

UNCLASSIFIED

AD NUMBER
AD083901
NEW LIMITATION CHANGE
TO Approved for public release, distribution unlimited
FROM Distribution authorized to U.S. Gov't. agencies and their contractors; Administrative/Operational Use; 01 MAY 1955. Other requests shall be referred to Rome Air Development Center, Griffiss AFB, NY.
AUTHORITY
RADC ltr, 23 Jul 1968

THIS PAGE IS UNCLASSIFIED

UNCLASSIFIED

AD NUMBER
AD083901
CLASSIFICATION CHANGES
TO
unclassified
FROM
confidential
AUTHORITY
31 May 1967, DoDD 5200.10

THIS PAGE IS UNCLASSIFIED

UNCLASSIFIED

AD NUMBER
AD083901
CLASSIFICATION CHANGES
TO
confidential
FROM
secret
AUTHORITY
31 May 1958, DoDD 5200.10

THIS PAGE IS UNCLASSIFIED

UNCLASSIFIED

AD _____

DEFENSE DOCUMENTATION CENTER

FOR

SCIENTIFIC AND TECHNICAL INFORMATION

CAMERON STATION .ALEXANDRIA. VIRGINIA

**DOWNGRADED AT 3 YEAR INTERVALS
DECLASSIFIED AFTER 12 YEARS
DOD DIR 5200.10**



UNCLASSIFIED

83901

Services Technical Information Agency

Reproduced by
DOCUMENT SERVICE CENTER
KNOTT BUILDING, DAYTON, 2, OHIO

WHEN GOVERNMENT OR OTHER DRAWINGS, SPECIFICATIONS OR OTHER DATA FOR ANY PURPOSE OTHER THAN IN CONNECTION WITH A DEFINITELY RELATED GOVERNMENT PROCUREMENT OPERATION, THE U. S. GOVERNMENT THEREBY INCURS NO LIABILITY, NOR ANY OBLIGATION WHATSOEVER; AND THE FACT THAT THE GOVERNMENT MAY HAVE FORMULATED, FURNISHED, OR IN ANY WAY SUPPLIED THE DRAWINGS, SPECIFICATIONS, OR OTHER DATA IS NOT TO BE REGARDED BY ANY PERSON OR OTHERWISE AS IN ANY MANNER LICENSING THE HOLDER OR ANY OTHER PERSON OR CORPORATION, OR CONVEYING ANY RIGHTS OR PERMISSION TO MANUFACTURE, OR TO USE, OR TO SELL ANY PATENTED INVENTION THAT MAY IN ANY WAY BE RELATED THERETO.

**Best
Available
Copy**

SECRET

Studies in Radar
Cross-Sections - XVI

Microwave Reflection Characteristics of Buildings

by H. Weil, R. R. Bonkowski,
T. A. Kaplan, and M. Leichter

Contract AF 30(602)-1070

Expenditure Order No. R 158-11 AD-16

1 May 1955

2255-12-T

University of Michigan
Engineering Research Institute
Willow Run Research Center
Willow Run Airport
Ypsilanti, Michigan

56AA 4875 FEB 17 1956

SECRET

NI-5991.

This document contains information affecting the national defense of the United States within the meaning of the Espionage Laws, (Title 18 U.S.C., Sections 793 and 794); its transmission or the revelation of its contents in any manner to an unauthorized person is prohibited by law.

SECRET

UNIVERSITY OF MICHIGAN

2255-12-T

STUDIES IN RADAR CROSS-SECTIONS

- I Scattering by a Prolate Spheroid, F. V. Schultz (UMM-42, March 1950), W-33(038)-ac-14222. UNCLASSIFIED
- II The Zeros of the Associated Legendre Functions $P_n^m(\mu')$ of Non-Integral Degree, K. M. Siegel, D. M. Brown, H. E. Hunter, H. A. Alperin, and C. W. Quillen (JMM-82, April 1951), W-33(038)-ac-14222. UNCLASSIFIED
- III Scattering by a Cone, K. M. Siegel and H. A. Alperin (UMM-87, January 1952), AF-30(602)-9. UNCLASSIFIED
- IV Comparison Between Theory and Experiment of the Cross-Section of a Cone, K. M. Siegel, H. A. Alperin, J. W. Crispin, H. E. Hunter, R. E. Kleinman, W. C. Orthwein, and C. E. Schensted (UMM-92, February 1953), AF-30(602)-9. UNCLASSIFIED
- V An Examination of Bistatic Early Warning Radars, K. M. Siegel (UMM-98, August 1952), W-33(038)-ac-14222. SECRET
- VI Cross-Sections of Corner Reflectors and Other Multiple Scatterers at Microwave Frequencies. R. R. Bonkowski, C. R. Lubitz, and C. E. Schensted (UMM-106, October 1953), AF-30(602)-9. SECRET (UNCLASSIFIED when Appendix is removed)
- VII Summary of Radar Cross-Section Studies Under Project Wizard, K. M. Siegel, J. W. Crispin, and R. E. Kleinman (UMM-108, November 1952), W-33(038)-ac-14222. SECRET
- VIII Theoretical Cross-Sections as a Function of Separation Angle Between Transmitter and Receiver at Small Wavelengths, K. M. Siegel, H. A. Alperin, R. R. Bonkowski, J. W. Crispin, A. L. Maffett, C. E. Schensted, and I. V. Schensted (UMM-115, October 1953), W-33(038)-ac-14222. UNCLASSIFIED
- IX Electromagnetic Scattering by an Oblate Spheroid, L. M. Rauch (UMM-116, October 1953), AF-30(602)-9. UNCLASSIFIED
- X The Radar Cross-Section of a Sphere, H. Weil (2144-6-T, to be published), DA-36(039)SC-52654. UNCLASSIFIED
- XI The Numerical Determinant of the Radar Cross-Section of a Prolate Spheroid, K. M. Siegel, B. H. Gere, I. Marx, and F. B. Sleator (UMM-126, December 1953), AF-30(602)-9. UNCLASSIFIED
- XII Summary of Radar Cross-Section Studies Under Project MIRO, K. M. Siegel, M. E. Anderson, R. R. Bonkowski, and W. C. Orthwein (UMM-127, December 1953), AF-30(602)-9. SECRET
- XIII Description of a Dynamic Measurement Program, K. M. Siegel and J. M. Wolf (UMM-128, May 1954) W-33(038)-ac-14222. CONFIDENTIAL
- XIV Cross-Sections of Ballistic Missiles, K. M. Siegel, M. L. Barasch, J. W. Crispin, I. V. Schensted, W. C. Orthwein, and H. Weil (UMM-174, September 1954), W-33(038)-ac-14222. SECRET
- XV Radar Cross-Sections of B-47 and B-52 Aircraft, C. E. Schensted, J. W. Crispin, and K. M. Siegel (2260-1-T, August 1954), AF-33(616)-2531. CONFIDENTIAL
- XVI Microwave Reflection Characteristics of Buildings, H. Weil, R. R. Bonkowski, T. A. Kaplan, and M. Leichter (2255-12-T, May 1955), AF-30(602)-1070. SECRET
- XVII Complete Scattering Matrices and Circular Polarization Cross-Sections for the B-47 Aircraft at S-Band, A. L. Maffett, M. L. Barasch, W. E. Burdick, R. F. Goodrich, W. C. Orthwein, C. E. Schensted, and K. M. Siegel (2260-6-T, June 1955), AF 33(616)-2531. CONFIDENTIAL

SECRET

SECRET

UNIVERSITY OF MICHIGAN

2255-12-T

PREFACE

This paper is the sixteenth in a series of reports growing out of studies of radar cross-sections at the Willow Run Research Center¹ of The University of Michigan. The primary aims of this program are:

1. To show that radar cross-sections can be determined analytically.
2. To elaborate means for computing cross-sections of various objects of military interest.
3. To demonstrate that these theoretical cross-sections are in agreement with experimentally determined values.

Intermediate objectives are:

1. To compute the exact theoretical cross-sections of various simple bodies by solution of the appropriate boundary-value problems arising from electromagnetic theory.
2. To examine the various approximations possible in this problem and to determine the limits of their validity and utility.
3. To find means of combining the simple-body solutions in order to determine the cross-sections of composite bodies.
4. To tabulate various formulas and functions necessary to enable such computations to be done quickly for arbitrary objects.
5. To collect, summarize, and evaluate existing experimental data.

Titles of the papers already published or presently in process of publication are listed on the back of the title page.

K. M. Siegel

¹Henceforth the Willow Run Research Center will be identified organizationally as Engineering Research Institute with a geographical designation as Willow Run Laboratories.

SECRET

NI-5991

SECRET

UNIVERSITY OF MICHIGAN

2255-12-T

TABLE OF CONTENTS

<u>Section</u>		<u>Page</u>
	Preface	ii
	List of Figures	vi
	List of Tables	x
I	Introduction	1
	1.1 Nature and Scope of the Work	1
	1.2 Summary of Experimental Work	2
	1.3 Summary of Theoretical Work	5
	1.4 Materials for Radar Camouflage	5
	1.5 Basic Assumptions	7
II	Camouflage Procedures	9
	2.1 Procedures	9
	2.2 Needed Field Tests	11
III	Radar Cross-Section of the East Side of the Willow Run Airport	13
	3.1 Radar Cross-Section for Individual Trihedral Reflectors	21
	3.2 Radar Cross-Section in the Cardinal Direction (Cardinal Point Effect)	44
	3.3 Method of Computation for Finite Conductivity	47
IV	Effect of Building Shape on Radar Returns	50
V	Recommendations	53
	5.1 Experimental Programs	53
	5.1.1 Camouflage Procedures	53
	5.1.2 Rough Surfaces	53
	5.1.3 Angle Errors	53
	5.1.4 Dielectric Constants of Soils and Common Building Materials	54
	5.1.5 Validity of Physical Optics	54
	5.1.6 Flight Tests for Data on Microwave Reflections	54

SECRET

SECRET

UNIVERSITY OF MICHIGAN

2255-12-T

TABLE OF CONTENTS (Continued)

<u>Section</u>	<u>Page</u>
5.1.7 Over-all Tests of Results of Section III	54
5.1.8 Further Analysis of Project Baltimore Data	55
5.2 Theoretical Programs	55
5.2.1 Rough Surfaces	55
5.2.2 Returns from Complex Targets	55
5.2.3 Geometric Areas for Trihedrals Including Effects of Non-Perpendicularity	56
5.2.4 Refined Computations of the Willow Run Scattering Patterns	56
5.2.5 Polarization	57
Appendix A Special Formulas for Dihedral and Trihedral Returns	A-1
A.1 General Theoretical Basis	A-1
A.2 Radar Cross-Section Formulas for Conventional Corner Reflectors	A-6
A.3 Radar Cross-Section of a Compensated and Truncated Trihedral Reflector	A-8
A.4 Radar Cross-Section of Two Walls in Tandem	A-19
A.5 Wavelength Dependence of the Non-Specular Return from 90-Degree Dihedral Reflectors	A-21
A.6 Angle Errors	A-23
Appendix B Complex Dielectrics in Dihedral and Trihedral Reflectors	B-1
B.1 The Problem	B-1
B.2 Basic Theoretical Considerations	B-1
B.3 Dihedral Reflectors	B-7
B.4 Trihedral Reflectors	B-19
B.5 X-Band Data on Lossy Dielectrics	B-51

SECRET

SECRET

UNIVERSITY OF MICHIGAN

2255-12-T

TABLE OF CONTENTS (Continued)

<u>Section</u>	<u>Page</u>
Appendix C Rough Surface Effects	C-1
Appendix D Summary and Analysis of Experiments	D-1
D. 1 Strategic Air Command, Radar Prediction Improvement Program "The Baltimore Project"	D-1
D. 2 The Ohio State University Results for Batavia, N. Y.	D-5
D. 3 Kurtz Laboratories Integration Techniques	D-6
D. 4 Engineering Research Associates, Inc., and Ford Instrument Company "Brilliance Measurements"	D-8
D. 5 Philco Corporation Research on Radar Terrain Reflection Characteristics	D-11
D. 6 Dihedral and Trihedral Reflector Experiments	D-13
References	E-1
Distribution	E-4

SECRET

SECRET

UNIVERSITY OF MICHIGAN

2255-12-T

LIST OF FIGURES

<u>Number</u>		<u>Page</u>
3-1	Map of the Willow Run Research Center; East Side of the Willow Run Airport	14
3-2	Aerial Photograph of the Willow Run Research Center; East Side of the Willow Run Airport	15
3-3	Radar Cross-Section of WRRC in Square Meters as a Function of Azimuth Angle ϕ for $\lambda = 0.03$ m	16
3-4	Radar Cross-Section WRRC, Dielectric Constant $\epsilon' = 2$	17
3-5	Radar Cross-Section WRRC, Dielectric Constant $\epsilon' = 4$	18
3-6	Radar Cross-Section WRRC, Dielectric Constant $\epsilon' = 6$	19
3-7	Radar Cross-Section WRRC, Dielectric Constant $\epsilon' = 8$	20
3-8	Radar Cross-Section of WRRC with Principal Trihedral Reflectors Camouflaged; Infinite Conductivity	22
3-9	Radar Cross-Section of WRRC with Principal Trihedral Reflectors Camouflaged; Dielectric Constant $\epsilon' = 2$	24
3-10	Geometrical Definition of Corner Dimensions Used in Table 3-1	31
3-11 - 3-22	Polar Diagrams Nos. 1-47	32 - 43
3-23	Effect of Beam Divergence	44
4-1	Geometry for Flat Plate	51
A. 1-1	Quantities Appearing in the Formula for the Scattered Field	A-2
A. 1-2	The Projection Vector \vec{P}	A-5

SECRET

SECRET

UNIVERSITY OF MICHIGAN
2255-12-T

LIST OF FIGURES (Continued)

<u>Number</u>		<u>Page</u>
A. 2-1	Geometry for Trihedral Reflector	A-7
A. 2-2	Geometry for Dihedral Reflector	A-7
A. 3-1	Geometry for Compensated and Truncated Trihedral Reflector	A-8
A. 3-2	Geometry for the Image Problem	A-9
A. 3-3	A Geometrical Optics Approximation to the Image Problem	A-10
A. 3-4	Introducing the Notation	A-11
A. 3-5	The Image of \mathcal{L} on the YZ-Plane as a Function of the Aspect Angle θ with Azimuth Angle ϕ Fixed	A-12
A. 3-6	The Image of \mathcal{L} on the YZ-Plane	A-15
A. 3-7a	Definition of Trihedral Reflector Sides	A-17
A. 3-7b	Definition of Trihedral Reflector Sides in the Image Problem	A-17
A. 4-1	Two Buildings with Similar Walls in Tandem	A-19
A. 4-2	Geometry for the Image Problem	A-20
A. 5-1	Geometry for the Image Problem	A-22
A. 6-1	Geometry for Dihedral with Arbitrary Angle	A-26
A. 6-2	Geometry for Dihedral with Non-Perpendicular Sides	A-27
A. 6-3	Geometry for the Image Problem	A-27
A. 6-4	Coordinate Systems for Plate L and L'	A-28
A. 6-5	Geometry Defining Beam Directions	A-31
A. 6-6	Formation of Various Equivalent Apertures	A-32

SECRET

SECRET

UNIVERSITY OF MICHIGAN

2255-12-T

LIST OF FIGURES (Continued)

<u>Number</u>		<u>Page</u>
A. 6-7	Parallelogram Aperture	A-33
A. 6-8	Relative Intensity of Diffraction through a Parallelogram Aperture	A-35
A. 6-9	Possible Aperture for Dihedral with Two Sides Finite	A-34
A. 6-10	Triangular Aperture	A-36
A. 6-11	Relative Intensity of Diffraction through a Triangular Aperture	A-39
B. 2-1	Illustration of Volume V and Surfaces S_1 and S_2	B-2
B. 2-2	Dihedral of Finite Conductivity	B-6
B. 3-1	Dihedral with Sides of Different Materials	B-8
B. 3-2	Dihedral Geometry	B-11
B. 3-3	Reflector Coefficients for Two Perpendicular Dielectric Walls of the Same Dielectric Constant (cf. ex. 1) Parallel Polarization	B-13
B. 3-4	Reflection Coefficients for Two Perpendicular Dielectric Walls of the Same Dielectric Constant (cf. ex. 2) Perpendicular Polarization	B-14
B. 3-5	A Dielectric Wall of Finite Dimensions on a Perfectly Conducting Plane of Infinite Extent	B-18
B. 3-6	The Image Problem	B-18
B. 4-1	Definition of Vectors Appearing in the Trihedral Problem	B-20
B. 4-2	Ray (123) in the X and X' Coordinate Systems	B-28
B. 4-3	Definitions of Various Coordinate Systems	B-33
B. 4-4	Reference Figure	B-37

SECRET

UNIVERSITY OF MICHIGAN

2255-12-T

LIST OF FIGURES (Continued)

<u>Number</u>		<u>Page</u>
B. 4-5	Equivalent Single Reflection Where Two Sides Are Perfectly Conducting	B-41
B. 4-6	Symmetric Square Corner Reflector, \vec{k} along Symmetry Axis	B-45
B. 4-7	Symmetric Square Corner Reflector with Walls of Finite Thickness	B-48
B. 5-1	Reflection Coefficients for Moist and Dry Soil	B-54
C-1	Vertical Wall in Rough Surface	C-1
C-2	Image Problem	C-2
C-3	Reflection of Rough Surface	C-3
C-4	Geometry for Rough Surface	C-5
C-5	Two Dimensional Pseudo-Isotropic Scatterer	C-7
D-1	Change in Brightness Due to Contrast Control	D-2
D-2	Illustrating PPI Returns from Batavia, N. Y.	D-7
D-3	Relative Intensity of Reflection from Square Corner Reflector	D-14
D-4	Corner Reflector Geometry	D-16
D-5	Modulation for Movable Side Corner Reflector (Single Side Displaced)	D-17
D-6	Modulation for Movable Side Corner Reflector (Two Sides Displaced Equal Amounts in the Same Direction)	D-18
D-7	Modulation for Movable Side Corner Reflector (Two Sides Displaced Equal Amounts in Opposite Directions)	D-19

SECRET

SECRET

UNIVERSITY OF MICHIGAN

2255-12-T

LIST OF FIGURES (Continued)

<u>Number</u>		<u>Page</u>
D-8	Diffusing Side Cylindrical Projection Corner Reflector	D-20
D-9	Multiple Dir Shutter Corner Reflector	D-21
D-10	Multiple Vertical Cylinder Diffuser Corner Reflector	D-22
D-11	Multiple Disc Diffuser Corner Reflector	D-23

LIST OF TABLES

<u>Number</u>		<u>Page</u>
3-1	Trihedral Reflector Data	25
3-2	Radar Cross-Section in the Cardinal Directions	47
4-1	Radar Cross-Section as a Function of Building Shape	52
A-1	Errors in Corners Versus db Drop in Signal Strength	A-25
B-1	Complex Dielectric Constants and Depth of Penetration	B-53
D-1	Variation of Cross-Section with Corner Side Length b	D-15

SECRET

UNIVERSITY OF MICHIGAN

2255-12-T

I

INTRODUCTION

This report presents the results obtained thus far in a theoretical study of the microwave reflection characteristics of buildings. The study was initiated 1 May 1954 at The University of Michigan, Willow Run Research Center (WRRC), under Contract AF-30(602)-1070 with the Rome Air Development Center. The aim of this study is to recommend methods suitable for camouflaging ground structures from X-band navigation radars operating at an altitude of 40,000 feet and at ranges up to 150 miles.

Recommended camouflage procedures are described in Section II. Recommendations for future work are contained in Section V.

1.1 NATURE AND SCOPE OF THE WORK

Before determining how to conceal the presence of buildings it is first necessary to know, in some detail, the effects of structural shapes and materials on the radar back-scattering patterns of buildings and groups of buildings located on various types of terrain. The attack on the problem was threefold:

1. Theory (Sec. 1.3) and experiment (Sec. 1.2 and App. D) on the radar characteristics of buildings and on existing and proposed camouflage materials (Sec. 1.4) were surveyed.
2. A theoretical basis and methods and formulas were developed for computing the approximate radar cross-sections of buildings and of groups of buildings at X-band (App. A, B, and C).
3. The methods and formulas developed under (2) were applied to a specific target complex, namely the group of buildings located on the east side of the Willow Run Airport, Ypsilanti, Michigan (Sec. III).

SECRET

UNIVERSITY OF MICHIGAN

2255-12-T

Although the radar camouflage problem treated in this report is related to the extremely complex radar prediction and interpretation problems for ground targets, it is simpler in some ways. It is generally unnecessary to calculate the scattering pattern of the entire complex group of structures which may fall within a radar pulse. Rather, it suffices to concentrate on the major returns which arise either from individual structures, or from combinations of neighboring structures. Furthermore, it is believed that conclusions adequate for recommending camouflage of structures against present-day X-band bombing radars can be drawn without detailed knowledge of the scattering behavior of the surrounding terrain (e. g., fine structure of the scattering pattern, echo amplitude probability distributions, and spectra). It suffices to consider the terrain surrounding the buildings to reflect specularly, isotropically, or in a simple superposition of these two ways. Additional basic assumptions made in the course of the analytic work are described in Section 1.5.

Although the present problem does allow many simplifications, there are, nevertheless, a number of quite complex considerations which were taken into account in varying degrees. These include the over-all shape and orientation of the buildings (Sec. IV), non-perpendicularity of walls (App. A. 6), finite conductivity of construction materials and the earth (App. B), and effects of rough surfaces (App. C).

1.2 SUMMARY OF EXPERIMENTAL WORK

Most of the applicable experimental work has consisted of measurement of the returns to airborne radars from terrain with and without man-made structures. These include:

1. "The Baltimore Project", an extensive investigation by the Strategic Air Command, Offutt Air Force Base, Nebraska, involving airborne PPI photography (App. D. 1). The final results of this investigation are not available at this writing; the experimental procedures and preliminary results are described in Reference 5.
2. Extensive analysis by Engineering Research Associates,

SECRET

SECRET

UNIVERSITY OF MICHIGAN

2255-12-T

Arlington, Virginia (App. D. 4), the Ford Instrument Company, Long Island City, N. Y., (App. D. 4), and The Ohio State University (App. D. 2) of several sets of airborne radar PPI photographs supplied by the Wright Air Development Center.

3. Investigation of various photographic integration methods for use on successive PPI photographs by Kurtz Laboratories, Yellow Springs, Ohio, using film supplied by the Wright Air Development Center, Dayton, Ohio (App. D. 3).
4. A considerable amount of data on terrain without man-made structures and a much smaller amount of data on terrain with structures obtained by the Philco Corporation, Philadelphia, Pennsylvania (App. D. 5).

Applicable laboratory experiments have been concerned primarily with gathering data on the radar cross-section of dihedral and trihedral reflectors (App. D. 6). In some cases, these experiments were scale-model tests using light instead of radar.

The general trends in the experimental results found by Strategic Air Command all point to the fact that the major radar echoes from complex ground targets are primarily due to specular reflection from dihedral and trihedral reflectors, whose sides are fairly smooth with respect to 3 cm radiation. These reflectors are formed, for example, by building walls and paved ground. The effect of windows in buildings was found to be not too great even though, for example, combinations of window frames and panes form trihedral corners. These results are to be expected, inasmuch as the angles between sills and panes are generally not very close to 90 degrees, and hence the corner-reflector effect would be considerably reduced as indicated indirectly by the experimental data in Appendix D. 6. 1.¹ Neglect of windows is also in line with the experimentally observed

¹The data given in this appendix verify various results obtained for corner reflectors by physical optics theory including some of the results on the reduction in radar return due to angle errors given in Table A-1.

SECRET

SECRET

UNIVERSITY OF MICHIGAN

2255-12-T

"cardinal point effect" in cities; that is, predominantly large returns are found in directions perpendicular to the streets (these directions are often, but not necessarily, the cardinal directions of the compass). An explanation of this effect is that the rows of buildings are contributing large returns from the many dihedrals formed by the walls and the street. If the walls were rough or if corners, such as those formed by windows, were important, this directional effect would be much less. The cardinal point effect is demonstrated clearly by the results obtained by Ohio State University (App. D. 2) and the Kurtz Laboratories (App. D. 3). It is an effect which is well known to Strategic Air Command; in fact, it is often used by bombardiers on bombing runs.

The surface irregularities of common external building materials are usually small compared to the 3-cm wavelength of interest. Hence it is to be expected that roughness has only a negligible effect on the radar returns from buildings when the foreground is also relatively smooth. This expectation is strengthened by the effects observed by Engineering Research Associates in their optical scale-model scattering tests (App. D. 6. 3)¹ where roughness of the order of 3 to 5 wavelengths still permitted strong cardinal point effects to be observed.

In addition to cross-section information, there is the need for X-band measurements of reflectivity and transmissivity or, equivalently, of the complex dielectric constants of construction materials and of various types of earth under different moisture and possibly temperature conditions. The small amount of such data available is summarized in Appendix B. 5.

¹Scale model tests using light sources in place of radar are of limited use for obtaining quantitative information on the validity of possible simplifying assumptions for treating the returns from buildings. Since the length scaling ratio is usually about 50,000:1, accurate reproduction of construction or surface details is, in general, impossible and the scaling of complex dielectric constants is very difficult.

SECRET

SECRET

UNIVERSITY OF MICHIGAN

2255-12-T

1.3 SUMMARY OF THEORETICAL WORK

No theoretical studies have been found which were directed primarily at the problem of camouflage of ground targets against radar, with the exception of the theory used in the design of absorbing materials. The Strategic Air Command has developed empirical formulas for relative intensity of ground targets as seen on PPI displays based on study of their own experimental data. There is, of course, extensive literature on radar cross-sections and scattering of electromagnetic waves in general. The work on perfectly conducting corner reflectors by Spencer (Ref. 10) and on these and other multiple scatterers in the sixth paper in this "Studies in Radar Cross-Sections" series (Ref. 11) is particularly applicable.

Formulas and computations of the type derived in Appendix A of this report, but somewhat less general, have been given by Engineering Research Associates (Ref. 1), and the results compared with optical tests as described in Appendix D. 6 3.

The contributions which have been made thus far under this contract lie (1) in the extensive study of experimental results in an effort to determine the probable type of target elements which contribute chiefly to the radar returns from ground structures; (2) in the treatment of corners each of whose sides is, in general, made of a material of different complex dielectric constant; (3) in the development of relatively convenient formulas to compute the effective area of dihedrals and corners subject to fairly general truncation and angle errors; (4) in a preliminary study of rough surface effects; and (5) in the study of the effect of over-all building shape on the principal reflections.

1.4 MATERIALS FOR RADAR CAMOUFLAGE

There are many absorbing materials which give very low radar reflections over wide frequency bands and ranges of angles of incidence. These materials have an impedance, at the air-material interface which is to be irradiated, which is close to the wave impedance of free space (120π ohms). The impedance then increases with distance from the air-material interface, an increasing resistive component accounting for the absorption.

SECRET

SECRET

UNIVERSITY OF MICHIGAN

2255-12-T

The materials so far developed may be divided into two groups: those which have mechanical properties which permit their use as structural materials, and those which can be used only as coverings. Various materials of the latter type have been in existence for many years and further development and evaluation is being carried out at present at the Naval Research Laboratory, Washington, D. C. (Refs. 12 and 13). One major type, "Darkflex", is made of animal hair impregnated with rubber containing carbon black. It is meant primarily for indoor use (e. g., in microwave model scattering experiments). It can be pulled or picked apart easily and probably is not suitable as a permanent outdoor material. Its absorptivity is somewhat decreased by moisture, but (according to the Naval Research Laboratory) not badly, and this effect could be lessened. Its reflectivity is only a few per cent except very near grazing incidence. Versions of this material are available commercially.

A second material being investigated at the Naval Research Laboratory is "Harp", a very dense, rubber-based material in which impedance tapering is obtained partly by loading with conducting flakes and partly by forming the low-impedance side into arrays of pyramid-shaped protuberances. This shaping can also be done with hair mats. It is a better outdoor material than the hair mats, but is highly absorptive only over a narrow frequency band.

Structural materials are being developed at Emerson and Cuming, Inc., Canton, Massachusetts (Ref. 14). The most successful and furthest developed are panels of a sandwich honeycomb structure. The front facing is a thin, low-dielectric-constant, low-loss sheet. The honeycomb is coated by successive dipping with a resistive coating whose resistivity increases with distance from the front face. The backing is a high-loss, structurally strong material. Flatwise compression and simple flexure tests have indicated adequate structural strength. The power reflected is less than five per cent of the incident power for all angles except those near grazing, and for all wavelengths from 2 to 12 cm.

All these materials are quite expensive. The hair material, which is only non-rigid facing, is about \$0.80 per square foot. Emerson and Cuming estimate that their presently developed sandwich materials, if in

SECRET

SECRET

UNIVERSITY OF MICHIGAN

2255-12-T

production, would run close to \$8.00 per square foot. By comparison, a four-inch-thick cinderblock wall erected in Ann Arbor, Michigan, costs about \$0.60 per square foot. Hence active developments aimed at lowering costs are being carried out at several organizations.

Some preliminary work has been done under this contract to explore the possibility of designing camouflage materials not based on absorption. These materials would contain arrays of scatterers which would scatter the energy so as to give a very low return back toward the transmitter for a wide range of angles of incidence.

1.5 BASIC ASSUMPTIONS

The complexity of the problem of computing radar cross-sections of buildings and groups of buildings has been reduced by keeping the camouflage aims of this contract in mind. A series of simplifying assumptions has been made, based upon the conclusions drawn in Section 1.2 from the experimental work and upon calculations such as those given in Section IV. It is believed that computations based on these assumptions provide values of radar cross-sections of sufficient accuracy for most camouflage needs. These assumptions, which overlap to some extent are:

1. Only the principal contributions to back scattering need be considered; i. e., the net contribution to the radar cross-section from all other scattering objects in the beam is much less than the contribution of a limited number of the largest scatterers.
2. Surface roughness of most building materials is not a predominant influence on the returns at a wavelength of 3 cm. Hence building walls reflect essentially specularly.
3. The reduction in maximum, or near maximum, return (as a function of aspect) due to windows, doors, railings, etc., may be neglected except in unusual situations where window or door areas form extremely high percentages of the wall areas.
4. There is relatively little re-radiation from the interiors of buildings except in very special cases.

SECRET

SECRET

UNIVERSITY OF MICHIGAN

2255-12-T

5. The ground is either a perfect specular reflector or, if rough, reflects a fraction of the energy specularly and the remainder isotropically over a hemisphere.

These assumptions together amount to assuming that the scattering complex may be replaced for computational purposes by a few smooth-walled, opaque structures having the over-all shape of the major buildings.

If these assumptions are valid, back scattering comes predominantly from flat surfaces, particularly those which form dihedral and trihedral reflectors. These surfaces, in general, have irregular shapes:

Often the sides do not intersect; one side (the ground) may be effectively infinite in extent, or partly smooth and partly rough; the angles will often not be 90 degrees so that perfect reversal of the main direction of energy flow will not take place. To handle these effects, which are not considered in sufficient generality in the literature, it was necessary to do considerable analysis, which is reported in Appendices A, B, and C.

SECRET

SECRET

UNIVERSITY OF MICHIGAN

2255-12-T

II

CAMOUFLAGE PROCEDURES

On the basis of the investigations performed under this contract, it is possible to recommend many means of camouflaging complex targets of moderate size against X-band airborne radars. However, these investigations were not concerned with the necessity of camouflaging targets. Hence, the procedures described below do not resolve such questions as "which targets are worth camouflaging?", "what amounts of time and money should be invested in camouflage under various situations?", or "how much camouflage will be necessary in the future?" Furthermore, no attention has been given to the important problems of camouflaging against radars of frequency other than X-band or of camouflaging simultaneously against surveillance with radar, infrared, and visible radiation.

The problems that arise in camouflaging a complex target area are determining which parts of the target should be camouflaged and determining how to achieve camouflage. Implicit in the solution to these two problems is the answer to the question "what do the surroundings look like?" There are three methods of camouflage; viz. to make the surroundings look like the target area in question, to make the target look like the surroundings, or to alter both the surroundings and the target area.

Camouflage procedures described in this section consider the second method and are directed at changing the appearance of a group of buildings so that they either disappear into the terrain or appear as lakes, smaller groups of buildings, etc. The former is achieved for present-day radars if the radar cross-sections of the target and terrain are approximately the same.

2.1 PROCEDURES

A determination of the radar cross-section of a group of buildings will usually show that certain buildings and combinations of buildings contribute far more strongly to the cross-section than others. For most

SECRET

SECRET

UNIVERSITY OF MICHIGAN

2255-12-T

aspects, these main contributors will be trihedrals formed by separate buildings and the ground, and trihedrals and dihedrals formed by a single building and the ground. The trihedrals formed by a single building are generally the most important except in the cardinal directions in which case the dihedrals will likely dominate. It will not be necessary to camouflage all corners but only the main contributors.

One criterion which may be used to determine whether or not the major reflectors contribute sufficiently large returns to need camouflaging is to compare their radar cross-section with that of the area on the ground (considered as an isotropic scatterer) which contributes to the instantaneous return at the receiver. The effects of angle errors and surface roughness should be taken into account, at least approximately.

If it is desired to make the area appear as rough terrain without buildings, it will be necessary to reduce the returns from all the corners determined by the above criterion approximately to that of rough terrain occupying the area in the ground plane occupied by, or shadowed by, the buildings. If it is desired to simulate a smaller or less complex group of buildings, it will suffice to reduce some of the major returns in this manner. Camouflaging the main group of contributors may, however, not be sufficient. In that case the next most important group of reflectors must also be camouflaged, and so on.

The reduction in radar return from dihedral and trihedral reflectors can be accomplished by destroying the right angles at the junctions of the sides. This can often be done easily by sloping the ground a degree or so from horizontal in the neighborhood of the buildings. It can also be achieved by putting wire mesh screens at an angle to the walls, or by building sloping walls, or curved walls as in quonset huts (Sec. IV). Roughening the foreground by plowing, planting shrubs and trees, or inserting arrays of plates will also greatly reduce these echoes, as would perhaps growing ivy on buildings. The relative efficiency of these methods should be investigated experimentally (Sec. 5.2).

Buildings are ordinarily built almost vertical. It would not be feasible to construct a steel-frame building which was not plumb, but a facing

SECRET

UNIVERSITY OF MICHIGAN

2255-12-T

slanted by one degree (say 10 inches for a 50-foot building) could be put on a vertical frame rather inexpensively while the building was being built, or over the present facing after the building was built (at somewhat greater expense). Such a sloped facing would reduce the peak X-band cross-section of most buildings by a factor of 1000-to-1 or more.

When constructing new installations, adjacent buildings should not be parallel or perpendicular to one another so as to avoid large returns from trihedral reflectors formed by walls of the adjacent buildings. Consideration should also be given to using special building shapes, such as quonset huts, inasmuch as over-all building shape has a large effect on the maximum return (Sec. IV).

If it is desired to make a group of buildings simulate a specular surface such as a lake (or in some other special situations) the use of absorbing materials may be warranted. However, generally these materials will not be needed.

Because airport runways or a large flat roof may appear conspicuously as a dark spot on the PPI it might be desirable to increase the cross-sections of such large flat surfaces by placing small corner reflectors on them.

In all this work, considerations of time and cost will determine the choice of particular methods.

2.2 NEEDED FIELD TESTS

The procedures given in Section 2.1 should be tried in the field. In the field test program, close attention should be paid to the following factors to avoid difficulties such as were encountered in past work involving observation of ground targets where quantitative results were desired.

SECRET

SECRET

UNIVERSITY OF MICHIGAN

2255-12-T

The target areas chosen should be representative, at least theoretically, of the different types of back-scatterers and should not include too great a diversity of types.

Careful airborne radar and visual observation of the site should be made before and after camouflage. A careful record of the physical characteristics important to radar returns should be obtained (e. g., roughness, angles, material of corners). Courses radar parameters, control settings, and photographic development procedures should be known and duplicated closely in each run. A procedure such as that used by the Strategic Air Command to increase the effective measurable range of inputs and to avoid difficulties caused by contrast control (App. D. 1) should be used. Information as a function of azimuth and of depression angle is of great importance. Hence, circular courses at several ranges may be desirable, but the effect of antenna tilt due to airplane banking must be accounted for or duplicated from run to run. Alternatively, several radial runs from well chosen azimuth directions should be used. Unless such care is taken the results will not be sufficiently reproducible to have meaning. If not enough target aspects are considered, the value of the camouflage will not be ascertained adequately.

Although the variety of targets and types of camouflage which might be of interest may be extremely large, it is necessary to limit the number of tests and yet obtain enough information. Hence, careful factorial design (Ref. 23 and 24, for example) of the experiments should be made.

SECRET

SECRET

UNIVERSITY OF MICHIGAN

2255-12-T

III

RADAR CROSS-SECTION OF THE EAST SIDE OF THE WILLOW RUN AIRPORT

The University of Michigan buildings on the east side of the Willow Run Airport were selected as a complex target with which to illustrate the camouflage criteria outlined at the beginning of Section 2.1. This area is shown in Figures 3-1 and 3-2. Only a small percentage of this area consists of buildings, while the remainder is mainly a level grass field cut by gravel roads. Adjoining this area to the west is the airport proper. At high altitudes and long ranges the airport runways will not stand out on a PPI so that the building reflections characterize the target and only these reflections must be analyzed. Therefore, the major dihedral and trihedral reflectors formed by the buildings and ground were determined and their net scattering patterns were computed as functions of azimuth for aircraft assumed to be flying at 40,000 feet at ranges of 20 and 100 miles. The radar wavelength was 3 cm and horizontal (electric vector) polarization was assumed throughout.

In all the computations smooth surfaces at right angles to each other were assumed. As a result, the computed radar cross-sections tend to over-estimate the true values. In obtaining Figure 3-3, the walls and ground were assumed to be perfectly conducting so that the pattern shown is due entirely to the effect of building shape and orientations. Figures 3-4 through 3-7 illustrate the scattering pattern when the conductivity is assumed to be zero for several values of dielectric constants in the range of building materials. The newly introduced zeros in the pattern may be ascribed to a "Brewster angle" effect. Actual non-metallic building materials generally have a small conductivity and will have patterns intermediate between the zero and infinite conductivity cases. For wooden buildings and the dielectric constant (relative to vacuum), $\epsilon' = 2$, for example, instead of a null occurring at the Brewster angle the cross-section is reduced from that for infinite conductivity by about 50 db.

SECRET

SECRET

UNIVERSITY OF MICHIGAN
2255-12-T

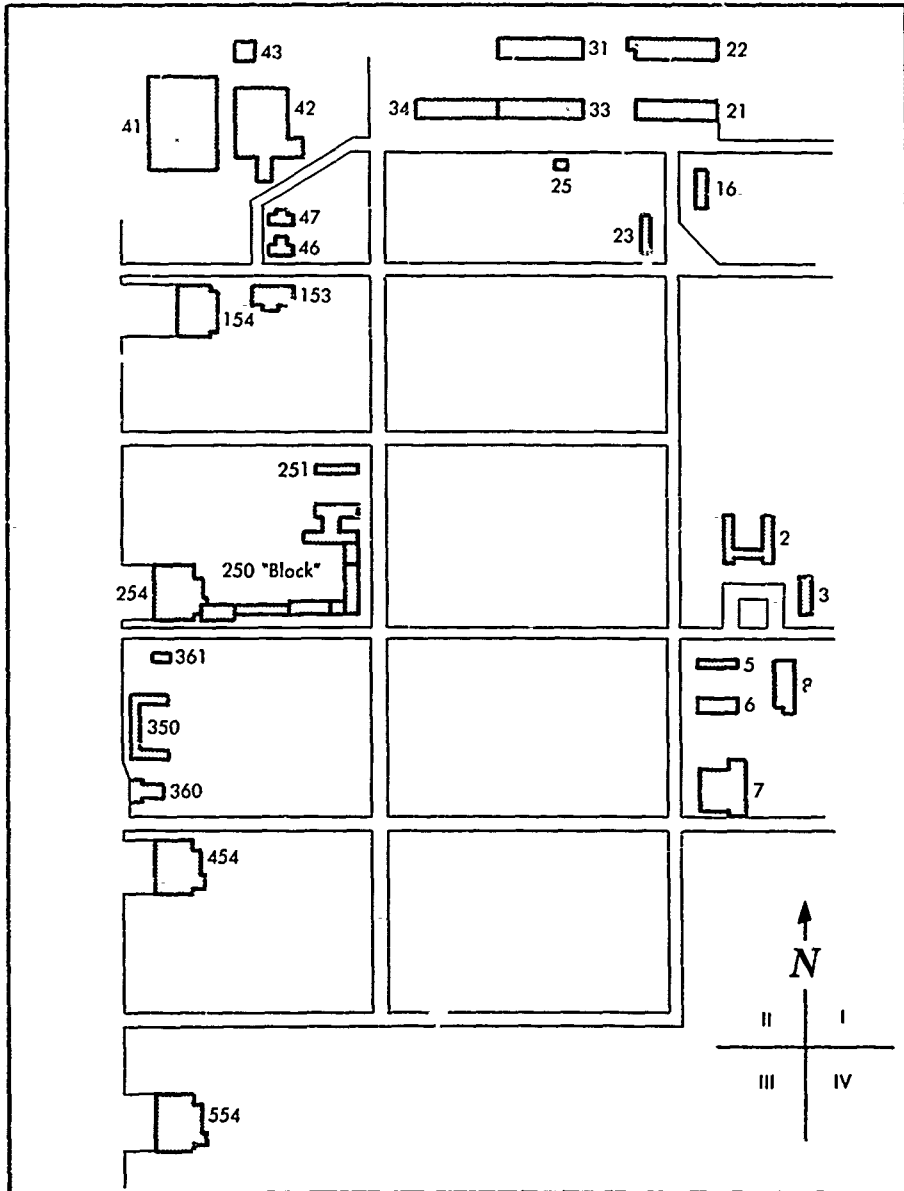


FIG. 3.1 MAP OF THE WILLOW RUN RESEARCH CENTER;
EAST SIDE OF THE WILLOW RUN AIRPORT

SECRET

SECRET

UNIVERSITY OF MICHIGAN



FIG. 3.2 AERIAL PHOTOGRAPH OF THE WILLOW RUN RESEARCH CENTER;
EAST SIDE OF THE WILLOW RUN AIRPORT

SECRET

SECRET

UNIVERSITY OF MICHIGAN

2255-12-T

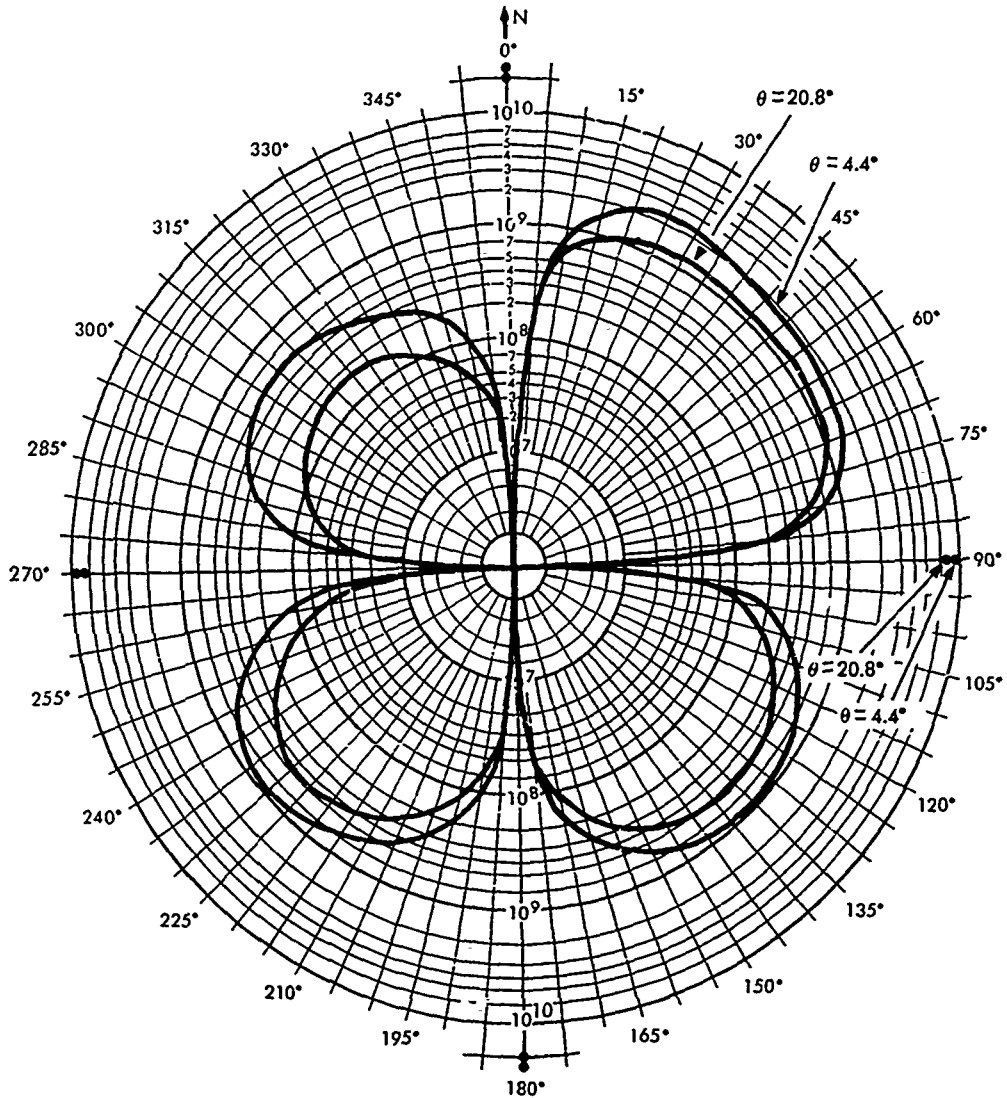


FIG. 3.3 RADAR CROSS-SECTION OF WIRC IN SQUARE METERS
AS A FUNCTION OF AZIMUTH ANGLE ϕ FOR $\lambda = 0.03$ m.

Figs. 3.3 through 3.9 & Figs. 3.11 through 3.22 have a Logarithmic Radial Scale

$\theta =$ Depression Angle $= 4.4^\circ$ for Airplane at a Range of 100 Miles and Altitude of 40,000 Feet
 $\theta = 20.8^\circ$ for Airplane at a Range of 20 Miles and Altitude of 40,000 Feet

SECRET

UNIVERSITY OF MICHIGAN

2255-12-T

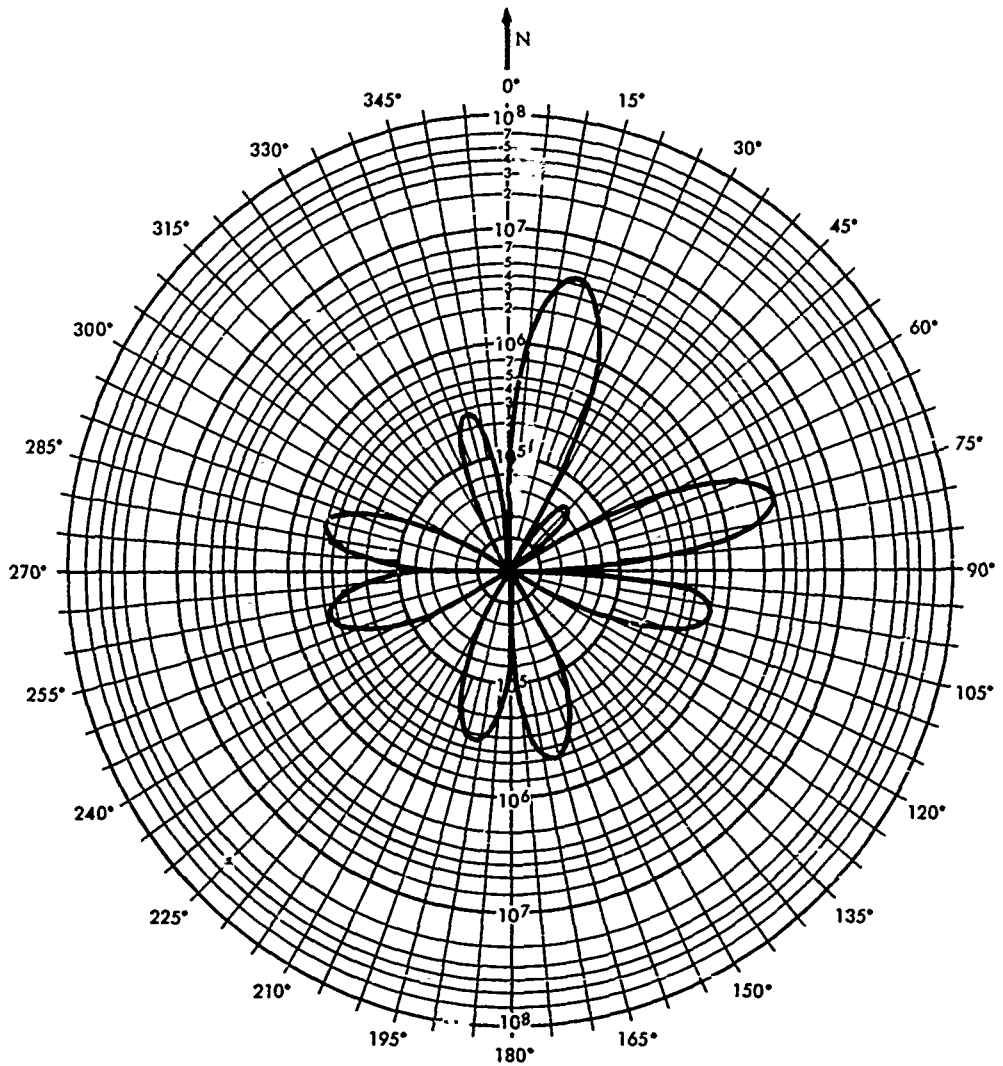


FIG. 3.4 RADAR CROSS-SECTION OF W R R C; DIELECTRIC CONSTANT $\epsilon = 2$
Cross-Section in Square Meters as a Function of Azimuth Angle ϕ for
 $\theta = 4.4^\circ$ and $\lambda = 0.03$ m.

SECRET

SECRET

UNIVERSITY OF MICHIGAN

2255-12-T

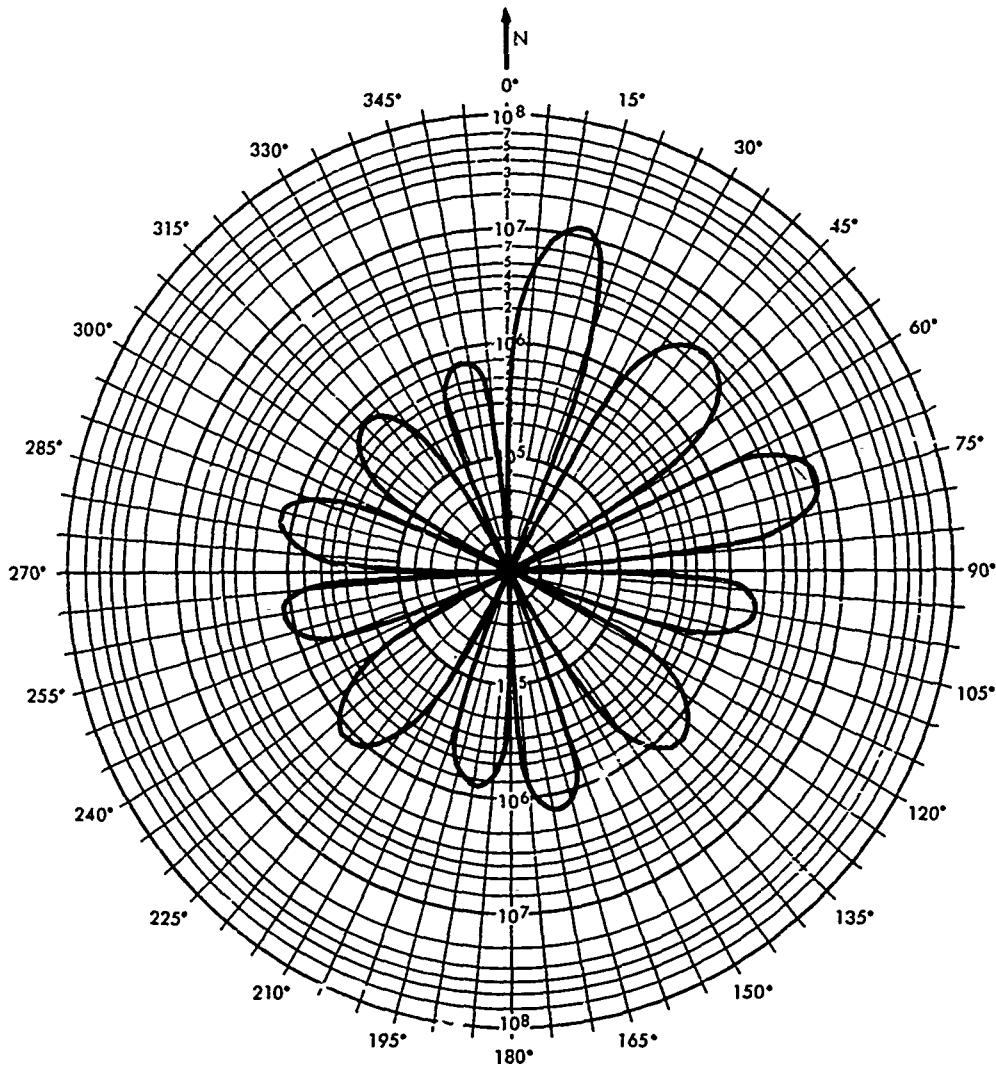


FIG. 3.5 RADAR CROSS-SECTION OF WRR; DIELECTRIC CONSTANT $\epsilon' = 4$
Cross-Section in Square Meters as a Function of Azimuth Angle ϕ for
 $\theta = 4.4^\circ$ and $\lambda = 0.03$ m.

SECRET

SECRET

UNIVERSITY OF MICHIGAN
2255-12-T

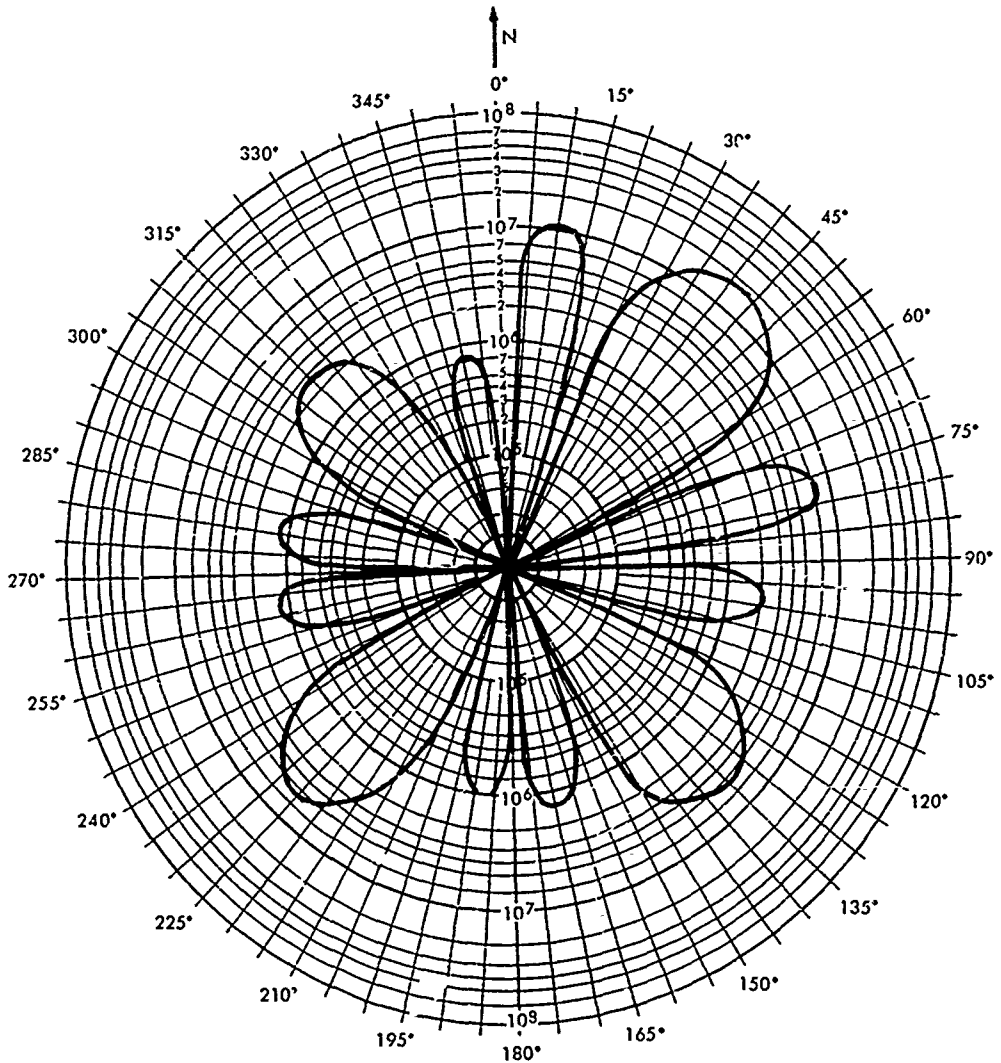


FIG. 3.6 RADAR CROSS-SECTION OF WRRC; DIELECTRIC CONSTANT $\epsilon=6$
Cross-Section in Square Meters as a Function of Azimuth Angle ϕ for
 $\theta=4.4^\circ$ and $\lambda=0.03$ m.

SECRET

SECRET

UNIVERSITY OF MICHIGAN

2255-12-T

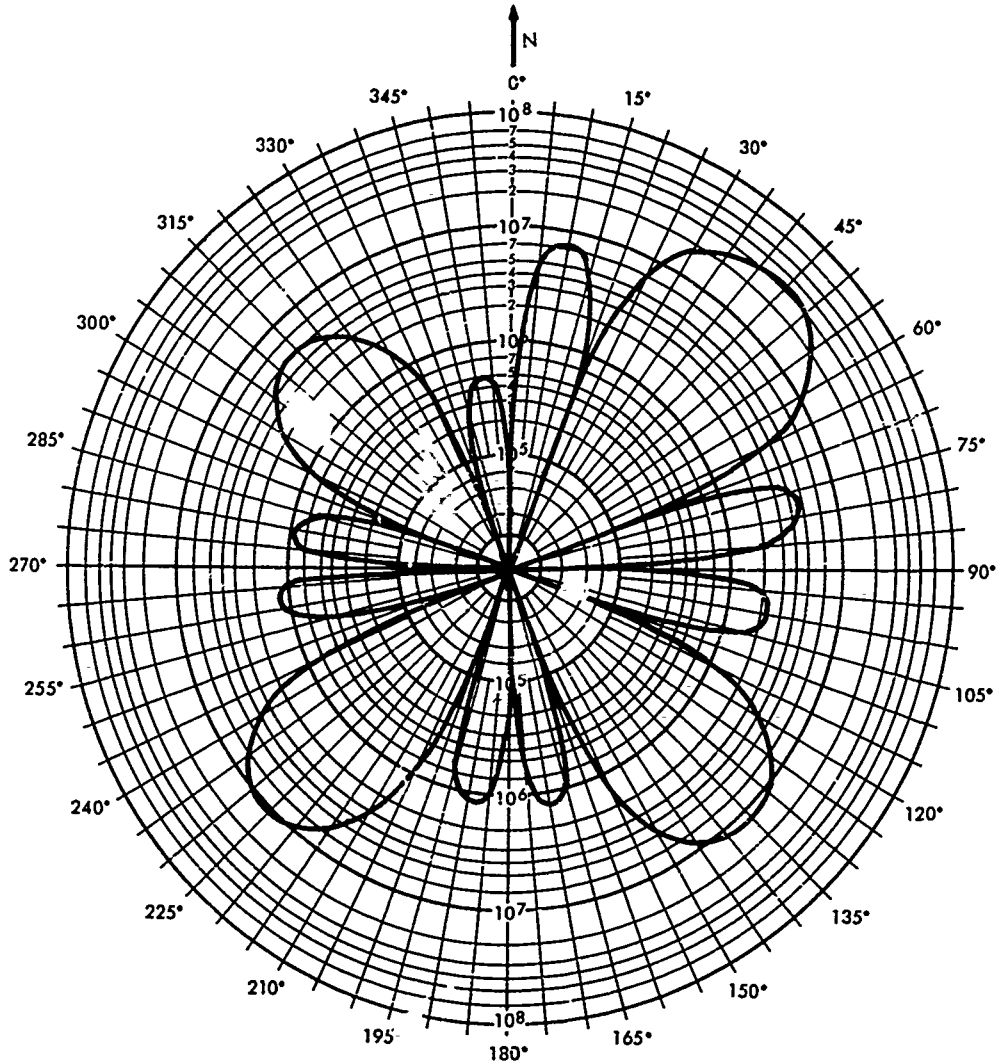


FIG. 3.7 RADAR CROSS-SECTION OF W R R C; DIELECTRIC CONSTANT $\epsilon = 8$
Cross-Section in Square Meters as a Function of Azimuth Angle ϕ for
 $\theta = 4.4^\circ$ and $\lambda = 0.03$ m.

SECRET

UNIVERSITY OF MICHIGAN

2255-12-T

The lobes in all of these figures are due to energy reflected from trihedrals. The amount of such energy drops off to zero as ϕ approaches one of the four cardinal points. Within a very narrow band of angles at the cardinal points there is a very strong echo due to the dihedrals. The maxima of these cardinal-point echoes are shown as points on Figure 3-3; they were not computed for the other figures.

There are several trihedral reflectors in each quadrant, the principal reflectors, whose effects are much larger than the others in their quadrant and many reflectors which, though less important, give returns large enough for them to be classed as important contributors according to the criterion of Section II. In this criterion, the returns from a corner are compared to the return which would result from isotropic ground. For a pulse length of roughly 300 meters, and beamwidth of 3 degrees, this is of the order of magnitude 10^5 square meters. For perfectly conducting surfaces Figure 3-8 illustrates the change in the scattering pattern of Figure 3-3 which would occur if the principal trihedral reflectors were camouflaged so that they gave no return. The results indicate that it is not sufficient to camouflage only these reflectors because the maximum cross-sections are reduced only by about 10 db, whereas to simulate isotropically scattering ground, roughly a 40 db decrease would be needed. To reduce the return to that from isotropically scattering ground it would be necessary to camouflage at least the smaller reflectors referred to above. However, the camouflage removes the azimuthal asymmetry in the scattering pattern. Figure 3-9 illustrates the effect of camouflage of the same trihedral reflectors for one case of zero conductivity and $\epsilon' = 2$. In this case camouflage of the principal reflectors is adequate to reduce the maximum returns to that of isotropic ground.

3.1 RADAR CROSS-SECTION FOR INDIVIDUAL TRIHEDRAL REFLECTORS

Table 3-1 contains the data used in computing radar cross-section values for the perfectly conducting trihedral reflectors from Equation A.3-7. The columns headed "corner and building specification", and "corner faces quadrant" were used in conjunction with Figure 3-1 to orient the individual trihedral reflectors in the area. The quantities h_1 , h_2 , ξ_1 ,

SECRET

UNIVERSITY OF MICHIGAN

2255-12-T

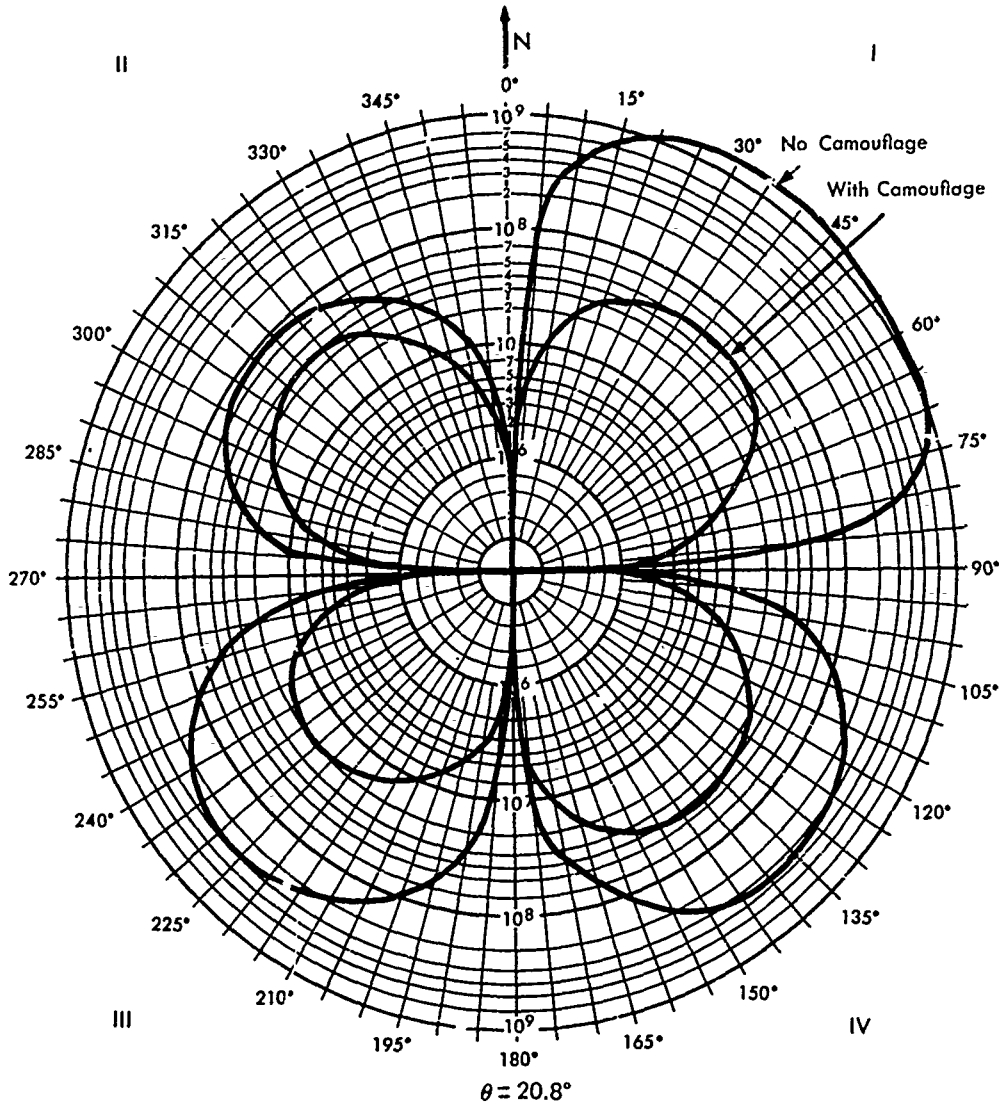


FIG. 3.8a RADAR CROSS-SECTION OF WRC WITH PRINCIPAL TRIHEDRAL REFLECTORS CAMOUFLAGED; INFINITE CONDUCTIVITY
(Compared with the "No Camouflage" case)

SECRET

UNIVERSITY OF MICHIGAN

2255-12-T

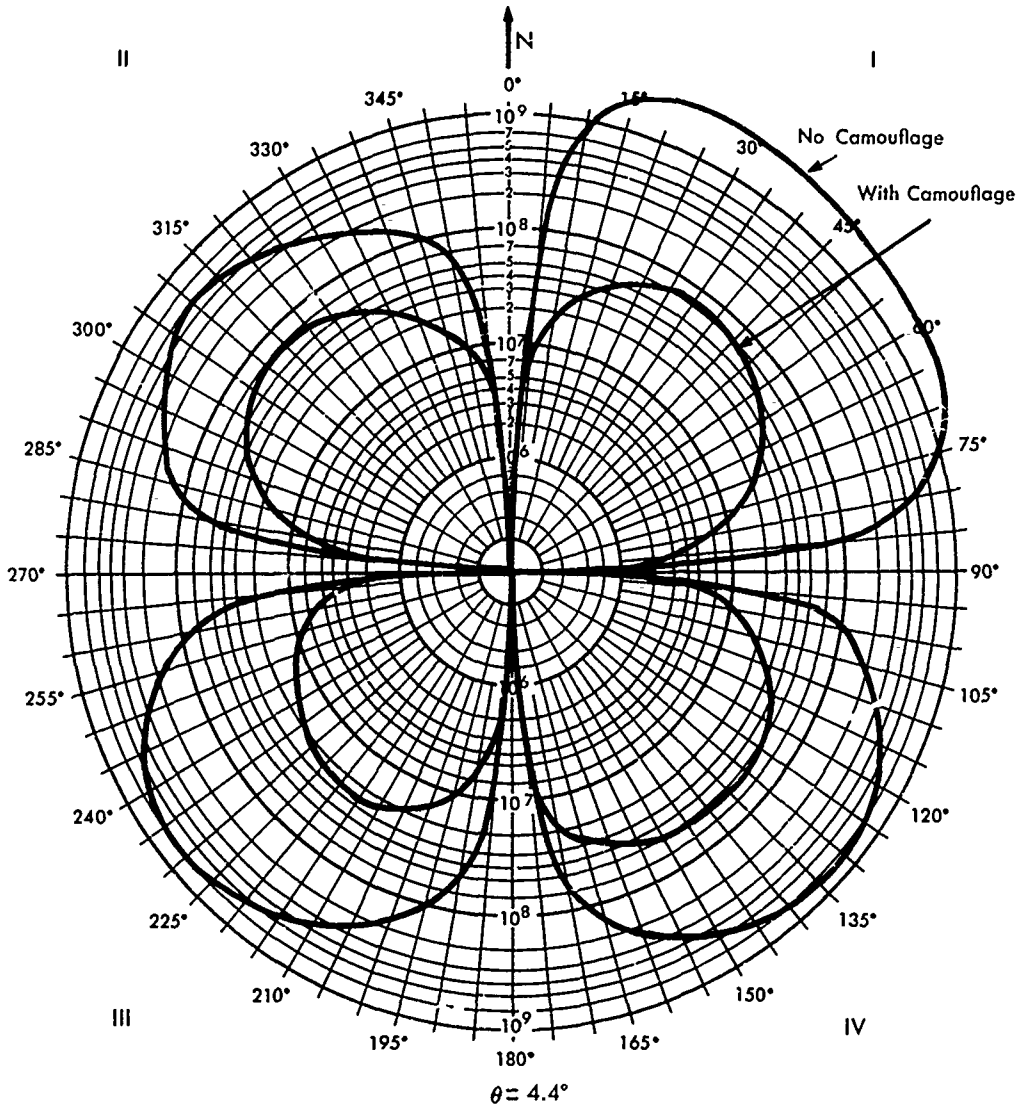


FIG. 3.8b RADAR CROSS-SECTION OF WIRC WITH PRINCIPAL TRIHEDRAL REFLECTORS CAMOUFLAGED; INFINITE CONDUCTIVITY (Compared with the "No Camouflage" case)

SECRET

UNIVERSITY OF MICHIGAN

2255-12-T

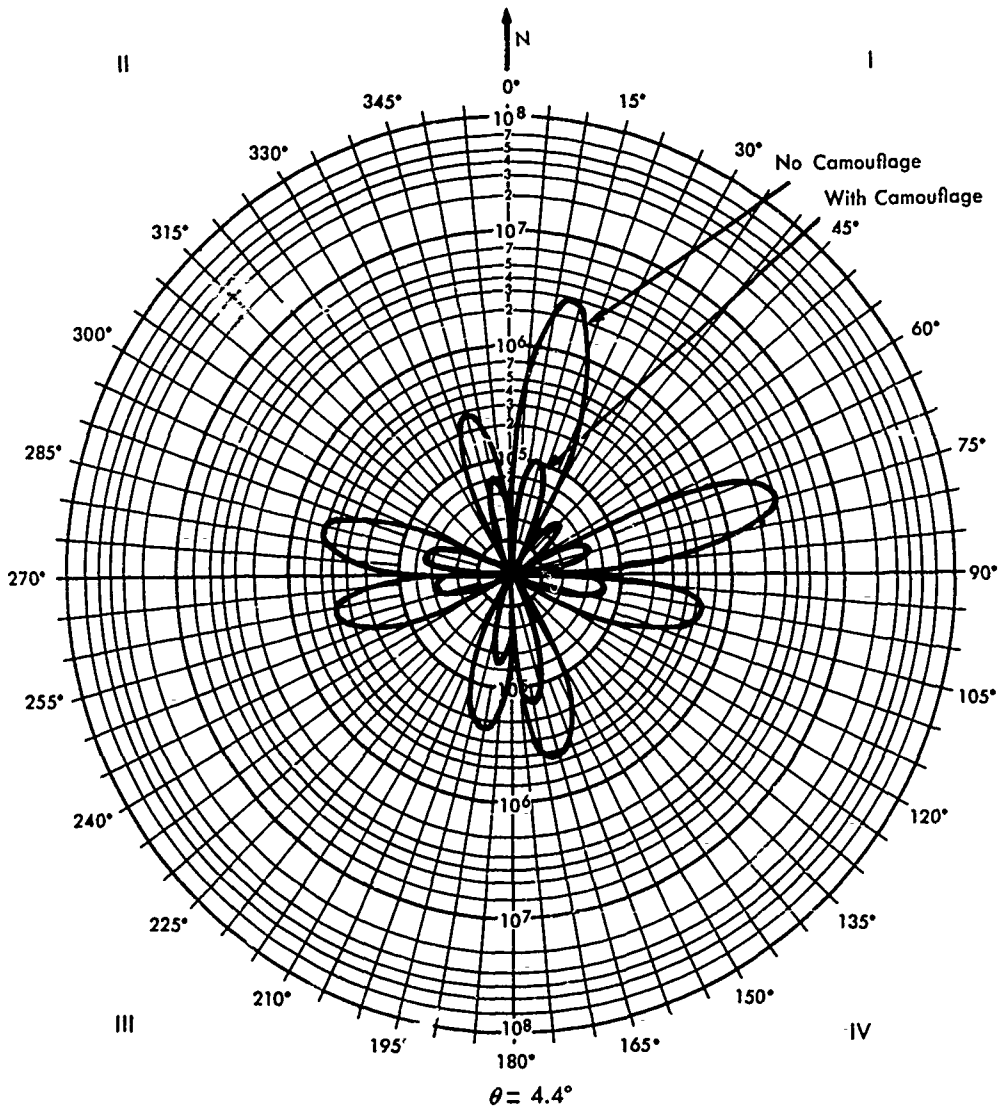
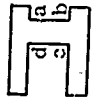
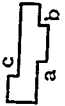
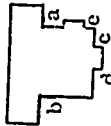


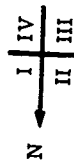
FIG. 3.9 RADAR CROSS-SECTION OF WRR C WITH PRINCIPAL TRIHEDRAL REFLECTORS CAMOUFLAGED; DIELECTRIC CONSTANT $\epsilon' = 2$ (Compared with the "No Camouflage" case)

SECRET

UNIVERSITY OF MICHIGAN
2255-12-T

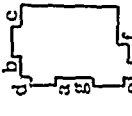
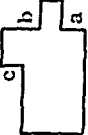
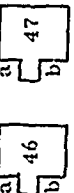
TABLE 3-1
TRIREDRAL REFLECTOR DATA

Corner and Building	Specification	Corner Faces Quadrant	Lengths in Meters				ξ_1	ξ_2	Remarks	Polar Diagram No.
			h_1	h_2	β_1	β_2				
 Bldg. 2	a	III	2.75	2.75	0	1.2	0	30.		1
	b	IV	2.75	2.75	0	30.	0	1.2		2
	c	I	2.75	2.75	0	23.4	0	30.	Principal	3
	d	II	2.75	2.75	0	30.	0	23.4	Principal	4
 Bldg. 3	a	II	3.	2.4	0	1.2	0	12.	Negligible	
	b	III	2.4	3	0	12.	0	1.2	Negligible	
	c	IV	3.	2.4	0	1.8	0	23.1	Negligible	
 Bldg. 7	a	III	3.6	3.6	0	11.	0	12.	Principal	5
	b	II	3.6	3.6	0	24.	0	6.3	Principal	6
	c	III	3.	6.6	0	6.	0	1.5		7
	d	II	6.6	3.	0	1.5	0	21.		8
	e	III	3.6	3.	0	1.2	0	13.	Negligible	
 Bldg. 8	a	II	3.	5.4	0	6.	0	0.9		9
	b	IV	5.4	3.	0	3.6	0	32.7	Principal	10
	c	I	5.4	3	0	0.9	0	10.	Negligible	
 Bldg. 16	a	I	2.4	4.8	0	6.	0	2.1		11
	b	IV	4.8	2.4	0	2.1	0	18.		12
	c	II	4.8	1.8	0	0.9	0	18.	Negligible	
	d	III	1.8	4.8	0	6.	0	0.9	Negligible	



SECRET

TABLE 3-1 (Continued)

Corner and Building	Specification Corner Faces	Length in Meters				Remarks	Polar Dia-gram No.	
		h ₁	h ₂	β ₁	β ₂			
 Bldg. 22	a	2.4	5.4	0	15.	0	1.5	13
	b	2.4	5.4	0	4.	0	1.5	14
	c	5.4	2.4	0	1.5	0	9.	15
	d	5.4	2.4	0	1.5	0	30.	16
	e	2.4	5.4	0	12.	0	1.2	17
	f	5.4	5.4	0	4.5	0	4.5	Principal
	g	5.4	2.4	0	1.2	0	5.	Negligible
 Bldg. 41	a	6.6	6.6	0	1.8	0	1.8	19
	b	6.6	6.6	0	1.8	0	1.8	19
	c	6.6	6.6	0	1.8	0	1.8	19
 Bldg. 42	a	6.6	3.3	0	15	0	15	Principal
	b	3.3	6.6	0	19	0	15	Principal
	c	6.6	6.6	0	30	0	12	Principal
 Bldgs. 46 and 47	a	3.	3.	0	4.5	0	3.	23
	b	3.	3.	0	3.	0	4.5	24
 Bldg. 153	a	2.6	3.	0	3.	0	9.	25
	b	3.	2.6	0	12.	0	3.	26

SECRET

UNIVERSITY OF MICHIGAN
2255-12-T

TABLE 3-1 (Continued)

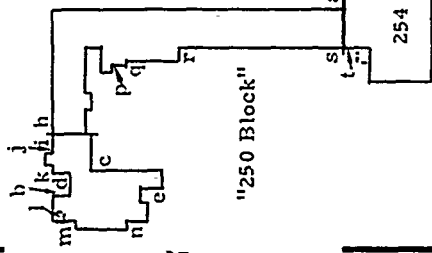
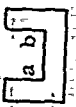
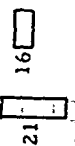
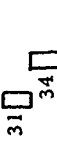
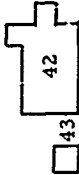
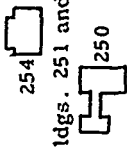
Corner and Building	Specification	Corner Faces	Length in Meters				Remarks	Polar Diagram No.		
			Quadrant	h_1	h_2	β_1			β_2	ξ_1
 Bldg. 154 - 454 - 554	I	I	10.5	8.1	0	4.5	0	22.5	Principal	27
	II	II	3.8	10.5	0	4.2	0	5.7	Principal	28
	IV	IV	10.5	3.8	0	5.7	0	4.2	Principal	29
	I	I	8.1	10.5	0	22.5	0	4.5	Principal	30
 "250 Block"	IV	IV	3	2.6	0	7.5	0	2.7		31
	IV	IV	3	3	0	6	0	3		32
	III	III	3	3	0	18	0	27	Principal	33
	I	I	3	3	0	3	0	6		34
	II	II	2.4	2.4	0	12	0	6		35
	II	II	8.1	3	0	22.5	0	1.5	Negligible	
	III	III	3	2	0	0.6	0	22.5	Negligible	
	IV	IV	2.6	3	0	0.6	0	30	Negligible	
	I	I	3	2.6	0	9	0	0.6	Negligible	
	IV	IV	2.6	2.1	0	1.8	0	9	Negligible	
	I	I	2.1	2.6	0	4.5	0	1.8	Negligible	
	I	I	3	3	0	4.5	0	3	Negligible	
	I	I	3	3	0	0.5	0	15	Negligible	
	II	II	3	3	0	3.7	0	0.5	Negligible	
	II	II	1.8	2.4	0	1.5	0	1.5	Negligible	
II	II	2.7	2.7	0	1.8	0	3.6	Negligible		
II	II	2.7	2.7	0	22.5	0	1.5	Negligible		
I	I	3	3	0	0.6	0	22.5	Negligible		
II	II	3	3	0	15	0	0.6	Negligible		

TABLE 3-1 (Continued)

Corner And Building	Specification	Corner Faces Quadrant	Length in Meters				ζ_1	ζ_2	Remarks	Polar Diagram No.
			h_1	h_2	β_1	β_2				
 Bldg. 251	a	II	3	2.1	0	1.2	0	4.2	Negligible	
	b	III	3	3	0	1.5	0	4.2		
 Bldg. 350	a	IV	2.75	2.75	0	23.4	0	30	Principal	3
	b	I	2.75	2.75	0	30	0	23.4		
 Bldg. 360	a	IV	3	4.8	0	3.6	0	18	Principal	36
	b	I	4.8	3	0	18	0	3.6		
 21 Bldgs. 21 and 16	-	III	4.8	4.8	30	60	0	40.5	Negligible	38
	-	IV	4.8	2.7	53	87	75	150		
 33 34 Bldgs. 33, 34, and 23	a	III	3	2.7	6	36	11	18.5	Principal	39
	b	IV	2.7	3	6	33	11	56		
 2 Bldgs. 2 and 3	a	III	3	2.7	6	36	11	18.5	Principal	40
	b	IV	2.7	3	6	33	11	56		

UNIVERSITY OF MICHIGAN 2255-12-T

TABLE 3-1 (Continued)

Corner and Building	Specification	Corner Faces Quadrant	Lengths in Meters				Remarks	Polar Diagram No.		
			h_1	h_2	β_1	β_2			ζ_1	ζ_2
 2 5 Bldgs. 2 and 5	-	II	2.75	2.75	0	16.5	67.5	97.5	Negligible	
 31 34 Bldgs. 31 and 34	-	II	4.8	4.8	0	57	27	42		41
 42 43 Bldgs. 42 and 43	-	I	6.6	3	18	30	0	21		42
 43 41 Bldgs. 43 and 41	-	II	3	6.6	15	43.5	7.5	19.5		43
 251 254 Bldgs. 251 and 254	-	II	3	8.1	71	93.5	60	67.5	Negligible	
 250 254 Bldgs. 250 and 254	a b	II II	3 3	8.1 8.1	73.5 63	96 85.5	31 15	42 24		44 45

SECRET

UNIVERSITY OF MICHIGAN
2255-12-T

TABLE 3-1 (Concluded)

Corner and Building	Specification	Corner Faces Quadrant	h_1	h_2	Lengths in Meters			ζ_2	Remarks	Polar Diagram No.
					β_1	β_2	ζ_1			
 254		II	10.5	2.7	0	15	45	83		46
 350										
Bldgs. 254 and 350										
 361		II	3	2.7	0	15	19	26.5	Negligible	
 350										
Bldgs. 361 and 350										
 454		III	4.8	8.1	24	60	3	9		47
 360										
Bldgs. 360 and 454										

SECRET

UNIVERSITY OF MICHIGAN

2255-12-T

ξ_2 , β_1 , and β_2 are defined geometrically in Figure 3-10. To reduce the amount of computation required, estimates were obtained for an upper bound for the cross-section of individual corners. When this upper bound was small (usually less than one per cent of the contributions obtained from other trihedral reflectors in the same quadrant) further computations were not performed and these reflectors were termed negligible.

Polar diagrams of radar cross-section versus azimuth angle for each of the trihedral corners listed in Table 3-1 are shown in Figures 3-11 through 3-22. The column entitled "polar diagram no." in Table 3-1 indicates which polar diagram corresponds to which corner.

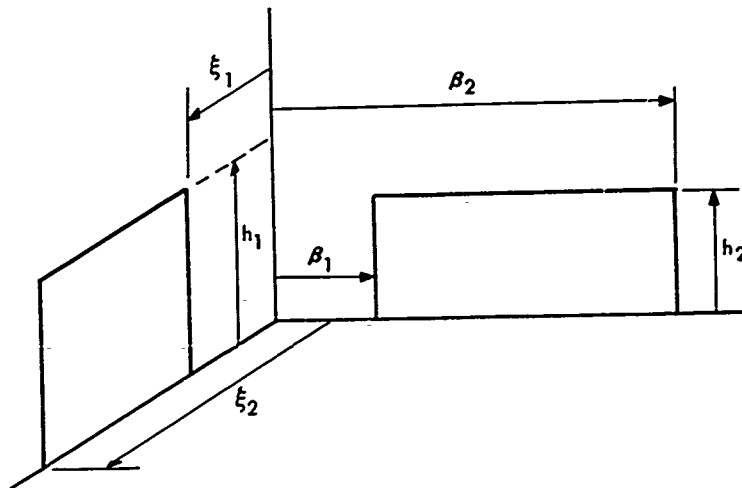


FIG. 3.10 GEOMETRICAL DEFINITION OF CORNER DIMENSIONS USED IN TABLE 3-1

**THIS
PAGE
IS
MISSING
IN
ORIGINAL
DOCUMENT**

SECRET

UNIVERSITY OF MICHIGAN

2255-12-T

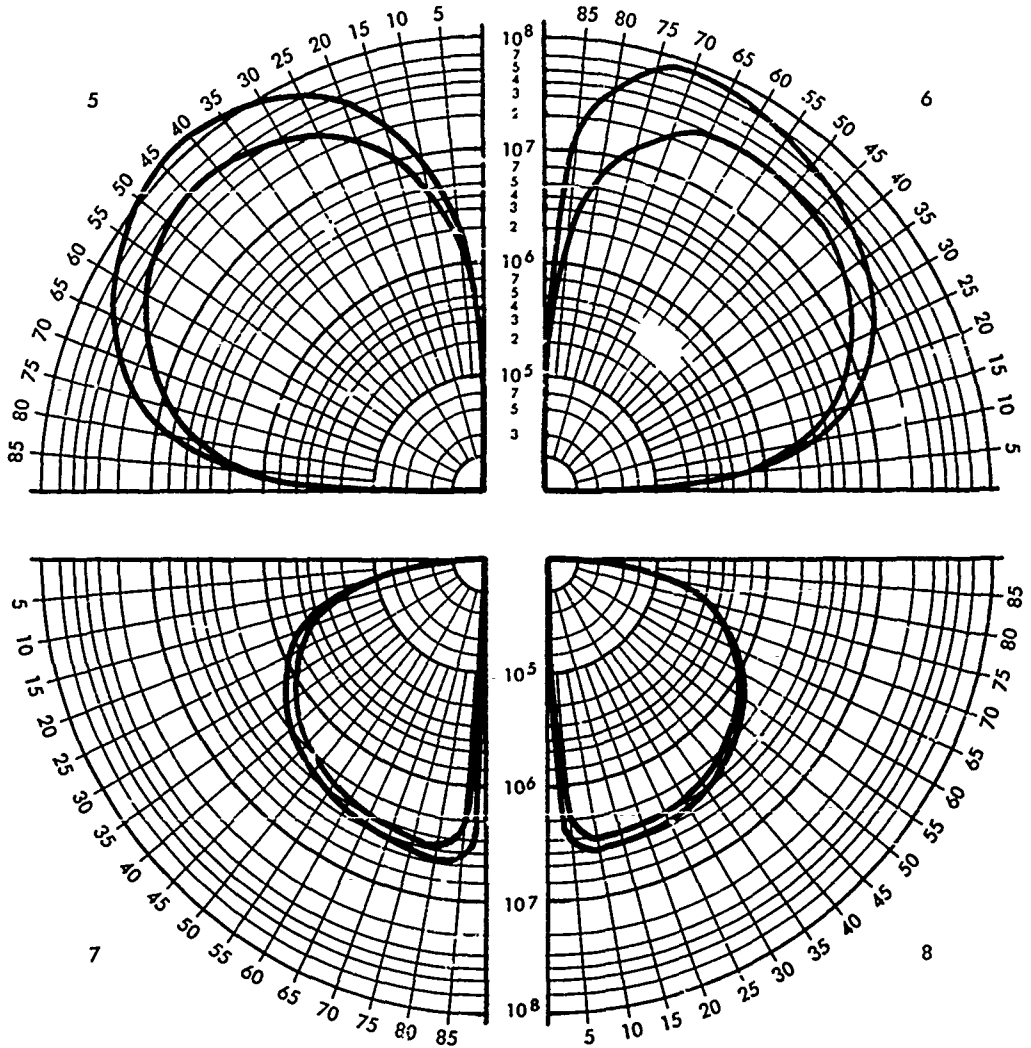


FIG. 3.12 POLAR DIAGRAM NOS. 5-8

SECRET

SECRET

UNIVERSITY OF MICHIGAN
2255-12-T

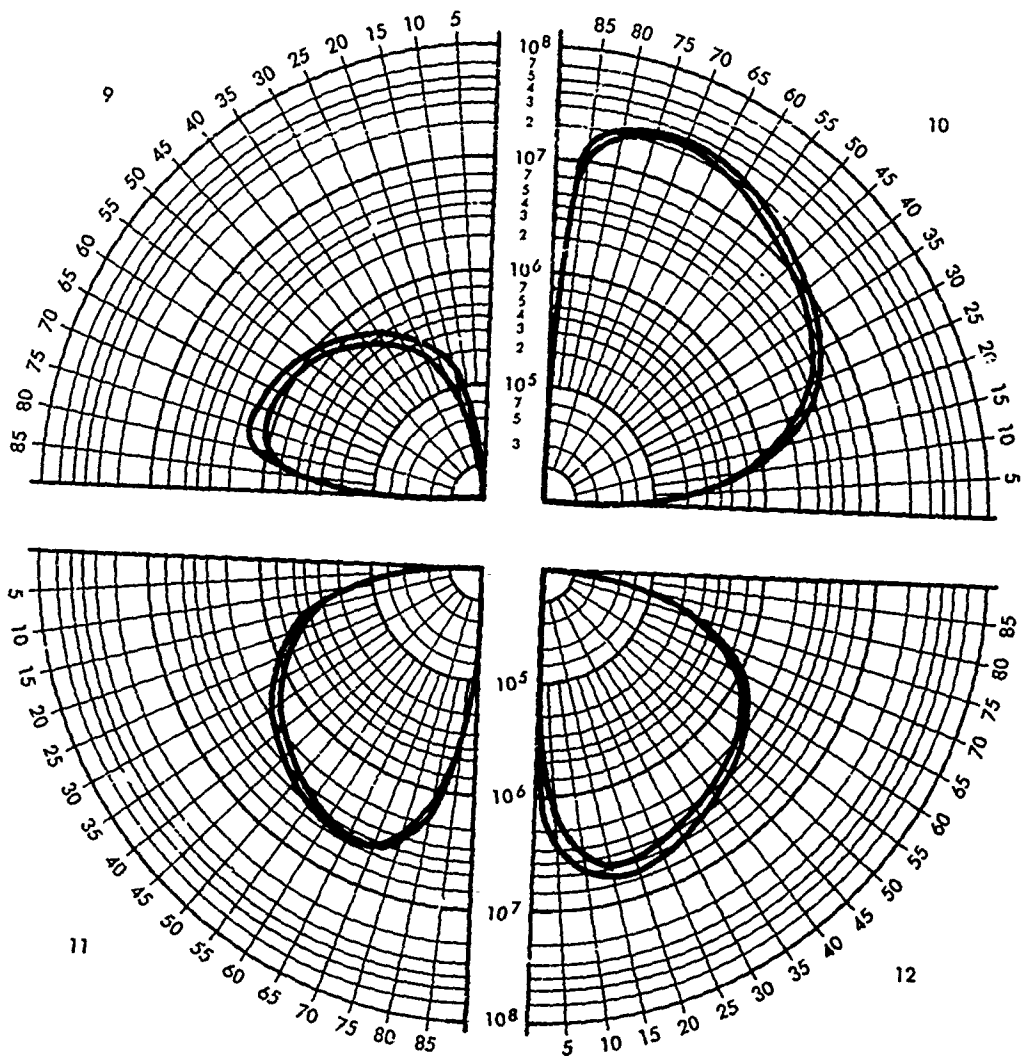


FIG. 3.13 POLAR DIAGRAM NOS. 9-12

SECRET

SECRET

UNIVERSITY OF MICHIGAN

2255-12-T

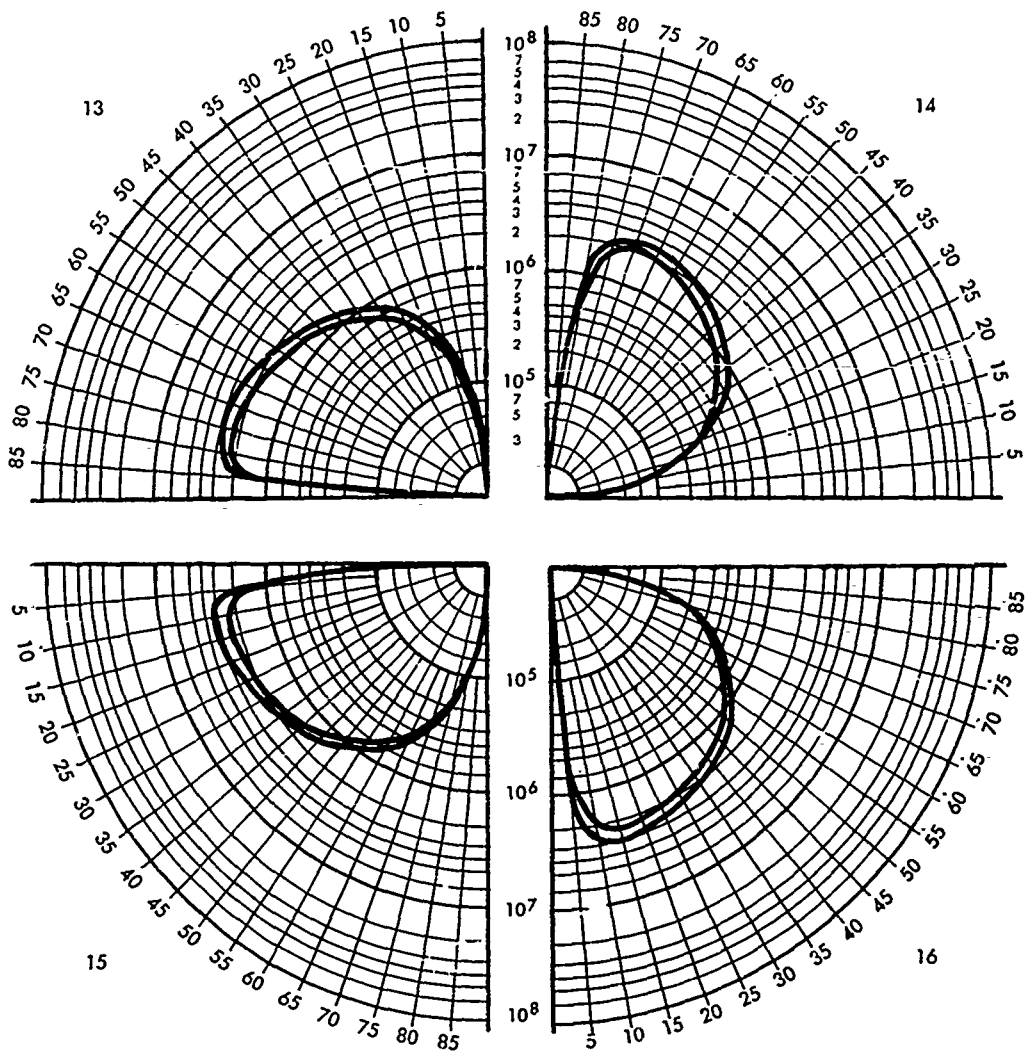


FIG. 3.14 POLAR DIAGRAM NOS. 13-16

SECRET

UNIVERSITY OF MICHIGAN

2255-12-T

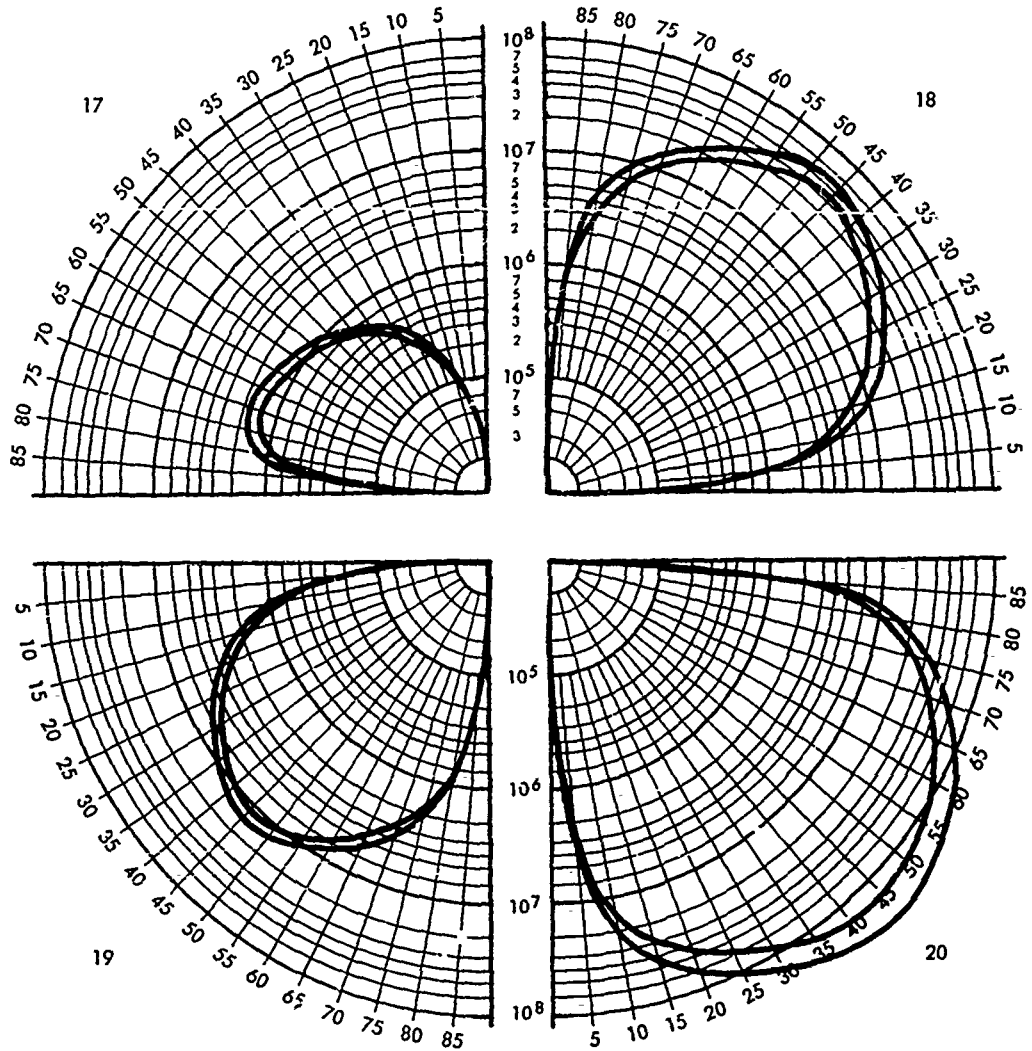


FIG. 3.15 POLAR DIAGRAM NOS. 17-20

SECRET

SECRET

UNIVERSITY OF MICHIGAN

2255-12-T

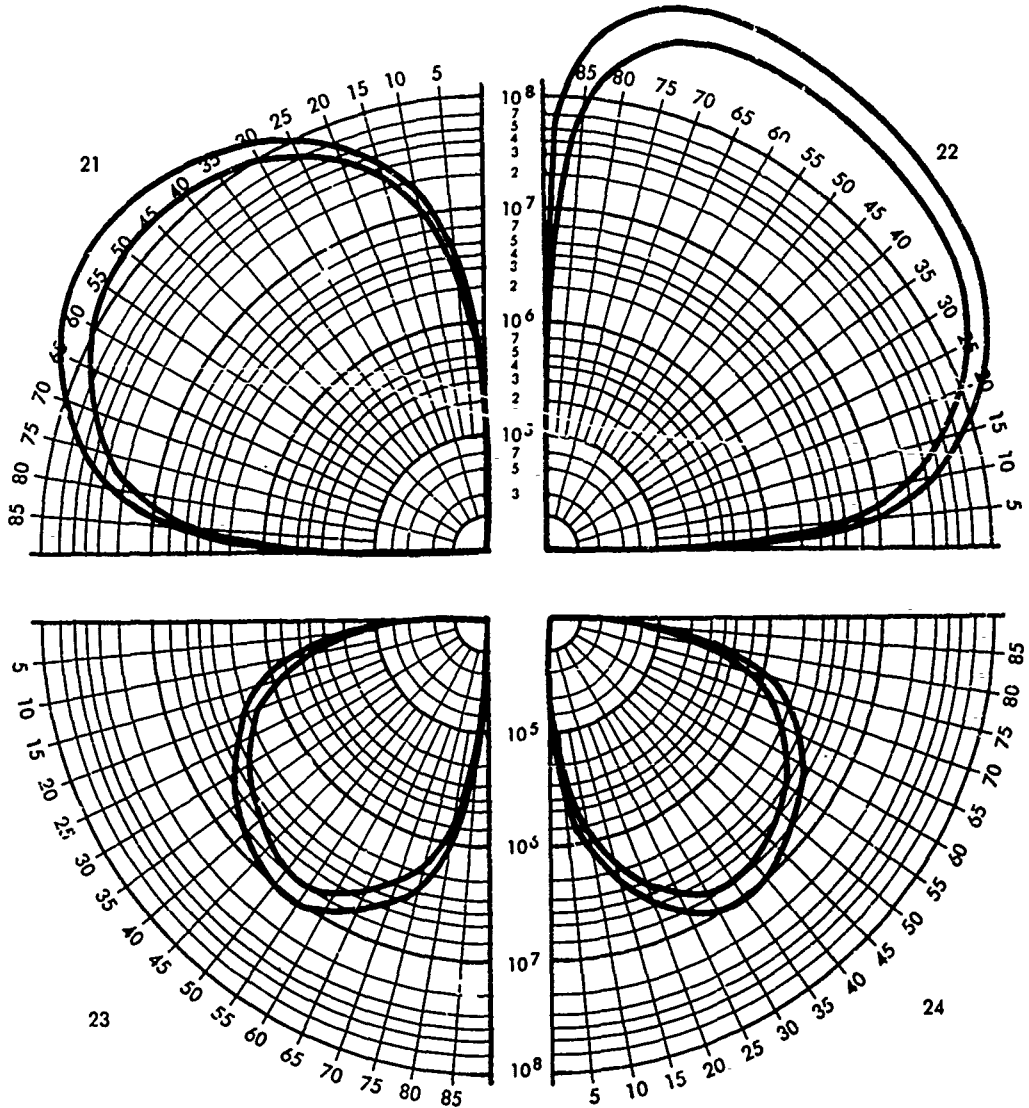


FIG. 3.16 POLAR DIAGRAM NOS. 21-24

SECRET

UNIVERSITY OF MICHIGAN

2255-12-T

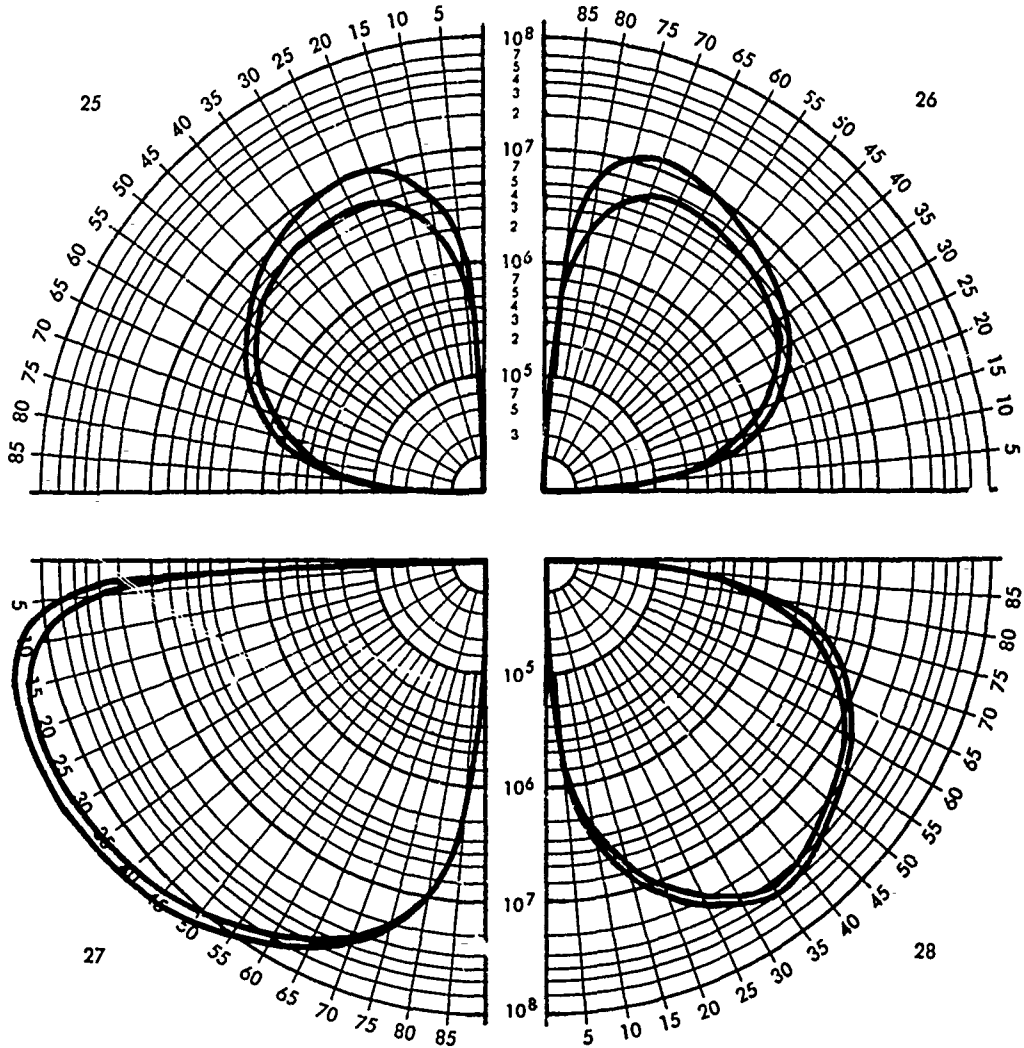


FIG. 3.17 POLAR DIAGRAM NOS. 25-28

SECRET

UNIVERSITY OF MICHIGAN

2255-12-T

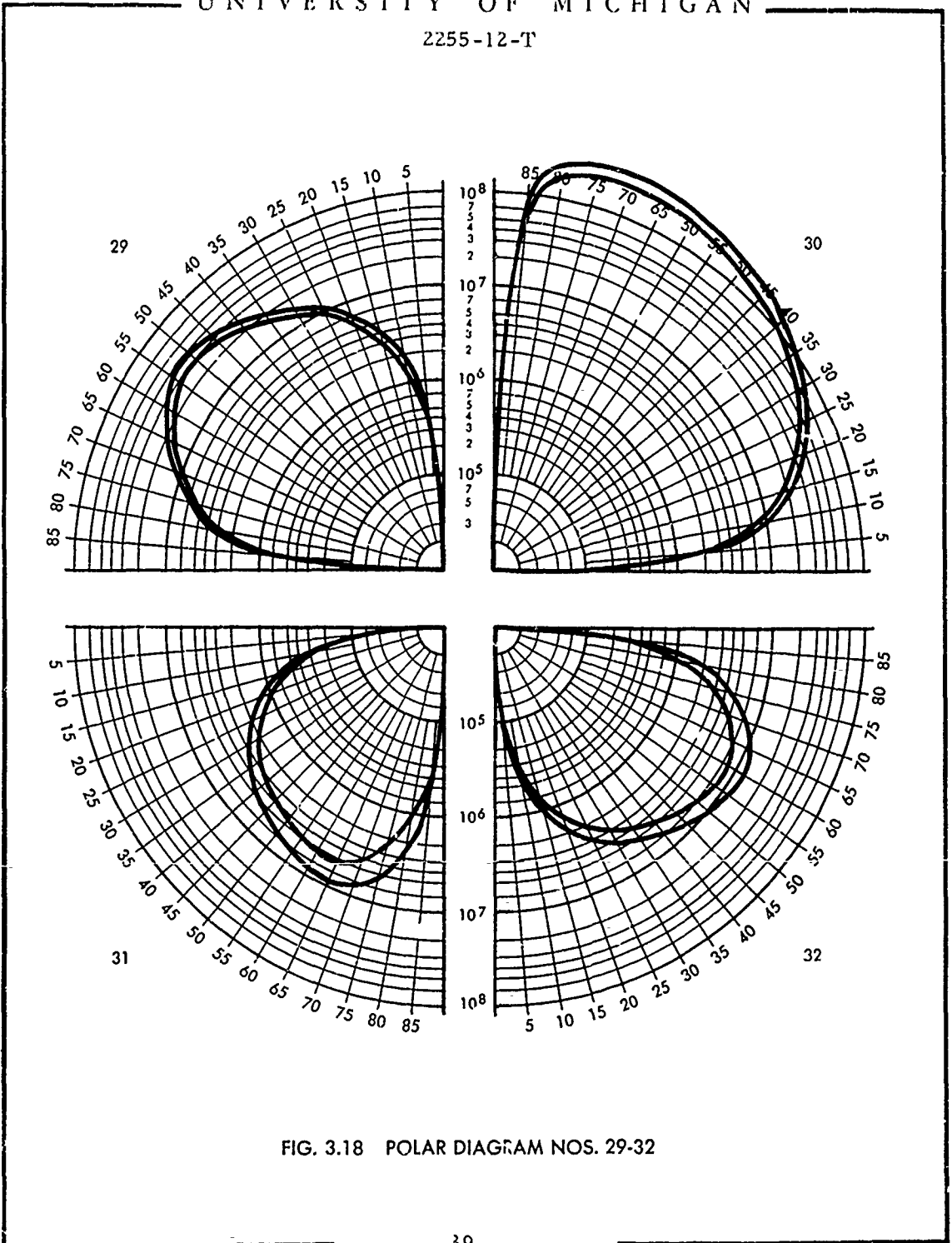


FIG. 3.18 POLAR DIAGRAM NOS. 29-32

SECRET

UNIVERSITY OF MICHIGAN

2255-12-T

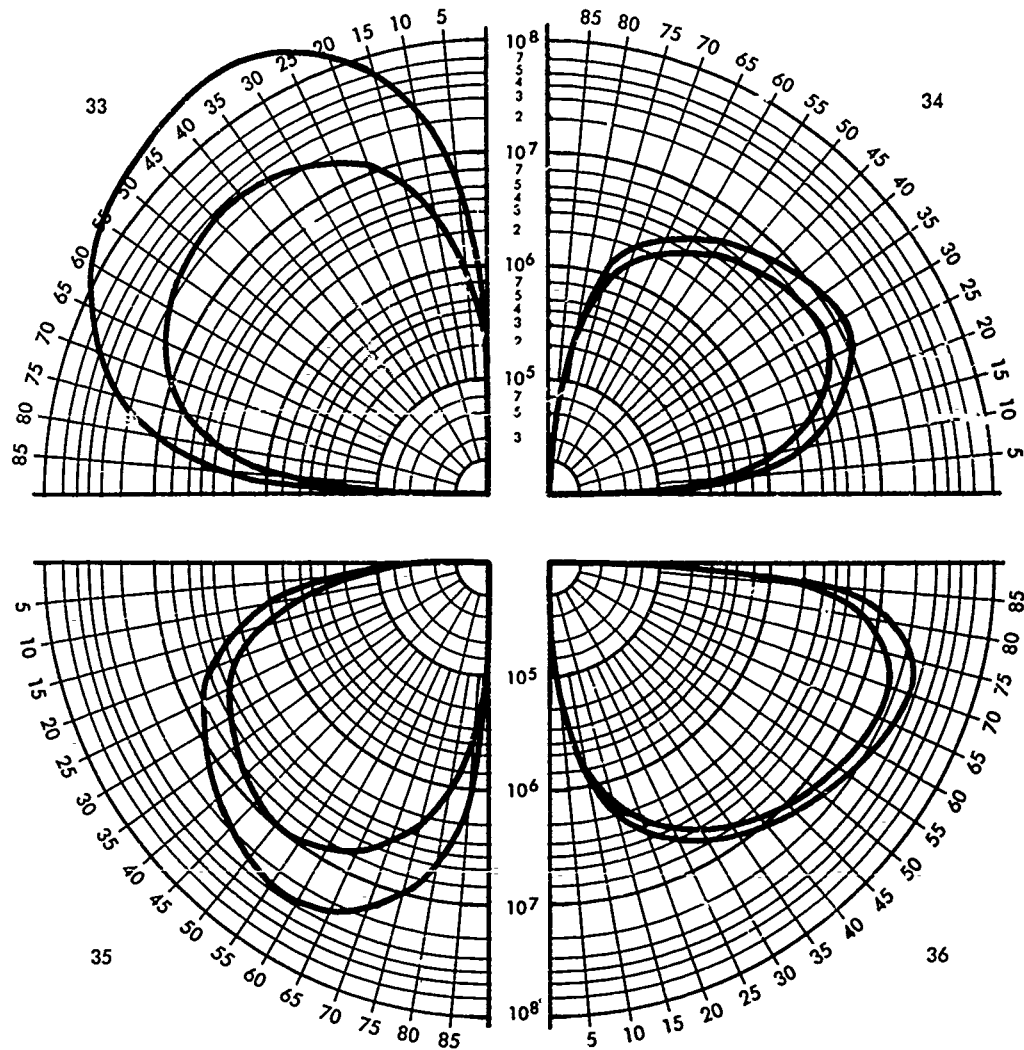


FIG. 3.19 POLAR DIAGRAM NOS. 33-36

SECRET

SECRET

UNIVERSITY OF MICHIGAN

2255-12-T

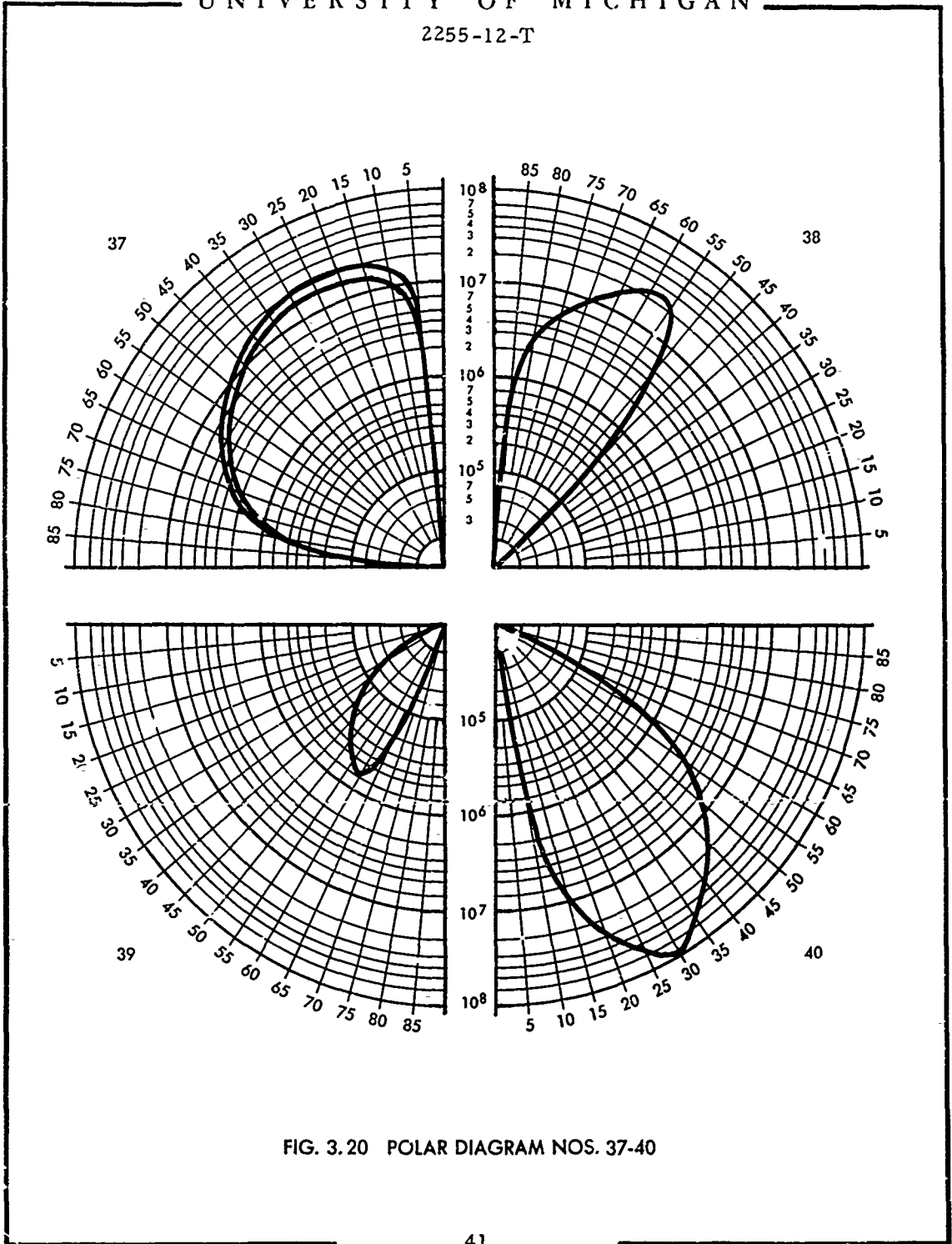


FIG. 3.20 POLAR DIAGRAM NOS. 37-40

SECRET

UNIVERSITY OF MICHIGAN

2255-12-T

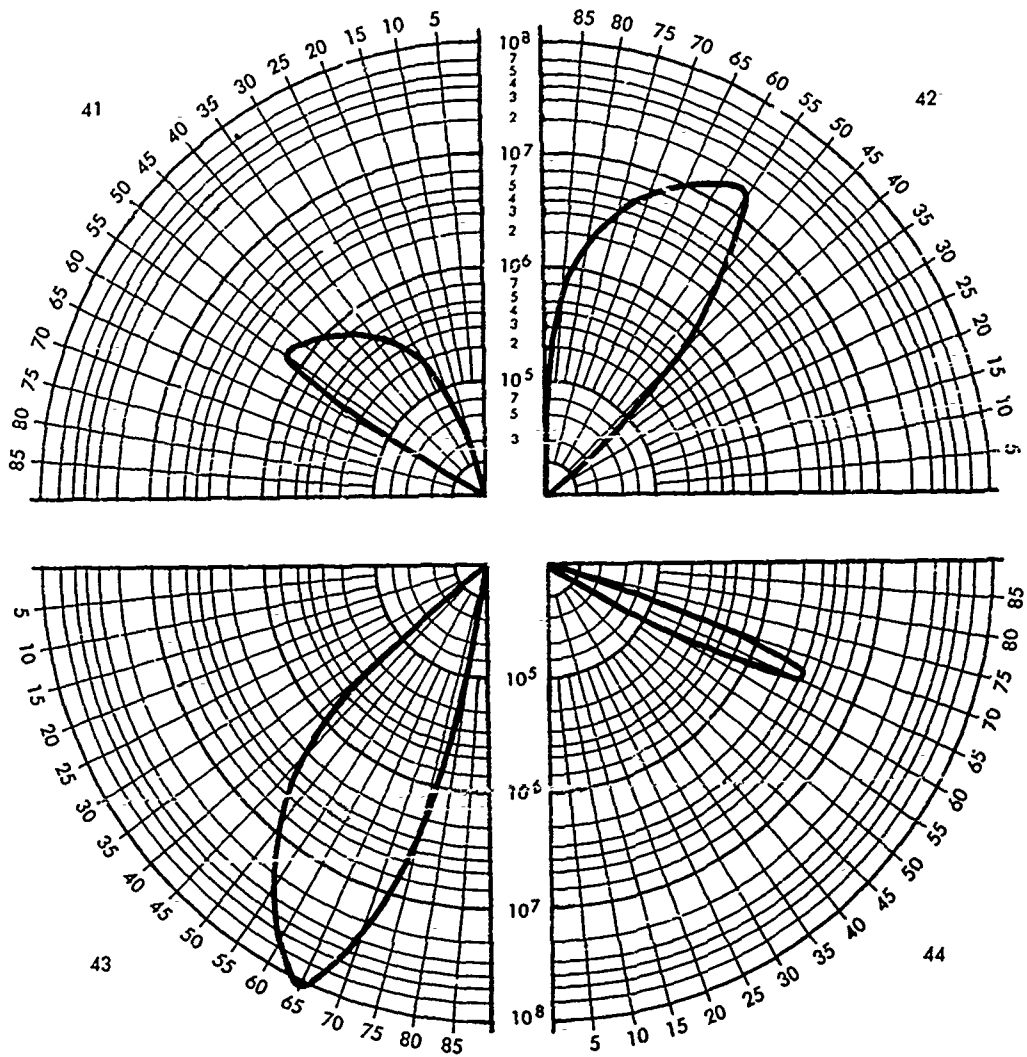


FIG. 3.21 POLAR DIAGRAM NOS. 41-44

SECRET

UNIVERSITY OF MICHIGAN

2255-12-T

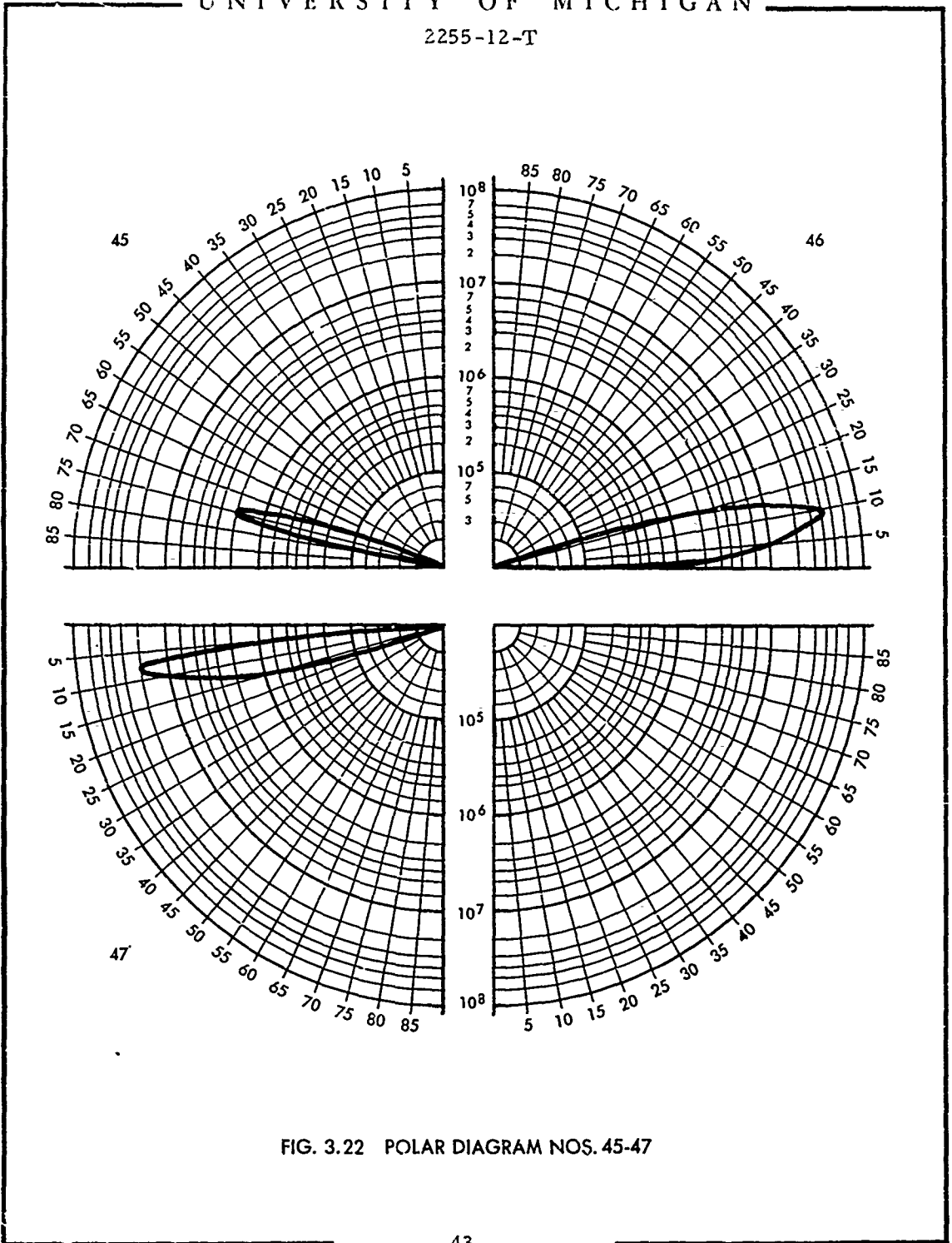


FIG. 3.22 POLAR DIAGRAM NOS. 45-47

SECRET

UNIVERSITY OF MICHIGAN
2255-12-T

3.2 RADAR CROSS-SECTION IN THE CARDINAL DIRECTION (CARDINAL POINT EFFECT)

As pointed out in Section 1.2, the cardinal directions from the radar point of view are the directions perpendicular to the streets in uniformly built up areas. In these directions, the dihedral reflectors are generally of primary importance in computing the radar cross-section. As shown by Figure 3.23, because of the beam divergence, part of the dihedral contribution is essentially specular (from dihedral reflector 3) while part will be non-specular (reflector 4 and parts of 2 and 5). Reflector (1) is not in the beam and therefore does not contribute to the returned signal.

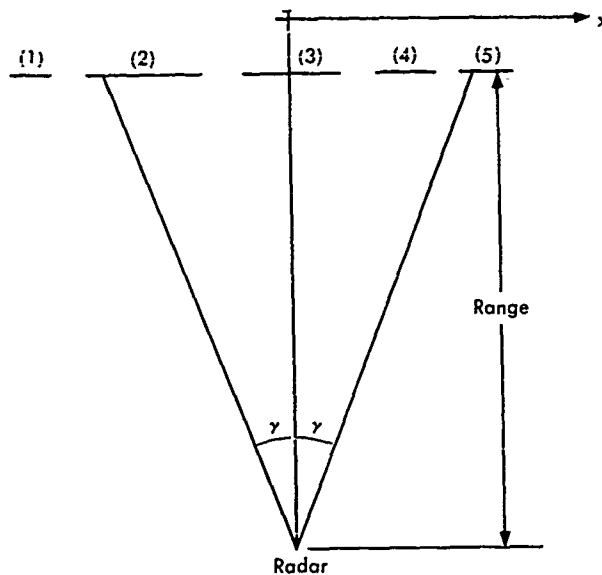


FIG. 3.23 EFFECT OF BEAM DIVERGENCE

When the radar radiation is incident in a plane nearly normal to the dihedral axis, specifically when

$$\frac{2\pi\ell}{\lambda} \sin \theta_r \cos \phi_r \ll \pi,$$

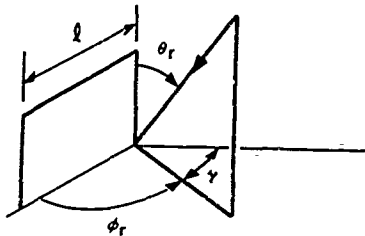
SECRET

UNIVERSITY OF MICHIGAN

2255-12-T

(for angles defined in the figure below), the back-scattering radar cross-section is much greater than when the direction of incidence is not nearly the normal to the dihedral axis, i. e., when

$$\frac{2 \pi \ell}{\lambda} \sin \theta_r \cos \phi_r \gg \pi .$$



This follows from the results of Appendix A.5 which show that subject to the latter inequality the cross-section σ is essentially wavelength independent (Eq. A.5-1), while near normal incidence it is inversely proportional to wavelength squared

$$\sigma = \frac{4 \pi}{\lambda^2} A^2$$

where A is the area of the dihedral projected in the plane perpendicular to the incident ray.

Assuming the much greater sign (\gg) to be equivalent to at least a factor of ten, the returns for which

$$\frac{2 \pi x}{\lambda} \sin \theta_r \cos \phi_r \geq 10 \pi \quad (x \text{ shown in Figure 3-23})$$

SECRET

UNIVERSITY OF MICHIGAN

2255-12-T

can be neglected. If $\lambda = 0.03\text{m}$, $\theta_r = 4.4^\circ$ and $\phi_r = \pi/2 - \gamma$ then

$$x \sin \gamma \geq \frac{27}{(4.4) \pi} \text{ m} .$$

But $\sin \gamma = x/R$, where $R = 1.6 \times 10^5$ so that

$$x^2 \geq \frac{(2.7)(1.6)}{(4.4) \pi} \cdot 10^6 \text{ m}^2 \text{ and } x \geq 5.6 \times 10^2 \text{ meters} .$$

Using this example with Figure (3.23) we see that if 5.6×10^2 is less than the distance out to the dihedral 2 (or 4) but greater than the extent of 3 then the return may be considered to be very large from parts of 3 (specular) and quite small from all other dihedrals shown in the figure.

The part of reflector (3) which gives a large return corresponds to the condition

$$\frac{2 \pi x}{\lambda} \sin \theta_r \cos \phi_r \leq \pi .$$

For $\lambda = 0.03\text{m}$, $\theta_r = 4.4^\circ$, and $R = 1.6 \times 10^5$ meters this corresponds to the condition $x \leq 100$ meters.

A similar calculation for $\theta_r = 29.8^\circ$ shows that for values of x larger than 115 meters any dihedral contribution is negligible compared with the specular return for x less than 65m.

From these considerations the radar cross-section in the cardinal directions was computed to be as shown in Table 3-2 and Figure 3-3.

These values represent an upper limit to the radar cross-section in accordance with the assumptions of infinite electrical conductivity, plane, smooth surfaces at right angles to each other, an exact perpendicularity between the dihedral axis and the radar-to-dihedral line-of-sight.

SECRET

SECRET

UNIVERSITY OF MICHIGAN

2255-12-T

TABLE 3-2

RADAR CROSS-SECTION IN THE CARDINAL DIRECTIONS

Cardinal Directions	Depression Angle in Degrees	Radar Cross-Section in Square Meters
N ($\phi = 0^\circ$)	20.8	2.0×10^{10}
	4.4	2.3×10^{10}
W ($\phi = 90^\circ$)	20.8	8.1×10^9
	4.4	9.3×10^9
S ($\phi = 180^\circ$)	20.8	2.0×10^{10}
	4.4	2.3×10^{10}
E ($\phi = 270^\circ$)	20.8	8.1×10^9
	4.4	9.3×10^9

3.3 METHOD OF COMPUTATION FOR FINITE CONDUCTIVITY

The effect of zero conductivity was obtained from the relation $\sigma_{\text{zero conductivity}}(\theta, \phi) = R_1 R_2 \sigma_{\text{infinite conductivity}}(\theta, \phi)$, where R_1 and R_2 are the energy reflection coefficients of the walls of the buildings (see App. B. 2). The ground was assumed to be perfectly reflecting and the materials of the two walls were taken to be the same (this last is actually the case for many of the reflectors considered). The calculations for zero conductivity were carried out only at the near-grazing incidence angle, $\theta = 4.4$ degrees. The reason for this choice was that at this angle the corner could be treated as if it were a dihedral, thereby simplifying the calculations greatly. Since horizontal electric vector polarization was assumed, the Brewster angle effect enters causing a very great difference between the lobe structures for the two extreme cases. Consider, for example, the northeast sectors of Figure 3-3 and 3-7. For infinite electrical conductivity there is only one lobe. For zero electrical conductivity this single lobe splits into three lobes. The effect of finite conductivity is to smooth the latter curve since at the Brewster angle, θ_b , the reflection

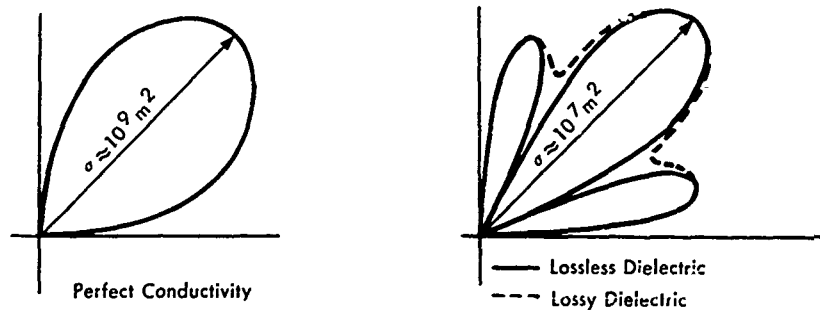
SECRET

SECRET

UNIVERSITY OF MICHIGAN

2255-12-T

coefficient is no longer zero. This result for the northeast sections of Figure 3-3 and 3-7 is reproduced qualitatively in the figure below.



If the loss tangent satisfies the inequality $\tan^2 \delta \ll 1$, the doubly reflected energy reflection coefficient $R_1 R_2 = |R_{11}(\theta_b)|^2$, is given by (App. B. 3, Example 1).

$$R_1 R_2 = \left| R_{11}(\theta_b) \right|^2 \cong \frac{1}{16} \left(\frac{\epsilon' - 1}{\epsilon'} \right)^2 \tan^2 \delta \left| \rho_{11}^2(\pi/2 - \theta_b) \right|, \tan^2 \delta \ll 1$$

where ϵ' = real part of the dielectric constant, and ρ_{11}^2 is the energy reflection coefficient for horizontal polarization. To obtain a large value of $|R_{11}(\theta_b)|^2$ but still satisfy $\tan^2 \delta \ll 1$, assume $\epsilon' = 6$ and $\tan \delta = 0.1$. Then $|R_{11}(\theta_b)|^2 \cong 10^{-5}$. This value gives a cross-section of the order of 10^4 square meters which is about 30 db less than the maximum values in the neighboring lobes. For wood, $\tan \delta \approx 10^{-2}$, $\epsilon' \approx 2$, (see Table B-1, App. B). These values give $|R_{11}(\theta_b)|^2 \ll 10^{-5}$. Thus even though the electrical properties of non-metallic construction materials at X-band are not well known, it is to be expected that the more complex lobe structure predicted for lossless dielectrics when horizontal polarization is used, will be observed in practice for non-metallic buildings. If ϵ' should be much larger than 6, the zeros in the radiation pattern would occur much closer to the $\phi = 0$ degrees

SECRET

UNIVERSITY OF MICHIGAN

2255-12-T

and $\phi = 90$ degrees angles, in which case the radiation pattern would not be significantly changed from that for perfect conductivity.

SECRET

SECRET

UNIVERSITY OF MICHIGAN

2255-12-T

IV

EFFECT OF BUILDING SHAPE ON RADAR RETURNS

The over-all shape of a building has a marked effect on its radar cross-section, particularly in directions from which specular returns are received. Hence, in designing new structures, serious consideration should be given to using building shape in conjunction with or in place of absorbent material as a means of reducing radar returns. The extent to which cross-section can be reduced in this way can be seen from Table 4-1. This table contains formulas for the maximum cross-section of several building shapes as a function of aspect and illustrative examples showing the cross-section of each of these shapes for a floor area of approximately 30,000 square feet. In preparing this table all surfaces were assumed to be smooth and perfectly conducting.

The numerical examples illustrate the fact that the return from dihedrals, under optimum conditions, is far greater than the return from curved surfaces. For example the ratio of cross-sections between the rectangular building and a quonset hut type shown in Table 4-1 is 10^3 . The reason for these differences is simply that the returns from corners are highly directional, returning much of the energy back toward the transmitter, whereas the curved surfaces reflect the energy more nearly isotropically.

The calculations in Table 4-1 took into account only the specular returns. Although the return from an object such as a building is specular at some aspects it is not at others. The non-specular return, however, is generally negligible compared to the specular. Consider a sloped roof which gives a specular return at normal incidence only. To obtain an approximate idea of relative radar cross-sections for the specular and non-specular returns assume the roof to be a flat plate isolated in space. Assuming perfect conductivity, the cross-section at normal incidence is given by

$$\sigma_n = \frac{4\pi}{\lambda^2} A^2 \quad (4-1)$$

SECRET

UNIVERSITY OF MICHIGAN

2255-12-T

where A is the area of the roof. For any other aspect (θ, ϕ) , with θ, ϕ not too close to 0 or $\pi/2$ the return is not specular and the cross-section (averaged over a small interval about (θ, ϕ)) is

$$\sigma_a = \frac{\lambda^2 \cos^2 \theta}{16\pi^3 \sin^4 \theta \sin^2 \phi \cos^2 \phi} \quad (4-2)$$

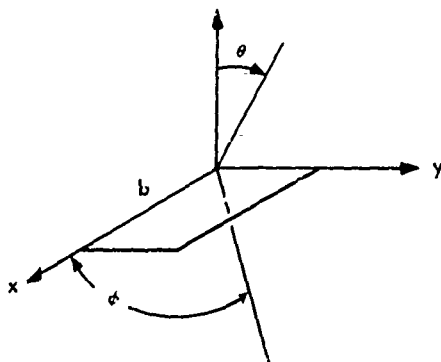


FIG. 4.1 GEOMETRY FOR FLAT PLATE

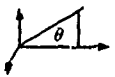
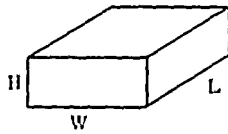
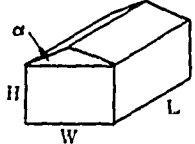
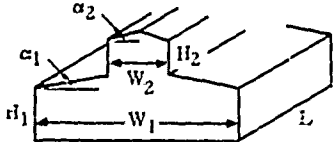
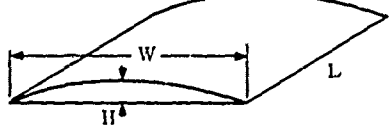
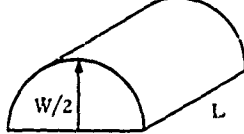
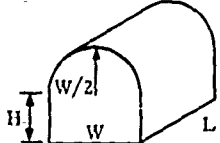
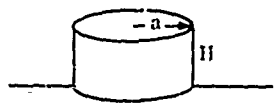
The ratio of the specular to non-specular return is

$$\frac{\sigma_n}{\sigma_a} = \frac{64\pi^4 A^2}{\lambda^4} \frac{\sin^4 \theta \sin^2 \phi \cos^2 \phi}{\cos^2 \theta} \quad (4-3)$$

As an example let $\lambda = 3$ cm, $A = \ell^2$, $\ell = 30$ feet, $\theta = 30$ degrees, and $\phi = 45$ degrees. In this case the ratio is

$$\sigma_n/\sigma_a \cong 10^{12} \quad (4-4)$$

This result illustrates that in estimating the cross-section of an area it is generally sufficient to take into account only the specular return.

BUILDING SHAPE (L = 3W)	CROSS-SECTION 	
	$\sigma = \pi \left(\frac{4HL \cos \theta}{\lambda} \right)^2$	H = 1 W = 1 L = 3
	$\sigma = \pi \left(\frac{4HL \cos \theta}{\lambda} \right)^2 \quad 0 < \frac{\pi}{2} - \alpha$ $\sigma_a = \pi \left(\frac{4HL \cos \theta}{\lambda} \right)^2 + \pi \left(\frac{WL}{\lambda \cos \alpha} \right)^2 \quad 0 > \frac{\pi}{2} - \alpha$	H = 1 W = 1 L = 3
	Same as in 2 with $\alpha = \alpha_1$ or α_2 and $H = H_1 + H_2$ where $0 > \tan^{-1} \left(\frac{2H_2}{W_1 - W_2} \right)$ $\sigma = \begin{cases} 0 & 0 > \tan^{-1} \left(\frac{2H_2}{W_1 - W_2} \right) \\ 1 - \frac{W_1 - W_2}{2H_2} (\tan \theta - \tan \alpha_1) & \tan^{-1} \left(\tan \alpha_1 + \frac{2H_2}{W_1 - W_2} \right) > 0 > \alpha_1 \\ 1 & 0 > \alpha_1 \end{cases}$	H1 = 1 H2 = 1 W1 = 1 W2 = 1 alpha1 = 1
	$\sigma = \frac{\pi(W^2 + 4H^2)L^2}{4\lambda H} \quad 0 > \frac{\pi}{2} - \tan^{-1} \frac{2H}{W}$	H = 1 W = 1 L = 3
	$\sigma = \frac{\pi WL^2}{\lambda} (1 + \cos \theta)$	W = 1 L = 3
	$\sigma = \pi \left(\frac{4HL \cos \theta}{\lambda} \right)^2 + \frac{\pi WL^2}{\lambda} (1 + \cos \theta)$	H + W = 1 W = 5
	$\sigma = \frac{8\pi a H^2 \cos \theta}{\lambda}$	H = 20 a = 97 H = 50 a = 56
	$\sigma = 2\pi a^2$	a = 97

SECRET

TABLE 4.1

SECRET

CROSS-SECTION 	NUMERICAL EXAMPLES FLOOR AREA CONST. = $3 \times 10^4 \text{ ft.}^2$ NUMERICAL DATA	σ (IN SQUARE METERS)
$\sigma = \pi \left(\frac{4HL \cos \theta}{\lambda} \right)^2$	H = 20 ft. (1 Floor) 30° W = 100 ft. L = 300 ft. H = 50 ft. (3 Floors) 30° W = 57.74 ft. L = 173.2 ft.	1.302×10^{10} 2.712×10^{10}
$\left(\frac{4HL \cos \theta}{\lambda} \right)^2 \quad \theta = \frac{\pi}{2} - \alpha$	H = 20 ft. (1 Floor) $\pi/2 - \alpha$ W = 100 ft. L = 300 ft. $(\alpha = 30^\circ)$	4.049×10^{10}
$\left(\frac{4HL \cos \theta}{\lambda} \right)^2 + \pi \left(\frac{WL}{\lambda \cos \alpha} \right)^2 \quad \theta = \frac{\pi}{2} - \alpha$	H = 50 ft. (3 Floors) $\pi/2 - \alpha$ W = 57.74 ft. L = 173.2 ft. $(\alpha = 30^\circ)$	1.306×10^{10}
$\left. \begin{array}{l} \alpha = \alpha_1 \text{ or } \alpha_2 \text{ and} \\ H_2 \text{ where} \\ (\tan \theta - \tan \alpha_1) \end{array} \right\} \begin{array}{l} \theta > \tan^{-1} \left(\frac{2H_2}{W_1 - W_2} \right) \\ \tan^{-1} \left(\tan \alpha_1 + \frac{2H_2}{W_1 - W_2} \right) > \alpha_1 \\ \theta > \alpha_1 \end{array}$	H ₁ = 30 ft. (1 Floor) H ₂ = 10 ft. $(1) \theta = 20^\circ$ W ₁ = 100 ft. L ₁ = 300 ft. W ₂ = 15 ft. L ₂ = 300 ft. $(2) \theta = \pi/2 = \alpha_1$ $\alpha_1 = 10^\circ$ $\alpha_2 = 15^\circ$	3.929×10^{10} 2.930×10^{10}
$\frac{(\pi^2) L^2}{\lambda^2} \quad \theta > \frac{\pi}{2} - \tan^{-1} \frac{2H}{W}$	H = 40 ft. 30° W = 100 ft. L = 300 ft.	2.736×10^7
$\sigma = \frac{\pi WL^2}{\lambda} (1 + \cos \theta)$	W = 100 ft. 30° L = 300 ft.	4.980×10^7
$\sigma = \pi \left(\frac{4HL \cos \theta}{\lambda} \right)^2 + \frac{\pi WL^2}{\lambda} (1 + \cos \theta)$	H + W/? = 50 ft. (3 Floors) 30° W = 57.74 ft. L = 173.2 ft.	4.853×10^9
$\sigma = \frac{8\pi a H^2 \cos \theta}{\lambda}$	H = 20 ft. (1 Floor) 30° a = 97.72 ft. H = 50 ft. (3 Floors) 30° a = 56.42 ft.	8.031×10^5 2.898×10^6
$\sigma = 2\pi a^2$	a = 97.72 ft.	5.574×10^3

TABLE 4.1

V

RECOMMENDATIONS

There is a considerable need for basic investigation of factors affecting the radar returns from building and terrain. Specific problems which should be studied experimentally and/or theoretically are described below.

5.1 EXPERIMENTAL PROGRAMS5.1.1 Camouflage Procedures

The camouflage procedures described in Section 2.1 should be field tested as described in Section 2.2.

5.1.2 Rough Surfaces

In the present study, the ground was assumed to reflect incident energy specularly, isotropically, or in a superposition of these two ways. It is felt that this assumption is sufficiently good for obtaining estimates of radar cross-sections for camouflage against present-day radars. However, because rough surfaces generally do not scatter isotropically as assumed, this assumption should be checked by investigating the effects of type and magnitude of roughness on the returns from dihedral and trihedral reflectors formed by smooth walls when the ground is covered by grass or shrubbery, is plowed, or contains irregularities such as natural gullies, holes, and rocks.

These results, together with considerations of time and cost, can be used to determine the most suitable means for reducing dihedral and trihedral reflections for camouflage. For this purpose, the effects of regular arrays of protuberances such as were studied by Cornell Aeronautical Laboratory (App. D. 6.2) should also be investigated.

5.1.3 Angle Errors

If the sides of a dihedral or trihedral reflector do not meet at exactly

SECRET

UNIVERSITY OF MICHIGAN

2255-12-T

90 degrees, the radar cross-section is reduced. The geometry and algebra involved in computing this change for a trihedral are lengthy and the results quite involved except for special cases (App. A.6). To get useful results in more general cases would require extensive numerical work. Hence, it may be advisable to investigate these effects experimentally (App. D.6.1).

5.1.4 Dielectric Constants of Soils and Common Building Materials

Radar returns depend markedly on the electrical properties of the ground and of building materials, as characterized by their complex dielectric constants. Inasmuch as little data are available on these constants at X-band for common building materials, combinations of materials, or soils (App. E), such data should be obtained.

5.1.5 Validity of Physical Optics

There is considerable experimental evidence available on the degree of validity of the physical optics approximations for perfectly conducting dihedral and trihedral reflectors. The validity of the physical optics results obtained in Appendix B for non-perfect conductors should be checked in similar ways.

5.1.6 Flight Tests for Data on Microwave Reflections

New experimental data should be obtained with airborne radars in well-controlled experiments. These tests should include the effects of various polarizations in transmission and reception, that is, the scattering matrix should be obtained.

5.1.7 Over-all Tests of Results of Section III

Flight test data on the microwave reflections from the buildings on the east side of the Willow Run Airport would be extremely useful. These data would make it possible to compare the theory and computations in this report directly with experiment and hence possibly to determine the over-all validity of the assumptions and methods employed in Section III. However, the computations should be refined for this comparison as indicated in Section 5.2.4.

SECRET

SECRET

UNIVERSITY OF MICHIGAN

2255-12-T

5.1.8 Further Analysis of "Project Baltimore" Data

The results of Project Baltimore (Ref. 4 and 5) appear to be degraded to a certain extent by inadequate target description (App. D.1). If this is true, the information which was lost could be regained by re-describing the target area and target characteristics and then re-analyzing the data. In carrying out this task, more theoretical information than was available to the Strategic Air Command should be used in selecting the critical target characteristics and in determining the amount of detail needed in the descriptions.

5.2 THEORETICAL PROGRAMS

5.2.1 Rough Surfaces

A geometric optics formula for the radar cross-section of a two-dimensional "rough" surface, assuming no multiple reflections, is developed in Appendix C. However, the exact shape of any particular section of ground would probably never be known; at best, only certain statistical properties of the surface would be known. Hence, the statistical aspects of the problem should be investigated.

The assumption of geometric optics, although probably quite good for slowly varying surfaces, is, for example, inapplicable to ground covered with trees or bushes. Problems of rapidly varying surfaces should be investigated to obtain a better theory of scattering by rough surfaces.

5.2.2 Returns from Complex Targets

A theoretical study should be undertaken of simplified models of groups of buildings in which the buildings are assumed to be arrays of rectangular blocks with certain statistical distributions of heights, widths, and spacings. This study is of interest to the general problem of radar cross-section prediction and camouflage. The dimensions are to be considered sufficiently large to apply physical optics.

An analysis should be made assuming that the contribution made by rays undergoing more than three reflections is negligible, that the building

SECRET

SECRET

UNIVERSITY OF MICHIGAN

2255-12-T

heights are statistically distributed, and that the building widths and spacings are constant. The computations would show how variations in height and different ratios among average height, width, and spacing will affect the cross-section. It would be of interest to compare such results with those of Project Baltimore (App. D. 1) where some of the parameters found to correlate highly with radar returns seen on PPI displays were variations in building height and the ratios of building height to spacing between buildings

5.2.3 Geometric Areas for Trihedrals Including Effects of Non-Perpendicularity

In Appendix B. 4, the cross-section for a trihedral reflector with walls of arbitrary complex dielectric constant is determined in terms of the areas occupied by various bundles of rays. Formulas for these areas in terms of reflector geometry (e. g. , the truncated corners dealt with in Appendix A. 3) and direction of incidence should be obtained in order to be able to use the general results of Appendix B. 4 for computational purposes.

Solution of the same problem, but for angles other than 90 degrees between walls, is necessary to handle the effects of non-perpendicularity. Extensive numerical calculations would be required to obtain usable results from the straightforward methods described in Appendix A. These numerical results, if obtained, should be analyzed with the aim of determining some simple general estimates of the angle error effects. It may be possible to avoid many of these computations by devising a more clever alternate scheme which would provide approximate answers for small angle errors.

5.2.4 Refined Computations of the Willow Run Scattering Patterns

If it desired to check the radar cross-section estimates made in Section III experimentally, as recommended in Section 5.1.3, the patterns which have been obtained (which overestimate the radar cross-sections) should first be refined by allowing for surface roughness and non-perpendicularity of the sides of the reflectors.

SECRET

SECRET

UNIVERSITY OF MICHIGAN

2255-12-T

In addition, the effects of small conductivity should be taken into account more accurately, particularly for situations in which the depression angle is not very small.

5.2.5 Polarization

The effects of varying polarization of the transmitter and receiver on the cross-section of building complexes should be studied analytically. The entire polarization scattering matrix should be considered. This work involves only straightforward application of the procedures and many of the completed results of Appendices A and B.

SECRET

SECRET

UNIVERSITY OF MICHIGAN

2255-12-T

APPENDIX A

SPECIAL FORMULAS FOR DIHEDRAL AND TRIHEDRAL REFLECTOR RETURNS

It was pointed out in Section I that the main contributors to the radar cross-section of buildings are most likely the dihedral and trihedral reflectors formed, for example, by the building walls and the earth. These reflectors are usually not the conventional corner reflectors which are used as beacons, reflection standards and so on. They often have one side effectively infinite in extent, or of an irregular shape; they may be truncated so that parts of the sides near the apex are missing; the sides of the dihedral may not meet at 90 degrees; and the materials of the sides are generally not all metallic and not all the same. Formulas have not been worked out in the past for many of these situations. Some of these formulas taking into account the special geometrical configurations, are derived in Sections A. 3 through A. 6.

A.1 GENERAL THEORETICAL BASIS

A.1.1 Back Scattering by Corner Reflectors

Corner reflectors will be considered whose dimensions are several wavelengths or larger, irradiated by a parallel beam of electromagnetic energy whose geometrical cross-section is larger than the reflector. Assume for the present that the reflector sides are at right angles with each other. The main effects of the reflector then are to reverse the direction of energy flow and to limit the cross-sectional extent of the reflected beam. The reflector acts very much like a flat plate perpendicular to the beam. It is, of course, well known that the edges of such a plate cause diffraction so that the beam actually spreads out around the direction of greatest energy flow. In the case of a corner reflector, however, the beam vignetting does not take place all in one plane, but parts of it occur at various distances along the beam, i. e., at the successive reflections from the walls. However, a comparison of computational procedures shows that the diffraction pattern can be adequately predicted from that of a flat plate.

SECRET

SECRET

UNIVERSITY OF MICHIGAN

2255-12-T

In general diffraction patterns can be fairly well approximated by applying physical optics as outlined, for example, in Reference 15. In essence this method is an application of Huygen's principle, whereby, the contributions of the elementary sources across the aperture are added (integrated) in phase. In Reference 11 this method is applied to a square trihedral corner first by integrating over the faces of the corner and alternatively by integrating over the equivalent flat plate. It was found that the heights and widths of the main lobes of the two diffraction patterns were practically the same. Also the envelopes of the sidelobes were similar although the fine structures were quite different. It is therefore a matter of indifference which method is used as far as accuracy is concerned; hence the simpler plane plate method will be used.

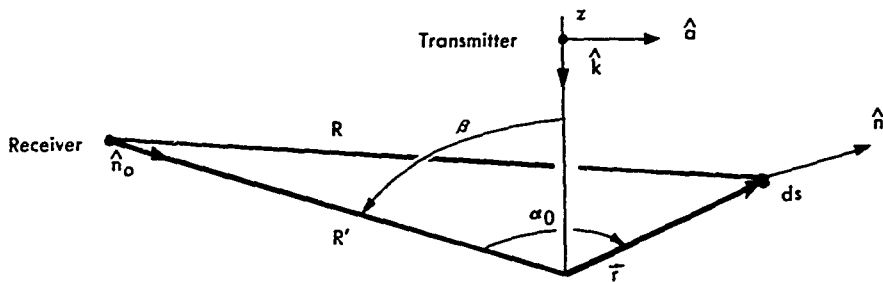


FIG. A.1-1 QUANTITIES APPEARING IN THE FORMULA FOR THE SCATTERED FIELD

In Reference 15 it is shown that the scattered magnetic field is

$$\bar{H}_{sc} = \frac{\exp(-ik R')}{R'} \bar{F}(\beta), \quad (\text{A.1-1})$$

for an incident magnetic field H_{inc} ,

SECRET

SECRET

UNIVERSITY OF MICHIGAN

2255-12-T

where,

$$\bar{F}(\beta) = \frac{ik}{2\pi} \left[(\hat{n}_0 \cdot \hat{a}) \bar{r} - (\hat{n}_0 \cdot \bar{r}) \hat{a} \right] H_{\text{inc}} \quad , \text{ and}$$

$$\bar{r} = \int_A \hat{n} e^{-ik\hat{r} \cdot (\hat{n}_0 + \hat{k})} ds \quad .$$

Here,

A = the area of the effective flat plate

R = the distance separating the receiver and the integration point

$R' = R + r \cos \alpha_0$, where $\cos \alpha_0 = \hat{n}_0 \cdot \bar{r}/|\bar{r}|$

β = the angle separating the transmitter and receiver

\hat{n}_0 = the unit vector directed from the receiver to the origin

\hat{a} = a unit vector in the direction of the incident magnetic field
(\hat{a} has the components a_x , a_y , and a_z .)

\hat{n} = the unit normal to the surface

\hat{k} = the unit vector directed from transmitter to origin

\hat{r} = radius vector from origin to integration point.

The radar cross-section is

$$\sigma = 4\pi \left(|F_x|^2 + |F_y|^2 + |F_z|^2 \right) \quad . \quad (\text{A.1-2})$$

If \hat{d} is the direction of the receiver's \bar{H} polarization the effective radar cross-section which measures the received energy taking polarization into account is

$$\sigma_e(\beta) = \frac{4\pi}{\lambda^2} \left| (\hat{n}_0 \cdot \hat{a}) (\bar{r} \cdot \hat{d}) - (\hat{n}_0 \cdot \bar{r}) (\hat{a} \cdot \hat{d}) \right|^2 \quad . \quad (\text{A.1-3})$$

SECRET

UNIVERSITY OF MICHIGAN

2255-12-T

For back scattering at normal incidence $\hat{n} = -\hat{k} = -\hat{n}_0, \vec{f} = \bar{n} A$, and

$$\sigma = \frac{4\pi A^2}{\lambda^2} \quad (\text{A.1-4})$$

A.1.2 Law of Reflection

The shape of the effective scatterer may be determined by ray tracing. For this purpose it is convenient to write the law of reflection (the angle of incidence equals the angle of reflection) in vector form. Let \hat{p}_i and \hat{p}_r be unit vectors in the directions of the incident and reflected rays; \hat{n} the unit normal to the reflecting surface at the point of reflection, directed positive toward the side where the ray is incident. Then the law of reflection is

$$\hat{p}_r = \hat{p}_i - 2(\hat{n} \cdot \hat{p}_i) \hat{n} \quad (\text{A.1-5})$$

In particular if, in a cartesian coordinate system (x, y, z) , $\hat{p}_i = (p_{ix}, p_{iy}, p_{iz})$ and, for example, if $\hat{n} = (1, 0, 0)$ then Equation (A.1-5) states that $p_r = (-p_{ix}, p_{iy}, p_{iz})$.

The direction of \hat{a} in the beam emerging from the reflector may be determined as though the walls were infinite in extent, by using the fact that the tangential component of the electric field vanishes on perfectly conducting surfaces.

A.1.3 Projections

Another general formula which is needed is for the projection along direction \hat{p} of a position vector \vec{P} (extending from the origin to a point P) onto a plane with normal \hat{n} passing through the origin (Fig. A.1-2). The projected vector \vec{P}' is

$$\vec{P}' = \vec{P} + s\hat{p} \quad (\text{A.1-6})$$

where s is determined by the condition

$$\vec{P}' \cdot \hat{n} = 0, \quad (\text{A.1-7})$$

SECRET

UNIVERSITY OF MICHIGAN

2255-12-T

or

$$s = - \frac{\vec{P} \cdot \hat{n}}{\hat{p} \cdot \hat{n}} \quad (A.1-8)$$

For the special case in which $\hat{n} = -\hat{p}$,

$$s = -\hat{p} \cdot \vec{P} \quad (A.1-9)$$

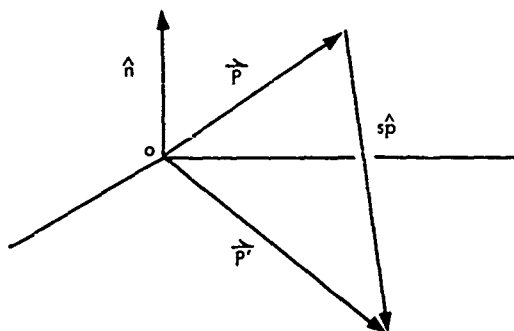


FIG. A.1-2 THE PROJECTION VECTOR \vec{P}

For determining the diffraction patterns it will in some cases prove desirable to express P' in terms of rectangular coordinates X, Y in the plane normal to \hat{n} , (Sec. A. 7). A convenient system is defined in terms of an arbitrary rectangular coordinate system $\hat{x}, \hat{y}, \hat{z}$, by the unit vectors

$$\hat{X} = \frac{\hat{y} \times \hat{n}}{|\hat{y} \times \hat{n}|} = \frac{1}{\sqrt{n_1^2 + n_3^2}} (n_3, 0, -n_1) \quad (A.1-10)$$

$$\hat{Y} = \hat{X} \times \hat{n} = \left[n_1 n_2, -(n_1^2 + n_3^2), n_2 n_3 \right] \frac{1}{\sqrt{n_1^2 + n_3^2}}$$

in this plane. Thus, if $\vec{P}' = (x', y', z')$, then, $\vec{P}' = \xi \hat{X} + \eta \hat{Y}$, with

SECRET

UNIVERSITY OF MICHIGAN

2255-12-T

$$\xi = (x' n_3 - z' n_1) \frac{1}{\sqrt{n_1^2 + n_3^2}}, \quad (\text{A.1-11})$$

$$\eta = \left[n_1 n_2 x' - (n_1^2 + n_3^2) y' + n_2 n_3 z' \right] \frac{1}{\sqrt{n_1^2 + n_3^2}}$$

A.2 RADAR CROSS-SECTION FORMULAS FOR CONVENTIONAL CORNER REFLECTORS

Three of the simplest reflectors are the trihedral reflector with square sides, the trihedral reflector with rectangular sides, and the dihedral with incident propagation vector normal to the dihedral axis. The back scattering cross-section formulas for these reflectors are well known. They are:

1. For the trihedral reflector with square faces--

$$\sigma = \begin{cases} \frac{64\pi}{\lambda^2} \frac{\ell^2 m^2}{n^2} a^4, & m \leq \frac{n}{2} \\ \frac{4\pi}{\lambda^2} \ell^2 \left(4 - \frac{n}{m}\right)^2 a^4, & m \geq \frac{n}{2} \end{cases}$$

where ℓ , m , n are the direction cosines for the incident radiation, a is the sidelength, and λ is the wavelength.

2. For the trihedral reflector with rectangular sides we have

$$\sigma = \begin{cases} \frac{4\pi \ell^2 b^2}{\lambda^2} \left(4c - \frac{n}{m} b\right)^2, & \left(\frac{m}{b} \geq \frac{n}{2c}\right) \\ \frac{64\pi \ell^2 m^2 c^4}{\lambda^2 n^2}, & \left(\frac{m}{b} \leq \frac{n}{2c}\right) \end{cases}$$

where the symbols are defined in Figure A.2-1, $\ell = \sin \theta \cos \phi$, $m = \sin \theta \sin \phi$, $n = \cos \theta$, and

SECRET

SECRET

UNIVERSITY OF MICHIGAN

2255-12-T

$$\left| \frac{l}{a} \right| \leq \left| \frac{m}{b} \right| \leq \left| \frac{n}{c} \right|.$$

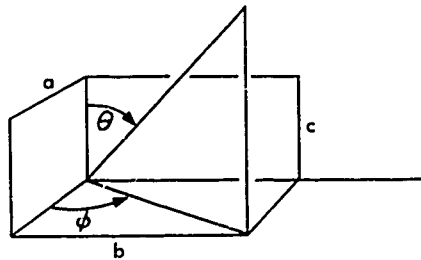


FIG. A-2.1 GEOMETRY FOR TRIHEDRAL REFLECTOR

3. For the dihedral with incident propagation vector normal to dihedral axis

$$\sigma = \frac{16\pi}{\lambda^2} a^2 L^2 \sin^2 \phi,$$

where a , L and ϕ are as shown in Figure A.2-2.

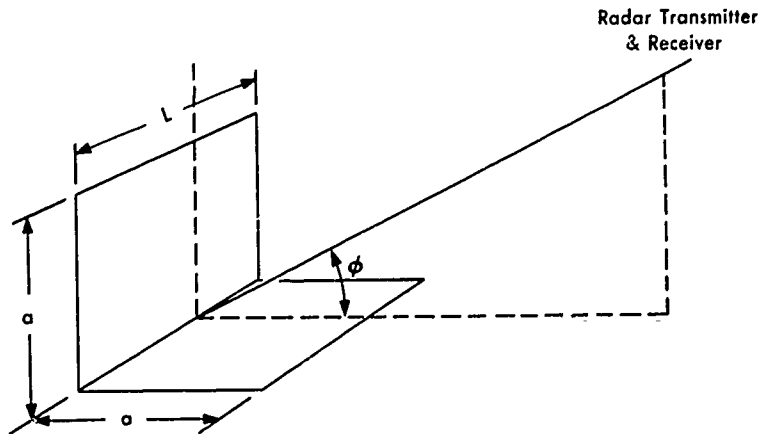


FIG. A-2.2 GEOMETRY FOR DIHEDRAL REFLECTOR

SECRET

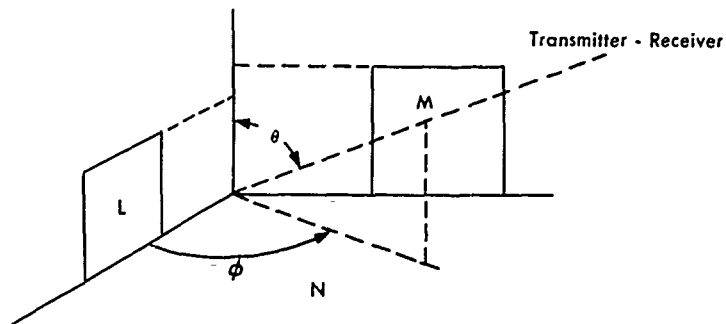
UNIVERSITY OF MICHIGAN

2255-12-T

A.3 RADAR CROSS-SECTION OF A COMPENSATED AND TRUNCATED TRIHEDRAL REFLECTOR

Reduction of the back scattered energy by modifying the corner reflector is called compensation since the reduction in back scattered energy is compensated by the increased energy scattered in other directions. The modification may be due to such causes as truncation (i. e., the removal of some of the reflecting surface), non-perpendicularity of the dihedrals, or roughness of the reflecting surfaces. It should be pointed out that truncating a corner reflector does not necessarily compensate it.

In this section the radar cross-section for the corner reflector shown in Figure A.3-1 will be determined. First, the method of images will be used to simplify the calculations and then the laws of geometrical optics will be applied to obtain the cross-section. The scattering surfaces are assumed to be perfectly plane and to have infinite electrical conductivity. A problem equivalent to that of Figure A.3-1 is obtained when



NOTE: Plane surfaces L, M and N form a corner reflector.
N is of infinite extent; L and M are of finite extent.

FIG. A-3.1 GEOMETRY FOR COMPENSATED AND TRUNCATED TRIHEDRAL REFLECTOR

SECRET

UNIVERSITY OF MICHIGAN

2255-12-T

surfaces L and M along with the transmitting antenna are imaged in the plane of N. Only those rays originating at the image transmitter can

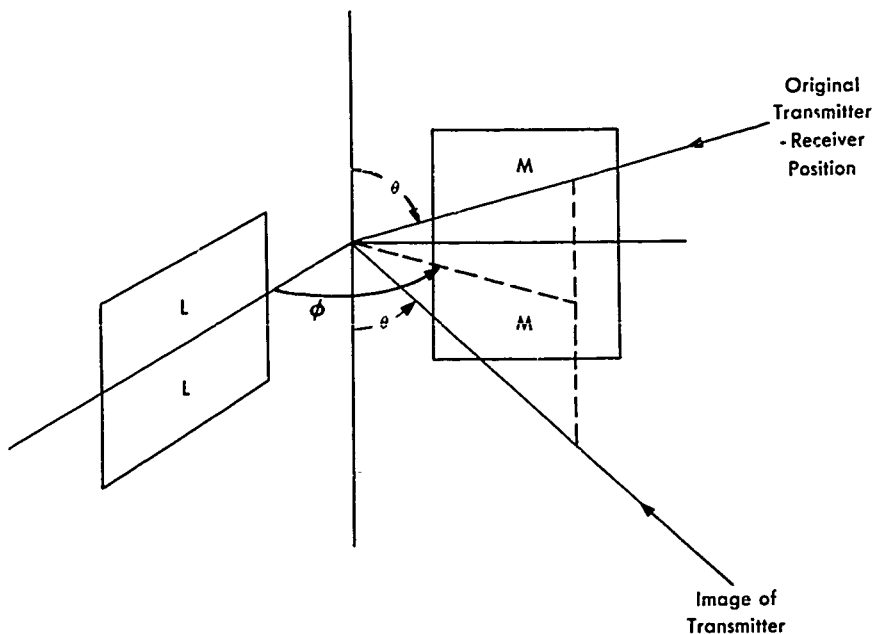


FIG. A-3.2 GEOMETRY FOR THE IMAGE PROBLEM

reach the indicated receiver position. Thus, only a transmitter placed at $\pi - \theta$ need be considered to determine the cross-section of the bundle of rays reaching the receiver position at θ . The problem becomes that of determining the cross-section of the bundle of rays that first strikes the surface L, or its image, then strikes M, or its image, and finally reaches the receiver. The rays that strike M, or its image, then L, or its image, are accounted for in a similar manner.

SECRET

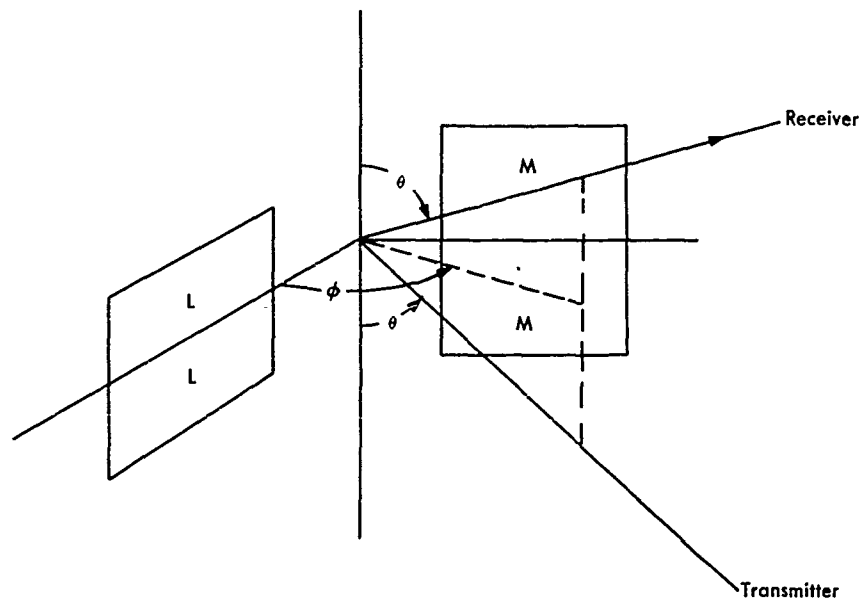


FIG. A-3.3 A GEOMETRICAL OPTICS APPROXIMATION TO THE IMAGE PROBLEM

Consider first the rays that strike L and then M, and introduce the notation shown in Figure A.3-4. The unit vector in the direction of the incident rays is $\hat{k} = -a\hat{i}_x - b\hat{i}_y + c\hat{i}_z$. The rays which are reflected from the surface in the xz plane have the direction numbers $(-a, b, c)$ and form an image of \mathcal{L} on the yz plane as they strike this plane. In the yz plane the image of \mathcal{L} , \mathcal{L}' , will take one of the three forms in Figure A.3-5. This figure indicates how the shape of \mathcal{L}' varies with the elevation angle at a fixed angle ϕ .

The point $(\xi_2, 0, h_2 + h_1)$ projects onto the point $(0, y_4, z_4)$. Similarly the points $(\xi_2, 0, h_2 - h_1)$, $(\xi_1, 0, h_2 + h_1)$, and $(\xi_1, 0, h_2 - h_1)$

SECRET

UNIVERSITY OF MICHIGAN

2255-12-T

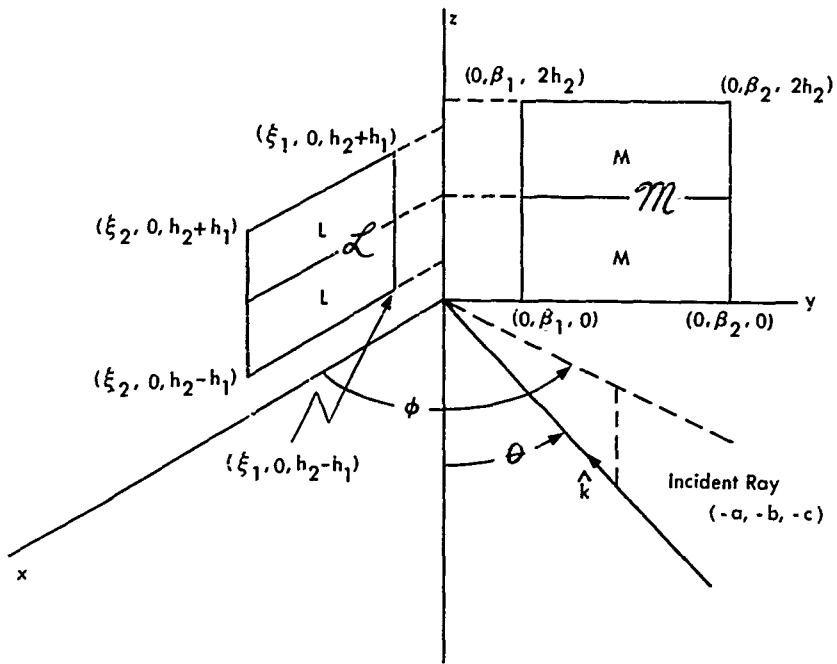


FIG. A-3.4 INTRODUCING THE NOTATION

SECRET

UNIVERSITY OF MICHIGAN

2255-12-T

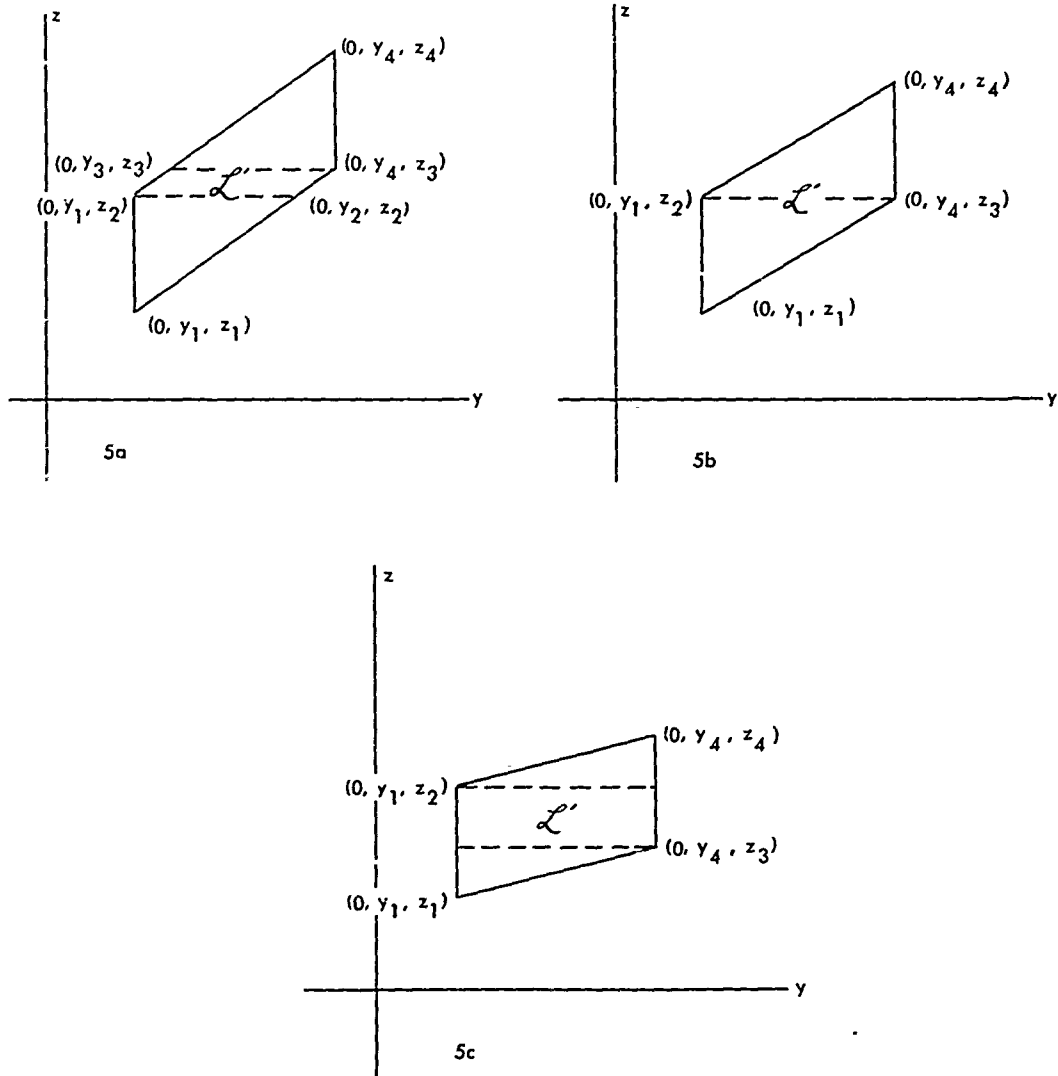


FIG. A-3.5 THE IMAGE OF \mathcal{L} ON THE YZ-PLANE AS A FUNCTION OF THE ASPECT ANGLE θ WITH AZIMUTH ANGLE ϕ FIXED

SECRET

UNIVERSITY OF MICHIGAN

2255-12-T

project onto the points $(0, y_4, z_3)$, $(0, y_1, z_2)$, and $(0, y_1, z_1)$ respectively in the direction $(-a, b, c)$. Therefore,

$$- \xi_2 : y_4 : z_4 - (h_2 + h_1) : : -a:b:c,$$

$$- \xi_2 : y_4 : z_3 - (h_2 - h_1) : : -a:b:c,$$

$$- \xi_1 : y_1 : z_2 - (h_2 + h_1) : : -a:b:c, \text{ and}$$

$$- \xi_1 : y_1 : z_1 - (h_2 - h_1) : : -a:b:c.$$

As a result

$$y_4 = \frac{b}{a} \xi_2 ; z_4 = h_1 + h_2 + \frac{c}{a} \xi_2 ; z_3 = h_2 - h_1 + \frac{c}{a} \xi_2 ; y_1 = \frac{b}{a} \xi_1 ;$$

$$z_2 = h_1 + h_2 + \frac{c}{a} \xi_1 ; \text{ and } z_1 = h_2 - h_1 + \frac{c}{a} \xi_1 .$$

The only rays that will reach the receiving antenna at (θ, ϕ) are those which reflect off the surface \mathcal{M} , so that the problem becomes that of determining the area common to \mathcal{M} and \mathcal{L}' . Once the area common to \mathcal{L}' and \mathcal{M} is found, it will be only necessary to project this area in the direction having direction numbers (a, b, c) in order to obtain the cross-sectional area of the bundle of rays finally reaching the receiving antenna.

Designate this area by A_{LM} . Carrying out a similar procedure leads to the area A_{ML} , where A_{ML} is the projection in the direction of the receiver of the area common to those rays that first strike \mathcal{M} and then \mathcal{L} . The radar cross-section in this approximation is

$$\sigma = \frac{4\pi}{\lambda^2} (A_{LM} + A_{ML})^2 . \tag{A. 3-1}$$

An expression for the areas common to \mathcal{L}' and \mathcal{M} will be obtained. There are three possibilities as shown in Figure A. 3-5. It is seen from the

SECRET

UNIVERSITY OF MICHIGAN

2255-12-T

figure that the area \mathcal{L}' is the same in all three cases. Considering only the y- limitation in the \mathcal{M} -plane then

$$A_{\text{common}} = (z_4 - z_3) \left[(y_4 \cap \beta_2) - (y_1 \cup \beta_1) \right], \quad (\text{A. 3-2})$$

where the symbols $(x \cap y)$ and $(x \cup y)$ mean the smaller of x and y and the larger of x and y respectively. The square parentheses shall be taken to mean, $[x] = 0$ if $x \leq 0$ and $[x] = x$ if $x > 0$. Therefore:

$$\begin{aligned} A_{LM} &= (A_{\text{common}} \hat{1}_x) \cdot (a \hat{1}_x + b \hat{1}_y + c \hat{1}_z) \\ &= (\sin \theta \cos \phi) A_{\text{common}} \end{aligned}$$

It is clear from the geometry that if $h_1 < h_2$, the line $x = 0, z = 0$ imposes no limitation on the area so that it is only necessary to consider the limitations due to the line $x = 0, z = 2h_2$. This yields (for $z_3 \geq z_2$)

$$\begin{aligned} A_{\text{common}} &= (z_4 - z_3) \left[(y_4 \cap \beta_2) - (y_1 \cap \beta_1) \right] - \frac{1}{2} \left[(z_4 \cap z''') - (2h_2 \cup (z_3 \cup z'_0)) \right] \\ &\cdot \left[(\beta_2 \cap y_4) - (y' \cup (y_{00} \cap y_3)) \right] - \left[(2h_2 \cup (z_3 \cap z'_0)) - (2h_2 \cup z_1 \cup z'_{00}) \right] \quad (\text{A. 3-3}) \\ &\cdot (y_4 - y_3) + \frac{1}{2} \left[(z_2 \cup z''_0) - (2h_2 \cup z_1 \cup z'_{00}) \right] \left[(y_1 \cup \beta_1) - (y' \cup y_0 \cup y'_0) \right]. \end{aligned}$$

The first term in Equation (A. 3-3) represents the parallelogram with no limitations imposed by the line $z = 2h_2$. The second term allows for the triangular area cut off by the line $z = 2h_2$ when $2h_2 < z_4$. The third term allows for the parallelogram cut off by the line $z = 2h_2$ when $2h_2 < z_3$ and the third and fourth terms allow for the trapezoidal area cut off by the line $z = 2h_2$ when $2h_2 < z_2$. In Equation (A. 3-3) y_0 is the intersection of

SECRET

UNIVERSITY OF MICHIGAN

2255-12-T

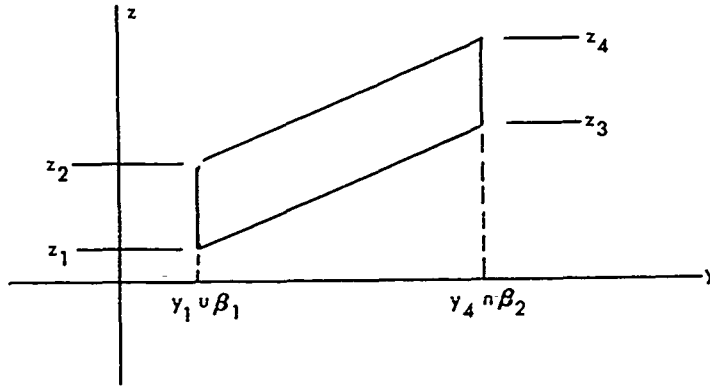


FIG. A-3.6 THE IMAGE OF \mathcal{L} ON THE YZ-PLANE

$z = z_1$ with the line (p) passing through the points $(0, y_4, z_4)$ and $(0, y_1, z_2)$, i. e.,

$$y_0 = y_4 + \frac{y_4 - y_1}{z_4 - z_2} (z_1 - z_4) = \frac{b}{a} \xi_1 - 2h_1 \frac{b}{c} ,$$

y' is given by the intersection of line $z = 2h_2$ with line p, i. e.,

$$y' = y_4 + \frac{y_4 - y_1}{z_4 - z_2} \left(\frac{b}{c} (h_2 - h_1) \right) ,$$

y_{00} is given by the intersection of the line $z = z'_0$ with line p where $z = z'_0$ is given by the intersection of the line (q) passing through the two points $(0, y_4, z_3)$ and $(0, y_1, z_1)$ with $y = \beta_2$.

$$y_{00} = y_1 + \left(\frac{y_4 - y_1}{z_4 - z_2} \right) \left\{ z_1 - z_2 + \frac{(\beta_2 - y_1)(z_3 - z_1)}{y_4 - y_1} \right\} = \beta_2 - 2h_1 \frac{b}{c}$$

SECRET

UNIVERSITY OF MICHIGAN

2255-12-T

y'_0 is given by the intersection of the line z'_{00} with line p where z'_{00} is given by the intersection of $y = \beta_1$ with line q, i. e.,

$$y'_0 = \beta_1 - 2h_1 \frac{b}{c}$$

z''' is the intersection of $y = \beta_2$ with line p; i. e., $z''' = h_1 + h_2 + \frac{c}{b} \beta_2$,

z''_0 is the intersection of $y = \beta_1$ with line p; i. e., $z''_0 = h_1 + h_2 + \frac{c}{b} \beta_1$, and

z'_0 is the intersection of $y = \beta_2$ with line q, i. e., $z'_0 = h_2 - h_1 + \frac{c}{b} \beta_2$.

Furthermore, $y_3 = y_4 + \frac{y_4 - y_1}{z_4 - z_2} (z_3 - z_4) = \frac{b}{a} \xi_2 - 2h_1 \frac{b}{c}$. From these relations, Equation (A.3-3) becomes,

$$\begin{aligned} A_{\text{common}} &= 2h_1 \left[\eta_2 - \eta_1 \right] - \frac{b}{2c} \left[2h_1 \cap \left(h_1 - h_2 + \frac{c}{b} \eta_2 \right) \right]^2 \\ &\quad - \frac{2bh_1}{c} \left[\frac{c}{b} (\eta_2 - \eta_1) \cap \left(-h_1 - h_2 + \frac{c}{b} \eta_2 \right) \right] \\ &\quad + \frac{b}{2c} \left[2h_1 \cap \left(h_1 - h_2 + \frac{c}{b} \eta_1 \right) \right]^2 \quad \text{if } \frac{a}{c} \leq \frac{\xi_2 - \xi_1}{2h_1}, \end{aligned} \quad (\text{A.3-4})$$

where

$$\eta_1 = \frac{b}{a} \xi_1 \cup \beta_1, \text{ and } \eta_2 = \frac{b}{a} \xi_2 \cap \beta_2. \quad (\text{A.3-5})$$

When $z_2 \geq z_3$, i. e., $\frac{c}{a} (\xi_2 - \xi_1) \leq 2h_1$, then by a similar method

$$\begin{aligned} A_{\text{common}} &= 2h_1 \left[\eta_2 - \eta_1 \right] - \frac{b}{2c} \left[\frac{c}{b} (\eta_2 - \eta_1) \cap \left(h_1 - h_2 + \frac{c}{b} \eta_2 \right) \right]^2 \\ &\quad - \left[\eta_2 - \eta_1 \right] \left[2h_1 \cap \left(h_1 - h_2 + \frac{c}{b} \eta_1 \right) \right] \\ &\quad + \frac{b}{2c} \left[\frac{c}{b} (\eta_2 - \eta_1) \cap \left(-h_1 - h_2 + \frac{c}{b} \eta_2 \right) \right]^2. \end{aligned} \quad (\text{A.3-6})$$

SECRET

UNIVERSITY OF MICHIGAN

2255-12-T

The area A_{ML} is equal to the area A_{LM} . This is proved as follows:

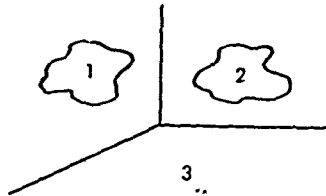


FIG. A-3.7a DEFINITION OF TRIHEDRAL REFLECTOR SIDES

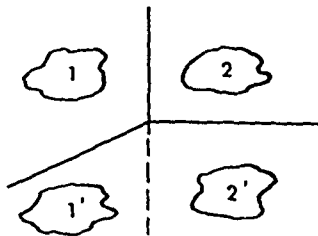


FIG. A-3.7b DEFINITION OF TRIHEDRAL REFLECTOR SIDES IN THE IMAGE PROBLEM

The triply reflected rays may be divided into two groups--those which strike (1) before (2) and those which strike (2) before (1). The first group consists of (1, 2, 3), (3, 1, 2) and (1, 3, 2); the second group contains (2, 1, 3), (3, 2, 1), and (2, 3, 1). Since every ray in the second group is the reverse of some ray in the first group consider for the moment only rays in the first group. In the image problem the ray (1, 2, 3) is represented by (1', 2'); (3, 1, 2) is represented by (1, 2); and (1, 3, 2) is represented by (1', 2). The area obtained by projecting (1) + (1') on

SECRET

UNIVERSITY OF MICHIGAN

2255-12-T

(2) + (2') (along the beam) and projecting the common area on the direction of incidence is the sum of the areas of the three beams (1, 2, 3), (3, 1, 2), and (1, 3, 2). The projection of (2) + (2') on (1) + (1') along the beam and projecting the common area on the direction of incidence is the area of the three beams (2, 1, 3), (3, 2, 1), and (2, 3, 1). Since the area consisting of the beams (1, 2, 3), (3, 1, 2), and (1, 3, 2) is the same as the area of the beams (2, 1, 3), (3, 2, 1), and (2, 3, 1) it follows that the projection of (1) + (1') on (2) + (2') and then in the direction of incidence is the same as the projection of (2) + (2') on (1) + (1') and then in the direction of incidence. Therefore, the radar cross-section is just

$$\sigma = \frac{16\pi}{\lambda^2} (A_{LM})^2 ,$$

or

$$\sigma = \frac{16\pi}{\lambda^2} \sin^2 \theta \cos^2 \phi A_{\text{common}}^2 , \quad (\text{A. 3-7})$$

where A_{common} is given by Equation (A. 3-4) if $(c/a)(\xi_2 - \xi_1) \geq 2h_1$, or by Equation (A. 3-6) if $(c/a)(\xi_2 - \xi_1) \leq 2h_1$.

For completeness the case $h_1 > h_2$ must be considered. To obtain the cross-section for this case it is only necessary to replace h_2 , β_1 , β_2 , ξ_1 , ξ_2 and ϕ by h_1 , ξ_1 , ξ_2 , β_1 , β_2 and $(\pi/2 - \phi)$ respectively in Equations (A. 3-5) and (A. 3-6) where ϕ is still to be measured from the x-axis. To simplify the numerical calculations of σ from Equation (A. 3-7), the expression for A_{common} derived above can be put in the following equivalent forms:

$$\begin{aligned} A_{\text{common}} = & \left[\eta_2 - \eta_1 \right] \left[2h_1 + \left(h_2 - h_1 - \frac{c}{b} \eta_1 \right) \cap \frac{c}{b} (\eta_2 - \eta_1) \right] \\ & - \frac{b}{2c} \left[\left(\eta_2 - \eta_1 - \frac{c}{b} \eta_1 \right) \cap \frac{c}{b} (\eta_2 - \eta_1) \right]^2 \\ & - \frac{b}{2c} \left[\left(h_2 + h_1 - \frac{c}{b} \eta_1 \right) \cap \frac{c}{b} (\eta_2 - \eta_1) \right] \left\{ \left[-h_2 - h_1 + \frac{c}{b} \eta_2 \right] + \frac{c}{b} \left[\eta_2 - \eta_1 \right] \right\} , \text{ and} \end{aligned}$$

(A. 3-8)

SECRET

SECRET

UNIVERSITY OF MICHIGAN

2255-12-T

$$A_{\text{common}} = \frac{K b}{2 c} \left\{ K + 2 \left[\left(h_2 - h_1 - \frac{c}{b} \eta_1 \right) \wedge \left(h_2 + h_1 - \frac{c}{b} \eta_2 \right) \wedge \left| 2h_2 - \frac{c}{b} (\eta_2 - \eta_1) \right| \right] \right\} \\ + \left[h_1 - h_2 + \frac{c}{b} \eta_2 + K \right] \left[\left(h_2 + h_1 - \frac{c}{b} \eta_2 \right) \wedge \left(h_2 - h_1 - \frac{c}{b} \eta_1 \right) \wedge \frac{c}{b} (\eta_2 - \eta_1) \wedge 2h_2 \right]$$

where

$$K = 2h_1 \wedge \frac{c}{b} (\eta_2 - \eta_1) \wedge \left(h_2 + h_1 - \frac{c}{b} \eta_1 \right) . \quad (\text{A. 3-9})$$

A.4 RADAR CROSS-SECTION OF TWO WALLS IN TANDEM

Consider the case of two buildings in tandem with similar walls parallel as in Figure A.4-1. For angles of incidence in a plane normal

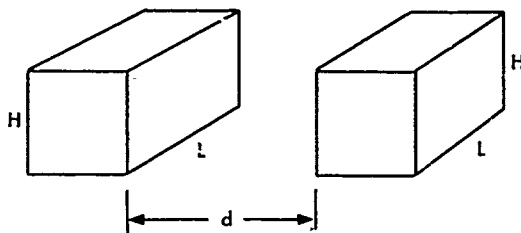


FIG. A-4.1 TWO BUILDINGS WITH SIMILAR WALLS IN TANDEM

to the surfaces the scattering cross-section can be determined by ray tracing as shown in Figure A.4-2. It can be seen that the incident radiation is ultimately reflected from the dihedral corner formed by the wall and the plane. Therefore, it is only necessary to determine the area common to the entrance and exit pupils of this dihedral reflector to obtain the cross-section of the wall. This area, A , is just the segment jc (on the line ag) times L . Inasmuch as $kl/kf = jc/kf = ac/af$, where $ac = d \sin \alpha$, $af = d$, and $kf = 2ke = 2ef$. Hence $jc = 2ke \sin \alpha$. To compute ke

SECRET

UNIVERSITY OF MICHIGAN

2255-12-T

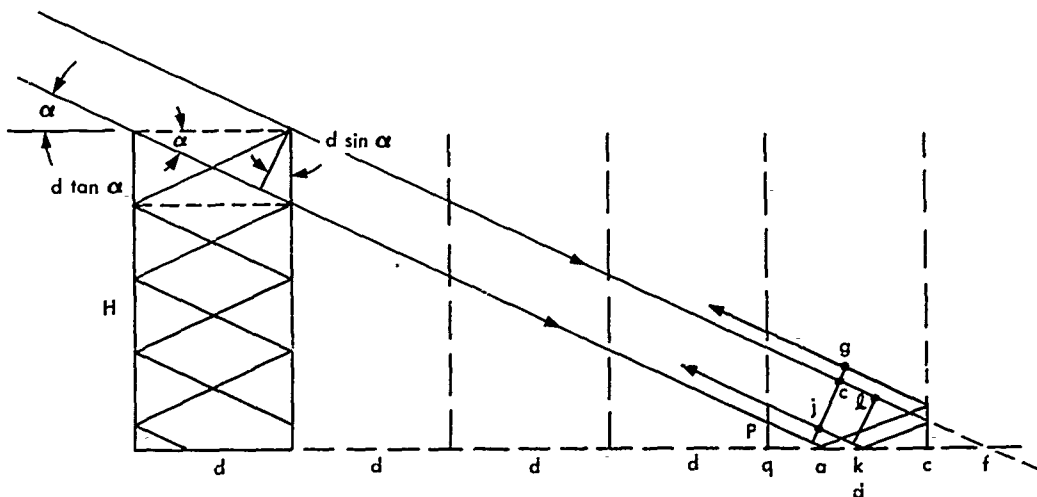


FIG. A-4.2 GEOMETRY FOR THE IMAGE PROBLEM

notice that $ke = ef = H \cot \alpha - nd$ where n is the number of reflections that occur before the incident wave reaches the dihedral corner.

Therefore, $jc = 2 \sin \alpha (H \cot \alpha - nd) = 2 (H \cos \alpha - nd \sin \alpha)$ and $A = 2L (H \cos \alpha - nd \sin \alpha)$. Hence,

$$\sigma = \frac{4\pi}{\lambda^2} (4L^2) (H \cos \alpha - nd \sin \alpha)^2 \quad . \quad (A.4-1)$$

The foregoing derivation is for the completely idealized case (of infinite conductivity). In application, the walls will often not be perfectly reflecting, and, of course, the ground never is. In such cases, the energy loss at each reflection will often make the returns after many reflections (n large) negligible compared to returns after one or two reflections (dihedrals and trihedral).

SECRET

UNIVERSITY OF MICHIGAN

2255-12-T

A. 5 WAVELENGTH DEPENDENCE OF THE NON-SPECULAR RETURN FROM 90-DEGREE DIHEDRAL REFLECTORS

Quite often it is necessary to consider the returns from dihedrals when the incident parallel rays do not lie in the plane containing both normals to the sides of the dihedrals. This situation occurs, for example, when taking into account the simultaneous returns from separated dihedral targets since the radar beam is not sharply collimated, but is divergent. This situation occurred in the computations for Section III of the text. The same situation also occurred in Section A. 3 where the problem of a trihedron with an infinite side was replaced by a dihedral in an imaging process. Non-specular dihedral returns are also of interest when the incident rays are normal to a wall which forms a dihedral with the ground, but in which the ground slopes along the wall.

In the special case to be considered in this section, in which one side of the dihedral is effectively infinite, imaging may be used to replace the dihedral problem by a particular bistatic flat plate diffraction problem which is readily solved.

While it is a well-known physical optics result that for radiation specularly reflected from a dihedral corner the scattering cross-section varies inversely with the square of the wavelength, it is not as well known that physical optics gives a cross-section essentially independent of wavelength¹ for back scattering from a dihedral when the propagation vector for the incident radiation is not perpendicular to the axis of the dihedral. Specifically, as shown in Figure A. 5-1, if the angle between the projection of the incident propagation vector on the xy-plane and the y-axis is γ , then

$$\sin \gamma > \frac{\lambda}{4 a \sin \theta}$$

is the condition for the back scattering to be independent of wavelength for the dihedral. θ is the angle measured from the polar axis which is

¹An average value has been given to the highly oscillatory wavelength dependent factor. However, the replacement of this factor by its average value is still within the spirit of the physical optics approximation, so that in this sense the resultant cross-section is independent of wavelength.

SECRET

SECRET

UNIVERSITY OF MICHIGAN

2255-12-T

normal to the azimuth plane. It will be noticed that physical optics is applicable only when $\frac{\lambda}{l} \ll 1$, thus the result is valid except in the vicinity of $\gamma \approx 0$, $\theta \approx 0$.

The method of images will be applied to find the radar cross-section of this dihedral reflector. The image problem is that shown in Figure A.5-1. In the image problem the transmitter position θ_i, ϕ_i is related to the receiver position θ_r, ϕ_r through the relations $\phi_r = 2\pi - \phi_i$ and $\theta_i = \theta_r$.

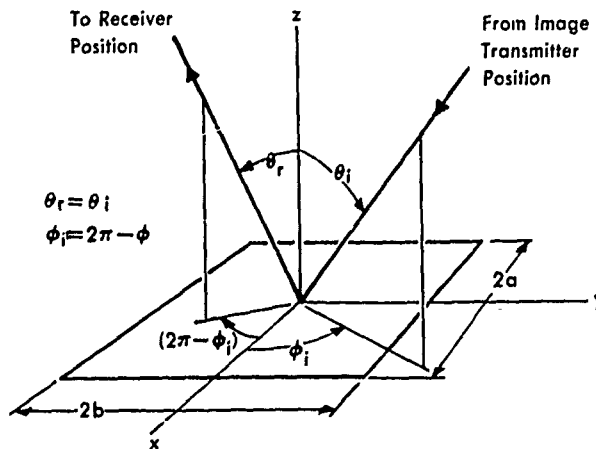


FIG. A - 5.1 GEOMETRY FOR THE IMAGE PROBLEM

To evaluate the radar cross-section given by Equation (A.1-2) note that now

$$\begin{aligned} \hat{n}_o &= -\hat{i}_x \sin \theta_r \cos \phi_r - \hat{i}_y \sin \theta_r \sin \phi_r - \hat{i}_z \cos \theta_r, \\ \hat{k} &= -\hat{i}_x \sin \theta_i \cos \phi_i - \hat{i}_y \sin \theta_i \sin \phi_i - \hat{i}_z \cos \theta_i, \text{ and} \\ \vec{r} \cdot (\hat{n}_o + \hat{k}) &= -2x \sin \theta_r \cos \phi_r - 2z \cos \theta_r. \end{aligned}$$

SECRET

UNIVERSITY OF MICHIGAN

2255-12-T

Therefore,

$$\vec{f} = \hat{i}_z \int_{-a}^{+a} \int_{-b}^{+b} e^{2ik(x \sin \theta_r \cos \phi_r + z \cos \theta_r)} dx dy .$$

Integrating gives,

$$\vec{f} = \hat{i}_z 4b e^{2ikz \cos \theta_r} \frac{\sin(2ka \sin \theta_r \cos \phi_r)}{2k \sin \theta_r \cos \phi_r} .$$

The radar cross-section becomes:

$$\sigma = \frac{4b^2 \sin^2(2ka \sin \theta_r \cos \phi_r)}{\pi \sin^2 \theta_r \cos^2 \phi_r} \left[(\hat{n}_o \cdot \hat{a})^2 - 2(\hat{n}_o \cdot \hat{i}_z)(\hat{n}_o \cdot \hat{a})(\hat{i}_z \cdot \hat{a}) + (\hat{n}_o \cdot \hat{i}_z)^2 \right] .$$

(A.5-1)

Since $\frac{2a}{\lambda} \gg 1$ in the usual physical optics approximation, the argument $2ka \sin \theta_r \cos \phi_r$ is much larger than π except for angular regions of ϕ_r near $\pi/2$ and θ_r near zero. When the argument is large, small changes in any of its factors changes its value greatly, so that, if $\sin^2(2ka \sin \theta_r \cos \phi_r)$ is replaced by its average value, a quantity of greater physical significance is obtained.

$$\bar{\sigma} = \frac{2b^2}{\pi \sin^2 \theta_r \cos^2 \phi_r} \left| (\hat{n}_o \cdot \hat{a})^2 - 2(\hat{n}_o \cdot \hat{i}_z)(\hat{n}_o \cdot \hat{a})(\hat{i}_z \cdot \hat{a}) + (\hat{n}_o \cdot \hat{i}_z)^2 \right| .$$

(A.5-2)

which is wavelength independent.

A.6 ANGLE ERRORS

Very often dihedrals formed by buildings and terrain will not be exactly 90 degrees. For example, for drainage purposes, land is often sloped away from the walls. In this case instead of one doubly reflected

SECRET

UNIVERSITY OF MICHIGAN

2255-12-T

beam there are two doubly reflected beams diverging with an angle given by Equation (A.6-6). The returned radiation at a distant point along the direction of incidence is therefore due only to diffraction out of the specular direction, even when this direction is in a plane perpendicular to the walls. To determine this back scattering the boundary of the cross-section of each reflected beam must be known since the radiation from each beam is diffracted approximately as though it were reflected from a flat plate of this cross-section. The back scattered energy is then determined by superimposing the two diffracted electric fields taking phase into account.

Similar remarks hold for a trihedral reflector. At each non-perpendicular junction of two walls, any incident beam is split into two diverging reflected beams so that there may be 2, 4, or 6 triply reflected beams accordingly as there are 1, 2, or 3, non-90-degree angles. The back scattering is again non-specular with the diffracted fields which are to be superposed, determined by the beam cross-sections.

A.6.1 Spencer's Results

For the specialized problem in which the incident radiation is along the axis of symmetry of a dihedral or trihedral reflector (with all 90-degree angles) the effects of slight rotations about the edges have been determined quite neatly by Spencer (Ref. 10). Spencer's results are summarized in Table A-1. The numbers in the last column give the product of side length times angle deviation from 90 degrees which corresponds to the indicated reduction in σ .

The work presented in this section has no such compact end result. The results in Sections A.6.2.2 and A.6.2.3 show that the decrease in back scattered energy for a given angle error is least for the angle of view considered in these tables. As a matter of fact this statement is almost the only one of some generality which can be made on the basis of the work which follows. The complexity of the problem in the general case is such, that it has not been possible as yet to come up with any general criterion by which a quick judgment of the effect can be made. Further theoretical analysis perhaps along different lines than used here or analysis of extensive computations of the deterioration in return as a function of angle error, computed on the basis of the results in this appendix or obtained experimentally, might lead to such criteria.

A-24

SECRET

SECRET

UNIVERSITY OF MICHIGAN

2255-12-T

TABLE A-1

ERRORS IN CORNERS VERSUS db DROP IN SIGNAL STRENGTH

Type of Reflection	Line of Sight	Number of Errors	Type of Corner	Error to Reduce by		
				1db	3db	10db
Double	45	One	Square	.17λ	.31λ	.61λ
Double	45	One	Triangular	.22	.39	.90
Triple	Symmetric	One	Square	.24	.40	.66
Triple	Symmetric	One	Triangular	.42	.70	1.21
Triple	Symmetric	Three	Square	.14	.24	.44
Triple	Symmetric	Three	Triangular	.20	.35	.62

A. 6.2 Dihedrals

A. 6.2.1 Ray Tracing

Consider the dihedral sides I and II in Figure A.6-1 to have normals

$$n_I = (\cos \theta, 0, \sin \theta), \text{ and}$$

$$n_{II} = (0, 0, 1) . \tag{A.6-1}$$

The specular directions of the rays are determined by applying the law of reflection (Eq. A.1-5). It is seen that rays which hit II first with direction

$$\hat{k} = k_x, k_y, k_z , \tag{A.6-2}$$

reflect from II with direction,

$$\hat{k}_1 = k_x, k_y, -k_z , \tag{A.6-3}$$

SECRET

UNIVERSITY OF MICHIGAN

2255-12-T

and then reflect from I with direction

$$\hat{k}_2 = -k_x \cos 2\theta + k_z \sin 2\theta,$$

$$k_y, -k_x \sin 2\theta - k_z \cos 2\theta. \quad (\text{A. 6-4})$$

On the other hand rays which strike I first, then II emerge with direction

$$\hat{k}'_2 = -k_x \cos 2\theta - k_z \sin 2\theta,$$

$$k_y, k_x \sin 2\theta - k_z \cos 2\theta. \quad (\text{A. 6-5})$$

The cosine of the angle ϕ between the emerging beams is there given by

$$\cos \phi = \hat{k}_2 \cdot \hat{k}'_2 = (1 - k_y^2) \cos 4\theta + k_y^2. \quad (\text{A. 6-6})$$

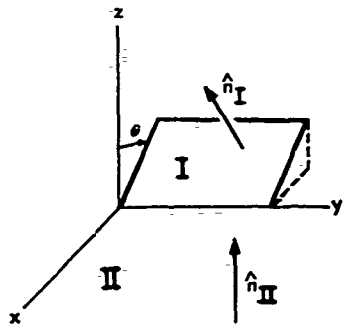


FIG. A - 6.1 GEOMETRY FOR DIHEDRAL WITH ARBITRARY ANGLE

SECRET

SECRET

UNIVERSITY OF MICHIGAN

2255-12-T

A. 6.2.2 One Infinite Side

In determining the diffraction in each beam and the net back scattered return we shall consider first the especially simple (but important) case where one side is infinite and the other side is a rectangle. The effective apertures normal to the reflected beams are then parallelograms (or simply rectangles if $k_y = 0$). However, in this problem it is perhaps simpler to use imaging which reduces the problem to bistatic scattering from two rectangular plates, neither one oriented perpendicular to the incident rays.

For the dihedral reflector shown in Figure A. 6-2 where M is the semi-infinite region $y > 0$ on the plane $z = 0$, and plane L is a rectangle the equivalent image problem is that of Figure A. 6-3 where the image of L is denoted by L' . Thus the scattered field at the receiver can be obtained by considering two plane waves incident on two rectangular flat

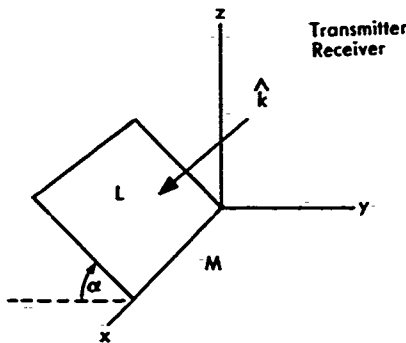


FIG. A - 6.2 GEOMETRY FOR DIHEDRAL WITH NON-PERPENDICULAR SIDES

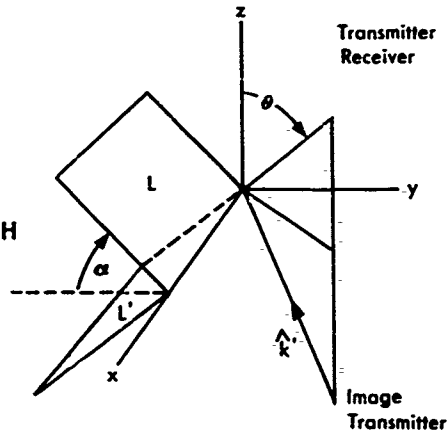


FIG. A - 6.3 GEOMETRY FOR THE IMAGE PROBLEM

SECRET

UNIVERSITY OF MICHIGAN

2255-12-T

plates. In the x, y, z coordinate system let the original transmitter-receiver position be indicated by the angles θ, ϕ and the image transmitter position by θ', ϕ' then a unit vector in the incident direction \hat{k} is

$$\hat{k} = \hat{i}_x \sin \theta \cos \phi + \hat{i}_y \sin \theta \sin \phi + \hat{i}_z \cos \theta, \text{ and}$$

$$\hat{k}' = \hat{i}_x \sin \theta' \cos \phi' + \hat{i}_y \sin \theta' \sin \phi' + \hat{i}_z \cos \theta', \quad (\text{A. 6-7})$$

for the image transmitter where $\phi = \phi'$ and $\theta' = \pi - \theta$. The receiver direction is $-\hat{n}_0 = -\hat{k}$.

For the plates L and L' introduce the coordinates of Figure A. 7-4. In these coordinate systems (θ_L, ϕ_L) , $(\theta_{L'}, \phi_{L'})$, and (θ_L^i, ϕ_L^i) , $(\theta_{L'}^i, \phi_{L'}^i)$ specify the position of the transmitter-receiver and image transmitter respectively.

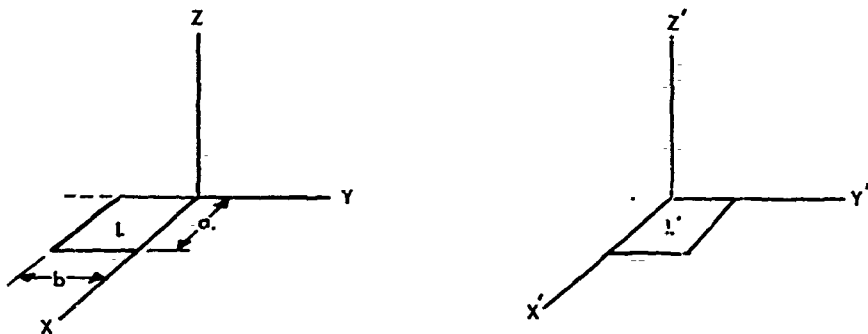


FIG. A-6.4 COORDINATE SYSTEMS FOR PLATE L AND L'

The equations of transformation are:

$$X = x$$

$$X' = x$$

$$Y = y \cos \alpha - z \sin \alpha$$

$$Y' = -y \cos \alpha - z \sin \alpha$$

$$Z = y \sin \alpha + z \cos \alpha$$

$$Z' = y \sin \alpha - z \cos \alpha. \quad (\text{A. 6-8})$$

SECRET

UNIVERSITY OF MICHIGAN

2255-12-T

The relations that will be of interest are:

$$\begin{aligned} \cos \theta_L &= \sin \theta \sin \phi \sin \alpha + \cos \theta \cos \alpha, \\ \sin \theta_L &= \left[1 - (\sin \theta \sin \phi \sin \alpha + \cos \theta \cos \alpha)^2 \right]^{1/2} \end{aligned} \quad (\text{A. 6-9})$$

$$\cos \phi_L = \frac{\sin \theta \cos \phi}{\left[1 - (\sin \theta \sin \phi \sin \alpha + \cos \theta \cos \alpha)^2 \right]^{1/2}}$$

$$\sin \phi_L = \frac{\cos \alpha \sin \theta \sin \phi - \cos \theta \sin \alpha}{\left[1 - (\sin \theta \sin \phi \sin \alpha + \cos \theta \cos \alpha)^2 \right]^{1/2}}$$

with a similar set for the primes, i. e.,

$$\begin{aligned} \cos \theta'_L &= \cos \theta' \sin \phi' \sin \alpha + \cos \theta' \cos \alpha, \text{ etc.}, \text{ and} \\ \cos \theta'_L &= \sin \alpha \sin \theta \sin \phi - \cos \theta \cos \alpha \\ \sin \theta'_L &= \left[1 - (\sin \alpha \sin \theta \sin \phi - \cos \alpha \cos \theta)^2 \right]^{1/2} \end{aligned} \quad (\text{A. 6-10})$$

$$\cos \phi'_L = \frac{\sin \theta \cos \phi}{\left[1 - (\sin \alpha \sin \theta \sin \phi - \cos \alpha \cos \theta)^2 \right]^{1/2}}$$

$$\sin \phi'_L = \frac{-(\sin \theta \sin \phi \cos \alpha + \cos \theta \sin \alpha)}{\left[1 - (\sin \alpha \sin \theta \sin \phi - \cos \theta \cos \alpha)^2 \right]^{1/2}}$$

also with a similar set for the primes, i. e.,

$$\cos \theta'_L = \sin \alpha \sin \theta' \sin \phi' - \cos \alpha \cos \theta'. \text{ etc.}$$

The unit vectors are related by:

SECRET

UNIVERSITY OF MICHIGAN

2255-12-T

$$\hat{i}_Z = \hat{i}_y \sin \alpha + \hat{i}_z \cos \alpha, \text{ and } \hat{i}_{Z'} = \hat{i}_y \sin \alpha - \hat{i}_z \cos \alpha.$$

By Equation (A. 1-2)

$$\sigma = 4\pi |\vec{F}|^2, \text{ where } \vec{F} = \frac{ik}{2\pi} \sum_{ij} \left[(\hat{n}_0 \cdot \hat{a}_j) \vec{f}_{ij} - (\hat{n}_0 \cdot \vec{f}_{ij}) \hat{a}_j \right] \quad (\text{A. 6-11})$$

where $H_{inc} = 1$, and

$$\vec{f}_{ij} = \int_{j^{\text{th}} \text{ plate}} \hat{n} e^{ik\vec{r} \cdot (\hat{n}_0 + \hat{k}_i)} ds.$$

The subscript $i = 1$ corresponds to the original transmitter, $i = 2$ the image transmitter, and the j 's correspond to plate L ($j = 1$) and plate L' ($j = 2$). Thus, for example, \vec{f}_{12} is the contribution of plate L' when irradiated by a plane wave coming from the original transmitter position.

From Figure A. 6-5 it is seen that if $\pi/2 - \theta < \alpha$ there are four beams, only two of which need be considered, namely, \vec{f}_{11} and \vec{f}_{22} . While for $\pi/2 - \theta > \alpha$ there are only the two beams, \vec{f}_{11} and \vec{f}_{22} . Thus F becomes,

$$\vec{F} = \frac{ik}{2\pi} \left[(\hat{n}_0 \cdot \hat{a}_2) \vec{f}_{22} - (\hat{n}_0 \cdot \vec{f}_{11}) \hat{a}_1 - (\hat{n}_0 \cdot \vec{f}_{22}) \hat{a}_2 \right], \quad (\text{A. 6-12})$$

since $\hat{n}_0 \cdot \hat{a}_1 = 0$. Transformation of coordinates and integration gives

$$\vec{f}_{11} = \hat{i}_z e^{2ikz \cos \theta_L} \left[\frac{e^{2ika \sin \theta_L \cos \phi_L} - 1}{2ik \sin \theta_L \cos \phi_L} \right] \left[\frac{1 - e^{-2ikb \sin \theta_L \sin \phi_L}}{2ik \sin \theta_L \sin \phi_L} \right], \text{ and} \quad (\text{A. 6-13})$$

$$\vec{f}_{22} = \hat{i}_z e^{2ikz' \cos \theta_{L'}} \left[\frac{e^{2ika \sin \theta_{L'} \cos \phi_{L'}} - 1}{2ik \sin \theta_{L'} \cos \phi_{L'}} \right] \left[\frac{e^{2ikb \sin \theta_{L'} \sin \phi_{L'}} - 1}{2ik \sin \theta_{L'} \sin \phi_{L'}} \right]. \quad (\text{A. 6-14})$$

SECRET

SECRET

UNIVERSITY OF MICHIGAN

2255-12-T

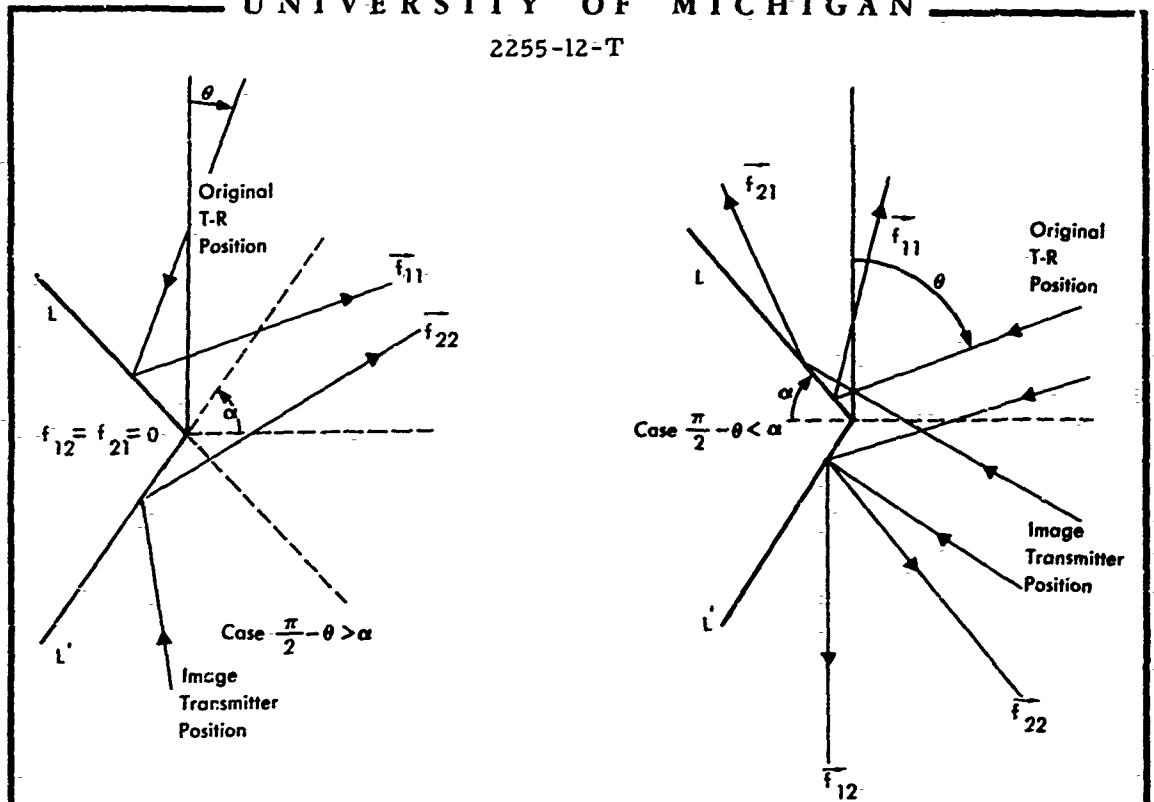


FIG. A-6.5 GEOMETRY DEFINING BEAM DIRECTIONS

A. 6.2.3 Two Finite Sides

If both sides of the dihedral are finite in extent, diffraction has to be considered as though the equivalent flat plates were made up of the area common to two overlapping parallelograms as shown in Figure A. 6-6. In each case, the common area is a parallelogram with one corner cut off.

In this problem the same shape of plate has to be considered whether or not an imaging procedure is used. If an imaging procedure is used, then as before, diffraction has to be considered when the incident wave is not normal to the plane of the aperture.

SECRET

SECRET

UNIVERSITY OF MICHIGAN

2255-12-T

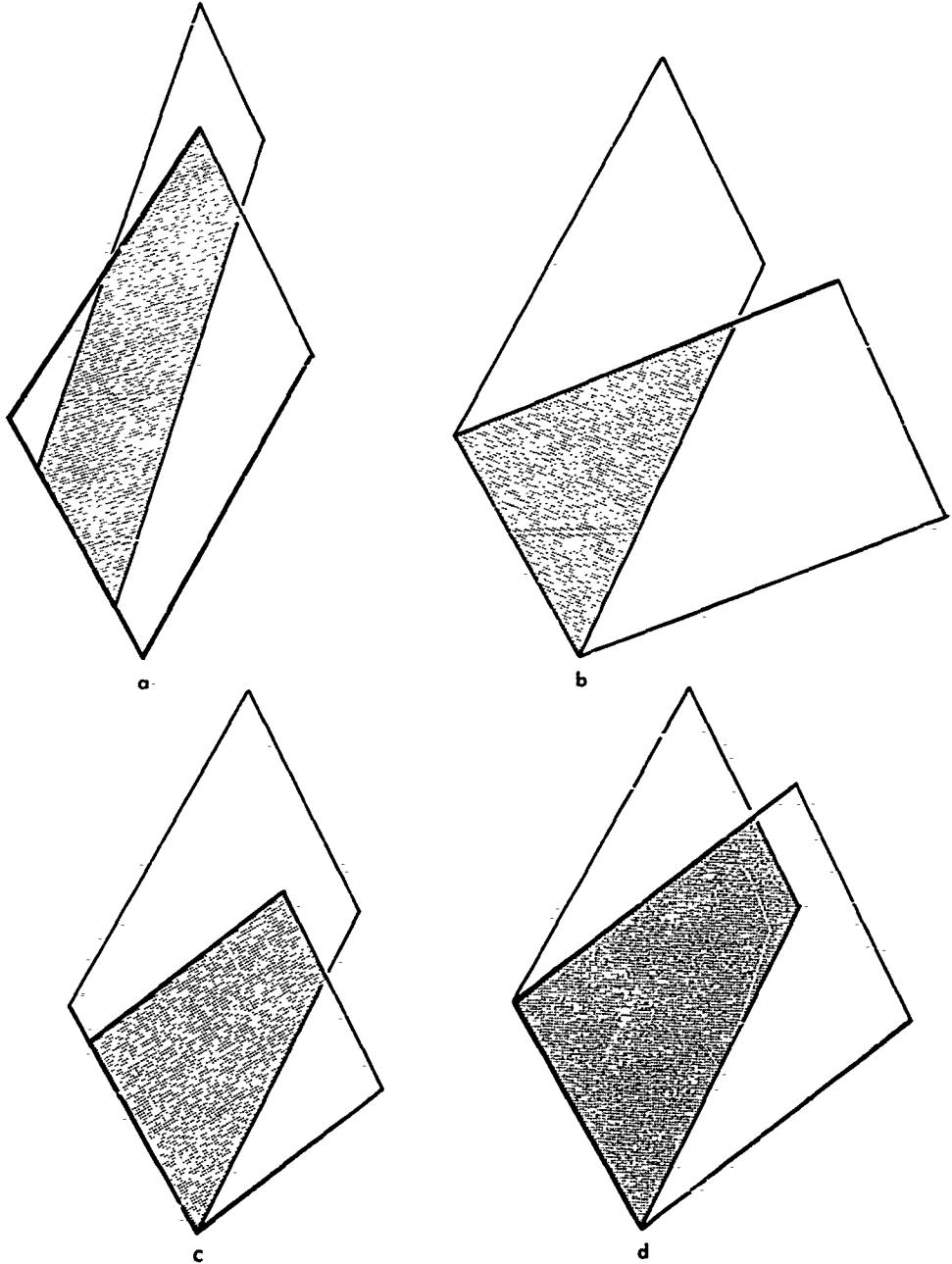


FIG. A-6.6 FORMATION OF VARIOUS EQUIVALENT APERTURES

SECRET

SECRET

UNIVERSITY OF MICHIGAN

2255-12-T

In the previous case of one infinite plane the imaging problem could be simplified by considering rectangular apertures, but now there is no simplification in using imaging. Hence the diffraction patterns for normal incidence are determined.

The field diffracted through these apertures can be obtained by subtracting the field diffracted by a triangular plate from the field diffracted by a parallelogram-shaped plate.

The detailed analysis required to determine the shape of the effective aperture directly parallels the work of Appendix A. 3 except that the non-perpendicularity of the dihedral must be taken into account in computing ray directions. This computation is not carried out here. However, the field patterns in various directions for certain families of parallelogram and triangular apertures are derived and graphed.

For the parallelogram aperture shown in Figure A. 6-7 application of Equation (A. 1-1) leads to an $|f|$ given by

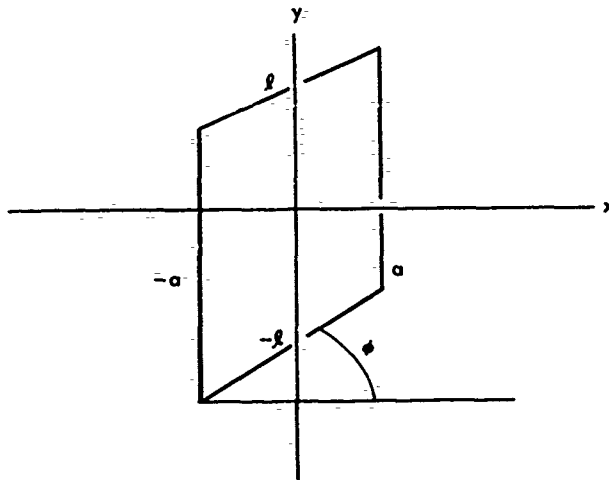


FIG. A-6.7 PARALLELOGRAM APERTURE

SECRET

UNIVERSITY OF MICHIGAN

2255-12-T

$$I = \frac{f}{4a\ell} = \frac{\sin k\beta\ell}{k\beta\ell} \frac{\sin kB\ell}{kB\ell} \quad (\text{A. 6-15})$$

where $a = \delta \ell$, and α and β are the x and y components of the vector from the receiver to the origin, and $B = (\alpha + \beta \tan \phi) \delta$. Graphs of I^2 for $B/\beta = 0, .5, 1, 5$ are shown on the Figure A.6-8. Note that for $B = .5, 1,$ and 5 the graphs of H all lie below the value for $B = 0$; thus the greatest angular spread of energy corresponds to $B = 0$, which for fixed δ and ϕ lies in the planes corresponding to

$$\alpha = \beta \tan \phi.$$

Consider next the clipped off corner shown in Figure A.6-9.

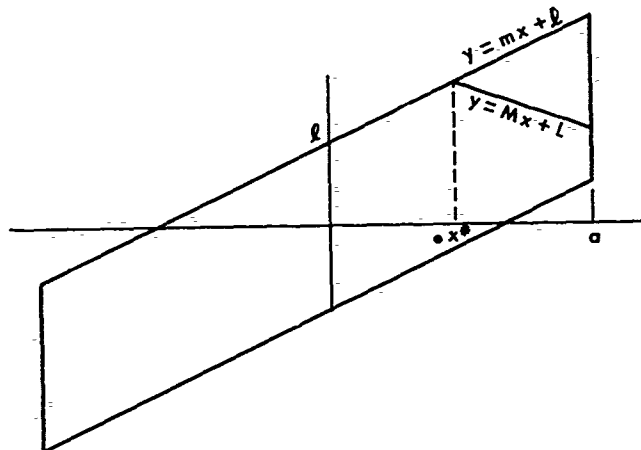


FIG. A-6.9 POSSIBLE APERTURE FOR DIHEDRAL WITH TWO SIDES FINITE

As extension of the definitions used for the Equation (A.6-15), define

SECRET

UNIVERSITY OF MICHIGAN
2255-12-T

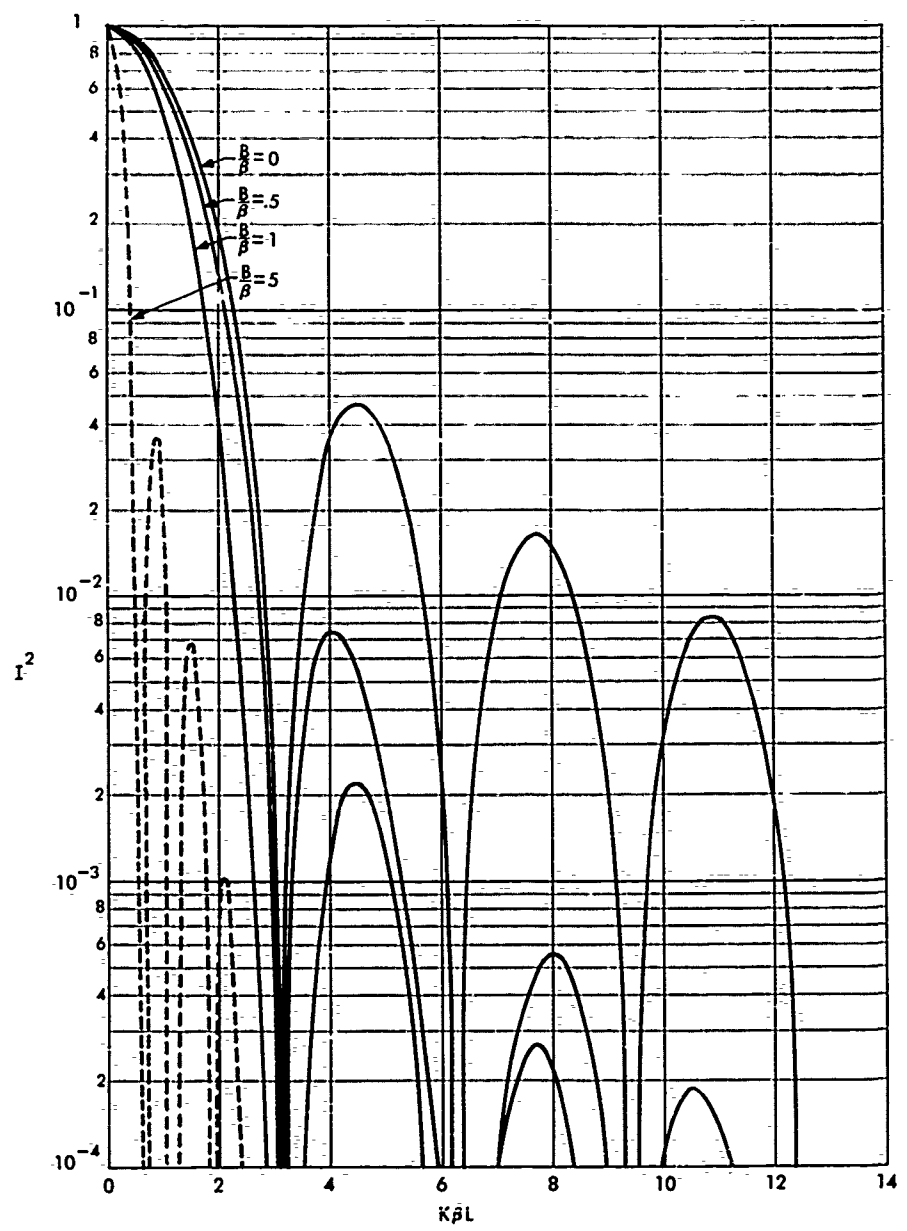


FIG. A-6.8 RELATIVE INTENSITY OF DIFFRACTION THROUGH A PARALLELOGRAM APERTURE

SECRET

SECRET

UNIVERSITY OF MICHIGAN

2255-12-T

$$\begin{aligned} x^* &= \frac{L-l}{m-M}, \quad B = (\alpha + \beta m)\delta, \quad B^* = (\alpha + \beta m)\delta^*, \quad C = (\alpha + \beta M)\delta, \quad C^* = (\alpha + \beta M)\delta^*, \\ x^* &= \delta^* l, \quad \frac{\Delta - l}{m - M} = \delta^*, \quad a = \delta l, \quad L = \Delta l. \end{aligned} \quad (\text{A. 6-16})$$

Then f for the triangle becomes

$$f = \frac{\delta e^{ik\beta l}}{k^2 B} (e^{ikB l} - e^{ikB^* l}) + \frac{\delta e^{ik\beta \Delta l}}{k^2 \beta C} (e^{ikC l} - e^{ikC^* l}), \quad (\text{A. 6-17})$$

or $f = \sqrt{|f|^2} e^{iv}$,

where $v = \tan^{-1} \frac{\frac{1}{B} (\sin a - \sin b) + \frac{1}{C} (\sin c - \sin d)}{\frac{1}{B} (\cos a - \cos b) + \frac{1}{C} (\cos a - \cos b)}$, and

$$\begin{aligned} |f|^2 &= \frac{2\delta^2}{k^4 b^2} \left\{ \frac{1 - \cos(a-b)}{B^2} + \frac{1 - \cos(c-d)}{C^2} \right. \\ &\quad \left. + \frac{\cos(a-c) - \cos(b-c) - \cos(a-d) + \cos(b-d)}{BC} \right\}. \end{aligned} \quad (\text{A. 6-18})$$

In Equation A. 6-18 $a = k\beta l (1 + \frac{B}{\beta})$, $c = k\beta l (1 + \frac{C}{\beta})$, and $b = k\beta l (\Delta + \frac{B^*}{\beta})$, $d = k\beta l (\Delta + \frac{C^*}{\beta})$.

In the special case of a right triangle shown in Figure A. 6-10 Equation (A. 6-18)

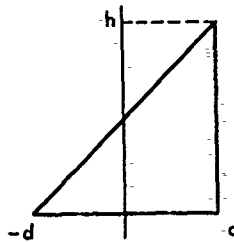


FIG. A-6.10 TRIANGULAR APERTURE

SECRET

UNIVERSITY OF MICHIGAN

2255-12-T

specializes to a form which is perhaps simpler. Comparison of Figures A. 6-10 and A. 6-9 shows that in this case $x = -d$, $a = d$, and hence $B = -B^*$ and $C = -C^*$. Also $M = L = 0$ and $m = \ell/d$, so that

$$f = \frac{2d}{ik\beta} \left[e^{ik\beta md} \frac{\sin k(\alpha + \beta m)d}{k(\alpha + \beta m)d} - \frac{\sin k\alpha d}{k\alpha d} \right] \quad (A. 6-19)$$

To plot f conveniently, define

$$X = k\alpha d; \quad N = \frac{\beta h}{2\alpha d}, \quad k(\alpha + \beta m)d = k\alpha d \left(1 + \frac{\beta h}{2\alpha} \right) = (1+N)x \quad (A. 6-20)$$

$$km\beta d = Nx; \quad \frac{2d}{k\beta} = \frac{hd}{Nx} .$$

Hence

$$f(N, x) = \frac{hd}{iNx} \left[e^{imx} \left(\frac{\sin(1+N)x}{(1+N)x} \right) - \frac{\sin x}{x} \right] \quad (A. 6-21)$$

and

$$\frac{|f(N, x)|^2}{h^2 d^2} = \frac{1}{N^2 x^2} \left[\left(\frac{\sin x}{x} \right)^2 + \left(\frac{\sin(1+N)x}{(1+N)x} \right)^2 - 2 \frac{\sin x}{x} \frac{\sin(1+N)x}{(1+N)x} \cos Nx \right] \quad (A. 6-22)$$

For $N = 0$ (or -1), Equation (A. 6-22) reduces further to

$$\frac{|f|^2}{h^2 d^2} = \left(\frac{\sin x}{x} \right)^2 \left[1 + \left(\frac{x \cot x - 1}{x} \right)^2 \right] \quad (A. 6-23)$$

By applying trigonometric identities, Equation (A. 6-22) can be reduced to the form

$$\frac{|f(N, x)|^2}{h^2 d^2} = \frac{1}{2N^2 (N+1)^2} \left\{ 1 + N(N+1)(1 - \cos 2x) + N \cos 2(N+1)x - (N+1) \cos 2Nx \right\}, \quad (A. 6-24)$$

which is quite convenient for computation, and more important, which also shows that

$$|f(m, x)|^2 = |f(-1 - m, x)|^2 \quad (A. 6-25)$$

But if N is a negative integer, $N \leq -2$

SECRET

SECRET

UNIVERSITY OF MICHIGAN

2255-12-T

$$\frac{|f(N, x)|^2}{h^2 d^2} = \frac{4}{N(N+1)} \left(\frac{\sin x}{x}\right)^4 \sum_{k=0}^{-N-2} (-1)^k \binom{-N+k}{2k+2} \frac{(2 \sin x)^{2k}}{k+2}$$

(A. 6-26)

Thus for all integers N except $N = \pm 1$ or zero, $|I|^2$, plotted as functions of x (Fig. A. 6-11) all drop off faster than the curves for $N = 0, -1$.

A. 6.3. Trihedral Reflectors

The most important reflectors for this investigation are those with one side (the ground plane) effectively infinite in extent. The angle error situation of most interest in this case is where the non-perpendicularities are at the junctions with the ground plane. However, if these angles are 90 degrees although the angle at the remaining edge is not in general 90 degrees the two finite walls may be imaged in the ground plane and the problem converted to a dihedral problem as in Section A. 6.2.3.

If one of the remaining walls is so large that it does not limit the beam, the more complete results of Section A. 6.2.2 are directly applicable.

Angle error effects in general trihedral reflectors can be handled by the methods described in the foregoing sections. The complexity of the analyses and results by this treatment is so great, that it has not been worked out on this contract. For a small deviation from 90-degree angles perhaps other approaches such as applied in Reference 10 for certain special cases would prove fruitful.

SECRET

SECRET

UNIVERSITY OF MICHIGAN
2255-12-T

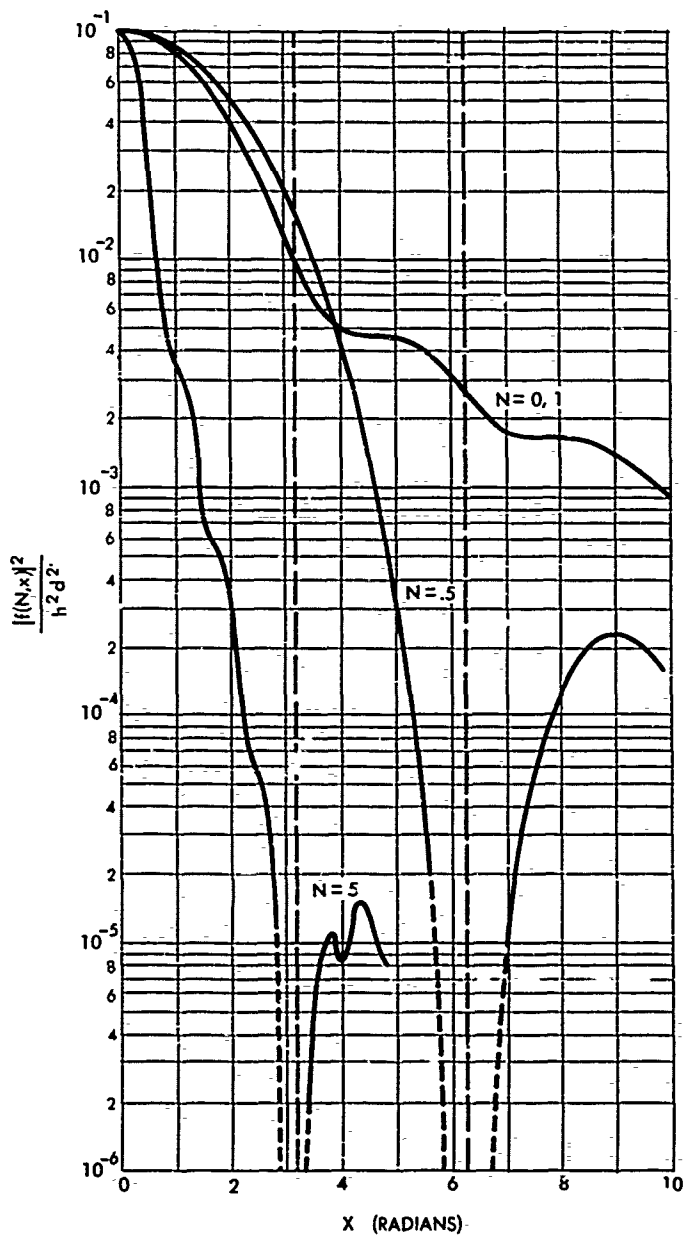


FIG. A-6.11 RELATIVE INTENSITY OF DIFFRACTION THROUGH A TRIANGULAR APERTURE

SECRET

SECRET

UNIVERSITY OF MICHIGAN

2255-12-T

APPENDIX B

COMPLEX DIELECTRICS IN DIHEDRAL AND TRIHEDRAL REFLECTORS

B. 1 THE PROBLEM

The fields scattered by objects constructed of materials of infinite conductivity have been investigated rather extensively by means of the physical optics approximation for objects whose characteristic dimensions are much greater than λ , the wavelength of the incident radiation. The main purpose of this appendix is to study the effect of finite conductivity in the case of dihedral and trihedral corner reflectors when use is made of an approximation analogous to the usual physical optics approximation as applied to perfect conductors.

B. 2 BASIC THEORETICAL CONSIDERATIONS

In Appendix A the basic theory behind the physical optics procedures was sketched to an extent adequate for the work in that appendix. However, to make clear how the effects of the dielectric constants of the scatterers enter the theory, a somewhat more detailed description is necessary.

The exact solution of Maxwell's equations in a closed region V containing no sources can be expressed as an integral over the surface S with unit outward normal \hat{n} bounding the region V . The fields are given by Stratton (Ref. 16, p. 466), as

$$\vec{H} = \frac{1}{4\pi} \int_S [i\omega\epsilon(\hat{n} \times \vec{E})\phi - (\hat{n} \times \vec{H}) \times \nabla\phi - (\hat{n} \cdot \vec{H}) \nabla\phi] dS, \quad (\text{B. 2-1})$$

$$\vec{E} = -\frac{1}{4\pi} \int_S [i\omega\mu(\hat{n} \times \vec{H})\phi + (\hat{n} \times \vec{E}) \times \nabla\phi + (\hat{n} \cdot \vec{E}) \nabla\phi] dS, \quad (\text{B. 2-2})$$

SECRET

SECRET

UNIVERSITY OF MICHIGAN

2255-12-T

where ϵ and μ are the dielectric constant (inductive capacity) and magnetic permeability of the medium filling V , the medium being assumed homogeneous, isotropic, and of zero conductivity. In all cases of interest here this medium may be considered to be free space. The above expression is for a time-periodic field of frequency ω ($e^{-i\omega t}$ time dependence) and ϕ is the Green's function $\phi = e^{ikr}/r$.

In actual applications the exact \vec{E} and \vec{H} fields on the surface S are generally not known so that it is necessary to approximate them. Before making any approximations however, it should be noted that the above surface integrals reduce to integrals over the surface of the scattering bodies only. To see this we consider scattering by a surface S_1 . To find the field at an arbitrary point P by applying Equations (B.2-1) and (B.2-2) we have to enclose P in some region V bounded by S_1 and S_2 .

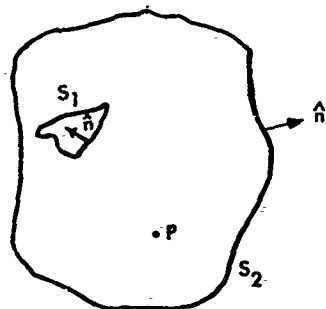


FIG. B-2.1 ILLUSTRATION OF VOLUME V
AND SURFACE S_1 AND S_2

B-2

SECRET

SECRET

UNIVERSITY OF MICHIGAN

2255-12-T

Then

$$\vec{H}(P) = \int_{S_1 + S_2} \quad (B.2-3)$$

where the integrand is that given in Equation (B.2-1). Since we are interested only in the scattered field at P we write the total field as the sum of an incident and a scattered field:

$$\vec{H}_{Tot} = \vec{H}_{Inc} + \vec{H}_{Sc}.$$

Then Equation (B.2-3) becomes

$$\vec{H}_{Inc}(P) + \vec{H}_{Sc}(P) = \int_{S_1 + S_2} (Inc + Sc). \quad (B.2-4)$$

If S_1 is an imaginary surface--i. e. not a real scattering body--then

$$\vec{H}_{Inc}(P) = \int_{S_1 + S_2} Inc. \quad (B.2-5)$$

If in particular there is no surface S_1 we get

$$\vec{H}_{Inc} = \int_{S_2} Inc. \quad (B.2-6)$$

Hence, combining Equations (B.2-5) and (B.2-6) we get

$$\int_{S_1} Inc = 0 \quad (B.2-7)$$

SECRET

UNIVERSITY OF MICHIGAN

2255-12-T

for a point P outside of S_1 . Hence Equation (B. 2-4) becomes

$$\vec{H}_{Sc}(P) = \int_{S_1} (Sc) + \int_{S_2} (Sc). \quad (B. 2-8)$$

If S_2 is chosen to be a sphere with arbitrarily large radius R (about the scattering body) then, since the scattered field falls off as $\frac{1}{R}$ (conservation of energy), the integral over S_2 approaches a constant (independent of the point P) which can be shown to be zero if only radiation fields are considered. This gives the final result

$$\vec{H}_{Sc}(P) = \int_{S_1} (Sc). \quad (B. 2-9)$$

It is from this result that the effect of finite conductivity in the physical optics approximation will be obtained.

As mentioned before it is necessary to make some approximations to the fields on the surface of the scatterer in order to apply Equation (B. 2-9) since the exact surface fields are not known. The simplest approximation is that used in physical optics as adapted to electromagnetic scattering problems by Spencer (Ref. 17) for perfect conductors in which one assumes that the fields on the surface (S_1) may be computed by geometric optics (Ref. 15). This approximation leads to discontinuities in \vec{E} and \vec{H} in Equation (B. 2-1), which necessitates some modification of the theory since the integral in Equation (B. 2-1) yields a solution of Maxwell's equations provided $(\hat{n} \times \vec{E})$, $(\hat{n} \times \vec{H})$, $(\hat{n} \cdot \vec{E})$ and $(\hat{n} \cdot \vec{H})$ (which may be interpreted as fictitious currents and charges) satisfy a continuity equation. Hence in order that the physical optics integral yield a solution of Maxwell's equation it is necessary to add to the surface integrals of B. 2-1 certain line integrals along the discontinuities in the geometric optics approximation (Ref. 16, p. 468). The integrands in the line integrals are linear in \vec{E} and \vec{H} . In the case of perfect conductors these additional terms vanish when Equation (B. 2-1) is used (but not for Equation B. 2-2) because the additional line integral corresponds to "magnetic charges" to balance the "magnetic current" $\hat{n} \times \vec{E}$ which is 0.

SECRET

SECRET

UNIVERSITY OF MICHIGAN

2255-12-T

The justification for the assumption of the geometric optics field on S_1 in the case of a square plate of side length l may be stated roughly. When $l \rightarrow \infty$ while λ remains finite, the geometric optics solution is exact; hence for l finite but $l \gg \lambda$ and $l \gg d$, the perpendicular distance from the plate to the point of observation, one would quite reasonably expect the geometric optics solution to be a very good approximation for $\xi \ll l/2$, where ξ is distance from the center of the plate. Furthermore as $d \rightarrow 0$, the region of validity will increase (but still be questionable near the edges). One then hopes that most of the contribution to the integral comes from the central region. As a matter of fact, the main contribution to the integral for back scattering at normal incidence does come from a central region, this also being true bistatically (normal incidence) for angles within the main lobe of the diffraction pattern, but for larger angles, the edge contribution increases; hence for these larger angles, the approximation becomes more doubtful.

Since the discussion of the previous paragraph applies whether or not the plate is a perfect conductor, the obvious extension of the physical optics approximation to non-perfectly conducting materials is to put the geometric optics fields into the right hand side of Equation (B.2-9) and, to add in the appropriate line integrals. It will suffice here to state the result obtained by this procedure. As in the case of perfectly conducting trihedral and dihedral corner reflectors, the scattered field in the geometric optics approximation consists of a number of beams of radiation which may be thought of as caused by reflections from perfectly conducting plates, normal to and of the same cross-sectional shape as the respective beams. Diffraction from each of these plates may then be handled by Equation (B.2-9) (or in the more explicit form of Equation B.2-9 for flat plates given by Equation A.1-1).

The approximate resulting field is obtained by adding the fields diffracted by the individual equivalent flat plates. The situation differs from the perfectly conducting case in that the geometric optics field incident on each equivalent flat plate is a function of the reflection

SECRET

UNIVERSITY OF MICHIGAN

2255-12-T

coefficients at the reflecting surfaces. Since these coefficients are not unity for finite conductivity but are functions of the angles of incidence of the rays and of the orientation of the \vec{E} and \vec{H} vectors with respect to the planes of incidence, the incident fields differ in phase and amplitude for each equivalent plate. In contrast, for the infinite conductivity case, the incident fields are all the same.

There are some interesting aspects associated with corners of finite conductivity. For infinitely conducting dihedrals and trihedrals the walls of which are at right angles, the geometric optics solution is the exact solution when the dimensions of the walls are infinite, whereas this is not generally true for finite conductivity. Consider for example the dihedral shown in Figure B.2-2 where medium (1) is air and (2) is some homogeneous material for which ϵ, μ, σ are finite.

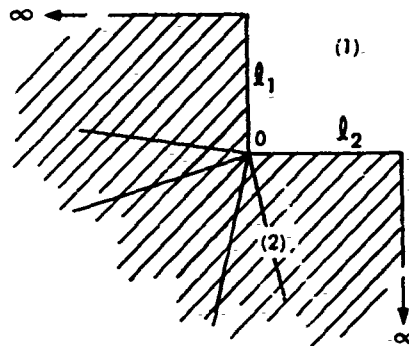


FIG. B-2.2 DIHEDRAL OF FINITE CONDUCTIVITY

The geometric optics solution within medium (2) (the transmitted beams) will be discontinuous along four rays through 0, and is therefore not a solution to Maxwell's equations in this region, even for $l_1 = l_2 = \infty$. Hence one cannot conclude that the geometrical optics solution in region (1) is the exact solution in that region, in spite of

SECRET

UNIVERSITY OF MICHIGAN

2255-12-T

the fact that it is a solution of Maxwell's equations in region (1) and, with the geometric optics solution in region (2), satisfies the boundary conditions across the dihedral surfaces. As far as we know, the exact solution for this problem has not been obtained. In the corresponding trihedral problem, the geometric optics solution is not a solution of Maxwell's equations in either region (1) or (2). (It is shown in Appendix B.4 that the geometric optics fields associated with the triply reflected rays are different for rays striking the three walls in different orders, leading to discontinuities in the field in region 1.) Incidentally, such difficulties do not disappear for perfectly-conducting corner reflectors when the angles between walls are not 90 degrees; the geometric optics field is again discontinuous.

B.3 DIHEDRAL REFLECTORS

Consider the dihedral formed by two planes intersecting at right angles as shown in Figure B.3-1. The shaded areas, regions (1) and (2), represent homogeneous media separated by a boundary B^2 . The region (0) is taken to be free space. The direction of incident radiation (a plane wave) is indicated by the wave vector \vec{k} lying in the x_1 - x_2 plane (the plane of incidence). Assuming that reflections from either plane obey the laws of reflection from a plane interface bounding two infinite media, we seek the fields associated with the rays traveling in the direction $\vec{k}_r = -\vec{k}$ (the geometric optics approximation). In terms of these fields, the physical-optics approximation is then obtained.

¹Except, in the dihedral, for angles of $90^\circ/n$, $n=1,2,3,\dots$ (Ref. 10).

²Boundary B is assumed to be such that no energy is reflected (geometrically) from it back into the region $x_1 > 0$, $x_2 > 0$. Also, the restriction that regions (1) and (2) be homogeneous may be weakened (e.g., Example 2, B.3). The essential restriction which we assume is such that the exact geometrical optics solution in the region (0) be characterized by a pair of reflection coefficients at each plane.

SECRET

SECRET

UNIVERSITY OF MICHIGAN

2255-12-T

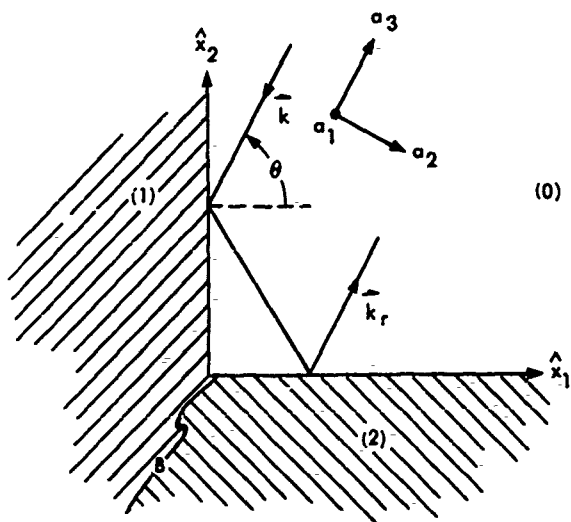


FIG. B-3.1 DIHEDRAL WITH SIDES OF DIFFERENT MATERIALS

The property that makes this problem simple is the following: if the incident wave is polarized perpendicular to the plane of incidence (the incident electric vector, \vec{E}^i , parallel to $\hat{x}_1 \times \hat{x}_2 = \hat{a}_3$, where \hat{x}_1 and \hat{x}_2 are unit vectors as shown), then the electric vector will be parallel to \hat{a}_1 after each reflection; similarly, for "parallel" polarization of the incident wave (the incident magnetic field, \vec{H}^i , parallel to \hat{a}_1), the magnetic vector will always be parallel to \hat{a}_1 . Letting \vec{E}^0 , \vec{H}^0 , \vec{E}^r , \vec{H}^r be the amplitudes of the incident and doubly reflected fields respectively, it follows that

$$\left. \begin{aligned} \vec{E}^r &= \rho_{\perp}^{(1)}(\theta) \rho_{\perp}^{(2)}\left(\frac{\pi}{2} - \theta\right) \vec{E}^0 \quad \text{for perpendicular polarization,} \\ \vec{H}^r &= \rho_{\parallel}^{(1)}(\theta) \rho_{\parallel}^{(2)}\left(\frac{\pi}{2} - \theta\right) \vec{H}^0 \quad \text{for parallel polarization,} \end{aligned} \right\} \text{(B.3-1)}$$

SECRET

SECRET

UNIVERSITY OF MICHIGAN

2255-12-T

where $\rho_{\perp}^{(j)}$, $\rho_{\parallel}^{(j)}$ are the reflection coefficients¹ for wall j. Where the regions (1) and (2) are homogeneous (Ref. 16 pp. 493, 494).

$$\rho_{\perp}^{(j)}(\theta) = \frac{\mu_j k \cos \theta - \mu_0 \sqrt{\kappa_j^2 - k^2 \sin^2 \theta}}{\mu_j k \cos \theta + \mu_0 \sqrt{\kappa_j^2 - k^2 \sin^2 \theta}}$$

$$\rho_{\parallel}^{(j)}(\theta) = \frac{\mu_0 \kappa_j^2 \cos \theta - \mu_j k \sqrt{\kappa_j^2 - k^2 \sin^2 \theta}}{\mu_0 \kappa_j^2 \cos \theta + \mu_j k \sqrt{\kappa_j^2 - k^2 \sin^2 \theta}}$$

(B.3-2)

$$\kappa_j^2 = \omega^2 \mu_j \epsilon_j + i\omega \mu_j c_j,$$

where

μ_j = magnetic permeability of medium j

ϵ_j = dielectric constant of medium j

c_j = conductivity of medium j

$$k = \frac{2\pi}{\lambda} = \kappa_0.$$

θ = angle of incidence measured from the normal.

¹The reflection coefficients are defined in terms of single plane reflections as follows. When the incident wave is polarized with the electric vector perpendicular to the plane of incidence, the reflected electric vector, \vec{E}^r is parallel to the incident electric vector, \vec{E}^i , so that \vec{E}^r is a scalar times \vec{E}^i , this scalar quantity being ρ_{\perp} : $\vec{E}^r = \rho_{\perp} \vec{E}^i$ for perpendicular polarization. Similarly, the reflection coefficient ρ_{\parallel} is defined by $\vec{H}^r = \rho_{\parallel} \vec{H}^i$ for parallel polarization of the electric vector.

SECRET

SECRET

UNIVERSITY OF MICHIGAN

2255-12-T

It should be noted that planes perpendicular to \vec{k} are planes of constant phase for all doubly reflected rays. Further, the reflected amplitudes are the same for all rays, so that this assumption of "ray tracing" leads to a reflected plane wave for each polarization.

For arbitrary polarization, we may write

$$\vec{E}^0 = \hat{a}_1 E_{01} + \hat{a}_2 E_{02} \quad (\text{B.3-3})$$

where

$$\hat{a}_1 = \frac{\vec{k} \times \hat{x}_1}{|\vec{k} \times \hat{x}_1|}, \quad \hat{a}_2 = \hat{a}_3 \times \hat{a}_1, \quad \hat{a}_3 = -\frac{\vec{k}}{k} \quad (\text{B.3-4})$$

It follows that after two reflections

$$\vec{E}^r = R_{\perp} E_{01} \hat{a}_1 - R_{\parallel} E_{02} \hat{a}_2 \quad (\text{B.3-5})$$

where

$$R_{\perp} = \rho_{\perp}^{(1)}(\theta_1) \rho_{\perp}^{(2)}\left(\frac{\pi}{2} - \theta_1\right) \quad (\text{B.3-6})$$

Note that \vec{E}^r is not parallel to \vec{E}^0 except when $\vec{E}^0 = E_{01} \hat{a}_1$ or $E_{02} \hat{a}_2$, this being true even in the limit of infinite conductivity where $R_{\perp} = R_{\parallel} = 1$. Furthermore, the reflected wave will be elliptically polarized in general.

The physical optics cross-section (for back scattering) is given, in accordance with the discussion of Section B. 2, by

$$\sigma = \frac{4\pi}{\lambda^2} A^2 \left| \frac{\vec{E}^r}{E^0} \right|^2$$

SECRET

UNIVERSITY OF MICHIGAN

2255-12-T

where A is the area perpendicular to \vec{k} occupied by all the doubly reflected rays.¹

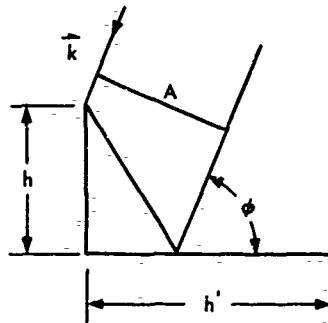


FIG. B-3.2 DIHEDRAL GEOMETRY

Clearly

$$\left| \frac{E^r}{E_0} \right|^2 = \frac{|R_{\perp}|^2 E_{01}^2 + |R_{\parallel}|^2 E_{02}^2}{E_{01}^2 + E_{02}^2} \quad (\text{B.3-7})$$

The reflection coefficients R_{\perp} , R_{\parallel} have been given in the literature as a function of ϕ for walls of various materials (Ref. 2, Interim Report No. 3).

¹Explicitly, $A=2h L \cos \phi$ (Fig. B.3-2), where L is the length perpendicular to the paper and $h \leq h' \tan \phi$.

SECRET

UNIVERSITY OF MICHIGAN

2255-12-T

The following examples, which were not found in the literature, are of interest in the specific problems with which this contract is concerned. The results of Example 1 were used in obtaining Polar Diagrams 50-57 of Section II.

Example 1: Two Dielectric Walls with the Same Dielectric Constant.

We consider non-magnetic materials so that $\mu_1 = \mu_2 = \mu_0$, the magnetic permeability of free space. Since the two walls are taken to be of the same materials, $\kappa_1^2 = \kappa_2^2 = \kappa^2$; writing $n^2 = \kappa^2 / k^2$, Equation (B.3-2) becomes

$$\rho_{\perp}(\theta) = \frac{\cos \theta - \sqrt{n^2 - \sin^2 \theta}}{\cos \theta + \sqrt{n^2 - \sin^2 \theta}}$$

$$\rho_{\parallel}(\theta) = \frac{n^2 \cos \theta - \sqrt{n^2 - \sin^2 \theta}}{n^2 \cos \theta + \sqrt{n^2 - \sin^2 \theta}}$$

If the material is taken to be a perfect, lossless dielectric, n^2 is real and equal to the ratio, ϵ' , of the dielectric constant to that of free space. The products

$$R_{\perp}(\phi) = \rho_{\perp}(\phi) \rho_{\perp}\left(\frac{\pi}{2} - \phi\right)$$

and

$$R_{\parallel}(\phi) = \rho_{\parallel}(\phi) \rho_{\parallel}\left(\frac{\pi}{2} - \phi\right)$$

have been plotted as functions of ϕ for $\epsilon' = 2, 4, 6, 8$ (Figs. B.3-3 and B.3-4). Note that $R_{\parallel}(\phi)$ always has two zeroes (at the Brewster angles, $\phi_b = \tan^{-1} \sqrt{\epsilon'}$, and $\frac{\pi}{2} - \phi_b$).

B-12

SECRET

SECRET

UNIVERSITY OF MICHIGAN

2255-12-T

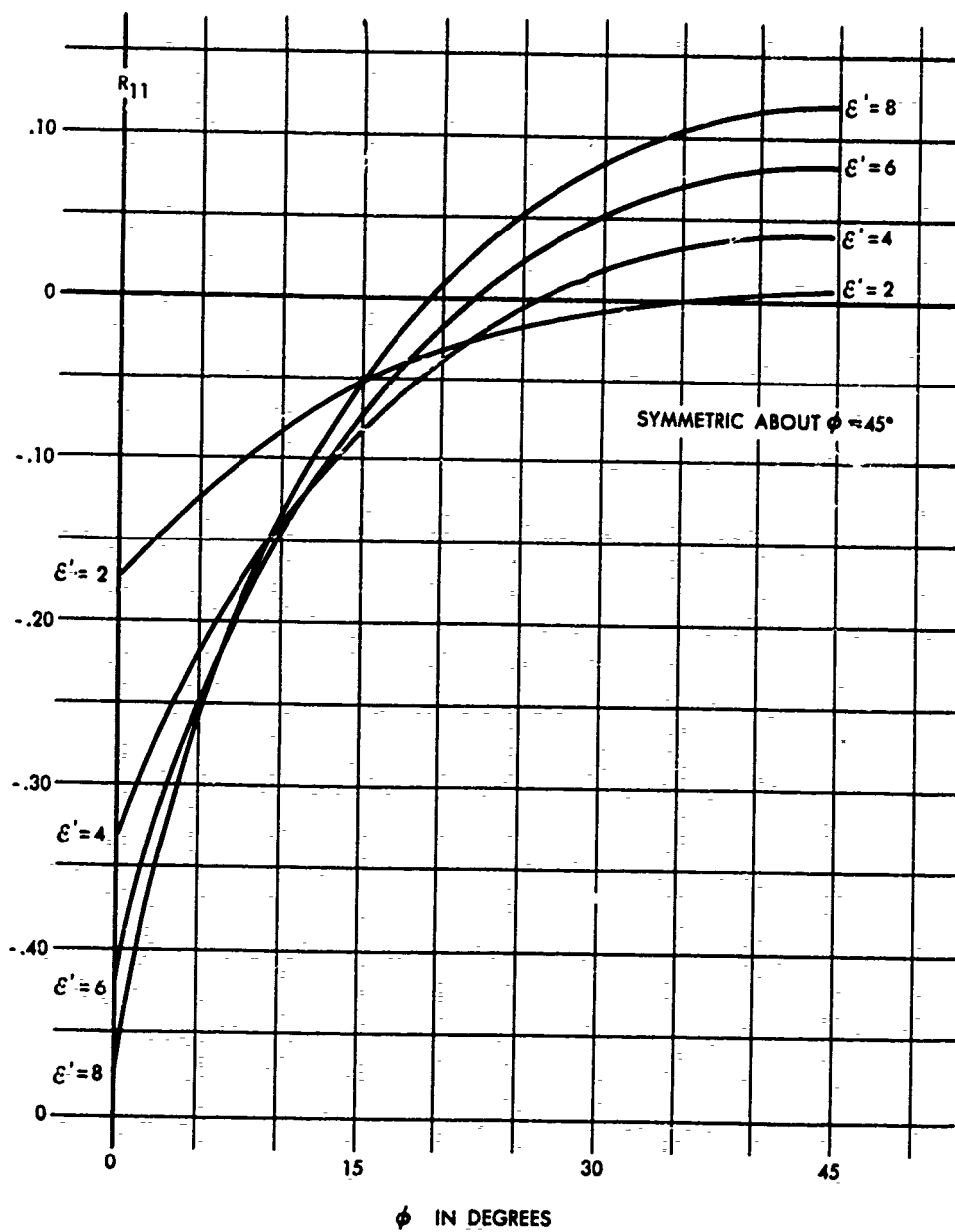


FIG. B-3.3 REFLECTION COEFFICIENTS FOR TWO PERPENDICULAR DIELECTRIC WALLS OF THE SAME DIELECTRIC CONSTANT (CF. EX. 1) PARALLEL POLARIZATION

B-13

SECRET

SECRET

UNIVERSITY OF MICHIGAN

2255-12-T

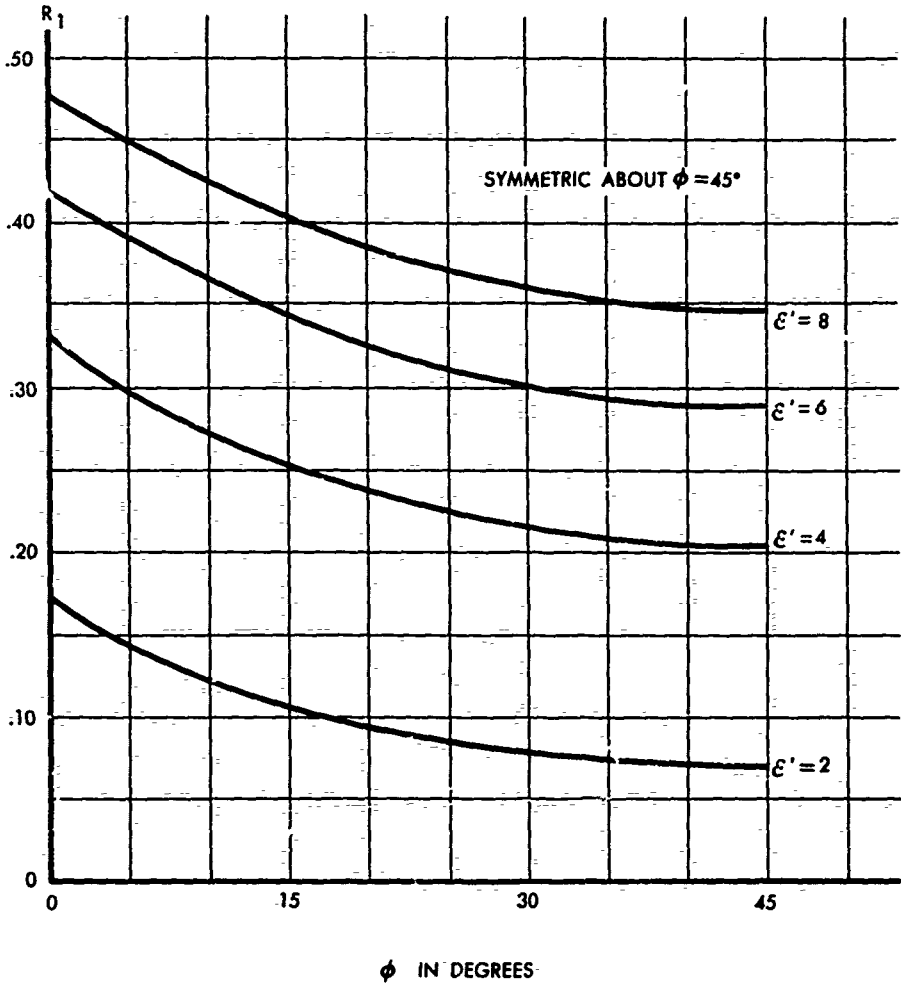


FIG. B-3.4 REFLECTION COEFFICIENTS FOR TWO PERPENDICULAR DIELECTRIC WALLS OF THE SAME DIELECTRIC CONSTANT (CF. EX. 1) PERPENDICULAR POLARIZATION

SECRET

UNIVERSITY OF MICHIGAN

2255-12-T

It is of interest to determine how $R_{11}(\theta)$ behaves at the Brewster angles when the dielectric is not lossless, in which case, n^2 is a complex number. Writing

$$n^2 = \alpha_1 + i\beta_1$$

we shall compute $R_{11}(\theta)$ assuming $(\beta_1/\alpha_1)^2 \ll 1$ and α_1 is roughly between 2 and 10. Putting

$$\sqrt{n^2 - \sin^2 \theta} = \alpha_2 + i\beta_2,$$

it is easy to show that

$$R_{11}(\theta) = \frac{(\alpha_1^2 + \beta_1^2) \cos^2 \theta - (\alpha_2^2 + \beta_2^2) + 2i \cos \theta (\beta_1 \alpha_2 - \beta_2 \alpha_1)}{(\alpha_1^2 + \beta_1^2) \cos^2 \theta + 2 \cos \theta (\alpha_1 \alpha_2 + \beta_1 \beta_2) + \alpha_2^2 + \beta_2^2}.$$

Also

$$\alpha_2 = \sqrt{\frac{\alpha_1 - \sin^2 \theta}{2}} \left[\sqrt{1 + \frac{\beta_1^2}{(\alpha_1 - \sin^2 \theta)^2}} + 1 \right]^{\frac{1}{2}}$$

$$\beta_2 = \sqrt{\frac{\alpha_1 - \sin^2 \theta}{2}} \left[\sqrt{1 + \frac{\beta_1^2}{(\alpha_1 - \sin^2 \theta)^2}} - 1 \right]^{\frac{1}{2}}$$

SECRET

UNIVERSITY OF MICHIGAN

2255-12-T

Now $\sin^2 \theta_b = a_1 / (a_1 + 1)$ so that $a_1 - \sin^2 \theta_b = a_1^2 / (a_1 + 1)$. Hence

$$\left(\frac{\beta_1}{a_1 - \sin^2 \theta_b} \right)^2 = \left(\frac{a_1 + 1}{a_1} \right)^2 \cdot \left(\frac{\beta_1}{a_1} \right)^2$$

Under our assumptions then,

$$a_2 \cong \sqrt{a_1 - \sin^2 \theta}$$

$$\beta_2 \cong \frac{1}{2 \sqrt{a_1 - \sin^2 \theta}}$$

At $\theta = \theta_b$

$$a_2 \cong \frac{1}{\sqrt{a_1 + 1}}, \quad \beta_2 \cong \frac{\sqrt{a_1 + 1}}{2 a_1} \beta_1$$

Using these approximations we obtain

$$\rho_{11}(\theta_b) \cong i \left\{ \frac{1 - a_1}{4 a_1} \right\} \left\{ \frac{\beta_1}{a_1} \right\}$$

In the notation of Section B. 5, $a_1 = \epsilon'$, the real part of the dielectric constant relative to vacuum and $-\beta_1/a_1 = \tan \delta$, the loss tangent. Hence

$$\left| R_{11}(\theta) \right|^2 = \frac{1}{16} \left\{ \left(\frac{\epsilon' - 1}{\epsilon'} \right)^2 \tan^2 \delta \right\} \left| \rho_{11} \left(\frac{\pi}{2} - \theta_b \right) \right|^2$$

In this approximation, $\rho_{11} \left(\frac{\pi}{2} - \theta_b \right)$ may be computed assuming no losses.

SECRET

UNIVERSITY OF MICHIGAN

2255-12-T

Example 2. A Dielectric Wall of Finite Dimensions on a Perfectly Conducting Plane of Infinite Extent

As discussed in Section B. 3, the "physical optics" cross-section is given by

$$\sigma = \frac{4\pi}{\lambda^2} A^2 \left| \frac{\vec{E}^r}{E^0} \right|^2$$

where \vec{E}^r is the geometric optics field propagating in the $-\vec{k}$ direction. It is interesting to note that since the exact solution to the electromagnetic problem of Figure B. 3-5 is the same as that for the image problem (in the upper half space) as shown in Figure B. 3-6, we see that the geometric optics solution is the exact solution to the problem in which h and depth $L \rightarrow \infty$. To compute E^r from Equation (B. 3-1), we have $\rho_{\perp}^{(2)} = -1$, $\rho_{\parallel}^{(2)} = 1$, and $\rho_{\perp}^{(1)}$ and $\rho_{\parallel}^{(1)}$ are given by the well-known expressions (Ref. 21) for reflection from an infinite plane slab of finite thickness¹; namely,

$$\rho_{\perp}^{(1)} = \frac{(r_{\perp}) (1 - F^2)}{1 - F^2 (r_{\perp})^2}, \quad (\text{B. 3-8})$$

where

$$F = e^{-iq},$$

$$q = \frac{2\pi a}{\lambda} \sqrt{\left(\frac{\kappa}{k}\right)^2 - \sin^2\theta},$$

¹This will be a good approximation for the finite slab provided $h \gg a \tan \theta$.

SECRET

UNIVERSITY OF MICHIGAN

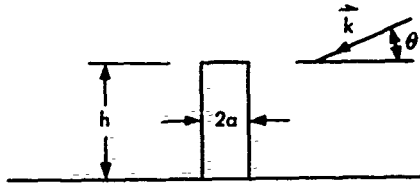


FIG. B-3.5 A DIELECTRIC WALL OF FINITE DIMENSIONS ON A PERFECTLY CONDUCTING PLANE OF INFINITE EXTENT

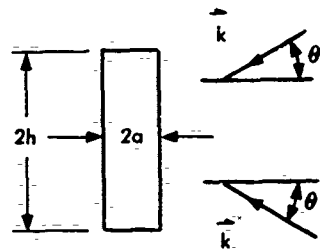


FIG. B-3.6 THE IMAGE PROBLEM

and r_{\perp} and r_{\parallel} are the special values of ρ_{\perp} and ρ_{\parallel} given by Equation (B.3-2) for a homogeneous medium. k is the propagation constant, $\sqrt{\omega^2 \mu \epsilon + i\omega\mu\sigma}$, for the slab.

Hence for the incident electric field, $\vec{E}^0 = \hat{a}_1 E_{01} + \hat{a}_2 E_{02}$, the physical optics cross-section is

$$\sigma = \frac{16\pi h^2 L^2 \cos^2 \theta}{\lambda^2} R^2, \quad (\text{B.3-9})$$

SECRET

UNIVERSITY OF MICHIGAN

2255-12-T

where

$$R^2 = \frac{|\rho_{\perp}|^2 |E_{01}|^2 + |\rho_{\parallel}|^2 |E_{02}|^2}{|\vec{E}_0|^2} \quad (B.3-10)$$

When the material of the slab is a perfect lossless dielectric ($c = 0$, $\epsilon = \epsilon^*$, $\mu = \mu_0$) and the incident wave is linearly polarized ($\vec{E}_{0i} = E_{0i}^*$),

$$R^2 = \frac{4 \sin^2 2q}{|E^0|^2} \left[\frac{r_{\perp}^2 E_{01}^2}{(1-r_{\perp}^2)^2 + 4r_{\perp}^2 \sin^2 2q} + \frac{r_{\parallel}^2 E_{02}^2}{(1-r_{\parallel}^2)^2 + 4r_{\parallel}^2 \sin^2 2q} \right] \quad (B.3-11)$$

We might point out that Equations (B.3-9) with (B.3-11) show that σ for $\vec{E}^0 = \hat{a}_1 E^0$ is always greater than σ for $\vec{E}^0 = \hat{a}_2 E^0$.

B.4 TRIHEDRAL REFLECTORS

We shall trace triply reflected rays under the same assumptions as to the reflections from each plane that were made in the case of the dihedral. Referring to Figure B.4-1, \hat{x}_i ($i=1, 2, 3$) are unit vectors perpendicular respectively to the three reflecting surfaces (i), each characterized by the constants ϵ_i , μ_i , c_i . We take the incident propagation vector to be

$$\vec{k} = k_1 \hat{x}_1 + k_2 \hat{x}_2 + k_3 \hat{x}_3 \quad (B.4-1)$$

SECRET

UNIVERSITY OF MICHIGAN

2255-12-T

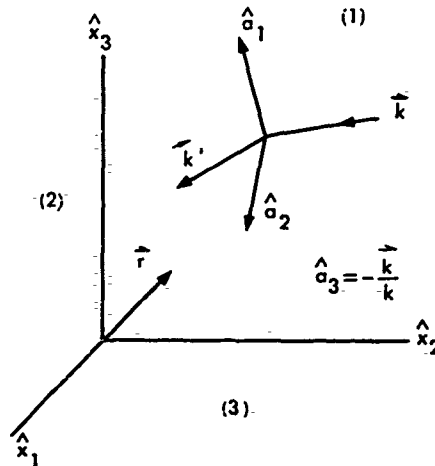


FIG. B-4.1 DEFINITION OF VECTORS APPEARING
IN THE TRIHEDRAL PROBLEM

Since at any single reflection, the propagation vector changes only by reversal in sign of the component normal to the reflecting plane, it follows simply that the propagation vector after three reflections (taken in any order) is $-\vec{k}$. Further, the angle of incidence made with any plane (j) is independent of the order of the reflections (e. g. if θ_1 is the angle of incidence made with plane (1), then for the rays striking this plane first, $\cos \theta_1 = -k_1/k$; since for rays striking plane (2) or (3) or both, before striking (1) the \hat{x}_1 component of the propagation vectors is not changed before striking (1), θ_1 will be the same for all rays). This enables us to define a single pair of reflection coefficients for each wall. We write

$$\rho_{||}^{(i)} = \xi_i, \quad \rho_{\perp}^{(i)} = \eta_i, \quad i = 1, 2, 3. \quad (B.4-2)$$

SECRET

UNIVERSITY OF MICHIGAN

2255-12-T

The complexity in this problem lies in the facts that if the incident \vec{E} (or \vec{H}) is parallel to the first reflecting plane, it will not be parallel to the succeeding planes, and the magnitudes of the two components of \vec{E} (or \vec{H}) will be changed by different amounts on any single reflection. The triply reflected fields are generally different for the six different rays given by the permutations, (123), (132), of i, j, k, where (ijk) denotes the ray striking planes (i), (j) and (k) in that order). The work is simplified considerably by the fact (to be shown) that the scattering matrix for ray (kji) is simply the transpose of that for (ijk).

These geometric optics results are then used to compute the reflected field in a physical optics approximation. Equations (B. 4-65) and (B. 4-71) give (in this approximation) the electric field vector and the radar cross-section from three mutually perpendicular walls of arbitrary shape in terms of the electrical properties of the walls, the areas (perpendicular to the incident direction of propagation) occupied by the different types of geometrically reflected rays, and the incident propagation vector. The formulas are evaluated explicitly for the special case where the three walls are made of the same material and form a symmetrical¹ corner reflector. The incident radiation is in the direction of symmetry, $k_1 = k_2 = k_3$. It is found to the accuracy of the present theory, that the back scattered field is identically zero independent of polarization when the material is a perfect dielectric with $\epsilon' = 8/3$. This is due, not to losses by transmission, but to interference between the six geometrically reflected rays.

B. 4.1 Scattering Matrix for a Single Plane Reflection

Considering the reflection from plane (1) for the incident propagation vector \vec{k} , we have

$$\vec{k}' = -k_1 \hat{x}_1 + k_2 \hat{x}_2 + k_3 \hat{x}_3 \quad . \quad (\text{B. 4-3})$$

¹That is, a corner reflector which is invariant under rotations of integral multiples of 120 degrees about the axis $\vec{r} = \hat{x}_1 + \hat{x}_2 + \hat{x}_3$.

SECRET

SECRET

UNIVERSITY OF MICHIGAN

2255-12-T

Since the incident electric field, $\vec{E}^i(\vec{r})$ is perpendicular to \vec{k} , we may write

$$\vec{E}^i(\vec{r}) = e^{i\vec{k} \cdot \vec{r}} (E_{01} \hat{a}_1 + E_{02} \hat{a}_2)^i, \quad (\text{B.4-4})$$

where the basis formed by the \hat{a}_i is defined by

$$\hat{a}_1 = \frac{\vec{k} \times \hat{x}_1}{|\vec{k} \times \hat{x}_1|}, \quad \hat{a}_2 = \hat{a}_3 \times \hat{a}_1, \quad \hat{a}_3 = -\frac{\vec{k}}{k}; \quad (\text{B.4-5})$$

(\hat{a}_1 and \hat{a}_2 are perpendicular and parallel, respectively, to the plane of incidence). If the electric field in the reflected ray is written

$$\vec{E}^r(\vec{r}) = e^{i\vec{k}' \cdot \vec{r}} (E_1^r \hat{a}_1 + \vec{E}^{r'}),$$

where $\hat{a}_1 \cdot \vec{E}^{r'} = 0$, then

$$E_1^r = \eta_1 E_{01}.$$

Further, if $E_{01} = 0$, the reflected \vec{H} would be, omitting the phase factor,

$$\vec{H}^{r'} = H_1^{r'} \hat{a}_1 = \xi_1 H_{01} \hat{a}_1 \quad (\text{for incident magnetic field } \vec{H}_0 = H_{01} \hat{a}_1). \text{ But}$$

from Maxwell's equations

$$\vec{E}^{r'} = -\frac{1}{\omega \epsilon} \hat{k}' \times \vec{H}^{r'} = -\frac{\xi_1 H_{01}}{\omega \epsilon} \hat{k}' \times \hat{a}_1, \quad (\hat{k}' = \vec{k}'/k);$$

where ϵ is for free space.

¹The time factor, $e^{-i\omega t}$, has been deleted.

SECRET

UNIVERSITY OF MICHIGAN

2255-12-T

Similarly,

$$E_{02} = \frac{H_{01} k}{\omega \epsilon}$$

Thus

$$\vec{E}^{r'} = -\xi_1 E_{02} \hat{k}' \times \hat{a}_1.$$

Writing

$$\hat{a}_1 \times \hat{k}' = a_2 \hat{a}_2 + a_3 \hat{a}_3,$$

we have

$$\vec{E}^r(\vec{r}) = e^{i\vec{k}' \cdot \vec{r}} (\eta_1 E_{01} \hat{a}_1 + \xi_1 a_2 E_{02} \hat{a}_2 + \xi_1 a_3 E_{02} \hat{a}_3). \quad (\text{B.4-6})$$

By direct computation

$$a_2 = \hat{a}_2 \cdot \hat{a}_1 \times \hat{k}' = -\hat{k}' \cdot \hat{a}_3 = \frac{\beta_1^2 - k_1^2}{k^2}$$

$$a_3 = \hat{a}_3 \cdot \hat{a}_1 \times \hat{k}' = \hat{k}' \cdot \hat{a}_2 = -2 k_1 \beta_1 / k^2,$$

where

$$\beta_1^2 = k^2 - k_1^2. \quad (\text{B.4-7})$$

SECRET

UNIVERSITY OF MICHIGAN

2255-12-T

The amplitudes, $\vec{E}^r = e^{-ik \cdot \vec{r}} \vec{E}^r(\vec{r})$ and $\vec{E}^0 = e^{-ik \cdot \vec{r}} \vec{E}^0(\vec{r})$, may be related by an operator S:

$$\vec{E}^r = S \vec{E}^0. \tag{B.4-8}$$

The representation, $S^{(a)}$, of S in the \hat{a} basis, is seen from Equation (B.4-6) to be the matrix

$$S^{(a)} = \begin{vmatrix} \eta_1 & 0 & A \\ 0 & \xi_{12}^a & B \\ 0 & \xi_{13}^a & C \end{vmatrix} \tag{B.4-9}$$

where A, B, and C are arbitrary¹. In other words, Equation (B.4-6) may be written

$$\begin{vmatrix} E_1^{r^a} \\ E_2^{r^a} \\ E_3^{r^a} \end{vmatrix} = \begin{vmatrix} \eta_1 & 0 & A \\ 0 & \xi_{12}^a & B \\ 0 & \xi_{13}^a & C \end{vmatrix} \begin{vmatrix} E_{01} \\ E_{02} \\ 0 \end{vmatrix}, \tag{B.4-10}$$

where $E_i^{r^a}$ are the components of \vec{E}^r in the \hat{a} basis.

¹This arbitrariness follows from the fact that $\hat{a}_3 \cdot \vec{E}^0 = 0$.

SECRET

UNIVERSITY OF MICHIGAN

2255-12-T

The representation in the \hat{x} -basis of S , $S^{(x)}$, is obtained from the relation

$$S^{(x)} = U^{-1} S^{(a)} U \quad (\text{B. 4-11})$$

where U is the matrix whose elements are given by

$$U_{ij} = \hat{a}_i \cdot \hat{x}_j \quad (\text{B. 4-12})$$

The inverse of U , U^{-1} , is the transpose of U ; that is

$$(U^{-1})_{ij} = U_{ji} \quad (\text{B. 4-13})$$

Writing Equation (B. 4-5) in the form

$$\begin{aligned} \hat{a}_1 &= \frac{1}{\beta_1} (k_3 \hat{x}_2 - k_2 \hat{x}_3) \\ \hat{a}_2 &= \frac{1}{k\beta_1} (\beta_1^2 \hat{x}_1 - k_1 k_2 \hat{x}_2 - k_1 k_3 \hat{x}_3) \\ \hat{a}_3 &= -\frac{k}{k} \end{aligned} \quad (\text{B. 4-14})$$

we see that

$$\bar{U} = \begin{vmatrix} 0 & k_3/\beta_1 & -k_2/\beta_1 \\ \beta_1/k & -k_1 k_2/k\beta_1 & -k_1 k_3/k\beta_1 \\ -k_1/k & -k_2/k & -k_3/k \end{vmatrix} \quad (\text{B. 4-15})$$

SECRET

UNIVERSITY OF MICHIGAN

2255-12-T

Choosing $A = B = C = 0$ and carrying out the multiplications indicated in Equation (B.4-11), we find that

$$\vec{S}^{(x)} = \begin{pmatrix} \frac{\beta_1^2}{k^2} \xi_1 & -\frac{k_1 k_2}{k^2} \xi_1 & -\frac{k_1 k_3}{k^2} \xi_1 \\ \frac{k_1 k_2}{k^2} \xi_1 & \frac{k_3^2}{\beta_1^2} \eta_1 - \left(\frac{k_1 k_2}{k \beta_1} \right)^2 \xi_1 & -\frac{k_2 k_3}{\beta_1^2} \left(\eta_1 + \frac{k_1^2}{k^2} \xi_1 \right) \\ \frac{k_1 k_3}{k^2} \xi_1 & -\frac{k_2 k_3}{\beta_1^2} \left(\eta_1 + \frac{k_1^2}{k^2} \xi_1 \right) & \frac{k_2^2}{k_1^2} \eta_1 - \left(\frac{k_1 k_3}{k \beta_1} \right)^2 \xi_1 \end{pmatrix} \cdot$$

(B.4-16)

An important property of this matrix is the following.

If

$$\vec{k}_{\text{rev}} \equiv -\vec{k} = k_1 \hat{x}_1 - k_2 \hat{x}_2 - k_3 \hat{x}_3 \tag{B.4-17}$$

then

$$\vec{S}^{(x)}(\vec{k}_{\text{rev}}) = \widetilde{\vec{S}^{(x)}}(\vec{k}) \tag{B.4-18}$$

where $\widetilde{\vec{S}^{(x)}}$ is the transpose of $\vec{S}^{(x)}$; that is

$$\vec{S}^{(x)}(\vec{k}_{\text{rev}})_{ij} = \vec{S}^{(x)}(\vec{k})_{ji} .$$

\vec{k}_{rev} is the incident propagation vector for the ray traveling in the opposite direction. Hence from this, Equation B.4-18, and the fact that

SECRET

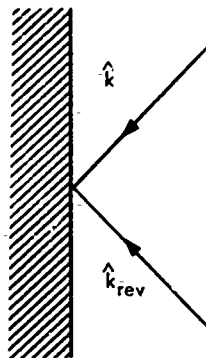
UNIVERSITY OF MICHIGAN

2255-12-T

for any two matrices A and B,

$$\tilde{A}B = \tilde{B}A,$$

it follows that the scattering matrix for a ray undergoing a series of plane reflections is simply the transpose of that for the ray traversing the path in the reverse direction.



B.4-2 Scattering Matrices for Triply Reflected Rays

We consider first the ray (123) as shown in Figure (B.4-2). If we denote the scattering matrices (x-representation) for the (1), (2) and (3) planes by $S_1^{(x)}$, $S_2^{(x)}$ and $S_3^{(x)}$, respectively, then the matrix $\mathcal{L}_{(123)}^{(x)}$ connecting the triply reflected ray with the incident ray will be given by

$$\mathcal{L}_{(123)}^{(x)} = S_3^{(x)} S_2^{(x)} S_1^{(x)}. \quad (\text{B.4-19})$$

The $S_i^{(x)}$ may be determined from (B.4-16) as follows. Writing (B.4-16) symbolically as

$$S^{(x)} = F(k_1, k_2, k_3, \rho_1),$$

SECRET

SECRET

UNIVERSITY OF MICHIGAN

2255-12-5

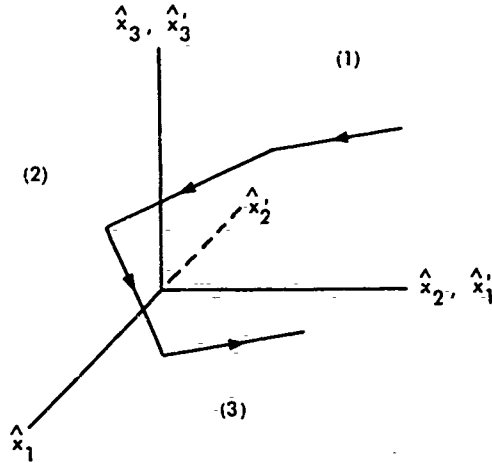


FIG. B-4.2 RAY (123) IN THE X & X' COORDINATE SYSTEMS

ρ_1 representing the pair of reflection coefficients ξ_1, η_1 , we have

$$S_1^{(x)} = F(k_1, k_2, k_3, \rho_1), \quad (\text{B. 4-20})$$

The ray reflected from (1) and incident on (2) has the wave vector

$$\vec{k}' = -\hat{x}_1 k_1 + \hat{x}_2 k_2 + \hat{x}_3 k_3. \quad \text{In terms of the coordinate system}$$

$$\hat{x}'_1 = \hat{x}_2, \quad \hat{x}'_2 = -\hat{x}_1, \quad \hat{x}'_3 = \hat{x}_3, \quad \text{we have } \vec{k}' = k_2 \hat{x}'_1 + k_1 \hat{x}'_2 + k_3 \hat{x}'_3$$

(\hat{x}'_1 is normal to surface (2).) In the \hat{x}' basis, then,

$$S_2^{(x')} = F(k_2, k_1, k_3, \rho_2). \quad (\text{B. 4-21})$$

SECRET

UNIVERSITY OF MICHIGAN

2255-12-T

$S_2^{(x)}$ is given by

$$S_2^{(x)} = U'^{-1} S_2^{(x')} U' \quad (\text{B.4-22})$$

where

$$U'_{ij} = (\hat{x}'_i \cdot \hat{x}'_j) = \begin{vmatrix} 0 & 1 & 0 \\ -1 & 0 & 0 \\ 0 & 0 & 1 \end{vmatrix} \quad (\text{B.4-23})$$

If (B.4-21) is $S_2^{(x')} = \{S'_{ij}\}$ then

$$S_2^{(x)} = \begin{vmatrix} S'_{22} & -S'_{21} & -S'_{23} \\ -S'_{12} & S'_{11} & S'_{13} \\ -S'_{32} & S'_{31} & S'_{33} \end{vmatrix} \quad (\text{B.4-24})$$

Similarly, for the scattering from surface (3) we introduce the basis $\hat{x}''_1 = \hat{x}_3$, $\hat{x}''_2 = -\hat{x}_1$, $\hat{x}''_3 = \hat{x}_2$. The \vec{k}'' vector incident on (3) is

$$\vec{k}'' = -k_1 \hat{x}_1 - k_2 \hat{x}_2 + k_3 \hat{x}_3 = k_3 \hat{x}''_1 - k_2 \hat{x}''_2 + k_1 \hat{x}''_3. \quad \text{Hence}$$

$$S_3^{(x'')} = F(k_3, -k_2, k_1, \rho_3). \quad (\text{B.4-25})$$

Further

$$S_3^{(x)} = U''^{-1} S_3^{(x'')} U'' \quad (\text{B.4-26})$$

SECRET

UNIVERSITY OF MICHIGAN

2255-12-T

where

$$U''_{ij} = \hat{x}''_i \cdot \hat{x}''_j = \begin{vmatrix} 0 & 0 & 1 \\ 0 & 1 & 0 \\ -1 & 0 & 0 \end{vmatrix} \quad (\text{B. 4-27})$$

If $S_3^{(x'')} = \{S''_{ij}\}$, (B. 4-26) gives

$$S_3^{(x)} = \begin{vmatrix} S''_{33} & -S''_{32} & -S''_{31} \\ -S''_{23} & S''_{22} & S''_{21} \\ -S''_{13} & S''_{12} & S''_{11} \end{vmatrix} \quad (\text{B. 4-28})$$

By means of Equations (B. 4-16, 21, 24, 25, 28), we obtain explicit expressions for the $S_1^{(x)}$: $S_1^{(x)}$ is given by (B. 4-16),

$$S_2^{(x)} = \begin{vmatrix} \frac{k_3^2}{\beta_2^2} \eta_2 - \left(\frac{k_1 k_2}{k \beta_2} \right)^2 \xi_2 & -\frac{k_1 k_2}{k^2} \xi_2 & \frac{k_1 k_3}{\beta_2^2} \left(\eta_2 + \frac{k_2^2}{k^2} \xi_2 \right) \\ \frac{k_1 k_2}{k^2} \xi_2 & \frac{\beta_2^2}{k^2} \xi_2 & -\frac{k_2 k_3}{k^2} \xi_2 \\ \frac{k_1 k_3}{\beta_2^2} \left(\eta_2 + \frac{k_2^2}{k^2} \xi_2 \right) & \frac{k_2 k_3}{k^2} \xi_2 & \frac{k_1^2}{\beta_2^2} \eta_2 - \left(\frac{k_2 k_3}{k \beta_2} \right)^2 \xi_2 \end{vmatrix}$$

(B. 4-29)

SECRET

UNIVERSITY OF MICHIGAN

2255-12-T

and

$$S_3^{(x)} = \begin{vmatrix} \frac{k_2^2}{\beta_3^2} \eta_3 - \left(\frac{k_1 k_3}{k \beta_3} \right)^2 \xi_3 & -\frac{k_1 k_2}{\beta_3^2} \left(\eta_3 + \frac{k_3^2}{k^2} \xi_3 \right) & -\frac{k_1 k_3}{k^2} \xi_3 \\ -\frac{k_1 k_2}{\beta_3^2} \left(\eta_3 + \frac{k_3^2}{k^2} \xi_3 \right) & \frac{k_1^2}{\beta_3^2} \eta_3 - \left(\frac{k_2 k_3}{k \beta_3} \right)^2 \xi_3 & -\frac{k_2 k_3}{k^2} \xi_3 \\ \frac{k_1 k_3}{k^2} \xi_3 & \frac{k_2 k_3}{k^2} \xi_3 & \frac{\beta_3^2}{k^2} \xi_3 \end{vmatrix}$$

(B. 4-30)

Here

$$\beta_i^2 = k^2 - k_i^2 \quad (B. 4-31)$$

The final scattering matrix in the a-basis is given by

$$S^{(a)}(123) = U S_3^{(x)} S_2^{(x)} S_1^{(x)} U^{-1} \quad (B. 4-32)$$

where U is defined in Equation (B. 4-15). The result obtained is

$$S^{(a)}(123) = \begin{vmatrix} A_{11} & A_{12} & 0 \\ A_{21} & A_{22} & 0 \\ 0 & 0 & 0 \end{vmatrix}, \quad (B. 4-33)$$

SECRET

UNIVERSITY OF MICHIGAN

2255-12-T

where

$$A_{11} = \frac{(k_1 k_2 k_3)^2 \xi_2 \eta_3 - (k_2 k_3)^2 \xi_2 \xi_3 + (k_1 k_2)^2 \eta_2 \xi_3 + (k_1 k_2 k_3)^2 \eta_2 \eta_3}{(\beta_1 \beta_2 \beta_3)^2} \eta_1 \quad (\text{B. 4-34})$$

$$A_{21} = \frac{k_1 k_2 k_3 (-k_2^2 \xi_2 \eta_3 - k_3^2 \xi_2 \xi_3 + k_1^2 \eta_2 \xi_3 - k_2^2 \eta_2 \eta_3)}{(\beta_1 \beta_2 \beta_3)^2} \eta_1$$

$$A_{12} = \frac{k_1 k_2 k_3 (-k_2^2 \eta_2 \xi_3 - k_3^2 \eta_2 \eta_3 + k_1^2 \xi_2 \eta_3 - k_2^2 \xi_2 \xi_3)}{(\beta_1 \beta_2 \beta_3)^2} \xi_1$$

$$A_{22} = \frac{-(k_1 k_2 k_3)^2 \eta_2 \xi_3 + (k_2 k_3)^2 \eta_2 \eta_3 - (k_1 k_2)^2 \xi_2 \eta_3 - (k_1 k_2 k_3)^2 \xi_2 \xi_3 \xi_1}{(\beta_1 \beta_2 \beta_3)^2}$$

Note that

$$A_{21}(\xi, \eta) = A_{12}(\eta, \xi)$$

$$A_{21}(\xi, \bar{\eta}) = -A_{11}(\eta, \xi)$$

An immediate check on (B. 4-33) is that the triply reflected electric field be perpendicular to \vec{k} ; this is obviously satisfied. Another is that in the limit of infinite conductivity, the final E should be the same as the incident \vec{E} . Now

$$\left. \begin{array}{l} \xi_i \rightarrow +1 \\ \eta_i \rightarrow -1 \end{array} \right\} \text{ as } c_i \rightarrow \infty \quad (\text{B. 4-35})$$

SECRET

UNIVERSITY OF MICHIGAN

2255-12-T

Clearly $A_{12} = A_{21} = 0$ in this limit. Computing A_{11} and A_{22} in this case does lead to the $A_{11} = A_{22} = 1$.

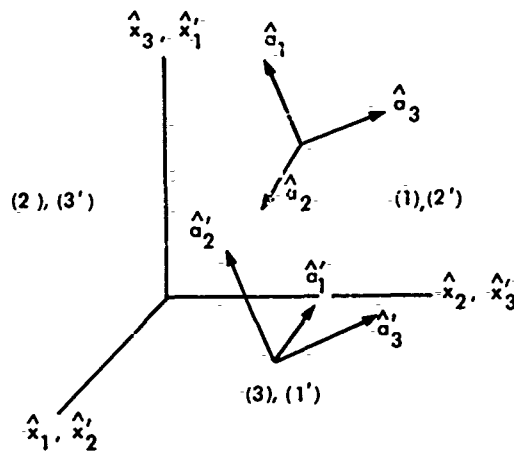


FIG. B-4.3 DEFINITIONS OF VARIOUS COORDINATE SYSTEMS

The matrices $\mathcal{L}^{(a)}_{(312)}$ and $\mathcal{L}^{(a)}_{(231)}$ (cyclic permutations) may be obtained from $\mathcal{L}^{(a)}_{(123)}$ by fairly simple operations. For example, consider the ray (312). In terms of the \hat{x}^i coordinates defined in Figure B-4.3, it is denoted by (1'2'3'). Defining

$$\hat{a}_1^i = \frac{\vec{k} \times \hat{x}_1^i}{|\vec{k} \times \hat{x}_1^i|}, \quad \hat{a}_2^i = \hat{a}_3^i \times \hat{a}_1^i, \quad \hat{a}_3^i = -\frac{\vec{k}}{k}, \quad (\text{B. 4-36})$$

it is evident that

$$\mathcal{L}^{(a')}_{(312)} = \mathcal{L}^{(a')}_{(1'2'3')} = A(k_1^i, k_2^i, k_3^i, \rho_1^i, \rho_2^i, \rho_3^i)$$

SECRET

UNIVERSITY OF MICHIGAN
2255-12-T

where we have defined

$$\mathcal{L}^{(a)}_{(123)} \equiv A (k_1, k_2, k_3, \rho_1, \rho_2, \rho_3). \quad (\text{B. 4-37})$$

Hence

$$\mathcal{L}^{(a')}_{(312)} = A (k_3, k_1, k_2, \rho_3, \rho_1, \rho_2). \quad (\text{B. 4-38})$$

If the elements of V are defined by

$$V_{ij} = \hat{a}'_i \cdot \hat{a}'_j, \quad (\text{B. 4-39})$$

then

$$\mathcal{L}^{(a)}_{(312)} = V^{-1} \mathcal{L}^{(a')}_{(312)} V. \quad (\text{B. 4-40})$$

From (B. 4-36)

$$a'_1 = \frac{1}{\beta_3} (k_2 \hat{x}_1 - k_1 \hat{x}_2); \quad a'_2 = \frac{1}{k\beta_3} (-k_3 k_1 \hat{x}_1 - k_3 k_2 \hat{x}_2 + \beta_3^2 \hat{x}_3); \quad \hat{a}'_3 = \hat{a}_3$$

(B. 4-41)

V may now be computed, yielding

$$V = \begin{vmatrix} -\frac{k_1 k_3}{\beta_1 \beta_3} & \frac{k k_2}{\beta_1 \beta_3} & 0 \\ -\frac{k k_2}{\beta_1 \beta_3} & -\frac{k_1 k_3}{\beta_1 \beta_3} & 0 \\ 0 & 0 & 1 \end{vmatrix} \quad (\text{B. 4-42})$$

SECRET

UNIVERSITY OF MICHIGAN

2255-12-T

Carrying out the operations indicated in (B. 4-40) and using (B. 4-33) and (B. 4-37), the result obtained is

$$\int^{(a)} (312) = \begin{vmatrix} B_{11} & P_{12} & 0 \\ B_{21} & B_{22} & 0 \\ 0 & 0 & 0 \end{vmatrix} \quad , \quad (\text{B. 4-43})$$

where

$$B_{11} = \frac{1}{(\beta_1^2 \beta_2 \beta_3)^2} \left\{ - (k k_1 k_2 k_3)^2 \xi_1 (\xi_2 + \eta_2) (\xi_3 + \eta_3) - \eta_1 \left[(k k_3)^2 \xi_2 - (k_1 k_2)^2 \eta_2 \right] \left[(k k_2)^2 \xi_3 - (k_1 k_3)^2 \eta_3 \right] \right\} ,$$

$$B_{21} = \frac{k k_1 k_2 k_3}{(\beta_1^2 \beta_2 \beta_3)^2} \left\{ \xi_1 (\xi_3 + \eta_3) \left[(k_1 k_2)^2 \xi_2 - (k k_3)^2 \eta_2 \right] + \eta_1 (\xi_2 + \eta_2) \left[(k k_2)^2 \xi_3 - (k_1 k_3)^2 \eta_3 \right] \right\} \quad (\text{B. 4-44})$$

$$B_{12}(\xi, \eta) = B_{21}(\eta, \xi) \quad ,$$

$$B_{22}(\xi, \eta) = -B_{11}(\eta, \xi) \quad .$$

SECRET

UNIVERSITY OF MICHIGAN

2255-12-T

The analogous procedure for ray (231) yields

$$\mathcal{L}^{(a)}_{(231)} = \begin{vmatrix} A_{11} & -A_{12} & 0 \\ -A_{21} & A_{22} & 0 \\ 0 & 0 & 0 \end{vmatrix} \quad . \quad (\text{B. 4-45})$$

The three rays obtained from (123) by non-cyclic permutations are obtained by means of the result obtained at the end of Section B. 4. 6. Namely:

$$\mathcal{L}^{(a)}_{(ijk)} = \overline{\mathcal{L}^{(a)}_{(kji)}} \quad . \quad (\text{B. 4-46})$$

B. 4. 3 Comparison of the Various Rays

First let us summarize the results:

$$\begin{aligned} (123) &= \begin{vmatrix} A_{11} & A_{12} \\ A_{21} & A_{22} \end{vmatrix} & (231) &= \begin{vmatrix} A_{11} & -A_{12} \\ -A_{21} & A_{22} \end{vmatrix} & (312) &= \begin{vmatrix} B_{11} & B_{12} \\ B_{21} & B_{22} \end{vmatrix} \\ (321) &= \begin{vmatrix} A_{11} & A_{21} \\ A_{12} & A_{22} \end{vmatrix} & (132) &= \begin{vmatrix} A_{11} & -A_{21} \\ -A_{12} & A_{22} \end{vmatrix} & (213) &= \begin{vmatrix} B_{11} & B_{21} \\ B_{12} & B_{22} \end{vmatrix} \end{aligned}$$

Here we have omitted the third row and column, and have abbreviated

$\mathcal{L}^{(a)}_{(ijk)}$ by (ijk).

Figure B. 4- 4 is for reference:

SECRET

UNIVERSITY OF MICHIGAN

2255-12-T

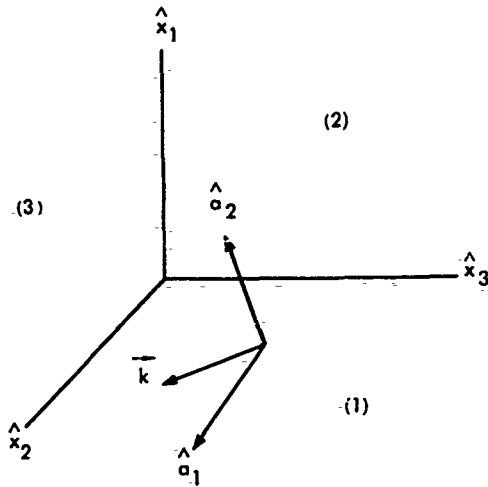


FIG. B-4.4 REFERENCE FIGURE

Consider the six differences between the four rays which strike (2) and (3) in succession:

$$(123) - (132) = (321) - (231) = \begin{vmatrix} 0 & A_{12} + A_{21} \\ A_{12} + A_{21} & 0 \end{vmatrix}$$

$$(123) - (231) = \widetilde{(321)} - \widetilde{(132)} = \begin{vmatrix} 0 & 2A_{12} \\ 2A_{21} & 0 \end{vmatrix}$$

SECRET

UNIVERSITY OF MICHIGAN

2255-12-T

$$(123) - (321) = (132) - (231) = \begin{vmatrix} 0 & A_{12} - A_{21} \\ -(A_{12} - A_{21}) & 0 \end{vmatrix} ;$$

also the difference

$$(312) - (213) = \begin{vmatrix} 0 & B_{12} - B_{21} \\ -(B_{12} - B_{21}) & 0 \end{vmatrix} .$$

(B.4-47)

Now

$$A_{12} \pm A_{21} = \frac{k k_1 k_2 k_3}{(\beta_1 \beta_2 \beta_3)^2} \left[-k^2 (\xi_1 \eta_2 \xi_3 \pm \eta_1 \xi_2 \eta_3) - k_3^2 (\xi_1 \eta_2 \eta_3 \pm \eta_1 \xi_2 \xi_3) \right. \\ \left. + k_1^2 (\xi_1 \xi_2 \eta_3 \pm \eta_1 \eta_2 \xi_3) - k_2^2 (\xi_1 \xi_2 \xi_3 \pm \eta_1 \eta_2 \eta_3) \right] , \quad (\text{B.4-48})$$

$$B_{12} \mp B_{21} = -\frac{k k_1 k_2 k_3}{(\beta_1 \beta_2 \beta_3)^2} \left\{ (\xi_2 + \eta_2) \left[k^2 k_2^2 (\pm \eta_1 \xi_3 - \xi_1 \eta_3) + k_1^2 k_3^2 (\xi_1 \xi_3 \mp \eta_1 \eta_3) \right] \right. \\ \left. + (\xi_3 + \eta_3) \left[k^2 k_3^2 (\eta_1 \xi_2 \mp \xi_1 \eta_2) + k_1^2 k_2^2 (\eta_1 \eta_2 \mp \xi_1 \xi_2) \right] \right\} . \quad (\text{B.4-49})$$

It can be seen that in general no two of the fields of the six different types of rays will be the same. We now proceed to investigate some special cases wherein the number of different reflected fields is reduced.

SECRET

UNIVERSITY OF MICHIGAN

2255-12-T

It might be expected intuitively that (123) = (132) in the special case $\rho_2 = \rho_3$, $k_2 = k_3$ and $\bar{E}_0 = E_{02} \hat{a}_2$. Letting $\Gamma = (k k_1 k_2 k_3) / (\beta_1 \beta_2 \beta_3)^2$, we have

$$A_{12} \pm A_{21} = -\Gamma \left\{ k_2^2 \left[\xi_1^2 \pm \eta_1 \eta^2 + (\xi_1 \pm \eta_1) \xi \eta \right] + k_3^2 \left[\xi_1 \eta^2 \pm \eta_1 \xi^2 + (\xi_1 \pm \eta_1) \xi \eta \right] \right\}, \quad (\text{B. 4-50})$$

when

$$\xi_2 = \xi_3 = \xi, \quad \eta_2 \eta_3 = \eta.$$

If in addition, $k_2 = k_3 = k'$,

$$A_{12} \pm A_{21} = -k'^2 (\xi_1 \pm \eta_1) (\xi + \eta)^2. \quad (\text{B. 4-51})$$

Thus, for finite conductivity, the fields are not the same even in this special case:

$$\bar{E}(123) = \begin{vmatrix} A_{12} & E_{02} \\ A_{22} & E_{02} \end{vmatrix}, \quad \bar{E}(132) = \begin{vmatrix} -A_{12} & E_{02} \\ A_{22} & E_{02} \end{vmatrix}, \quad \text{for } \bar{E}_0 = \hat{a}_2 E_{02}. \quad (\text{B. 4-52})$$

This may be made plausible by the following discussion. The reason for the intuitive feeling that they be the same is the picture containing the corner, the \bar{k} -vector and the \bar{E}_0 -vector is invariant under reflection in the plane containing \hat{x}_1 and $\hat{x}_2 + \hat{x}_3$. However, the H_0 -vector reverses direction under such a reflection, causing a change in the physical situation. Note that when $c_1 = \infty$, $\rho_2 = \rho_3$ and $k_2 = k_3$, (123) = (132), (321) = (231), the number of different rays reduces from six to four. Referring to the Equations (B. 4-33) and (B. 4-45) (the expressions for A_{ij} and B_{ij}),

SECRET

UNIVERSITY OF MICHIGAN

2255-12-T

we see that,

$$A_{12} = A_{21} = B_{12} = B_{21} = 0 \text{ when } c_2 = c_3 = \infty \text{ for arbitrary } \bar{k}, \text{ and} \quad (\text{B.4-53})$$

$$A_{11} = \frac{-\eta_1}{(\beta_1 \beta_2 \beta_3)^2} \left[(k k_1 k_3)^2 + (k k_2 k_3)^2 + (k k_1 k_2)^2 - (k_1 k_2 k_3)^2 \right],$$

$$A_{22} = \frac{\xi_1}{(\beta_1 \beta_2 \beta_3)^2} \left[(k k_1 k_3)^2 + (k k_2 k_3)^2 + (k k_1 k_2)^2 - (k_1 k_2 k_3)^2 \right],$$

$$B_{11} = \frac{-\eta_1}{(\beta_1^2 \beta_2 \beta_3)^2} \left[(k k_3)^2 + (k_1 k_2)^2 \right] \left[(k k_2)^2 + (k_1 k_3)^2 \right], \text{ and}$$

$$B_{22} = \frac{\xi_1}{(\beta_1^2 \beta_2 \beta_3)^2} \left[(k k_3)^2 + (k_1 k_2)^2 \right] \left[(k k_2)^2 + (k_1 k_3)^2 \right],$$

which reduce to

$$A_{11} = B_{11} = -\eta_1, \text{ and } A_{22} = B_{22} = \xi_1, \quad (\text{B.4-54})$$

when $c_2 = c_3 = \infty$, for arbitrary \bar{k} .

Thus we may conclude that when any two of the walls are perfectly reflecting, the fields on all six triply reflected rays are the same; the triple reflection is equivalent (when $c_2 = c_3 = \infty$) to a single reflection from the (1) plane if the incident wave has the wave vector $-\bar{k}' = k_1 \hat{x}_1 - k_2 \hat{x}_2 - k_3 \hat{x}_3$, and electric vector $\bar{E}^{0'} = -E_{01} \hat{b}_1 + E_{02} \hat{b}_2$, as shown in Figure B.4-5. Note that as the conductivity of (1) goes to infinity, $A_{11} = B_{11} \rightarrow +1$ and $A_{22} = B_{22} \rightarrow +1$ so that the scattering matrices approach the identity matrix, as expected.

SECRET

UNIVERSITY OF MICHIGAN

2255-12-T

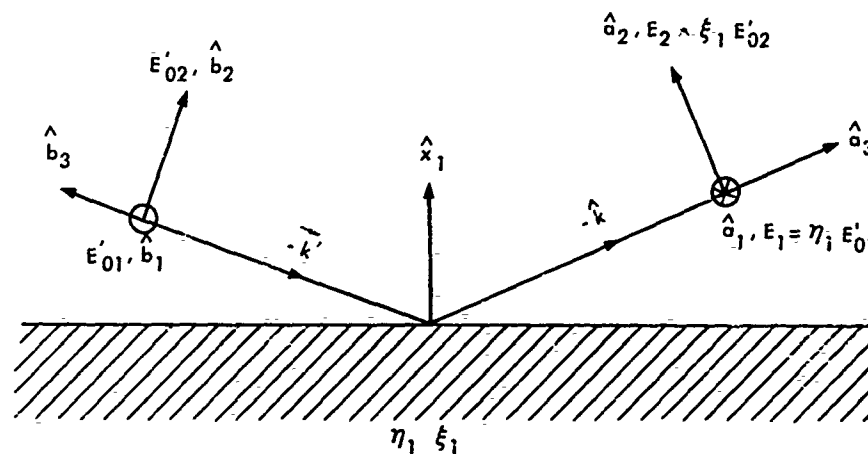


FIG. B-4.5 EQUIVALENT SINGLE REFLECTION WHERE TWO SIDES
ARE PERFECTLY CONDUCTING

B.4.4 Physical Optics Field and Radar Cross-Section

We have seen that the geometric optics solution consists of six beams of radiation, each characterized by the same propagation vector, $-\vec{k}$, but each having different field vectors, (\vec{E}_i, \vec{H}_i) , $i = 1, 2, \dots, 6$ and occupying different areas, a_i (normal to \vec{k}). As discussed in B.2 the physical optics approximate field is

$$\vec{E}(R) = \frac{ike}{2\pi R} \sum_{i=1}^6 \vec{E}_i a_i, \quad (\text{B.4-55})$$

where R is the distance from the observation point to the corner.

SECRET

SECRET

UNIVERSITY OF MICHIGAN

2255-12-T

Defining

$$\bar{\epsilon} = \frac{1}{a} \sum_{i=1}^6 \bar{E}_i a_i, \quad (\text{B. 4-56})$$

where

$$a = \sum_{i=1}^6 a_i, \quad (\text{B. 4-57})$$

(a is the total area for triply reflected radiation), we have

$$\bar{E}(R) = - \frac{ike^{ikR - i\omega t}}{2\pi R} a \bar{\epsilon}. \quad (\text{B. 4-58})$$

Let the numbers $i = 1, 2, \dots, 6$ correspond to the rays (ijk) as:

$$\begin{array}{lll} (123) \rightarrow 1 & (231) \rightarrow 3 & (312) \rightarrow 5 \\ (321) \rightarrow 2 & (132) \rightarrow 4 & (213) \rightarrow 6, \end{array}$$

and let

$$A_i^{kk} = A_{kk}, \quad i = 1, 2, 3, 4, \text{ and } k = 1, 2; \quad A_i^{kk} = B_{kk}, \quad i = 5, 6, \text{ and } k = 1, 2,$$

$$A_1^{kl} = A_{kl}, \quad A_2^{kl} = A_{lk}, \quad A_3^{kl} = -A_{kl}, \quad A_4^{kl} = -A_{lk}, \quad A_5^{kl} = B_{kl},$$

$$A_6^{kl} = B_{lk}, \quad l \neq k. \quad (\text{B. 4-59})$$

(The A_{kl} and B_{kl} are defined in Equations (B. 4-34) and (B. 4-45)), Then

$$\epsilon^{01} = \frac{1}{a} \left\| \begin{array}{l} E_{01} \sum_1^6 A_i^{11} a_i + E_{02} \sum_1^6 A_i^{12} a_i \\ E_{01} \sum_1^6 A_i^{21} a_i + E_{02} \sum_1^6 A_i^{22} a_i \end{array} \right\|$$

SECRET

UNIVERSITY OF MICHIGAN

2255-12-T

or

$$\vec{e}_0 = \begin{vmatrix} C_{11} & C_{12} \\ C_{21} & C_{22} \end{vmatrix} \begin{vmatrix} E_{01} \\ E_{02} \end{vmatrix}, \quad (\text{B. 4-60})$$

where

$$C_{kl} = \frac{1}{a} \sum_{i=1}^6 A_i^{kl} a_i. \quad (\text{B. 4-61})$$

Note that

$$\sum_{i=1}^4 A_i^{kl} = 0, \quad k \neq l. \quad (\text{B. 4-62})$$

Also, the areas for any two rays, (ijk) and its reverse (kji), are obviously equal, so that

$$a_1 = a_2, \quad a_3 = a_4, \quad a_5 = a_6. \quad (\text{B. 4-63})$$

Using (B. 4-59) and (B. 4-63), it follows that

$$C_{12} = C_{21}. \quad (\text{B. 4-64})$$

The physical significance of Equation (B. 4-64) (which is in agreement with the general reciprocity relationships associated with Maxwell's equations) is the following. If the incident field were $\vec{E}_0 = \hat{a}_1$, then $\hat{a}_2 \cdot \vec{E} = C_{21}$ whereas, if the incident field were $\vec{E}'_0 = \hat{a}_2$, then $\hat{a}_1 \cdot \vec{E}' = C_{12}$.

The C_{ij} may be written:

SECRET

UNIVERSITY OF MICHIGAN

2255-12-T

$$C_{11} = \frac{2}{a} \left[(a_1 + a_3) A_{11} + a_5 B_{11} \right] ,$$

$$C_{12} = \frac{1}{a} \left[(a_1 - a_3) (A_{12} + A_{21}) + a_5 (B_{12} + B_{21}) \right] = c_{21} ,$$

$$C_{22} = \frac{2}{a} \left[(a_1 + a_3) A_{22} + a_5 B_{22} \right] . \quad (\text{B. 4-65})$$

When

$c_1 = c_2 = c_3 = \infty$, $A_i^{kl} = 0$, $k \neq l$, $A_i^{kk} = 1$. Then $\{c_{ij}\}$ reduces to $\begin{pmatrix} 1 & 0 \\ 0 & 1 \end{pmatrix}$.

The cross-section, σ , is given by:

$$\sigma = \frac{4\pi a^2}{\lambda^2} \left| \frac{\vec{E}}{E_0} \right|^2 , \quad (\text{B. 4-66})$$

where we have assumed $|\vec{E}_0| = 1$. Clearly

$$\begin{aligned} \left| \frac{\vec{E}}{E_0} \right|^2 &= \left| C_{11} E_{01} + C_{12} E_{02} \right|^2 + \left| C_{21} E_{01} + C_{22} E_{02} \right|^2 \\ &= D_1 |E_{01}|^2 + D_2 |E_{02}|^2 + D_{12} E_{01} E_{02}^* + D_{21} E_{01}^* E_{02} , \end{aligned} \quad (\text{B. 4-67})$$

where

$$D_1 = |C_{11}|^2 + |C_{21}|^2 , \quad D_2 = |C_{12}|^2 + |C_{22}|^2 ,$$

$$D_{12} = C_{11} C_{12}^* + C_{12} C_{22}^* = D_{21}^* . \quad (\text{B. 4-68})$$

SECRET

UNIVERSITY OF MICHIGAN

2255-12-T

Example--Symmetric Corner Reflector; \vec{k} Along Axis of Symmetry

Assume \vec{k} to be along the axis of symmetry, $\hat{x}_1 + \hat{x}_2 + \hat{x}_3$. For this situation, $a_1 = a_3 = a_5$. (An example is the "square" corner reflector pictured in Figure B-4.6.)

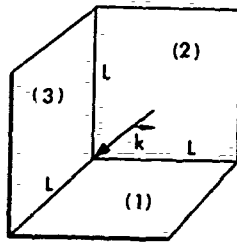


FIG. B-4.6 SYMMETRIC SQUARE CORNER REFLECTOR, \vec{k} ALONG SYMMETRY AXIS.

Equation (B.4-61) now becomes

$$C_{k\ell} = \frac{1}{6} \sum_{i=1}^6 A_i^{k\ell},$$

or

$$C_{11} = \frac{1}{3} (2A_{11} + B_{11}), \quad C_{22} = \frac{1}{3} (2A_{22} + B_{22}),$$

$$C_{12} = \frac{1}{6} (B_{12} + B_{21}) = C_{21}.$$

SECRET

UNIVERSITY OF MICHIGAN

2255-12-T

Using the facts that $k_1 = k_2 = k_3 = -k/\sqrt{3}$, $\beta_i^2 = 2k^2/3$ and writing $\eta_i = \eta$, $\xi_i = \xi$, $i = 1, 2, 3^1$, Equations (B.4-34) and (B.4-44) yield

$$A_{11} = \frac{3}{8} \left(\frac{1}{3} \eta^2 + 2\eta\xi - \xi^2 \right) \eta,$$

$$A_{22} = -\frac{3}{8} \left(\frac{1}{3} \xi^2 + 2\eta\xi - \eta^2 \right) \xi,$$

$$A_{21} = \frac{\sqrt{3}}{8} \eta (\xi + \eta)^2,$$

$$A_{12} = \frac{\sqrt{3}}{8} \xi (\xi + \eta)^2,$$

$$B_{11} = -\frac{1}{16} \left(3\xi^2 + 15\eta\xi^2 - 3\eta^2\xi + \eta^3 \right),$$

$$B_{22} = \frac{1}{16} \left(3\eta^2 + 15\xi\eta^2 - 3\xi^2\eta + \xi^3 \right), \text{ and}$$

$$B_{21} = \frac{9}{8\sqrt{3}} (\xi + \eta) \left[\xi \left(\frac{1}{3} \xi - \eta \right) + \eta \left(\xi - \frac{1}{3} \eta \right) \right] = -B_{12}.$$

Hence,

$$C_{12} = C_{21} = 0. \quad (\text{B.4-69})$$

Furthermore,

$$2A_{11} + B_{11} = \frac{3}{16} \left(\eta^3 + 9\eta^2\xi - 9\xi^2\eta - \xi^3 \right) = 2A_{22} + B_{11}.$$

¹ $\eta_1 = \eta_2 = \eta_3$ and $\xi_1 = \xi_2 = \xi_3$ since not only are the reflecting surfaces the same, but the angles of incidence, $\psi_i = \cos^{-1}(-k_i/k)$, are also the same.

SECRET

UNIVERSITY OF MICHIGAN

2255-12-T

giving

$$C_{11} = C_{22} = \frac{1}{16} (\eta^3 + 9\eta^2\xi - 9\xi^2\eta - \xi^3) \equiv C. \quad (\text{B.4-70})$$

Hence in this example, the reflected field is always parallel to the incident field independent of the initial polarization, and the cross-section is given by:

$$\sigma = \frac{4\pi a^2}{\lambda^2} |C|^2, \quad (\text{B.4-71})$$

which is also independent of initial polarization. Note that for perfect conductivity ($\eta = -1$, $\xi = 1$), $C = 1$, as it should.

Assuming the expressions (B-3.2) for the reflection coefficients, we have

$$\eta = \frac{1 - \sqrt{3\gamma - 2}}{1 + \sqrt{3\gamma - 2}}, \quad \xi = \frac{\gamma - \sqrt{3\gamma - 2}}{\gamma + \sqrt{3\gamma - 2}}, \quad (\text{B.4-72})$$

where we have used the fact that $\cos \psi_i = \sqrt{3}/3$, and

$$\gamma = n^2 \equiv \frac{k_i^2}{k^2} = \frac{\mu}{\mu_0} \frac{\epsilon}{\epsilon_0} - i \frac{\mu c}{\omega \mu_0 \epsilon_0}. \quad (\text{B.4-73})$$

For a perfect, lossless dielectric, γ is real and equal to ϵ/ϵ_0 ; (in this case $\mu = \mu_0$ and $c = 0$). Writing (B.4-70) as

$$C = \frac{1}{16} (\eta - \xi) (\eta^2 + 10\eta\xi + \xi^2),$$

we see that $C = 0$ when

$$\eta = (-5 - 2\sqrt{6})\xi,$$

which in turn occurs for $n^2 = \epsilon/\epsilon_0 = 8/3$, as may be verified through

SECRET

SECRET

UNIVERSITY OF MICHIGAN

2255-12-T

Equation (B.4-72). The other roots of $C = 0$ will not be obtained from (B.4-72) for n^2 real and >1 . In other words, physical optics predicts the back-scattered field from a symmetric corner to be identically zero, independent of incident polarization and wavelength¹, for symmetric incidence when the reflecting material is a perfect dielectric with $\epsilon/\epsilon_0 = 8/3$, provided we assume the reflection coefficients to be given by Equation (B.3-2). One should note that this zero result is due essentially to the interference between the six reflected fields rather than any phenomenon associated with each wall.

In any real situation, the finite thickness, t , of the walls must be considered as in Figure B.4-7 which represents a symmetric square

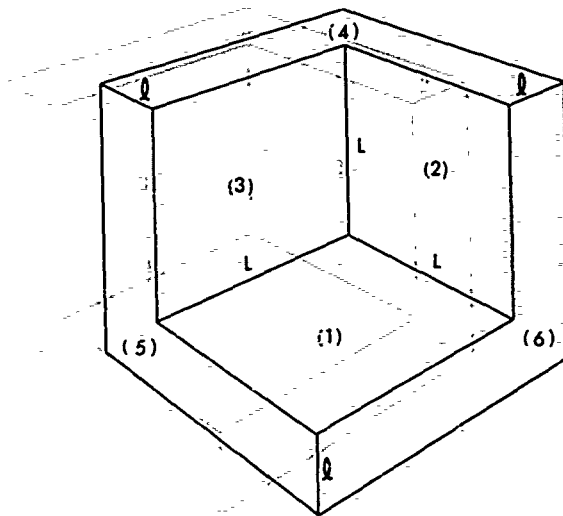


FIG. B-4-7 SYMMETRIC SQUARE
CORNER REFLECTOR WITH WALLS
OF FINITE THICKNESS

¹Provided of course $\lambda \ll$ dimensions of the corner.

SECRET

SECRET

UNIVERSITY OF MICHIGAN

2255-12-T

corner reflector viewed along the axis of symmetry. However, all materials will exhibit some absorption, causing the intensity to drop by the fraction $1/e$ in a distance $l_0 = 1/\beta$, where $K = \alpha + i\beta$. If $l \gg l_0$, then the reflection coefficients will be given to a very good approximation by those obtained using Equation (B. 3-2) (which assume $l \rightarrow \infty$)¹.

We would now like to determine the order of magnitude of l required for the fulfillment of this condition and the value of C assuming the material to be a plastic, Lumarith No. 22361, for which $n^2 = 2.67(1 - 2.56 \times 10^{-2} i) \cong 8/3$ at a temperature of 24°C and 3 cm wavelength (Ref. 18). Writing

$$n^2 = \epsilon_1 - i\epsilon_2, \quad \sqrt{3n^2 - 2} = A' + iB' \quad , \quad (\text{B. 4-74})$$

we find that Equation (B. 4-72) becomes:

$$\eta = \frac{1 - A'^2 - B'^2 - 2iB'}{(1 + A')^2 + B'^2} \quad ,$$
$$\xi = \frac{\epsilon_1^2 + \epsilon_2^2 - A'^2 - B'^2 - 2i(\epsilon_1 B' + \epsilon_2 A')}{(\epsilon_1 + A')^2 + (\epsilon_2 - B')^2} \quad . \quad (\text{B. 4-75})$$

From (B. 4-74),

$$A' = \frac{1}{\sqrt{2}} \left[3\epsilon_1 - 2 + \sqrt{(3\epsilon_1 - 2)^2 + 9\epsilon_2^2} \right]^{1/2} \quad ,$$
$$B' = \frac{1}{\sqrt{2}} \left[-(3\epsilon_1 - 2) + \sqrt{(3\epsilon_1 - 2)^2 + 9\epsilon_2^2} \right]^{1/2} \quad . \quad (\text{B. 4-76})$$

¹The condition $l \gg l_0$ insures that the fields of the beams obtained by reflections from the rear walls of the transmitted beams will be small.

SECRET

UNIVERSITY OF MICHIGAN

2255-12-T

We have $3\epsilon_1 - 2 \cong 6$ and $\epsilon_2 \cong 6.85 \times 10^{-2}$; hence

$$A' \cong \sqrt{3\epsilon_1 - 2} \quad ,$$

$$B' \cong \frac{3}{2} \frac{\epsilon_2}{\sqrt{3\epsilon_1 - 2}} \quad (\text{B.4-77})$$

Thus $B' \cong .042$. Letting η_0 and ξ_0 be the values of η and ξ when $\epsilon_2 = 0$ and $\epsilon_1 = 8/3$, writing $\eta = \eta_0 + \eta' + i\eta_2$, $\xi = \xi_0 + \xi' + i\xi_2$, and assuming $\epsilon_2 \ll \epsilon_1$, we obtain

$$\eta' \cong -\frac{2B'^2}{(1+A')^3} \quad , \quad \eta_2 \cong -\frac{2B'}{(1+A')^2} \quad ,$$

$$\xi' \cong \frac{2(\epsilon_2 A' + \epsilon_1 B')}{(\epsilon_1 + A')^3} (\epsilon_2 - B') \quad , \quad \xi_2 \cong -\frac{2(\epsilon_1 B' + \epsilon_2 A')}{(\epsilon_1 + A')^2} \quad .$$

Taking $\epsilon_1 = 8/3$, $\epsilon_2 = (8/3)(2.56)(10^{-2})$, we find that $|C|^2 \cong 10^{-5}$. Furthermore, $l_0 = 1/\text{Im}K \cong \lambda/\pi \sqrt{1/\epsilon_1} \cdot 1/\tan\delta$, where $\tan\delta = \epsilon_2/\epsilon_1$; so $l_0 \cong 1/4$ meter, for $\lambda = 3$ cm. Hence if l is taken to be ~ 1 meter, we would expect a cross-section for the trihedral corner made of this dielectric material to be of the order of 10^{-5} times that for the perfect conducting trihedral reflector with the same geometry. We mention that in the actual physical situation, the diffraction from sides (4), (5), and (6) should be checked for the non-perfect conducting case since the diffraction might be of the same order as the trihedral contribution. Referring to Equations (4-3) and (4-4), and noting that $\sigma_n/\sigma_a \sim l^4$, we see that $c_n/c_a \sim 10^8$ for a perfect conductor for which $l \sim 1$ meter, this being approximately true for the dielectric. If $L \sim l$ then $\sigma_a = 10^{-8} (4\pi a^2)/\lambda^2$ as compared to the trihedral contribution $10^{-5} (4\pi a^2/\lambda^2)$, which seems to show that the diffraction effects due to sides (4), (5), and (6) are negligible.

SECRET

SECRET

UNIVERSITY OF MICHIGAN

2255-12-T

B.5 X-BAND DATA ON LOSSY DIELECTRICS

Extensive tables of electrical properties of various materials which were measured at the Massachusetts Institute of Technology Laboratory for Insulation Research are given in Reference 18 in terms of the quantities $\epsilon' = \epsilon/\epsilon_0$ "dielectric constant relative to vacuum" and $\tan \delta = \epsilon''/\epsilon'$, the "dielectric loss tangent" or "dissipation factor." These are defined as follows: Taking the fields to have $e^{-i\omega t}$ time dependence, in Reference 18, Maxwell's equations are written as:

$$\nabla \times \mathbf{E} = -\mu_0 \frac{\partial \mathbf{H}}{\partial t}, \quad \nabla \times \mathbf{H} = \epsilon^* \frac{\partial \mathbf{E}}{\partial t},$$

assuming the medium to be non-magnetic, (μ_0 is the free space magnetic permeability). Here, $\epsilon^* = \epsilon' - i\epsilon''$. From this it follows that

$$\nabla^2 \mathbf{H} + \kappa^2 \mathbf{H} = 0, \quad \nabla^2 \mathbf{E} + \kappa^2 \mathbf{E} = 0,$$

where,

$$\kappa^2 = \omega^2 \mu_0 \epsilon^* = \omega^2 \mu_0 \epsilon' (1 - i \tan \delta).$$

In terms of the quantities, ϵ and c , the dielectric constant and conductivity respectively, as defined in Stratton, (Ref. 16):

$$\kappa^2 = \omega^2 \mu_0 \epsilon + i\omega \mu c.$$

Writing $\epsilon = \epsilon_1 - i\epsilon_2$, we see that $\epsilon' = \epsilon_1$, $\epsilon'' = \epsilon_2 - c/\omega$. The quantity $\omega\epsilon''$ is commonly referred to as the "conductivity." If $k^2 = \omega^2 \mu_0 \epsilon_0$ (k is the free space propagation constant), then $\kappa^2/k^2 = \epsilon'(1 - i \tan \delta)$. The reflection coefficients for a single plane reflection from a plane air-medium interface may be written:

$$p_{\perp} = \frac{\cos \theta - \sqrt{(\kappa/k)^2 - \sin^2 \theta}}{\cos \theta + \sqrt{(\kappa/k)^2 - \sin^2 \theta}},$$

$$p_{\parallel} = \frac{(\kappa/k)^2 \cos \theta - \sqrt{(\kappa/k)^2 - \sin^2 \theta}}{(\kappa/k)^2 \cos \theta + \sqrt{(\kappa/k)^2 - \sin^2 \theta}}.$$

SECRET

UNIVERSITY OF MICHIGAN

2255-12-T

Note that if $\kappa^2 = A + iB = (\alpha + i\beta)^2$, ($\kappa = \alpha + i\beta$), then

$$\alpha = \sqrt{\frac{A}{2}} \left[\sqrt{1 + \tan^2 \delta} + 1 \right]^{1/2}, \quad (\text{propagation constant}),$$

$$\beta = \sqrt{\frac{A}{2}} \left[\sqrt{1 + \tan^2 \delta} - 1 \right]^{1/2}, \quad (\text{attenuation constant}).$$

For $\tan^2 \delta \ll 1$, $\beta \cong (\pi/\lambda) \sqrt{\epsilon'} \tan \delta$.

The values of ϵ' and $\tan \delta$ given in Table B.1 are taken from References 18 and 19, for $\lambda = 3$ cm. When numbers are followed by values in parentheses, the numbers are rough averages, the values in parentheses giving the variation; unless otherwise specified, the data are from von Hippel, (Ref. 18), and at $\nu = 10^{10}$ cps. The values of $l_0 = 1/\beta$ (the distance in which the amplitude is reduced by the factor $1/e$) are also given.

There is qualitative agreement among the soil measurements: for dry soil, $\epsilon' \cong 2.4$ to 2.8 , $\tan \delta \cong .001$ to $.005$; both ϵ' and $\tan \delta$ increase with moisture content with values as large as $\epsilon' = 20$, $\tan \delta = .29$ for wet soil.

The effect of variation in $\tan \delta$ upon the reflection properties of soil, is illustrated in Reference 20, page 374, where the magnitude, $|\rho|$ and phase ψ of the reflection coefficient¹, are plotted as a function of the angle of incidence $\theta = (\pi/2 - \psi)$ for the different polarizations, and for values of $(\epsilon', \tan \delta) = (7, 0)$, $(7, 3/7)$, $(25, 0)$ and $(25, 19/25)$. These curves are reproduced in Figure B.5-1.

Noting that when $\tan \delta = 0$, $\phi_{\perp} = 180$ degrees for all ψ and $\phi_{\parallel} = 180$ degrees for ψ less than the Brewster angle ψ_0 , $\phi_{\parallel} = 0$ for $\psi > \psi_0$, we see that the approximation $\tan \delta = 0$ is fairly good except for $\psi \cong \psi_0$.

¹For two semi-infinite, homogeneous media.

SECRET

TABLE B. 1
COMPLEX DIELECTRIC CONSTANTS AND DEPTH OF PENETRATION
FOR VARIOUS MATERIALS AT X-BAND

Material	Type	Temperature, °C.	ϵ'	$\tan \delta$	$t_0 = 1/\beta$ (cm)
Wood		25	2(1.4-3.2)	3×10^{-2} (1.7-4.6) $\times 10^{-2}$	22.5
Glass ¹		25	6(5-7)	1.5×10^{-2} (.3-2.4) $\times 10^{-2}$	26
Water	with conductivity	5	41	.95	0.17
		15	49	.70	0.21
		25	55	.54	0.25
Seawater		28	65	.47	0.26
Ice		-12	3.17	0.07×10^{-2}	763
Soil	dry	25	2.53	0.36×10^{-2}	167
Soil, Sandy	2.18 moisture	25	2.50	6.5×10^{-2}	9.3
Soil, Sandy	3.88 moisture	25	4.40	12×10^{-2}	3.8
Soil, Sandy	16.8 moisture	25	20	29×10^{-2}	0.74
Soil, Loamy	dry	25	2.44	0.14×10^{-2}	437
Soil, Loamy	2.2 moisture	25	3.50	3×10^{-2}	17
Soil, Loamy	13.77 moisture	25	13.80	18×10^{-2}	1.4
Soil, Arizona ²	As found	not given	3.2	5.9×10^{-2}	9.1
Soil, Arizona	16 parts soil, 1 part water	not given	8.1	26×10^{-2}	1.3
Soil, Arizona	4 parts soil, 1 part water	not given	19	25×10^{-2}	0.88
Soil, Austin, Texas	Very dry	not given	2.8	0.51×10^{-2}	112
Soil, Austin, Texas	10 parts soil, 1 part water	not given	4.6	9.2×10^{-2}	4.8

¹Soda-Silica glasses (commonly used for windows); composition a per cent Na₂O, b per cent SiO₂, with (a, b) varying from (9, 91) to (30, 70); both ϵ' and $\tan \delta$ increase with a.

²Reference 19. Here $\nu = .937 \times 10^{10}$ cps; also 'dielectric constant' and 'conductivity' \equiv 'c' as used here, are taken to mean ϵ' and $\omega\epsilon''$ respectively so that $\tan \delta = 'c'/\omega\epsilon'$.

SECRET

UNIVERSITY OF MICHIGAN
2255-12-T

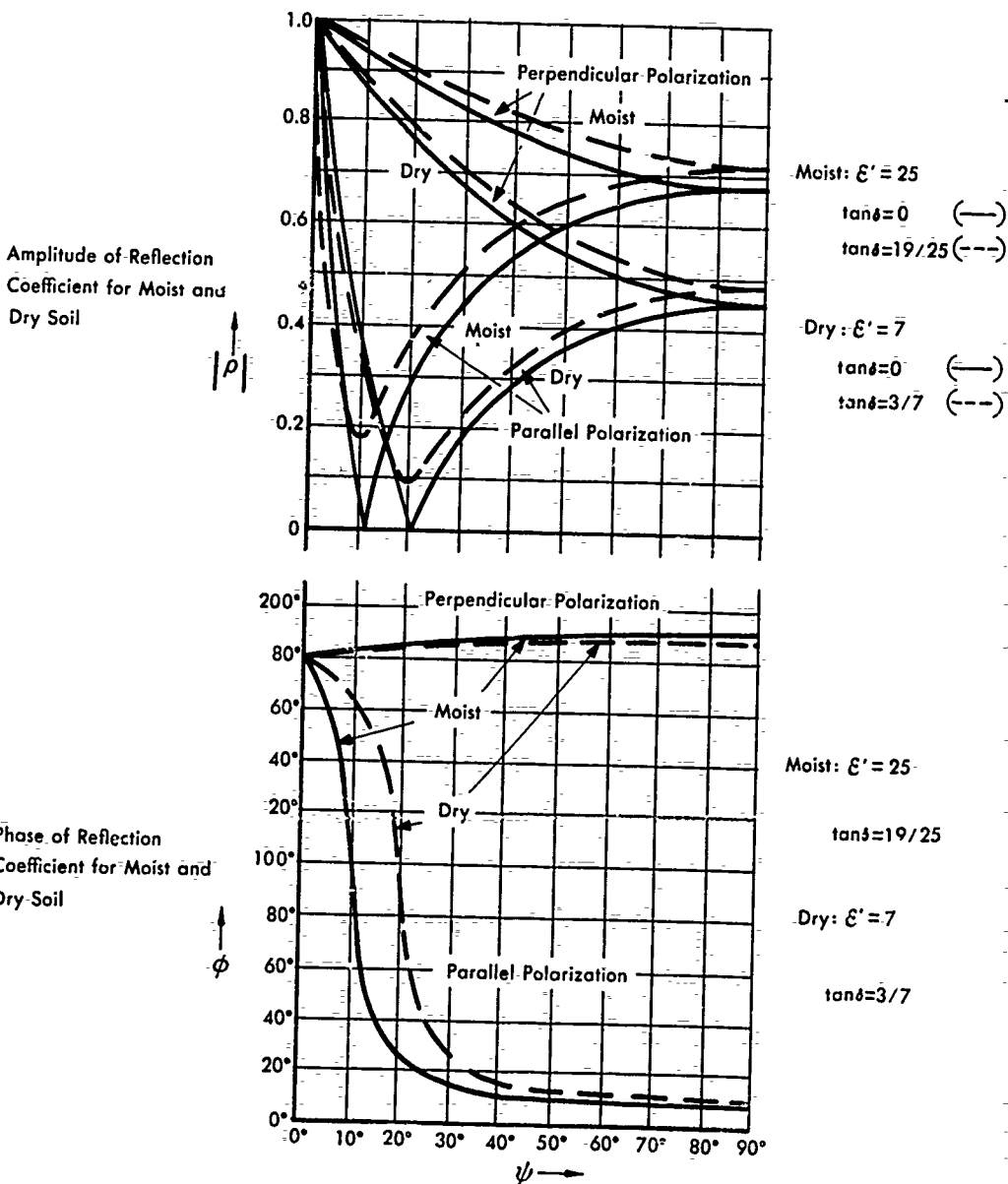


FIG. B-5.1 REFLECTION COEFFICIENTS FOR MOIST AND DRY SOIL

SECRET

SECRET

UNIVERSITY OF MICHIGAN

2255-12-T

APPENDIX C

ROUGH SURFACE EFFECTS

The radar cross-sections of the dihedrals and trihedrals formed by the ground and buildings were computed under the assumption that the ground is a smooth, perfect conductor. Inasmuch as unpaved ground is actually rough compared to the 3-cm wavelength considered, it is desirable to have some estimate of the effect of the roughness on the corner cross-section.

If it is assumed that the ground is an isotropic scatterer, then the effect of the corner is virtually nullified. This can be seen by considering the change in the cross-section of a dihedral when one face is made an isotropic scatterer. If the plane in Figure C-1 is smooth, the cross-section of the dihedral formed by a vertical wall on the plane, for the incident beam shown is given by:

$$\sigma = \frac{4\pi}{\lambda^2} A^2,$$

where A is obtained by imaging in the horizontal plane:

$$A = (2h \cos \theta) l, \quad 0 < \theta < \pi/2.$$

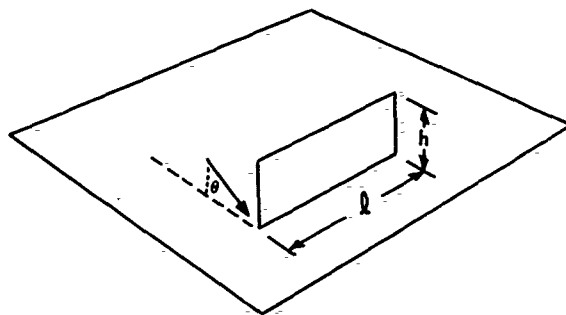


FIG. C-1 VERTICAL WALL IN ROUGH SURFACE

C-1

SECRET

SECRET

UNIVERSITY OF MICHIGAN

2255-12-T

If the plane is an isotropic scatterer, an equivalent problem in the region of physical optics may be obtained by imaging in the smooth wall (Fig. C-1 and C-2). Thus, instead of a corner, there is only the contribution of an isotropic scatterer with two incident beams.

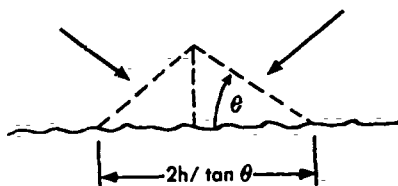


FIG. C-2 IMAGE PROBLEM

A quantitative estimate is obtained as follows: For an isotropic scatterer, the radar cross-section is equal to the area seen from the direction of incidence which is $2hl \cos \theta$ (Fig. C-2). Taking into account the image beam, the scattering cross-section for the "isotropic" corner is $\sigma_i = 4hl \cos \theta$. The contribution of the part of the rough surface affected by the vertical wall (Fig. C-2) is just doubled in the physical optics approximation. The ratio of the two cross-sections is

$$\frac{\sigma_i}{\sigma} = \frac{1}{4\pi \cos \theta} \frac{\lambda}{h} \frac{\lambda}{l}, \quad 0 < \theta < \pi/2.$$

For the cases of interest $\lambda/h \ll 1$ and $\lambda/l \ll 1$ so that $\sigma_i/\sigma \ll 1$ for θ not too close to $\pi/2$. For θ near $\pi/2$ the above expressions are no longer good approximations and hence the ratio has no meaning. However, the θ near $\pi/2$ case is not of importance in the present work.

In the literature there are several theoretical studies of the effects of surface roughness on radar return (Ref. 25). However, most of the work is not applicable to the present problem. Hence the following analysis, aimed at determining the conditions under which terrain might be expected to

SECRET

UNIVERSITY OF MICHIGAN

2255-12-T

scatter isotropically has been carried out. It is shown that a one-dimensional surface cannot scatter isotropically unless there is considerable shadowing of parts of the surface by adjacent parts.

Consider a perfectly conducting surface $y = y(x)$ whose roughness is large compared to the wavelength so that the reflection at each point may be considered specular. If the slope at some point is y' , and if the direction of the incident beam is given by β then the direction θ of the beam scattered from the point (having slope y') is given by (Fig. C-3):

$$\theta = 2\alpha + \beta, \quad (\text{C-1})$$

where

$$y' = \tan \alpha, \quad (\text{C-2})$$

(It has been implicitly assumed that the ray is not multiply scattered.)

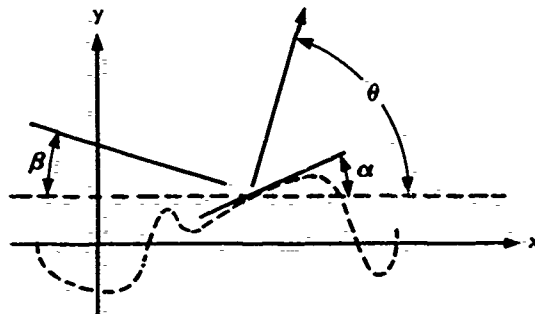


FIG. C-3 REFLECTION OF ROUGH SURFACE

If $p(\theta)$ is the probability of scattering into $d\theta$ at θ then $p(\theta)$ is proportional to the scattering cross-section $\sigma(\theta)$ per unit area of surface (Eq. C-11), $p(\theta)$ depends on α , β and on the shadowing of the surface, as parameters. It can be expressed also in terms of the distribution of slopes.

SECRET

UNIVERSITY OF MICHIGAN

2255-12-T

For each fixed β

$$\begin{aligned} P(y') dy' &= p(\theta) d\theta \\ P(y') &= p(\theta) d\theta/dy' \end{aligned} \tag{C-3}$$

where $d\theta/dy'$ is to be calculated from Equations (C-1) and (C-2):

$$\frac{d\theta}{dy'} = 2 \frac{d\alpha}{dy'} = \frac{2}{1+y'^2} ,$$

and therefore,

$$\begin{aligned} P(y') &= \frac{2}{1+y'^2} p(\theta) \\ &= \frac{2}{1+y'^2} p(2 \tan^{-1} y' + \beta) . \end{aligned} \tag{C-4}$$

For an isotropic scatterer:

$$\begin{aligned} p_i(\theta) &= \text{constant} = 1/\pi \\ P_i(y') &= \frac{2}{\pi(1+y'^2)} . \end{aligned} \tag{C-5}$$

$P(y')$ is the probability density distribution of surface elements of slope y' which are seen from the direction of incidence β . This function will now be found explicitly in terms of β , for a given curve $y(x)$ on the assumption of single scatterings only.

In Figure C-4 let Δs_i represent a small part of the curve $y(x)$ and let $\Delta y'$ be the change in y' along Δs_i . Then, if Δl_i is defined as shown in Figure C-4, the probability $P(y') \Delta y'$ of seeing a slope y' in the range $\Delta y'$ is given by:

$$P(y') \Delta y' = \sum \frac{\Delta l_i}{L \sin \beta} , \tag{C-6}$$

where the sum is over all points having the same y' (and not shadowed by another part of the curve).

SECRET

SECRET

UNIVERSITY OF MICHIGAN

2255-12-T

$$\Delta l_i = \Delta s_i \cos(\pi/2 - \alpha - \beta) = \Delta s_i \sin(\alpha + \beta)$$

$$\Delta x_i = \Delta s_i \cos \alpha$$

$$\Delta y' = y''_i \Delta x_i .$$

Assuming that $y''_i \neq 0$, and combining the last three equations with Equation (C-6):

$$P(y') \Delta y' = \sum \frac{\sin(\alpha + \beta)}{L \sin \beta \cos \alpha} \frac{\Delta y'}{y''_i} , \text{ or}$$

$$P(y') = \left(\frac{y'}{\tan \beta} + i \right) \left(\frac{1}{L} \sum \frac{1}{y''_i} \right) , \quad (C-7)$$

where y'' is to be expressed as a function of y' . The quantity in the second parenthesis on the right is essentially an average and hence is independent of L for sufficiently large L .

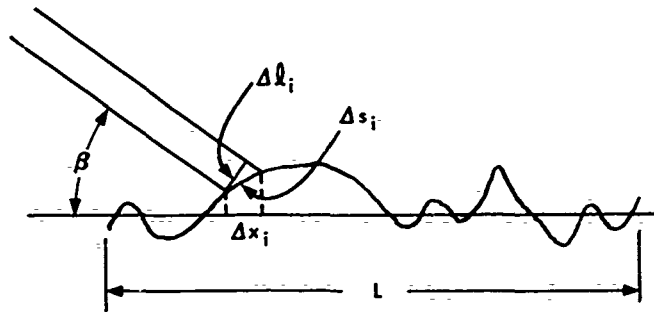


FIG. C-4 GEOMETRY FOR ROUGH SURFACE

It is evident from Equation (C-7) that a surface cannot be an isotropic scatterer for all incident directions if the sum reduces to a single term. In fact, since $P(y')$ is to be independent of β , it follows that the $\sum 1/y''_i$ must depend on β which means that as β varies new parts of the surface must be exposed and previously exposed parts shadowed, if the

SECRET

UNIVERSITY OF MICHIGAN

2255-12-T

scatterer is to be isotropic for all angles of incidence. When there is no shadowing, surfaces can be found which scatter isotropically for given values of β . For example, let $\beta = \pi/2$, and assume further that the sum in Equation (C-7) reduces to a single term for each y' . In this case Equations (C-5) and (C-7) give

$$\frac{2}{\pi(1+y'^2)} = \frac{1}{L y''} \quad (C-8)$$

A first integration gives

$$\frac{\pi x}{2L} + c_1 = \sin^{-1} \frac{y'}{\sqrt{1+y'^2}} .$$

The arbitrary constant c_1 may be set equal to 0, since it only shifts the origin. Solving for y' :

$$y' = \pm \tan \frac{\pi x}{2L} ,$$

which gives

$$\cos \frac{\pi x}{2L} = c_2 e^{\pm \frac{\pi y}{2L}} .$$

The constant c_2 may be set equal to 1 since it merely affects the average value of y , and the introduction of new variables

$$u = \frac{\pi x}{2L} \quad \text{and} \quad v = \frac{\pi y}{2L}$$

gives

$$\cos u = e^{\pm v} .$$

Choosing the plus sign and negative v , yields

$$\cos u = e^{-v} . \quad (C-9)$$

Equation (C-9) is plotted in Figure C-5.

SECRET

SECRET

UNIVERSITY OF MICHIGAN

2255-12-T

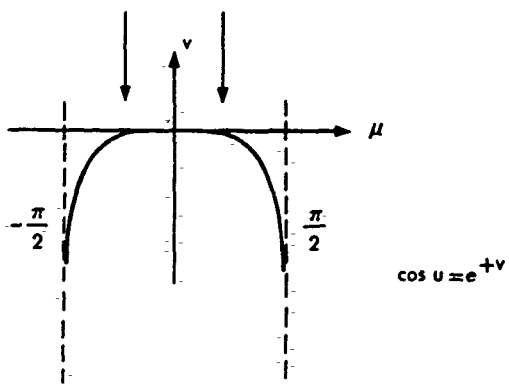


FIG. C-5 TWO-DIMENSIONAL PSEUDO-ISOTROPIC SCATTERING

It is obvious however, that Equation (C-9) does not scatter isotropically for all angles of incidence but only for $\beta = \pi/2$.

From Equation (C-7) the geometric optics cross-section for the surface $y(x)$ can be obtained. Since $\sigma(\theta)$ is proportional to $p(\theta)$, and

$$\int_0^\pi p(\theta) d\theta = 1, \quad \int_0^\pi \sigma(\theta) d\theta = \sigma_0 \tag{C-10}$$

where σ_0 is the total cross-section. Hence

$$\sigma(\theta) = \sigma_0 p(\theta) = \sigma_0 \frac{dy'}{d\theta} P(y') \tag{C-11}$$

From Equations (C-1) and (C-2)

$$\frac{dy'}{d\theta} = 1/2 \sec^2 \frac{\theta - \beta}{2} .$$

SECRET

UNIVERSITY OF MICHIGAN

2255-12-T

Also,

$$\sigma_o = L \sin \beta .$$

Therefore,

$$\sigma = (1/2) \sec^2 \left(\frac{\theta - \beta}{2} \right) \left[y' \cos \beta + \sin \beta \right] \sum \frac{1}{y_i''} \quad (C-12)$$

where the sum is now to be expressed in terms of θ by using Equations (C-1) and (C-2).

If the surface is defined statistically this formula would be used to obtain a probability distribution for σ .

C-8

SECRET

SECRET

UNIVERSITY OF MICHIGAN

2255-12-T

APPENDIX D

SUMMARY AND ANALYSIS OF EXPERIMENTS

D.1 STRATEGIC AIR COMMAND, RADAR PREDICTION IMPROVEMENT PROGRAM- -"THE BALTIMORE PROJECT"

To improve their predictions of the radar PPI presentations to be expected during bombing runs, the Strategic Air Command (SAC) conducted an extensive series of tests to obtain data from which to correlate the relative magnitudes of echoes from targets as seen on a PPI display with physical characteristics of these targets detectable photographically. More specifically, SAC wanted to determine which structures and patterns of structures give relatively strong, persistent radar returns as aspect changed and which give fluctuating (and hence unreliable) returns, which items of information are required, and which factors are insignificant in radar PPI scope prediction.

At present writing, a final report on this work (Ref. 4) is nearly complete but not yet available. The details given below are based on a semifinal report (Ref. 5) and on further data obtained during a visit to Headquarters, SAC, Offutt Air Force Base, Nebraska, by one of the authors.

Although some of the work of the Baltimore Project has been criticized, the results obtained appear to be of considerable value.

To obtain data, SAC chose 60 different, fairly homogeneous structure groupings in the Baltimore, Md., area for study. An AN/APS-23 radar was flown at an altitude of 30,000 feet in circular paths of radii 10, 15, 25, 30, and 40 miles about the center of Baltimore. The PPI presentation was photographed on each scan. Successive scans were made with a successively increasing gain for ten scans, after which the gain cycle was repeated. A cycle lasted about 12 seconds. The relative echo strength of a target was determined in each cycle by the lowest gain

SECRET

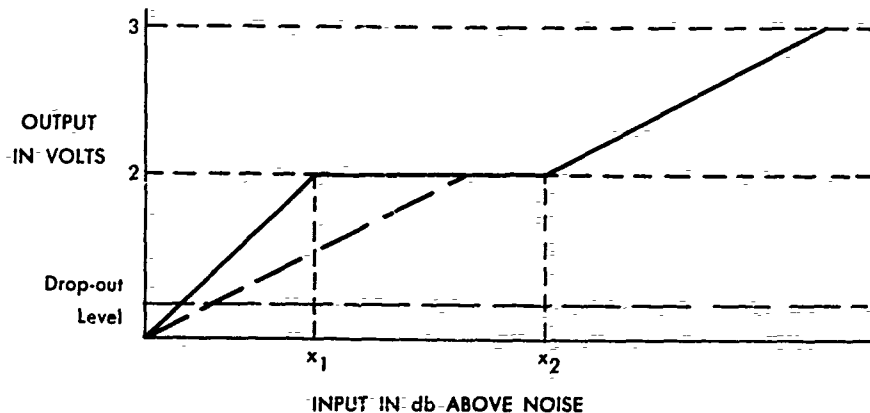
SECRET

UNIVERSITY OF MICHIGAN

2255-12-T

setting at which it was visible on the photograph. Returns visible on the lowest gain setting were labeled No. 1 intensities; those visible on the second lowest but not the lowest setting were labeled No. 2 intensities, and so on.

This procedure has three advantages over procedures such as were used by Engineering Research Associates and Ford Instrument Company (App. D. 4). It eliminates the need for careful photometric readings which are quite difficult and time consuming. More important, it eliminates the error caused by the AN/APS-23 contrast control.



Note: Brightness is monotonically but not linearly related to output voltage

FIG. D-1 CHANGE IN BRIGHTNESS DUE TO CONTRAST CONTROL

SECRET

SECRET

UNIVERSITY OF MICHIGAN

2255-12-T

To achieve maximum contrast between the brightest targets and the background, the transfer characteristic of the APS-23 is made, by means of a dual i-f strip, to have the form shown by the solid line in Figure D-1. x_2 may be set arbitrarily by the operator from x_1 to some maximum value (the contrast control). Hence, all inputs between x_1 and x_2 have the same output.

The effect of decreasing the receiver gain is simply to decrease the slope of the curve below the 2-volt output as from the solid to the dashed line in the figure. Hence, the shape of the curve above the 2-volt output (which is adjustable by the contrast control) has no bearing on the SAC results.

Finally, by using a variable gain, a much wider range of relative echo strengths could be considered than when the gain is fixed.

Data on twenty-seven inherent characteristics of the target groupings were obtained from the study of stereo-pair photographs made vertically from the air at scales of 1:8000 and 1:2000 and from ground photographs of each target from several angles and distances. The degree of correlation of the relative echo strengths with these twenty-seven characteristics and with range and aspect was determined, as were the correlations with many combinations of two factors. The target characteristics which SAC's analysis of the results indicate to be quite significant in affecting radar returns of targets which have fairly constant magnitude as aspect and range change, and which SAC expects to use in radar predictions, are:

1. Predominant outside building material (metal; metal and concrete; stone, brick, and concrete; and wood give returns whose magnitudes decrease in that order),
2. Relative number of separate reflecting surfaces in the group,
3. Horizontal size (buildings of greater over-all lengths gave greater returns),

SECRET

SECRET

UNIVERSITY OF MICHIGAN

2255-12-T

4. Predominant structure height (echo increased with height),
5. Variation in structure heights (the more variation; the greater the return), and
6. Presence of trees, shrubs, and vines around the buildings (even a moderate covering very markedly reduced the returns).

SAC has decided that consideration of these factors is sufficient for a good prediction scheme. Certain other significant factors did not need to be considered inasmuch as they apparently are highly correlated with the above factors (e. g., most metal walls are also smooth). These other factors are described in Reference 5. Those which are of direct interest in drawing inferences on which to base the computations of this report are:

1. Monitor and saw-tooth roofs gave much larger returns than gable and hipped roofs.
2. Percentage of vertical surfaces occupied by windows is not too important.
3. Water foregrounds and built-up foregrounds enhanced returns as compared to wooded areas and open fields.
4. Smooth wall and roof surfaces give much greater returns than rough surfaces.
5. A large amount of associated equipment (e. g., tractors, box cars, derricks, and tanks) greatly increase returns.

The principal objection which has been raised to the validity of the Baltimore Project results is that the target complex in many cases, particularly at the longer ranges, did not occupy the entire area on the ground which was reflecting signals to the radar. Thus the target descriptions did not describe all the contributions to the return. This objection is answered, at least partly, by the fact that among the factors considered were the characteristics of the area in the foreground of the target, the

SECRET

SECRET

UNIVERSITY OF MICHIGAN

2255-12-T

ground range of the target, and the percentage of the beamwidth occupied by the structure grouping. As long as the last factor was above 10 per cent, there appeared to be little dependence on it. In any case, this possible defect would degrade the results principally at the longer ranges, and hence the over-all results, but would not make them useless.

A second objection is that the target descriptions were not always adequately detailed. For example, a measure of variation in structure heights was taken to be the greatest difference in structure heights in the target complex.

A third objection is the size of sample; sixty targets may be an inadequate sample because it may result in too few samples in certain categories. Thus some of, but not all, the conclusions may be based on an inadequate sample size. Certain other objections to the statistical procedures have been heard by the authors but the validity or importance of these objections cannot be decided before studying the final report (which is to contain much detailed information on the data and data reduction procedures) and perhaps studying the raw data itself and the data reduction sheets.

Despite these objections, it is to be reiterated that the SAC data appear to be of considerable value.

D.2 THE OHIO STATE UNIVERSITY RESULTS FOR BATAVIA, N. Y.

The Mapping and Charting Research Laboratory of the Ohio State University Research Foundation has obtained some results which illustrate very clearly the dominant effects of trihedral and dihedral reflectors in returns from certain regular arrays of buildings (Ref. 22)¹. These results were obtained by examining PPI display photographs for two flights past Batavia, N. Y., with an AN/APS-23. The flight paths

¹These results were learned of by personnel of this project only after practically all of the work described in this report was completed. Hence, the results were not used in formulating the simplifying assumptions (Sec. 1.4), but do serve to indicate their correctness.

SECRET

SECRET

UNIVERSITY OF MICHIGAN

2255-12-T

were such that radar depression angles near 0 degrees or 90 degrees were avoided. The street pattern in Batavia is quite regular, as indicated in Figure D-2. The buildings are almost exclusively wooden houses except in a relatively small business area. The extent of the return on the PPI for successive positions along the flight path is indicated in the figure. The results shown in the figure were explained by assuming that the ground and the walls of adjacent buildings formed arrays of trihedral reflectors which gave large responses where the radar beam was not obstructed so as to shadow the adjacent wall or where the angle of depression was not so great that rays striking the ground would go over the tops of the walls. Ohio State University ray-tracing computations, based on average building sizes and spacings, demonstrated that it was precisely in those regions where the aspect prevented the trihedral effect that the return practically disappeared.

When the line-of-sight was perpendicular or parallel to the two street directions (or almost so), the walls and ground were considered to form arrays of dihedral reflectors which would be expected to provide very large returns, as was the case.

It is of importance to note that the successful explanation was based on a very simplified geometrical model in which only average spacings and heights were used, and in which no account was taken of surface roughness or dielectric constants. In addition, no account was taken of the few scattered large structures in Batavia which did not fit into the above patterns of buildings.

D. 3 KURTZ LABORATORIES INTEGRATION TECHNIQUES

The Kurtz Laboratories have done some interesting work on integrating successive frames on a strip of PPI film by photographic means with the objective of separating the returns from targets which are highly directional from those which are not (Ref. 9). Kurtz Laboratories interest is in development of these photographic techniques, but some of the results they have uncovered incidentally are of interest to the present work. In addition, the techniques hold considerable potential value for future attempts at radar PPI interpretations, and for obtaining qualitative information useful in formulating radar prediction methods.

D-6

SECRET

CHART OF BATAVIA RETURNS

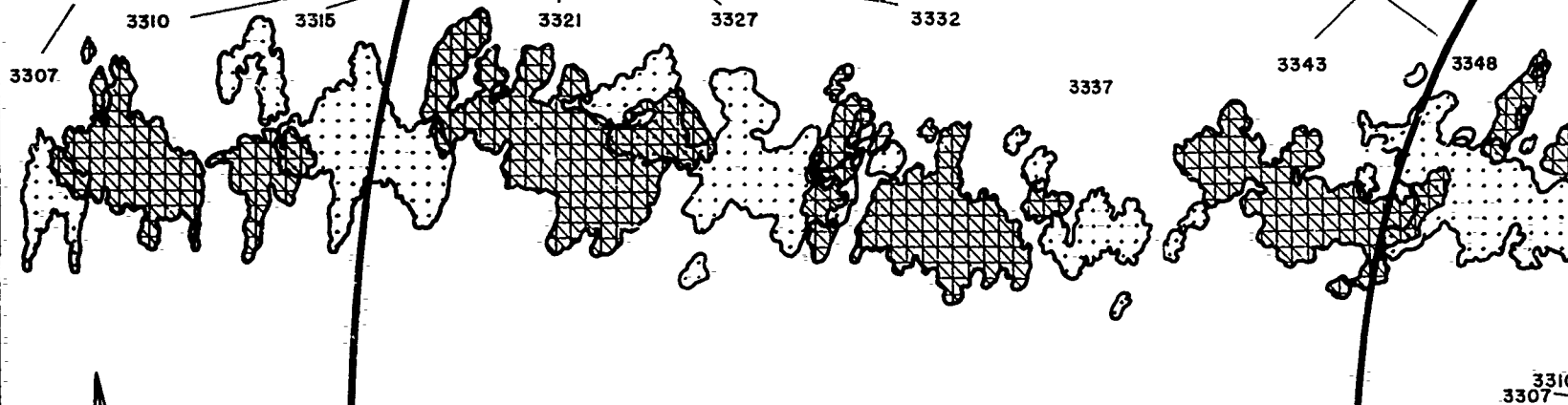
Position of lesser returns. Tangential distortion apparent.

Positions approximating 0° to large block units, 45° to small sections.

Position of lesser returns.

Positions approximating 0° and 45° to large block units.

Position effect



Heading Marker

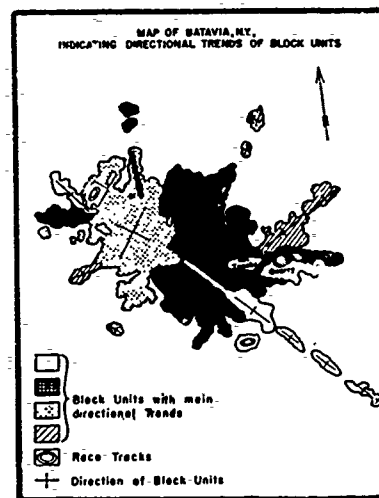
Range Marker

Range Marker

Scale 1:125,000
 Altitude = 20,000 ft.
 Mission No. 4
 Westbound Flight

20 N.M.

10



1

SECRET

FIG. D-2 ILLUSTRATING PPI RETURNS FROM
 (Reproduced from Ref.)

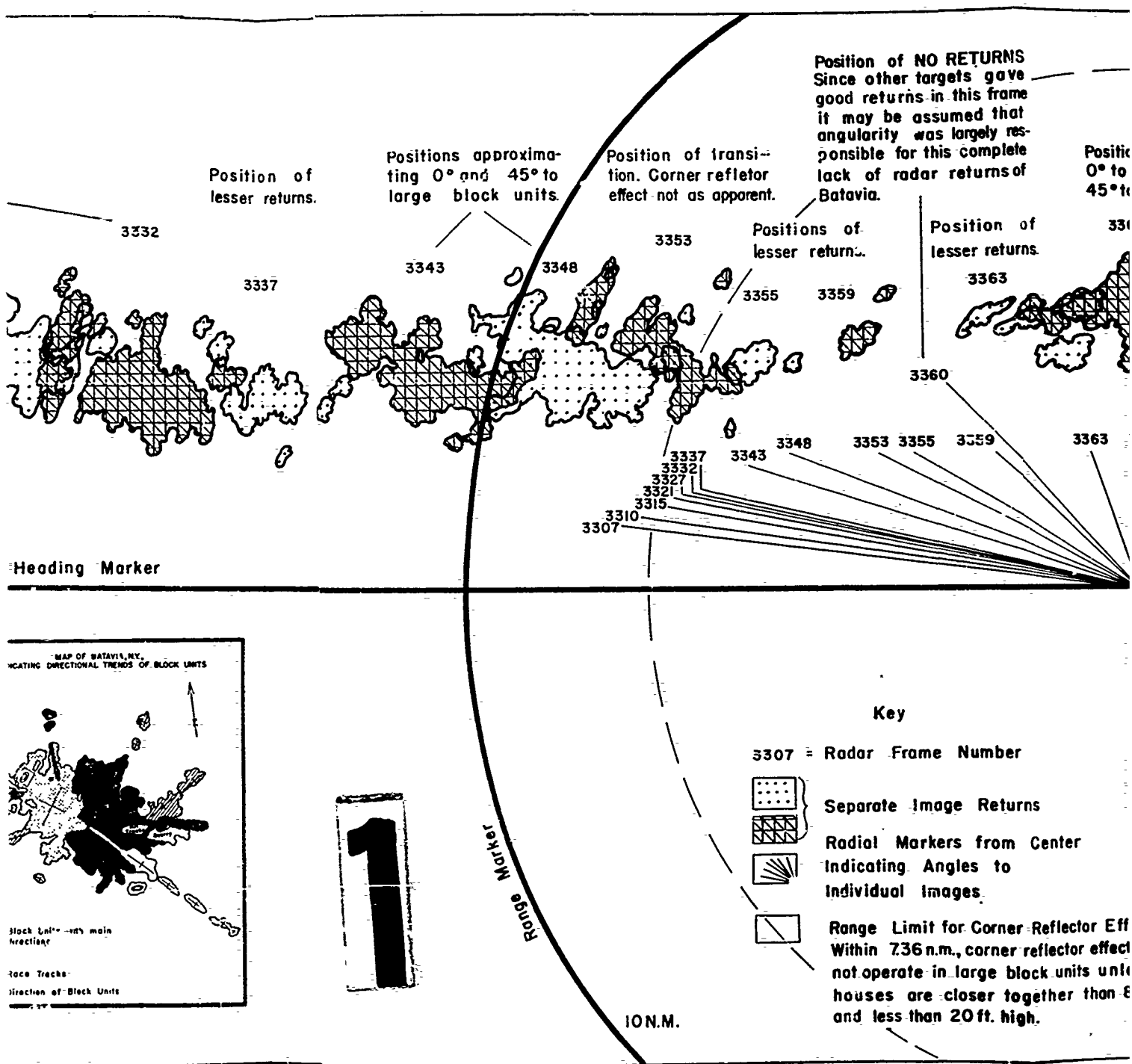


FIG. D-2 ILLUSTRATING PPI RETURNS FROM BATAVIA, NEW YORK
(Reproduced from Ref. 22)

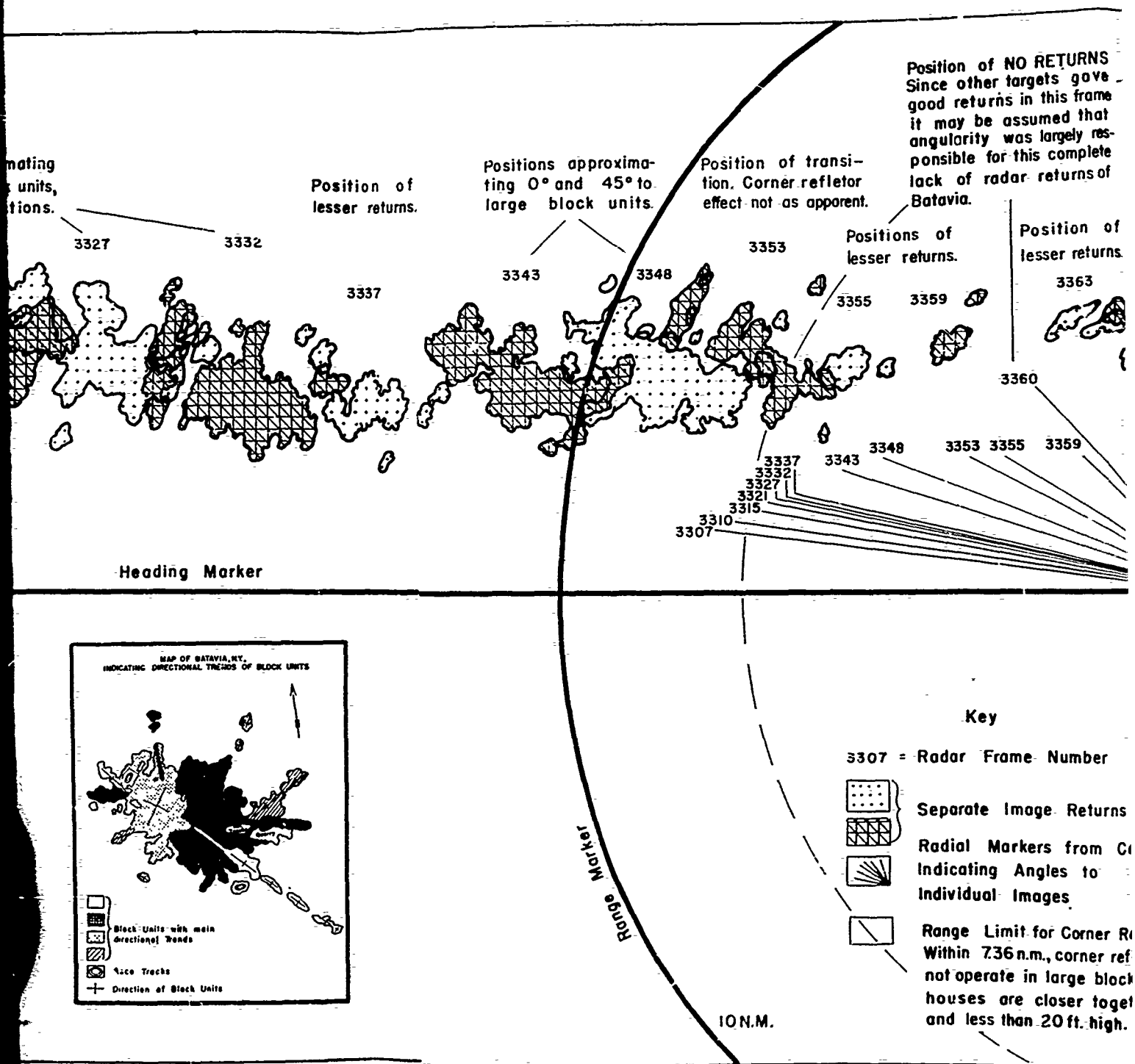
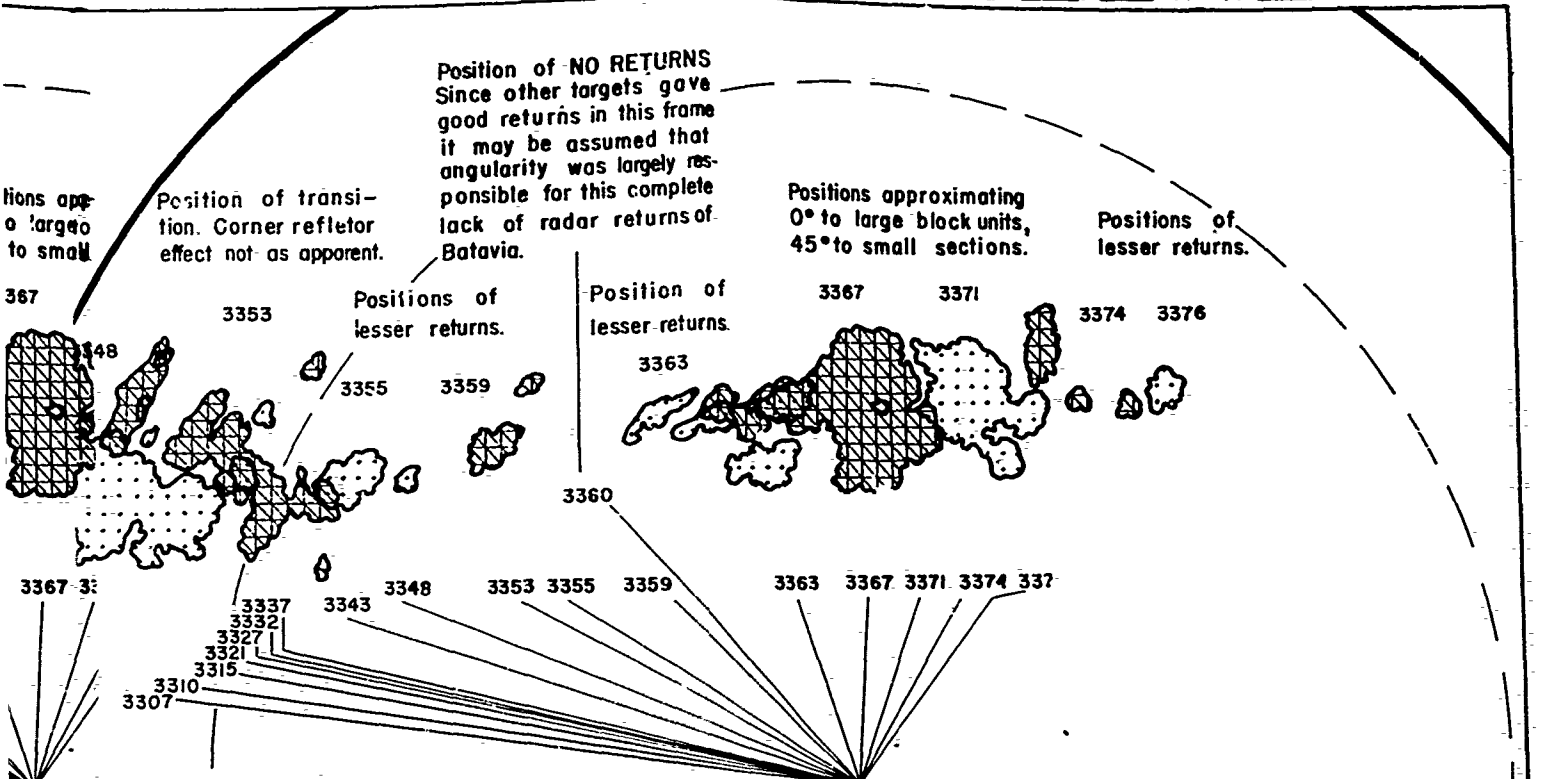
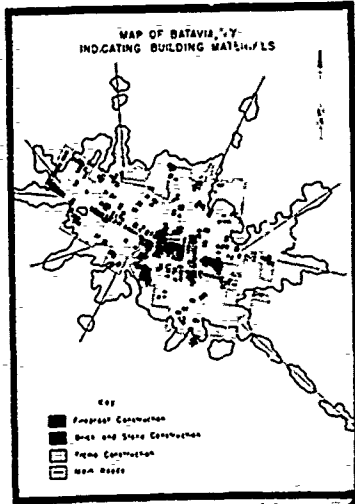


FIG. D-2 ILLUSTRATING PPI RETURNS FROM BATAVIA, NEW YORK
(Reproduced from Ref. 22)



Key

- 3307 = Radar Frame Number
- Separate Image Returns
- Radial Markers from Center Indicating Angles to Individual Images
- Range Limit for Corner Reflector Effect. Within 736 n.m., corner reflector effect will not operate in large block units unless houses are closer together than 80 ft. and less than 20 ft. high.



Effect. ct will less 80 ft.

10 N.M.

RETURNS FROM BATAVIA, NEW YORK
(from Ref. 22)

D-7

2

SECRET

UNIVERSITY OF MICHIGAN

2255-12-T

The main technique being developed is "chromatic glitter integration" (CGI). This is a technique in which several successively recorded film frames are stacked in register and bound to form a "sandwich". Three such sandwiches are formed from film corresponding to successive portions of flight. The successive sandwiches are printed onto Kodak dye transfer matrices from which a single composite color print is then made in the usual fashion by dye transfer.

Several distinct colors arising from the combinations of red, green, and blue where there is superposition: white (blue & green & red), magenta (red & blue), cyan (blue & green), and yellow (red & green). The final print also has the single colors red, blue, and green. The color displayed at a given area on the print indicates the portions of the flight path from which the area was seen on the PPI. Thus red, green or blue indicates a highly directional target, white an isotropic one.

By stacking undyed transfer matrices, and printing the composite picture, a picture representing the isotropic targets only is obtained, the so-called hard core of the scattering pattern.

CGI pictures of Detroit seen by the authors showed strong directional effects which appeared to illustrate the cardinal point effect (Sec. 1.2). In Reference 9, Ypsilanti is reported to have appeared colored in a CGI print, except for scattered white areas. The General Motors factory area at the Willow Run Airport was white. Since this area is extremely complex, having many corner reflectors oriented in all directions, this result appears reasonable.

D. 4 ENGINEERING RESEARCH ASSOCIATES, INC. AND FORD INSTRUMENT COMPANY "BRILLIANCE MEASUREMENTS"

Engineering Research Associates, Inc. (Ref. 1), and the Ford Instrument Company (Ref. 2 and 3) have conducted laboratory programs in which they measured the light transmission of selected target areas of radar PPI photographs furnished by the Wright Air Development Center. At ERA for example, the pictures were enlarged by projection onto an opaque screen.

SECRET

SECRET

UNIVERSITY OF MICHIGAN

2255-12-T

An aperture in the screen fitting the area of interest permitted light to strike a phototube. The amplified phototube response was divided by the response for clear film and corrected for nonlinearity in the amplification to get a quantity termed brilliance by ERA. The aperture size corresponded to 0.21 square miles on the ground.

From these data brilliance versus radar depression angle curves were constructed, ignoring azimuths. To emphasize differences between the curves (the differences were not great), a prescribed brilliance was subtracted at each point. At Engineering Research Associates an "average brilliance" based on some experimental data was subtracted. Its determination involved averaging over azimuth at fixed ranges for four film frames. At Ford Instrument Company the brilliance subtracted was the greatest brilliance in the film being measured at the range of the target, which was generally the saturation value. At Engineering Research Associates the curves are called "brilliance curves"; at Ford Instrument Company they are called "contrast history" curves. At Engineering Research Associates for each curve (i. e., for each target considered in a run) computations were made of the mean value of the ordinates, the standard deviation, the standard deviation per entry, and standard deviation per number of quantized brilliance levels occurring, and the asymmetry or differences in means on approach and departure.

The targets were described at ERA by word pictures such as given by this example (Ref. 1):

"Union Station, Cincinnati, Ohio. . . . 20 per cent Union Station (domed roof), 20 per cent railroad yards 60 per cent residential or business district. Almost 100 per cent . . . ; levee area at west-most edge (probably filled in since topographic map was made). Separated from flight path by hills 30 feet higher than area."

An attempt was made to relate the statistical parameters of the brilliance curves with the various types of targets. The best result was to show a tendency (with many exceptions) for the measurements for industrial areas to have much larger standard deviations than the measurements for farmlands.

SECRET

SECRET

UNIVERSITY OF MICHIGAN

2255-12-T

About 50 APS-23 PPI film strips were analyzed. Only two were comparable in flight path; however, these were at 3000- and 9000-foot altitudes, and all radar settings (e. g., contrast control) differed for these two strips.

At Ford Instrument Company the contrast intervals were generally quantized into four levels. The target classifications were very general ones such as railroads, industrial, waterways, and residential flatlands, with occasional combinations of industrial and railroads. Two types of statistical information were then recorded to form what Ford calls "target identification keys" for a given target type. Early in their work, Ford made histograms of the relative number of times the returns from targets of a given class changed from one contrast level to the next for a given depression angle θ_0 as the depression angle passed through θ_0 . These sets of histograms are called "change point keys". The later type of key, called a "contrast history key", is a set of histograms of the relative number of times a given contrast was achieved in a given θ interval. Variations of these keys were also used. The keys were then used as prediction devices, the idea being that if a set of histograms for an unidentified target were obtained, the target would most likely be a member of the target class whose key it fit most closely. Criteria for fitting were considered in detail.

About 40 per cent accuracy in identification was achieved with the change point keys, and 55 per cent with contrast history keys as compared to about 20 per cent which would occur by pure chance. It should be borne in mind that most of the evaluations of the keys used the same film strips as were used to form the keys.

Incidentally, it is evident that by no means all the properties of the target return are used in these keys. This was sharply brought out at Ford where it was found that the girls who did the film reduction could obtain very much higher prediction accuracy by examining film strips and using no keys. As a result, a program was started (but not complete as yet) to find out what attributes of the target pictures the girls were using for identification.

SECRET

SECRET

UNIVERSITY OF MICHIGAN

2255-12-T

In general, the target areas, even in the less general classifications used by Engineering Research Associates, such as "railroad roundhouse", embraced such a variety of types of reflectors that it would have been remarkable if much more success had been obtained in either investigation. The number of target areas studied is far too small to iron out the effects of these variations. Even if clear-cut results had been obtained, it would have been very difficult to draw conclusions useful for the purposes of this contract from the results on such complex targets.

In any case, there were other factors which reduce the value of these results. There was no uniformity in the radar control settings; in fact these settings were generally unknown. The same is true for the photography and development procedures for the PPI films. Both firms are well aware of these difficulties.

The question of radar control settings is unusually important with an AN/APS-23 radar because of the presence of the "contrast control" (App. D.1.).

D. 5 PHILCO CORPORATION RESEARCH ON RADAR TERRAIN REFLECTION CHARACTERISTICS

The Philco Corporation has carried out an extensive program in which they obtained a considerable amount of X-band pulse-to-pulse data on the radar returns from various types of terrain (Ref. 6). The quantity measured was A-scope amplitude, y , as recorded on film, the successive traces occurring 1600 times per second and extending for 3 microseconds.

From these data the following quantities were computed:

$W_1(y)$, the first probability density function

$\rho(\tau)$, the suppressed autocorrelation function

SECRET

UNIVERSITY OF MICHIGAN

2255-12-T

In general, the target areas, even in the less general classifications used by Engineering Research Associates, such as "railroad roundhouse", embraced such a variety of types of reflectors that it would have been remarkable if much more success had been obtained in either investigation. The number of target areas studied is far too small to iron out the effects of these variations. Even if clear-cut results had been obtained, it would have been very difficult to draw conclusions useful for the purposes of this contract from the results on such complex targets.

In any case, there were other factors which reduce the value of these results. There was no uniformity in the radar control settings; in fact these settings were generally unknown. The same is true for the photography and development procedures for the PPI films. Both firms are well aware of these difficulties.

The question of radar control settings is unusually important with an AN/APS-23 radar because of the presence of the "contrast control" (App. D.1.).

D.5 PHILCO CORPORATION RESEARCH ON RADAR TERRAIN REFLECTION CHARACTERISTICS

The Philco Corporation has carried out an extensive program in which they obtained a considerable amount of X-band pulse-to-pulse data on the radar returns from various types of terrain (Ref. 6). The quantity measured was A-scope amplitude, y , as recorded on film, the successive traces occurring 1600 times per second and extending for 3 microseconds.

From these data the following quantities were computed:

$W_1(y)$, the first probability density function

$\rho(\tau)$, the suppressed autocorrelation function

SECRET

UNIVERSITY OF MICHIGAN

2255-12-T

$\psi(\tau)$, the non-suppressed¹ autocorrelation function

σ_0 , the normalized² radar echoing area.

The targets observed consisted of four fairly extensive, homogeneous, flat New Jersey terrains; sand (an emergency landing field for small aircraft), grass (6-inch high wheat), scrub-pine (3 to 5 feet high), and forest (dense covering of pine trees 20 to 30 feet high); and four others; a river and river bank, a village of 60 houses along a railroad track a metal building with a 90-foot tower and a 100-foot water tank surrounded by some low cement block buildings; a railroad siding, and a pond surrounded by trees. More adequate descriptions and photographs are given in Reference 6.

The main results of interest to the present investigation are the values of σ_0 . It was found that only for sand and grass did σ_0 approximately vary as

$$\sigma_0(\theta) = \text{constant} \cdot \sin \theta$$

with depression angle θ . This result is the one which would be obtained if the terrain were scattered isotropically. Sand and grass were also the targets for which $W_1(y)$ was most nearly a Rayleigh distribution. $\sigma_0(\theta)$ for scrub pine and forest increased with decreasing θ .

The other data obtained by Philco are of interest to this program only indirectly. They showed that certain parameters of $W_1(y)$, $\rho(\tau)$, and $\psi(\tau)$ could be used with moderate success to differentiate among the various types of targets. These parameters are certainly not used explicitly for target identification in present-day radars, although this knowledge is of possible value for more long-range camouflage planning.

¹"Suppressed" is used by Philco to mean that the average value is subtracted from the data at each pulse before the correlation is carried out.

² σ_0 is the conventional radar cross-section divided by the area of the ground irradiated.

SECRET

SECRET

UNIVERSITY OF MICHIGAN

2255-12-T

The Philco Corporation obtained a large amount of data and conducted a thorough analysis of the results and their validity. Their analysis, as well as some separate considerations of their data made during the present study, indicate that the quantity of data, i. e., the sample size, is rather marginal for drawing some of their conclusions.

D. 6 DIHEDRAL AND TRIHEDRAL REFLECTOR EXPERIMENTS

All the computations made in this report place heavy emphasis on the returns from dihedral and trihedral reflectors. Hence, experimental data on the returns from corner reflectors are of interest, particularly the results of controlled tests which can be used to verify the approximate theoretical formulas used for the computations. Data for cases in which it is known that the approximations made in developing the theory are poor are particularly important in exploring the range of validity of the results. These cases include those in which the irradiating wavelength is comparable to the lengths of the sides of the corner or to the scale of surface roughness and those from which the theory determining the effects of non 90-degree angles at the edges of the corners can be checked. Data from three sources are described below.

D. 6.1 MIT Radiation Laboratory

R. D. O'Neal, in Reference 7, compared experimental returns from corner reflectors with the theoretical back-scattering radar cross-section result $\sigma = 4\pi A^2/\lambda^2$ which is used in this report. His results for a square corner reflector are reproduced in Figure D-3. A description of this work given in Reference 11 follows.

"The experimental dependence of the cross-section on the size of the reflector is shown in Table D-1 for a square corner reflector. A one-foot corner reflector was used to obtain the constant K. For the 6-inch reflector, whose dimensions are of the same order of magnitude as the wavelength of the incident radiation, the cross-section deviated from that predicted by physical optics by a factor of approximately 1.6. The discrepancies between physical optics theory and experiment for the 3 and 4-foot reflectors can be attributed to non-perpendicularity of the reflector sides."

SECRET

SECRET

UNIVERSITY OF MICHIGAN
2255-12-T

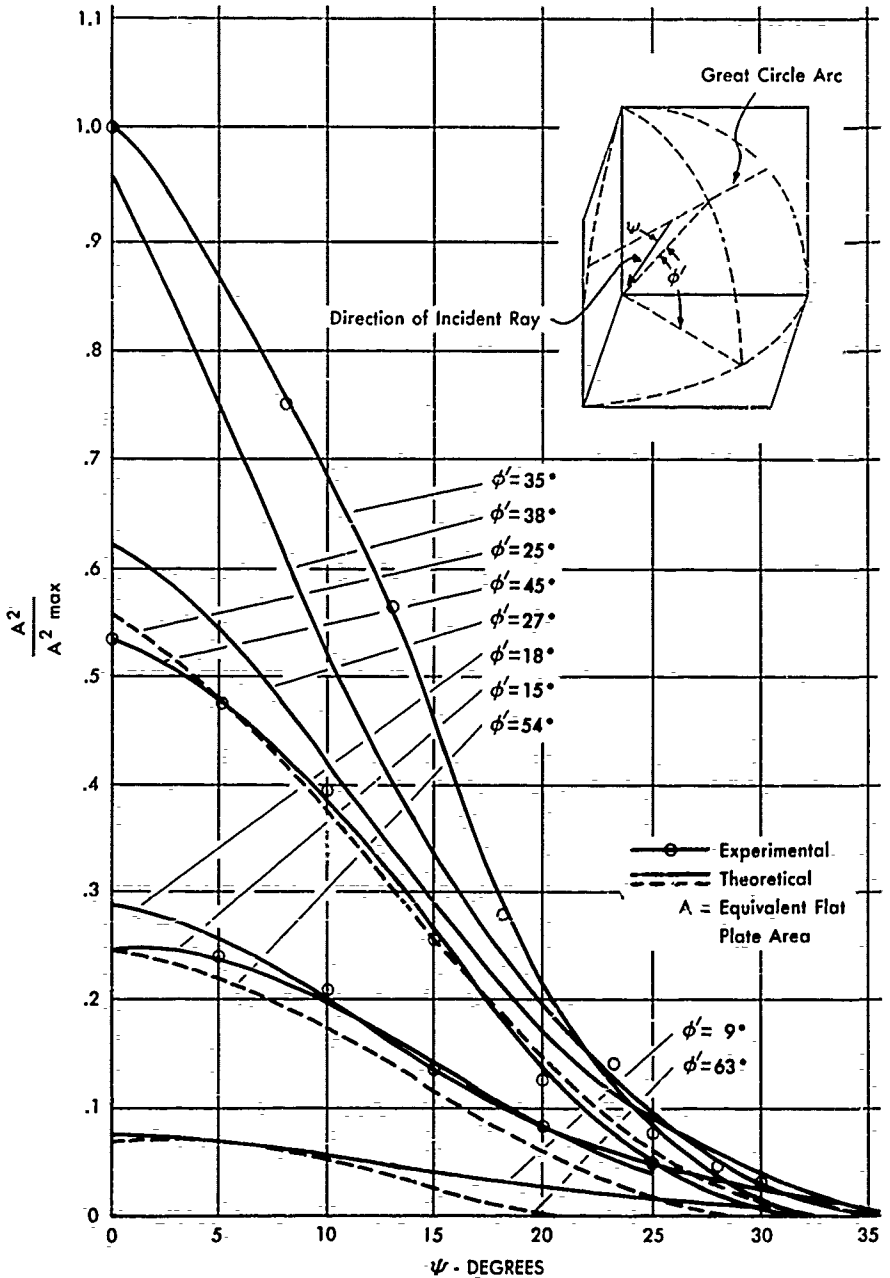


FIG. D-3 RELATIVE INTENSITY OF REFLECTION FROM SQUARE CORNER REFLECTOR.

D- 14

SECRET

SECRET

UNIVERSITY OF MICHIGAN

2255-12-T

TABLE D-1

VARIATION OF CROSS-SECTION WITH CORNER SIDE LENGTH b

($\lambda = 9.1$ cm)

<u>Side Length</u>	<u>Value of n in $\sigma = Kb^n$</u>
6 inches	3.3
2 feet	4.0
3 feet	3.8
4 feet	3.8

D.6.2 Cornell Aeronautical Laboratory

In Reference 3, the Cornell Aeronautical Laboratory presents the results of an extensive series of tests to determine effective means of modulating corner reflector echoes by changing the dihedral angles, truncating the corner reflectors, and using diffusing or absorbing surfaces. Many of these results are of direct interest to the present program. Some of them are of value as an aid in predicting the principal returns from buildings, and some because certain of the modulation methods could perhaps also be applied to camouflage.

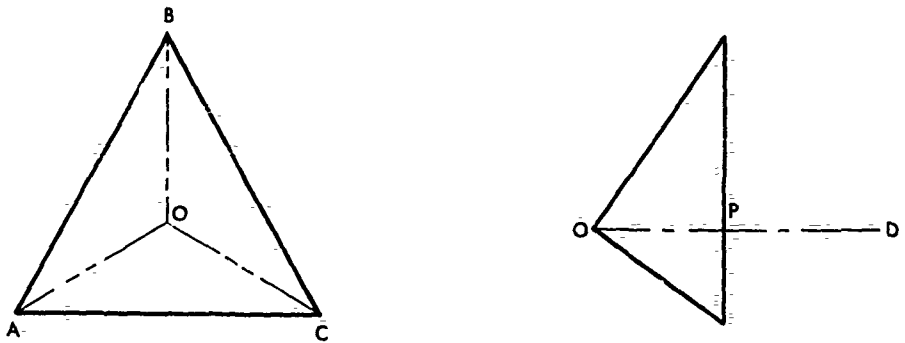
The corner reflectors were located on a paved parking lot with absorbing shielding placed to eliminate ground reflections. The radar was an AN/APS-15 X-band set, modified to furnish a 3-degree beamwidth, located on a tower 50 feet above ground level and 600 feet from the corner reflectors. Unfortunately for present purposes, the corner reflectors had triangular sides rather than the rectangular sides of primary interest in building returns. Figures D-4 through D-7, reproduced from Reference 8, illustrate the reduction of radar echo as a function of angle error for a given side length to wavelength ratio. In these tests this ratio was approximately 9. The results are of the magnitude indicated in Reference 10.

Figures D-8 through D-11 illustrate various protuberances placed on the walls of the corner reflectors. A reduction of about 20 db in maximum echo strength was found for each of these reflectors and hence such schemes should be considered as possible camouflage devices.

SECRET

SECRET

UNIVERSITY OF MICHIGAN



AO, BO, CO = Edge of Corner

AOB, BOC, COA = Side of Corner

ABC = Face of Corner

OPD = Axis of Corner Perpendicular to Face ABC

θ = Azimuth Angle of Corner Reflector Axis with Respect to Line of Sight to Radar

ψ = Elevation Angle of Corner Reflector Axis with Respect to Line of Sight to Radar

FIG. D-4 CORNER REFLECTOR GEOMETRY

SECRET

SECRET

UNIVERSITY OF MICHIGAN
2255-12-T

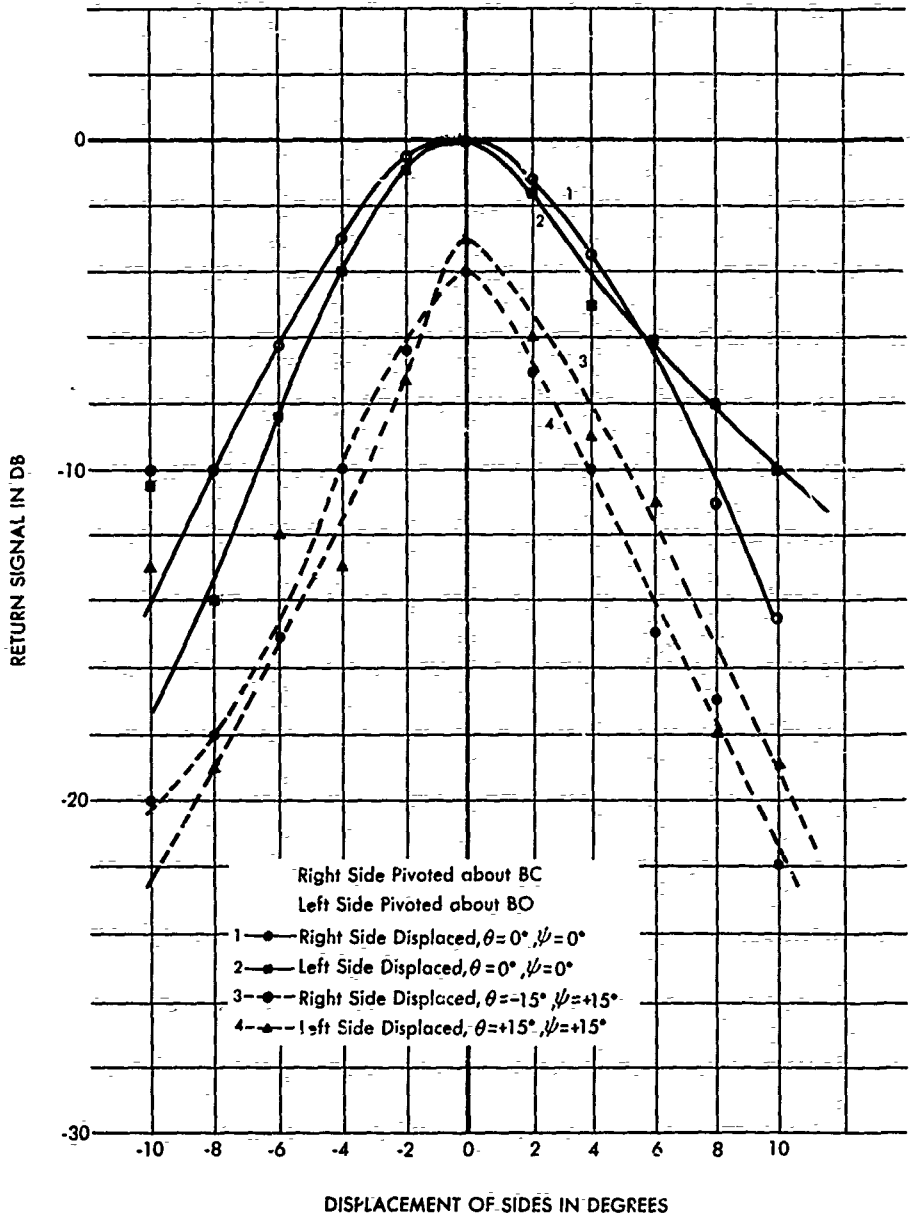


FIG. D-5 MODULATION FOR MOVABLE SIDE CORNER REFLECTOR
(Single Side Displaced)

D-17

SECRET

SECRET

UNIVERSITY OF MICHIGAN
2255-12-T

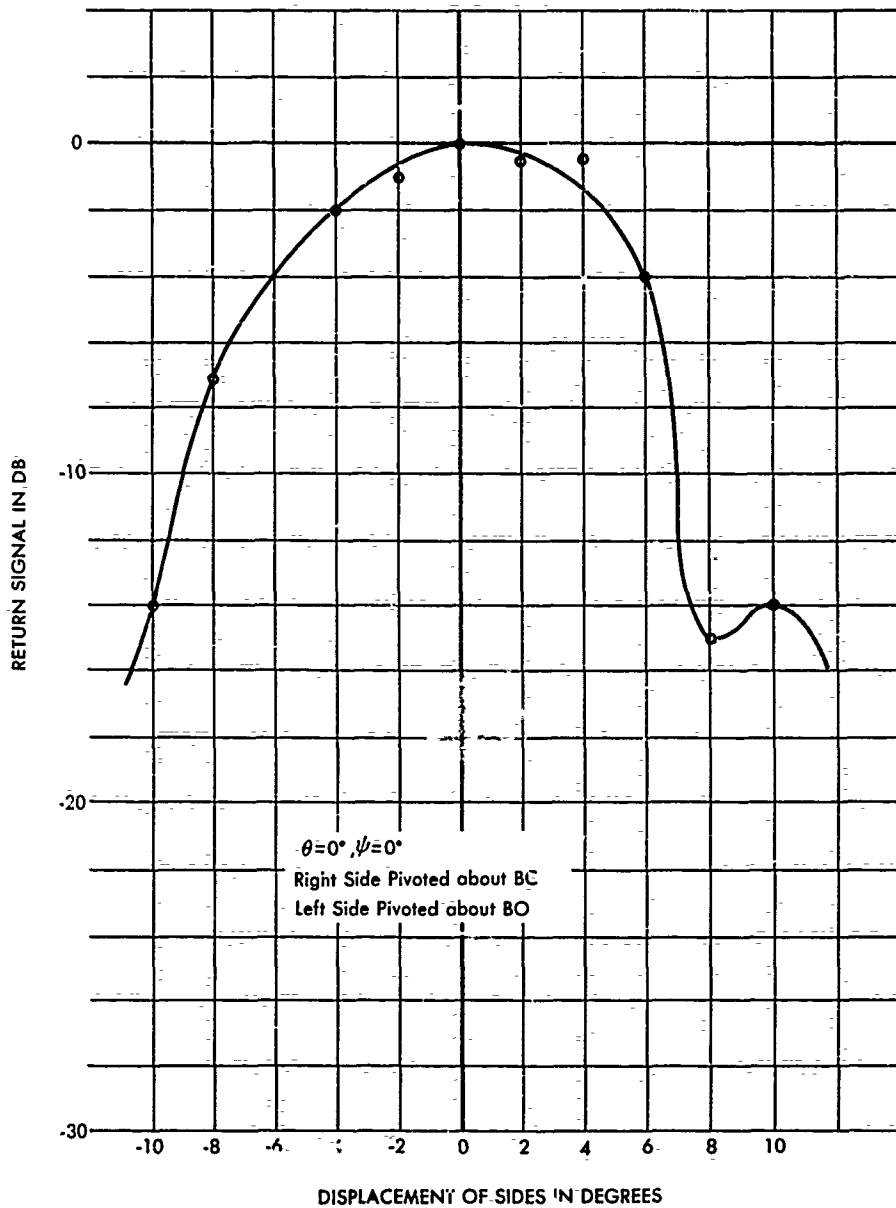


FIG. D-6 MODULATION FOR MOVABLE SIDE CORNER REFLECTOR.
(Two Sides Displaced Equal Amounts in the Same Direction)

D-18

SECRET

SECRET

UNIVERSITY OF MICHIGAN
2255-12-T

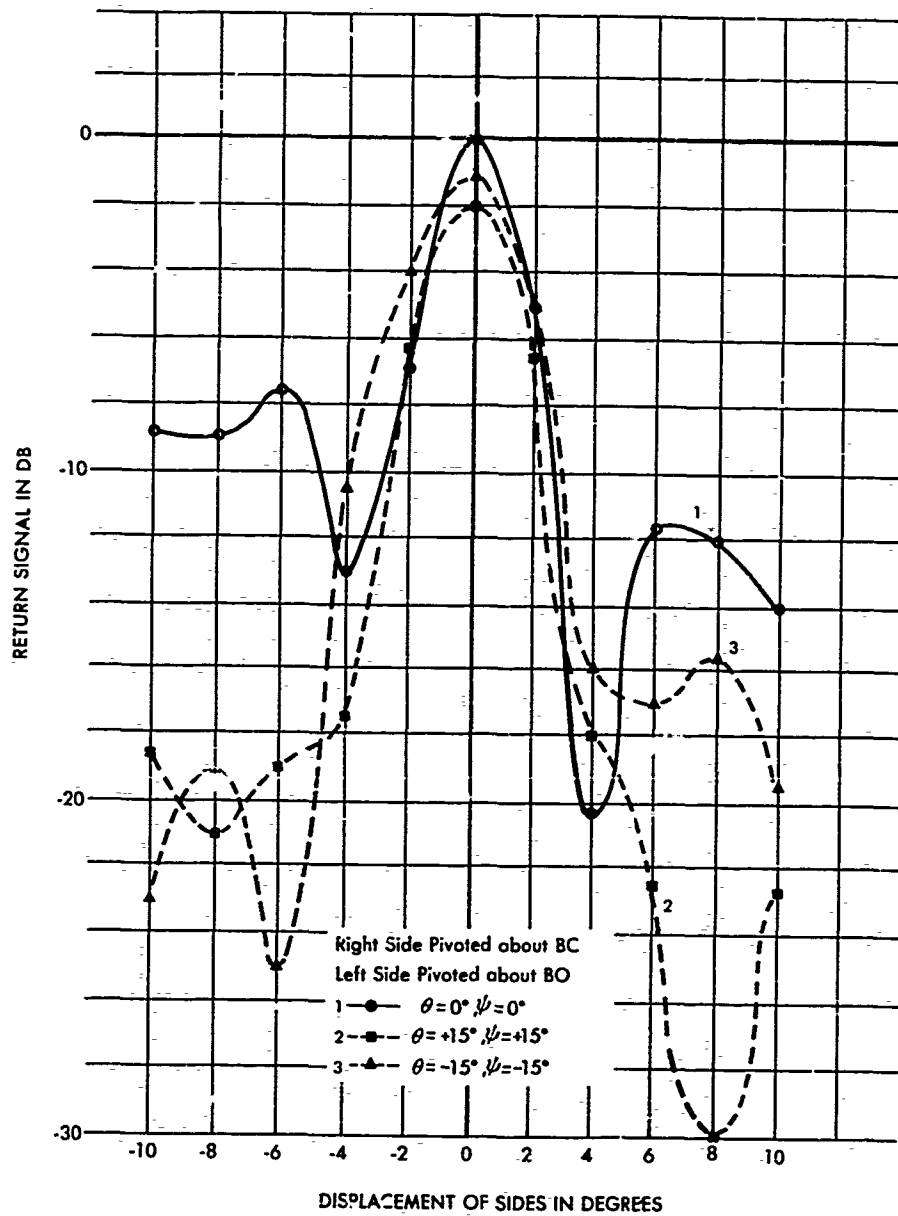


FIG. D-7 MODULATION FOR MOVABLE SIDE CORNER REFLECTOR
(Two Sides Displaced Equal Amounts in the Opposite Directions)

D-19

SECRET

BETTY W. HOMETT

SECRET

UNIVERSITY OF MICHIGAN

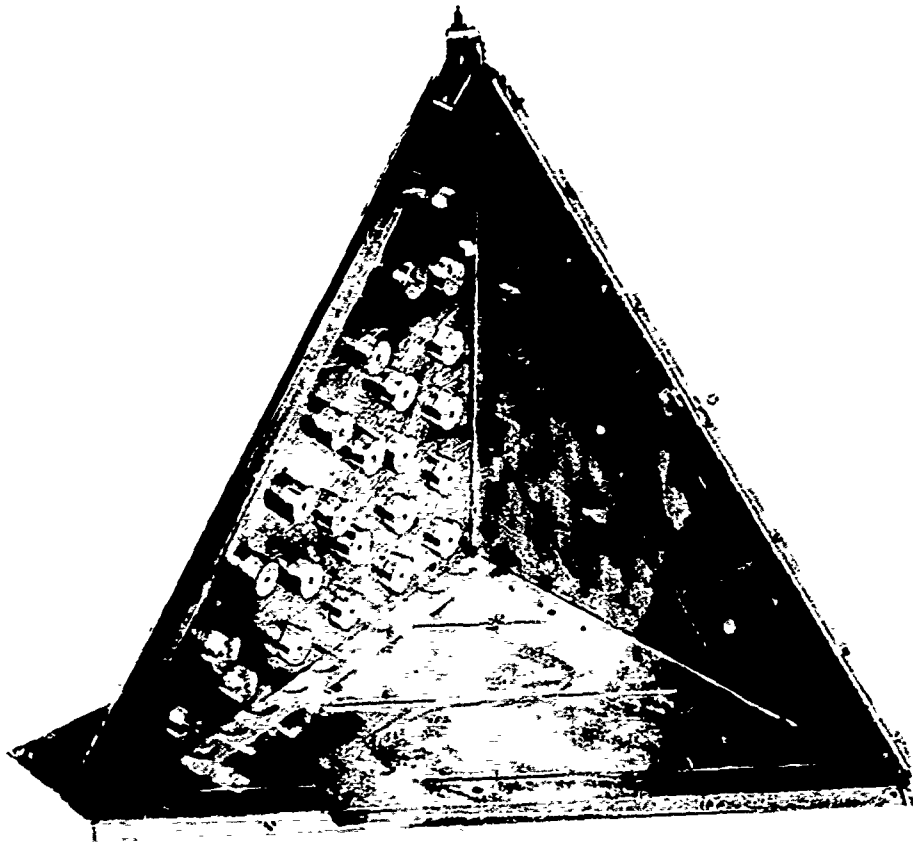


FIG. D-8 DIFFUSING SIDE CYLINDRICAL PROJECTION CORNER REFLECTOR

D-20

SECRET

SECRET

UNIVERSITY OF MICHIGAN

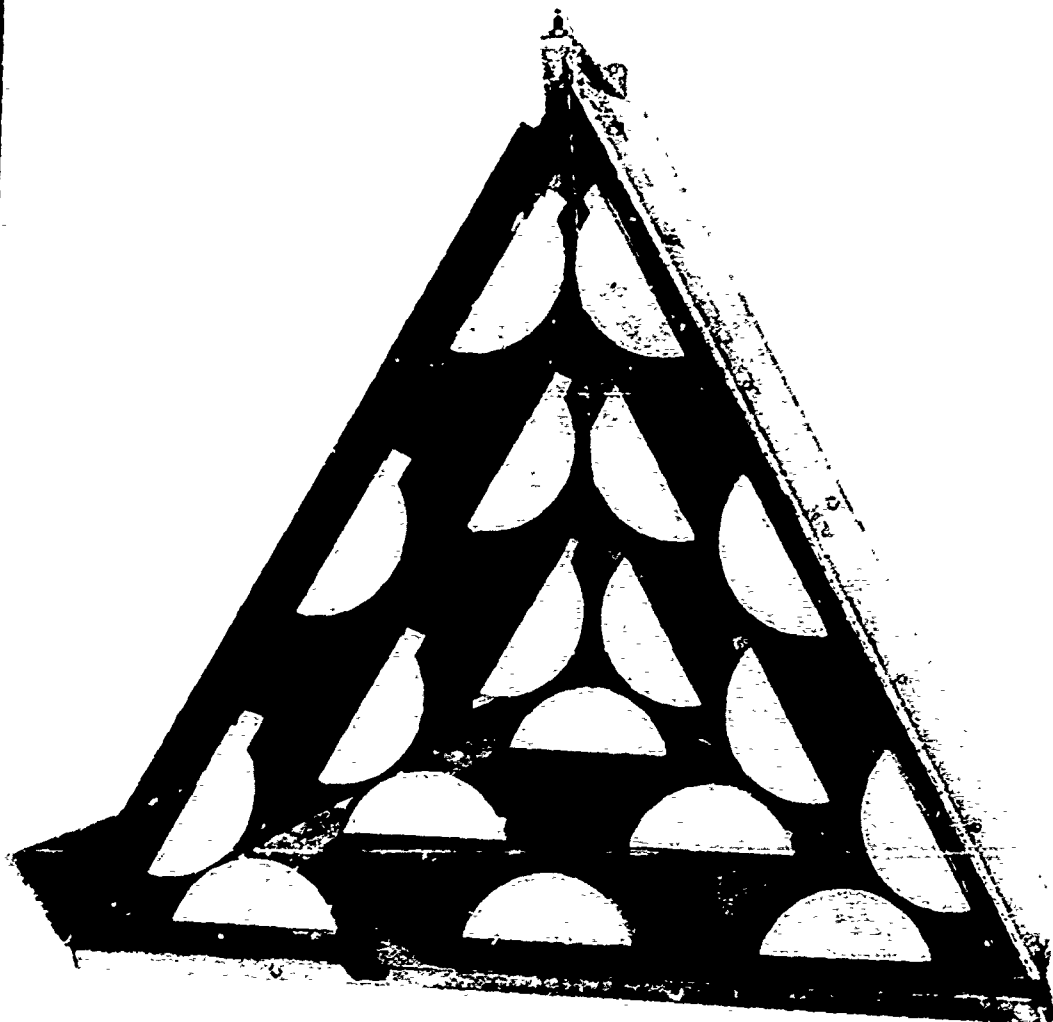


FIG. D-9 MULTIPLE DISC SHUTTER CORNER REFLECTOR

D-21

SECRET

SECRET

UNIVERSITY OF MICHIGAN

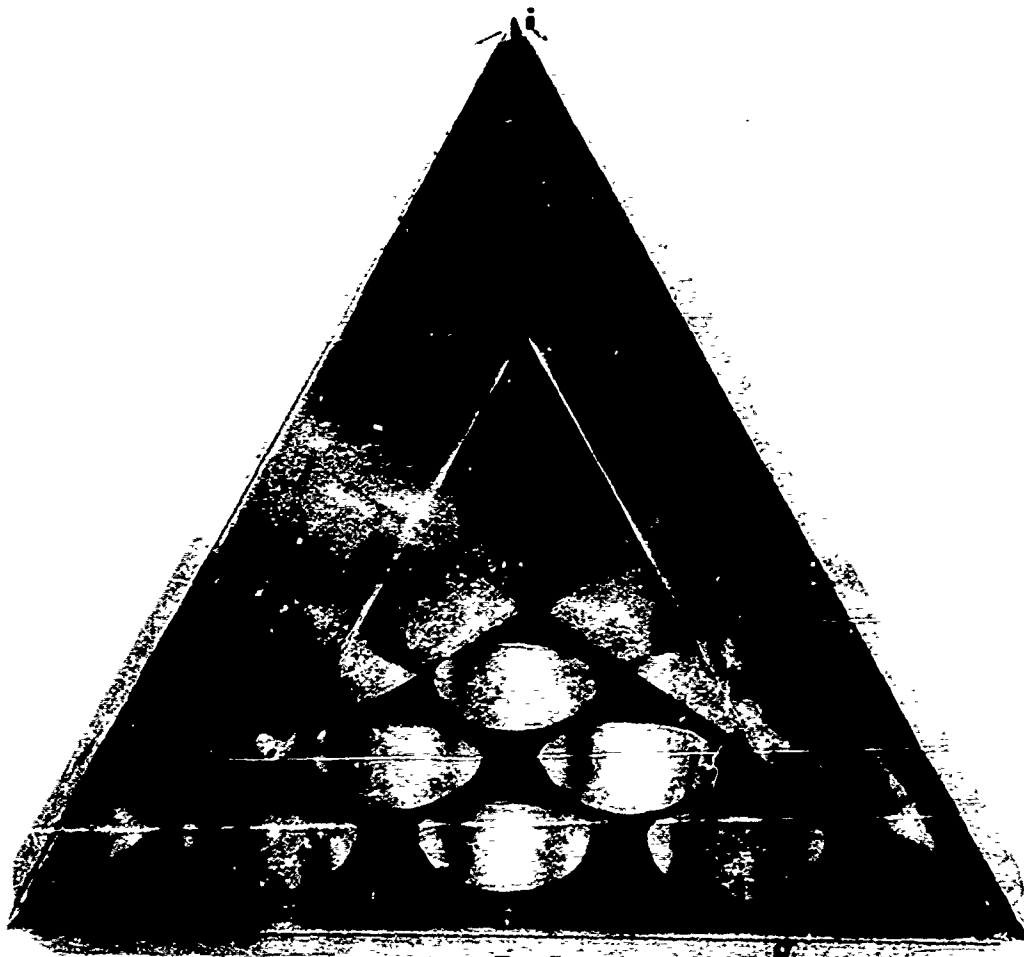


FIG. D-10 MULTIPLE VERTICAL CYLINDRICAL DIFFUSER CORNER REFLECTOR

D-22

SECRET

SECRET

UNIVERSITY OF MICHIGAN

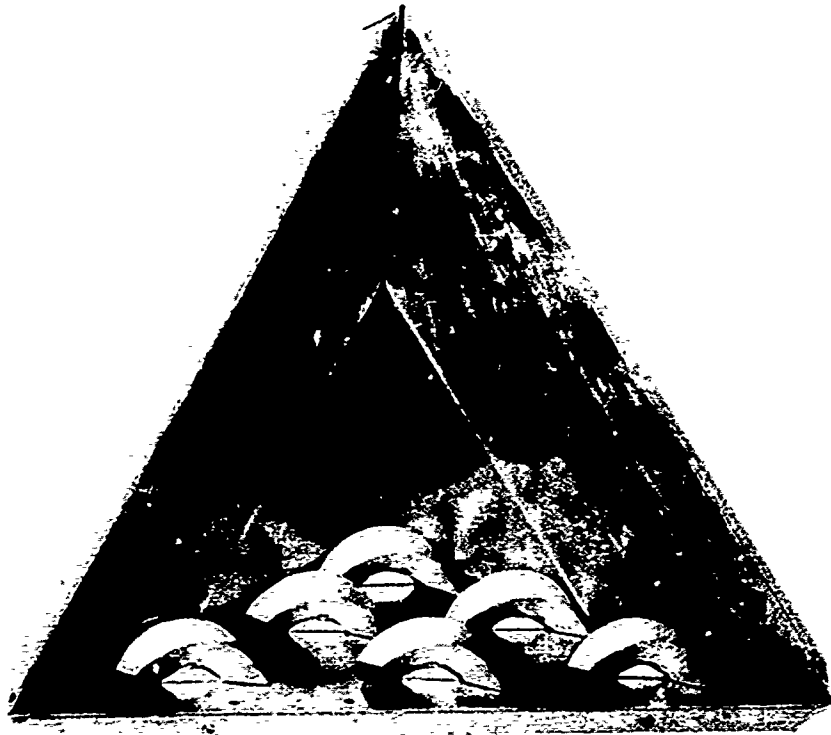


FIG. D-11 MULTIPLE DISC DIFFUSER CORNER REFLECTOR

D-23

SECRET

SECRET

UNIVERSITY OF MICHIGAN
2255-12-T

D. 6. 3 Engineering Research Associates Optical Models

An experimental laboratory study of scattering patterns has been made by Engineering Research Associates (Ref. 1). This experiment involved an unpolarized light beam as the source and a photocoell receiver. The re-radiation pattern of a group of toy plastic building blocks was investigated. A three-dimensional model of the observed radar pattern was compared with a similar model constructed according to physical optics computations of the type used in Appendix A of this report, neglecting energy returned after more than three bounces and neglecting all but specular returns. The theoretical and measured patterns had the same general shape. The differences are attributed by Engineering Research Associates to the use of non-parallel incident light in the experiment and the assumption of perfectly smooth surfaces in the theory.

A more sophisticated version of this experimental set-up which automatically recorded on facsimile paper the back scattering returns over an entire hemisphere was then used for additional measurements of trihedrals, dihedrals, and arrays of blocks. The results provide qualitative illustrations of the effects of rough surfaces, truncation and angular errors, and surface curvature on the returns. A result of special interest was that strong dihedral effects were observed even with surface roughness of three to five wavelengths.

D-24

SECRET

SECRET

UNIVERSITY OF MICHIGAN

2255-12-T

REFERENCES

1. Final Report and Interim Engineering Reports 1 - 12 on Contract AF 33(038)-14317 "Radar Target Intelligence Information Theory and Techniques." Engineering Research Associates, Inc.
2. Engineering Reports 1 through 12 on Contract AF 33(038)-23697, "Radar Presentation Intelligence Interpreter's Manual and Radar Presentation Intelligence Interpreter Equipment", Ford Instrument Co., Long Island City, N. Y. CONFIDENTIAL
3. Interim Engineering Report No. 2, on Contract AF 33(616)-400, "Radar Presentation Intelligence Predictor Equipment Study", Ford Instrument Co., Long Island City, N. Y. (September 1953). CONFIDENTIAL
4. SAC Manual 96-1, SAC Headquarters, Offutt Air Force Base, Omaha, Nebraska (to be published).
5. Semi-Final Report--The Radar Prediction Program, SAC Headquarters, Offutt Air Force Base, Omaha, Nebraska, (16 October 1953). CONFIDENTIAL
6. Final Engineering Reports on Contract AF 33(038)-9219, "Research on Radar Terrain Reflection Characteristics", Philco Corporation, Philadelphia, Pa. (Vol. I, December 1950, Vol. 3, July 1951). CONFIDENTIAL
7. R. D. O'Neal, "The Application of Corner Reflectors to Radar (Experimental)" Report No. RL-280, M. I. T. Radiation Laboratory, (July 1, 1953).
8. C. F. Kiefer and L. H. Bauer, "Modulated Corner Reflectors", Report No. GM-776-T-33 on Contract AF 18(600)-22, Cornell Aeronautical Laboratory, Inc., Buffalo, N. Y., (December 20, 1954).
SECRET

E-1

SECRET

SECRET

UNIVERSITY OF MICHIGAN

2255-12-T

9. Final Engineering Report and Interim Engineering Report 541-5 on Contract AF 33(616)-2343, Kurtz Laboratories, Yellow Springs, Ohio, (December 13, 1954).
10. R. C. Spencer, "Optical Theory of the Corner Reflector", Report No. 433, M.I.T. Radiation Laboratory, (March 2, 1944).
11. UMM-106 "Studies in Radar Cross-Sections VI, Cross - Sections of Corner Reflectors and Other Multiple Scatterers at Microwave Frequencies, R. R. Bonkowski, C. R. Lubitz and C. E. Schensted, University of Michigan, Willow Run Research Center. (October 1953). SECRET. (UNCLASSIFIED if Appendix is removed.)
12. H. A. Tanner, A. G. Sands, M. V. McDowell, "Darkflex - a Fibrous Microwave Absorber", Report 4137, Naval Research Laboratory, Washington, D. C., (April 20, 1953).
13. R. W. Wright and Johnson, "Removal of Mast Reflections by Harp in the S. G. Installation Aboard Destroyers", NRL R 3036
14. J. H. Davis and W. R. Cuming, Final Report on Contract NObsr 63054, BuShips Index No. -NE-071406, Subtask No. 2, Emerson and Cuming Inc., Canton, Mass. (November 1953).
15. UMM-115, "Studies in Radar Cross-Sections VIII - Theoretical Cross-Section as a Function of Separation Angle Between Transmitter and Receiver at Small Wavelengths, K. M. Siegel, H. A. Alperin, R. R. Bonkowski, J. W. Crispin, A. L. Maffett, C. E. Schensted, and I. V. Schensted, University of Michigan, Willow Run Research Center, (October 1953). UNCLASSIFIED
16. J. A. Stratton, "Electromagnetic Theory", McGraw Hill Book Co., New York, (1941 and 1954).
17. R. C. Spencer, "Back Scattering from Conducting Surfaces", Report No. CRL-R-E5070, Cambridge Air Force Research Center, (April 1951).

E-2

SECRET

SECRET

UNIVERSITY OF MICHIGAN
2255-12-T

18. A. R. von Hippel (ed.) "Dielectric Materials and Applications", Technology Press of M.I.T. and John Wiley and Sons, Inc., New York, (1954).
19. A. W. Straiton and W. C. Tolbert, "Measurement of the Dielectric Properties of Soils and Water at 3.2 cm. Wavelength", Journal of the Franklin Institute, Vol. 246, (July 1948).
20. C. R. Burrows and S. S. Attwood, "Radio Wave Propagation", Academic Press, Inc., New York, (1949).
21. Cady, Karelitz, Turner, "Radar Scanners and Radomes", M.I.T. Radiation Laboratory Series, No. 26, McGraw-Hill Book Company, New York.
22. Summary Report on Contract AF 18(600)-90, "Radar Mensuration, Interpretation and APS-23 Instrumentation Studies", Ohio State University Research Foundation, Technical Paper No. 186, (June 1954).
23. R. A. Fisher, "Design of Experiments", Oliver and Boyd, Edinburgh, (1951).
24. O. Kempthorne, "The Design and Analysis of Experiments", John Wiley and Sons, Inc., New York, (1952).
25. D. E. Kerr, "Propagation of Short Radio Waves", M.I.T. Radiation Laboratory Series, No. 13 McGraw Hill Book Company, Inc. New York, (1951).

E-3

SECRET

SECRET

UNIVERSITY OF MICHIGAN

2255-12-T

DISTRIBUTION

To be distributed in accordance
with the terms of the contract.

E-4

SECRET

N1-5901